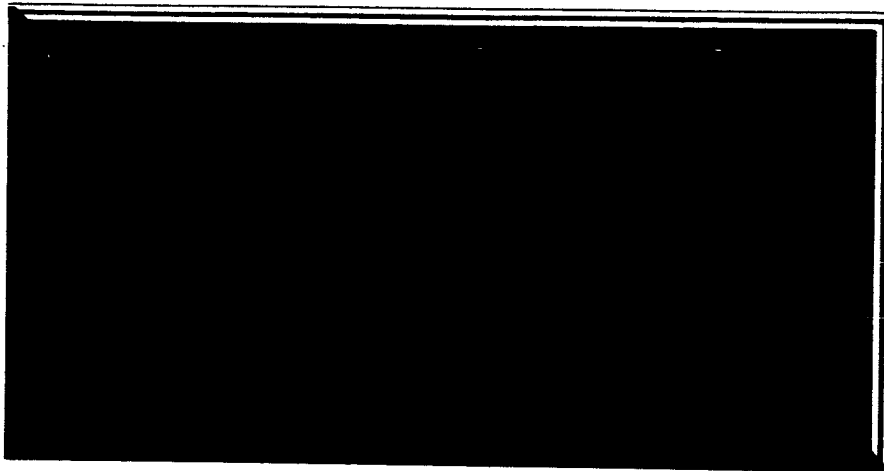


# SPACECRAFT DEPARTMENT

MISSILE AND SPACE DIVISION



GPO PRICE \$ \_\_\_\_\_

CFSTI PRICE(S) \$ \_\_\_\_\_

Hard copy (HC) \$ 6.00

Microfiche (MF) \$ 1.00

7 653 July 65

FACILITY FORM 602  
N66 25544  
(ACCESSION NUMBER)  
271  
(PAGES)  
OR 74953  
(NASA CR OR TMX OR AD NUMBER)

(THRU) \_\_\_\_\_  
(CODE) 1  
28  
(CATEGORY)

GENERAL  ELECTRIC

.66SD4255

15 MARCH 1966

**FINAL REPORT**

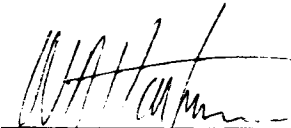
**FEASIBILITY ASSESSMENT OF A SOLID  
PROPELLANT ELECTRIC THRUSTER (SPET)**

**PREPARED FOR JET PROPULSION LABORATORY  
CALIFORNIA INSTITUTE OF TECHNOLOGY**


This work was performed for the Jet Propulsion Laboratory,  
California Institute of Technology, sponsored by the  
National Aeronautics and Space Administration under  
Contract NAS7-100.

**JET PROPULSION LABORATORY CONTRACT 951102**

APPROVED BY:



W.A. HARTMAN  
PROGRAM MANAGER



A.V. LARocca, MANAGER,  
ADVANCED PROPULSION DEVELOPMENT



T.W. SHIDLER, MANAGER.  
ADVANCED TECHNOLOGIES

**GENERAL  ELECTRIC**

**SPACECRAFT DEPARTMENT**

*A Department of the Missile and Space Division*

**Valley Forge Space Technology Center**

**P. O. Box 8555 • Philadelphia, Penna. 19101**

# TABLE OF CONTENTS

Section		Page
1	INTRODUCTION . . . . .	1-1
	1.1 Report Organization . . . . .	1-1
	1.2 Functional Description of SPET . . . . .	1-2
	1.3 Advantages . . . . .	1-5
	1.4 Accomplishments . . . . .	1-6
	1.5 Objectives of the Study . . . . .	1-10
2	SUMMARY OF STUDY RESULTS . . . . .	2-1
3	STUDY RESULTS . . . . .	3-1
	3.1 Thermofluidynamic Considerations . . . . .	3-1
	3.1.1 Summary . . . . .	3-1
	3.1.2 General Discussion . . . . .	3-1
	3.1.3 Discussion of Sample Calculations . . . . .	3-3
	3.1.4 Conclusions. . . . .	3-4
	3.1.5 Recommendations. . . . .	3-12
	3.2 Gas Phase Kinetics . . . . .	3-13
	3.3 A Preliminary Analysis of the Phase Transition in the SPET. . . . .	3-26
	3.3.1 Statement of the Problem . . . . .	3-26
	3.3.2 Phase Transition . . . . .	3-26
	3.3.3 Propagation of Disturbance and Shock Formation . . . . .	3-30
	3.4 SPET Spacecraft Interface Studies . . . . .	3-32
	3.4.1 Applicability of SPET-Class Thrusters to Typical Spacecraft Missions . . . . .	3-34
	3.4.2 Reliability and Redundance Considerations . . . . .	3-53
	3.4.3 Command Interfaces . . . . .	3-53
	3.4.4 Telemetry and Instrumentation Consideration . . . . .	3-55
	3.4.5 Center of Mass Migration . . . . .	3-55
	3.4.6 Contamination of Spacecraft Surfaces . . . . .	3-56
	3.4.7 Vehicle Acceleration and Vibration Effects . . . . .	3-57
	3.4.8 Separation of Power Conditioning Circuitry from the Thruster . . . . .	3-57
	3.4.9 SPET Handling . . . . .	3-58
	3.4.10 SPET Testing . . . . .	3-58
	3.4.11 Attitude Control Considerations . . . . .	3-60
	3.4.12 EMI Tests of SPET . . . . .	3-62
	3.5 Engineering Design Considerations . . . . .	3-79
	3.5.1 Typical Firing Circuit . . . . .	3-79
	3.5.2 Power Profiles . . . . .	3-93
	3.6 Propellant and Feed Considerations . . . . .	3-100
	3.7 High Energy Propellant for SPET-D . . . . .	3-107
	3.7.1 SPET-D Fuel Concepts . . . . .	3-107

## TABLE OF CONTENTS (Cont.)

<u>Section</u>	<u>Page</u>
3.8 Physio-Chemical Considerations of SPET Propellants . . .	3-112
3.9 References . . . . .	3-116
Appendix A FLUID PHYSICS OF SPET IN THE DETONATION MODE	A-1
Appendix B EQUILIBRIUM COMPOSITION OF THE COMBUSTION PRODUCTS. . . . .	B-1
Appendix C VACUUM BALANCE IMPULSE MEASUREMENT . . . . .	C-1
Appendix D DEFINITION OF AVERAGE PARAMETERS OF PULSED PROPULSION DEVICES . . . . .	D-1
Appendix E A CHARACTERIZATION OF THE SPET-A . . . . .	E-1
Appendix F RESULTS OF SPET-D LABORATORY DEMONSTRATIONS . . .	F-1



# LIST OF ILLUSTRATIONS

<u>Figure</u>	<u>Title</u>	<u>Page</u>
1-1	SPET Configurations and Performance Ranges . . . . .	1-8
1-2	Functional Demonstration Unit SPET-A Thrusters . . . . .	1-11
1-3	SPET Units Undergoing Functional Performance Checks . . . . .	1-12
1-4	SPET System Firing . . . . .	1-13
1-5	Two-Dimensional SPET-D Thrusters . . . . .	1-14
3-1	Injection of Combustible Gas . . . . .	3-5
3-2	Mass Fraction of Combustible Gas . . . . .	3-6
3-3	Propagation of Shock Wave in SPET Chamber (Without Combustion) . . . . .	3-7
3-4	Propagation of Detonation Wave in SPET Chamber (Without Combustion) . . . . .	3-8
3-5	Temperature Distribution in SPET Chamber (Without Combustion) . . . . .	3-9
3-6	Temperature Distribution in SPET Chamber (With Combustion) . . . . .	3-10
3-7	Density Distribution in SPET Chamber (With and Without Combustion) . . . . .	3-11
3-8	Shock Hugoniot Curve (Stoichiometric $H_2-O_2$ System . . . . .	3-25
3-9	Optimized Propulsion System Weights $W_{ps}$ Per 1,000 Pound-Sec Optimum . . . . .	3-43
3-10	Optimizing Specific Impulses . . . . .	3-44
3-11	30° Slewing Time vs Moment of Inertia . . . . .	3-45
3-12	90° Slewing Time vs Moment of Inertia . . . . .	3-47
3-13	Initial Acquisition Time vs Moment of Inertia . . . . .	3-48
3-14	Redundant Thruster Switching . . . . .	3-54
3-15	Deadband Limits . . . . .	3-61
3-16	Representative Test Setup - SPET EMI Measurements . . . . .	3-70
3-17	Broadband and Pulsed CW Radiated Interference (Measured at One Foot) . . . . .	3-71
3-18	Broadband and Pulsed CW Radiated Interference Measured at Various One-Foot Antenna Positions (Configuration No. 1) . . . . .	3-72
3-19	Broadband and Pulsed CW Radiated Interference Measured at Various One-Foot Antenna Positions (Configuration No. 2) . . . . .	3-73
3-20	Broadband and Pulsed CW Radiated Interference Measured at Antenna Position 1 . . . . .	3-74
3-21	Broadband and Pulsed CW Conducted Interference (Current Probes) (2 Sheets) . . . . .	3-75
3-22	Typical Firing Circuit for SPET Engines . . . . .	3-79
3-23	SPET Power Supply Block Diagram . . . . .	3-82
3-24	SPET Power Supply Timing Diagram . . . . .	3-83

# LIST OF ILLUSTRATIONS (Cont'd)

Figure		Page
3-25	SPET Power Supply Schematic . . . . .	3-85
3-26	Resonant Charging Circuit . . . . .	3-88
3-27	Internal Trigger Firing Circuit . . . . .	3-92
3-28	SPET Power Supply Block Diagram with Internal Trigger Engine .	3-92
3-29	Characteristic Current Pulses . . . . .	3-94
A-1	Injection of Combustible Gas . . . . .	A-21
A-2	Mass Fraction of Combustion Gas . . . . .	A-22
A-3	Propagation of Shock Wave in SPET Chamber (Without Combustion) . . . . .	A-23
A-4	Propagation of Detonation Wave in SPET Chamber (With Combustion) . . . . .	A-24
A-5	Temperature Distribution in SPET Chamber (Without Combustion) . . . . .	A-25
A-6	Temperature Distribution in SPET Chamber (Without Combustion) . . . . .	A-26
A-7	Density Distribution in SPET Chamber (With and Without Combustion) . . . . .	A-27
A-8	Schematic Diagram of Expansion Process. . . . .	A-29
A-9	Freezing of the Temperature $T_{11}$ (Knudsen Number = 1,000) . .	A-35
C-1	Engine Impulse - Balance Fixture . . . . .	C-10
C-2	Displacement Due to a 10 mg Mass Dropping Through Known Distance. . . . .	C-12
C-3	Electrical Impulse - Balance Calibration . . . . .	C-14
C-4	Disk Force vs. Voltage . . . . .	C-16
C-5	Dynamic Calibration Electrical Impulse . . . . .	C-17
C-6	Pulse Generator Circuit . . . . .	C-19
C-7	Thruster Impulse Measurement . . . . .	C-20
E-1	Dimensions of Current Carrying Leads . . . . .	E-4

# LIST OF TABLES

<u>Table</u>		<u>Page</u>
1-1	Milli/Micro Pound Thrust Requirements for Future Spacecraft Missions . . . . .	1-9
3-1	Analysis of Plane Detonation Wave . . . . .	3-16
3-2	Detonability Limits . . . . .	3-17
3-3	Detonation Velocities of Mixtures at Room Temperature and Atmosphere Pressure . . . . .	3-18
3-4	Detonation Parameters as a Function of Initial Pressure . . . . .	3-19
3-5	Effect of Preheat on Chapman-Jouguet Detonation Parameters (Stoichiometric H <sub>2</sub> -O <sub>2</sub> Mixture) . . . . .	3-19
3-6	Effect of Temperatures and Pressure on Detonation Velocity for a Stoichiometric = H <sub>2</sub> -O <sub>2</sub> Systems . . . . .	3-20
3-7	Reaction Scheme for H <sub>2</sub> /O <sub>2</sub> System . . . . .	3-21
3-8	Kinetic Coefficients for H <sub>2</sub> /O <sub>2</sub> System . . . . .	3-22
3-9	Collisional Efficiencies of Dissociation - Recombination Reactions. . . . .	3-23
3-10	Kinetic Considerations in H <sub>2</sub> /O <sub>2</sub> System . . . . .	3-24
3-10A	Milli/Micro Pound Thrust Requirements for Future Spacecraft Missions . . . . .	3-33
3-11	Assumed Constants of Vehicles . . . . .	3-34
3-12	Optimum I <sub>sp</sub> for Micro/Milli Pound Thrusters . . . . .	3-38
3-13	Mariner "C <sup>n</sup> " Parameters . . . . .	3-51
3-14	Comparison of SPET vs Cold Gas . . . . .	3-52
3-15	SPET Power Supply Component Parts Lists . . . . .	3-87
3-16	Candidate Fuels . . . . .	3-114
C-1	Impulse Calibration Dropping Mass Method . . . . .	C-13
C-2	Impulse Response Calibration Data . . . . .	C-21
C-3	Thruster Impulse Data . . . . .	C-21
E-1	Typical Engine Characteristics . . . . .	E-2
F-1	I <sub>sp</sub> vs. Electrical Energy . . . . .	F-5

## ACKNOWLEDGEMENT

Acknowledgement is gratefully extended to Dr. A. V. LaRocca, the inventor and developer of the SPET concept, Drs. S. Scala, P. Gordon and B. Hamel of the Space Science Laboratory for fluiddynamic analyses, to W. Browne and Dr. P. S. Ku of the Re-entry System Department for reaction kinetics and phase transition studies. Also to P. Malherbe for SPET testing supervision and the majority of the engineering design considerations presented herein, Dr. A. Tweedie for propellant research and physio-chemical property characterization, Dr. J. Sivinski for testing the SPET-D prototype, and to R. Wanger and S. Millman for mission analyses and application studies.

## SECTION 1

### INTRODUCTION

#### 1.1 REPORT ORGANIZATION

This is the final report on results of our study of feasibility of the Solid Propellant Electric Thruster (SPET) operating in the detonation mode. In the interest of more comprehensive and meaningful subject treatment, we have included a great deal of information pertinent to the so-called SPET-A system, which operates in a different performance regime, was conceived and developed on Company funds, and is not a subject of this funded program. Notification of an impending patent grant for SPET-A has been received by General Electric Company.

References to SPET-A are especially prevalent in the report sections pertaining to systems application, where comparisons of SPET-A and SPET-D performance are made, and in the report section dealing with EMI test results which is based entirely on SPET-A. The company-sponsored efforts beyond contractual scope are principally discussed in Appendices A, C, D, E and F, and General Electric reserves the right to use this material at its discretion.

The remainder of this introductory section contains a functional description of both SPET-A and SPET-D, advantages of the SPET concept, a summary of accomplishments to date, a summary of the objectives of this funded program, and a reproduction of pertinent sections of the Work Statement.

Each paragraph of the Work Statement has been assigned a "finding key" which directs the reader to the section of this report wherein the appropriate work result description can be found.

Section 2 of this report is a summary of program results, keyed to appropriate work statement paragraphs. It is intended to provide a quick overview of the conclusions which have arisen from this program and was written for the reader limited in time. Section 3, the

body of this report, contains study results in more detail. Due to the rather complex analytical nature of this contract, some of the equation derivations and analytical details were felt to be inappropriate for inclusion in the body of this report, and they have been relegated to appendices. In some cases, the appropriate appendix is in itself a complete report on some aspect of the work, and in Section 3 will be found verbatim quotes from the appendix. There is thus some planned redundancy in the material.

Appendix A is a treatise on the fluid physics of the SPET, operating in the detonation mode.

Appendix B treats the equilibrium composition of typical SPET-D combustion products.

Appendix C is a description of the impulse measurement apparatus currently in use at General Electric for performance tests of SPET thrusters.

Appendix D contains three short descriptions of generalized performance terminology pertinent to characterization of pulsed thruster systems.

Appendix E is a description of some of the program history and current results of the SPET-A development program.

Appendix F is a description of the laboratory test results on SPET-D thruster.

## 1.2 FUNCTIONAL DESCRIPTION OF SPET

The Solid Propellant Electric Thruster (SPET) engine consists of a propellant, a propellant reservoir and feed arrangement, and a means for generating an electrical discharge across a surface of the propellant. The device can be considered as a form of pulse plasma accelerator with a unique method of propellant feed.

An electrical discharge occurring between appropriate electrodes causes the ablation of a self-replenishing film of propellant. A charged HV capacitor is utilized as the energy source. By changing the energy, the total number and the frequency of the discharges, the amount and physical characteristics of the gas resulting from propellant ablation can be varied. Thus, thrust and specific impulse can be varied.

Due to the fact that this scheme has characteristics analogous to those of a restartable solid propellant rocket, and that the propellant is kept in the firing chamber and, when needed, is used "in loco" with no actuation, the name "Solid Propellant Electrical Thruster" (SPET) is given to the device. This is done even though the propellant may be a solid-liquid dispersion, a liquid, or a viscous paste rather than completely in the solid state.\* The amount of electrical energy may be limited only to that required by the change of phase, the acceleration of the resulting charge being possibly left to other thermofluidynamic means. In other words, the device may be made to operate as an exploding film or wafer rocket. This operating mode of the thruster concept is referred to as SPET-D throughout this report. In this manner, it has achieved a regime of operation analogous to that of a low density supersonic burning hot gas rocket.

Successive electrothermal energy addition may be made to occur by having the electrical discharge reinforce the explosive shock. This gives a mode of operation analogous to that of a supersonic low density arc rocket, SPET-A.

In those applications requiring still higher specific impulses further acceleration processes of fluid-magneto-dynamic nature can be applied by means of Hall or Lorentz forces and thus operate as a pulse plasma device, another version of SPET-A.

When operating at a fixed power input, the value of specific impulse at which the unit operates is determined by appropriately adjusting the propellant feed rate and ablation to match the

---

\*Solid state fuels are not excluded by this reference

thrust requirement. An appropriate matching is thus required because of the thrust-specific impulse relation which depends on the mass and energy efficiencies of a given design point. It is appropriate to point out that the pulse plasma accelerator also has the specific advantage of being capable of delivering thrust at different levels by varying the number of pulses per second. This capability implies that different levels of power expenditure can be allotted for the propulsion systems over the duration of a mission.

Actually, one of the simplest modes of operation would be obtained at a constant specific impulse by changing the pulses per second directly, while operating at a constant voltage and with a given capacitance, provided the energy efficiency remains constant. This requires the increase of the propellant flow rates in the same ratio as the thrust, with the assumption that the propellant loading times are within a given percentage of the cycle time.

The fact that the flow rate requirements are directly proportional to the thrust, or for the above-described mode of operation, directly proportional to the firing rate (i.e., number of pulses per second), has suggested a propellant feed system based on surface phenomena.

The feeding of a propellant by means of natural physical processes represents a unique solution in-as-much as no mechanical actuation is involved, and it can be made dependent upon the pulse rate and the amount of energy discharge per firing. By capillary action and other surface phenomena, the exposed surface of the plug inside the thrust nozzle is maintained permanently coated with the propellant. The ions in the low vapor pressure carrier give a sufficiently low breakdown potential to establish a discharge along this surface. As a consequence, the propellant is exploded in amounts depending on the characteristic of the electrical discharge.

Surface adhesion and capillarity phenomena of the combination of a high surface tension carrier and porous plug minimize the evaporation of propellant between firings. By appropriate sizing of the porous plug surface, the plug porosity, the propellant physical characteristics, the number, geometry and location of the triggering electrodes, the amount of propellant for each firing can be maintained constant over a range of a given number of firings per second.



It is therefore possible to operate at constant specific impulse if each firing is made to deliver the same amount of energy.

This mode of operation, although not necessarily the most efficient, is one of the most convenient since it permits changing the average thrust levels simply by varying the firing rate with a constant voltage and given capacitance. This statement should not obscure the fact that the SPET engine possesses the capability of covering a wide range of specific impulses from as low as a few hundred seconds to as high as several thousand seconds. Because of this, optimized propulsion systems (i.e., properly matched) can be designed. Furthermore, the capability of a wide variation of thrust and/or specific impulse around a nominal or design value permits a further refinement in the optimization procedure such that matching over the entire thrust profile of the mission may be achieved.

Conversely, by judiciously selecting the design parameters, the SPET system can be made to operate in a region of rather flat performance characteristics close to the optimum. This permits a flexibility in design with little degradation of performance.

The schemes incorporated in the SPET design can provide higher mass and energy efficiency than is possible with conventional gaseous feed of propellant to pulse plasma accelerators. This is due to the fact that the propellant charge is generated at the appropriate location and times, thus avoiding loss of mass and poor energy coupling. The initial conductive sheet formation may be appropriately controlled to eliminate the early inset of fluid magneto dynamic instabilities, since this conductive sheet is generated from a uniform substrate of appropriate geometry.

### 1.3 ADVANTAGES

Some specific advantages of the SPET concept, in addition to greatly improved performance are:

- a. No mechanical moving parts
- b. Mass flows can be precisely delivered as follows:

1. At very low levels
  2. At levels variable over wide ranges
  3. With nearly unlimited start/restart capabilities
- 
- c. Problems associated with extremely small throat areas are by-passed.
  - d. Problems associated with valves capable of metering and/or sealing small flows are avoided.
  - e. The dust contamination problem in production and assembly is eliminated.
  - f. Extremely small bits of impulse can be delivered and may be selectively and precisely varied.
  - g. Control is greatly simplified; solid state variable frequency circuits with only digital command can be used.
  - h. The thruster is rugged and compact and promises greatly improved reliability and life time.
  - i. The thruster lends itself to natural growth to the high power levels. This is true because of the unique features represented by the efficient delivery of mass flows of ionized gases at the most favorable locations and times, thus insuring mass and energy efficiencies otherwise unobtainable.

Of particular significance is that the SPET system has proven the fact that high performance electrical thrusters are feasible for the level of power which are now available.

#### 1.4 ACCOMPLISHMENTS

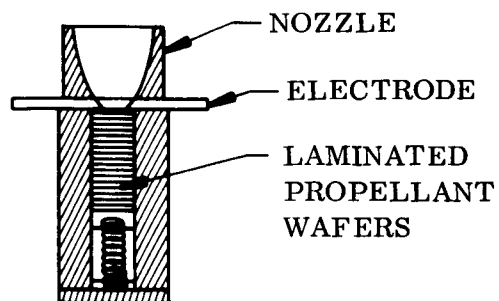
In the short time span of the SPET engine development, a number of significant accomplishments have been made:

- 4.6 million firings of a SPET-A thruster operating at one joule firing once per second.
- Successful development of a vacuum analytical balance technique for the measurement of micro-pound impulses.
- Thrust measured by direct reaction on pendulum and analytical balance.
- First solution of time dependent complete (one dimensional) Navier Stokes Equations, and first application thereof to the SPET-D phenomenon.
- High thrust/power 1 to  $3 \times 10^{-5}$  pound/watt demonstrated on SPET-A.
- $1 \times 10^{-4}$  to  $1 \times 10^{-6}$  pound thrust demonstrated feasible on SPET-A thruster at power levels of 5 to 0.5 watts.
- Specific impulse measured 800 to 4,500 seconds on SPET-A.
- Impulses of 1.1 to  $1.8 \times 10^{-4}$  pound second/pulse measured a single shot basis, at energy inputs of 0.02 and 1.1 joules, and Isp of 20 and 37 respectively (SPET-D).
- Power conditioning and logic developed and packaged.
- Feed system of five years fuel capacity - developed.
- Self triggering mode demonstrated.
- Supersonic arc-standing waves modes demonstrated (rails removed and comparable Isp achieved).
- Multistaging and series clustering demonstrated.

## SPET CONFIGURATIONS

## PERFORMANCE RANGE

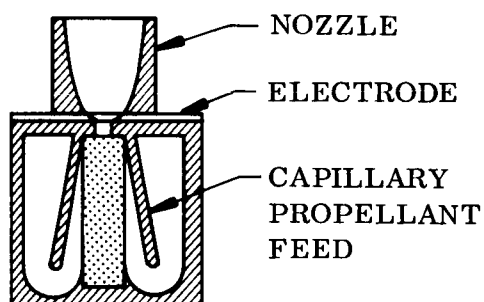
### I SPET "D" EXPLODING WAFER



SPECIFIC IMPULSE (SEC)	IMPULSE BIT (LB-SEC)	POWER INPUT (WATTS)
------------------------------	----------------------------	---------------------------

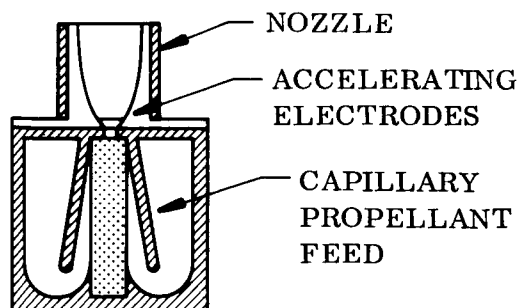
TO 200	$10^{-5} - 10^{-2}$	.01 - 10
--------	---------------------	----------

### II SPET "A" SUPERSONIC LOW DENSITY ARC



200-3000	$10^{-7} - 10^{-4}$	.5-20
----------	---------------------	-------

### III SPET "A" PULSE PLASMA ACCELERATOR



1000-5000	$10^{-8} - 10^{-5}$	.5-20
-----------	---------------------	-------

Figure 1-1. SPET Configurations and Performance Range

TABLE 1-1. MILLI/MICRO POUND THRUST REQUIREMENTS FOR FUTURE SPACECRAFT MISSIONS

	Continuous Thrusting (lb)				
	Vehicle Wt. 10 lb	Vehicle Wt. 100 lb	Vehicle Wt. 1000 lb	Vehicle Wt. 10,000 lb	Vehicle Wt. 100,000 lb
Required Operation	Decoys	GGTS Galactic Probe Adv. Pioneer	ATS-4 ATS 5,6 AM-FM Microwave Nimbus D	Voyager AM-FM P4 AAP	
E-W Stationkeeping	$5.2 \times 10^{-8}$	$5.2 \times 10^{-7}$	$5.2 \times 10^{-6}$	$5.2 \times 10^{-5}$	$5.2 \times 10^{-4}$
N-S Stationkeeping*	$9 \times 10^{-6}$	$9 \times 10^{-5}$	$9 \times 10^{-4}$	$9 \times 10^{-3}$	$9 \times 10^{-2}$
Orbit Adjust*	$1.4 \times 10^{-8}$	$1.4 \times 10^{-7}$	$1.4 \times 10^{-6}$	$1.4 \times 10^{-5}$	$1.4 \times 10^{-4}$
Drag Make-up	$10^{-5}$	$10^{-4}$	$10^{-3}$	$10^{-2}$	$10^{-1}$
110 NM/200 NM					
Attitude Maintenance	$2.3 \times 10^{-11}$	$2.7 \times 10^{-9}$	$1.4 \times 10^{-6}$	$5.9 \times 10^{-4}$	$2.7 \times 10^{-2}$
Attitude Changes	$1.3 \times 10^{-6}$	$2 \times 10^{-5}$	$2.8 \times 10^{-4}$	$4.4 \times 10^{-3}$	$6.5 \times 10^{-2}$
Spin Axis Precession*	$1.7 \times 10^{-8}$	$2.6 \times 10^{-5}$	$3.6 \times 10^{-6}$	$5.7 \times 10^{-5}$	$8.4 \times 10^{-4}$
Inversion Maneuver	$9.3 \times 10^{-7}$	$1.4 \times 10^{-5}$	$1.9 \times 10^{-4}$	$3.1 \times 10^{-3}$	$4.5 \times 10^{-2}$
Station Changes	$7 \times 10^{-7}$	$7 \times 10^{-6}$	$7 \times 10^{-5}$	$7 \times 10^{-4}$	$7 \times 10^{-3}$
Midcourse Correction	$0.3$	$3.0$	$30$	$300$	$3000$

# NOTES

\*Not Continuous, 16.7% "ON" Duty Cycle

SPET-A Applicable to items enclosed by .....

SPET-D Applicable to items shaded by 

To graphically indicate the wide range of applicability of the SPET family of thrusters, Table 1-1 shows thrust required for typical spacecraft operations as a function of vehicle weight. Note that SPET is eminently suitable for an extremely wide spectrum of operations. This chart is discussed in more detail in Section 3 of this report. SPET configurations and performance range are shown in Figure 1-1.

The following photographs depict the SPET-A thruster concept. While SPET-A is not the primary subject of this program, it is considered similar enough in configuration to SPET-D (yet to be built in any but a crude laboratory configuration) to make these photographs useful in visualizing the concept.

Figure 1-2 shows a family of laboratory functional demonstration unit SPET-A thrusters. Figure 1-3 shows two self-contained SPET units undergoing functional performance checks in vacuum. Figure 1-4 is an unretouched photograph of a SPET system being fired. The plume is evident upon examination of the orifice area.

Figure 1-5 illustrates the crude laboratory models of a "two-dimensional" SPET-D thruster. The units shown have been successfully fired in vacuum, and pertinent performance data is given in this report.

## 1.5 OBJECTIVES OF THE STUDY

The general objectives of this study were to:

- a. Assess analytically the feasibility of the SPET-D systems.
- b. Investigate the interface of SPET with typical spacecraft.
- c. Provide engineering data on certain SPET subsystems.

The following is a reproduction of the Work Statement with references to the sections of this report wherein the pertinent study results will be found.

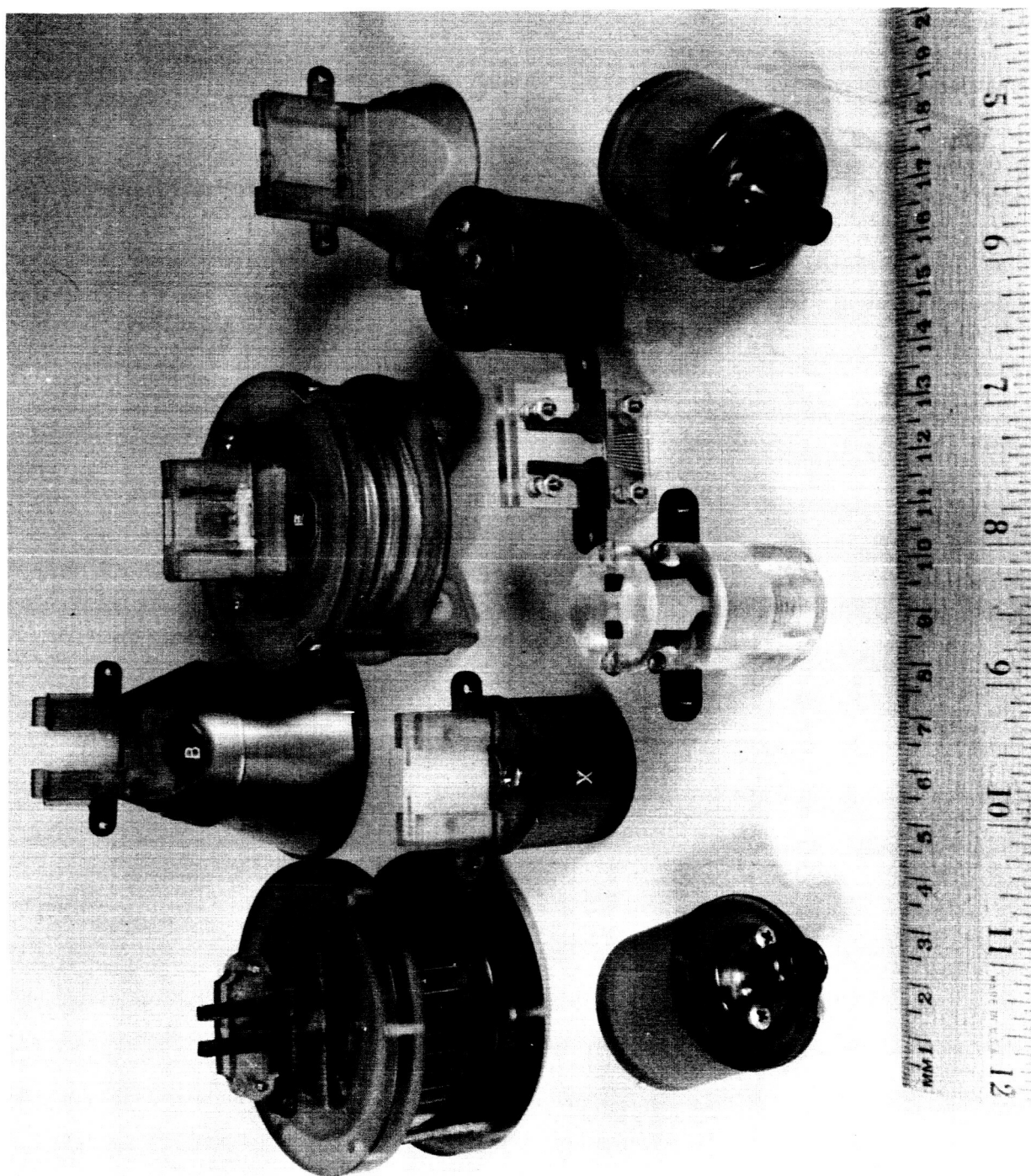


Figure 1-2. Functional Demonstration Unit SPET-A Thrusters

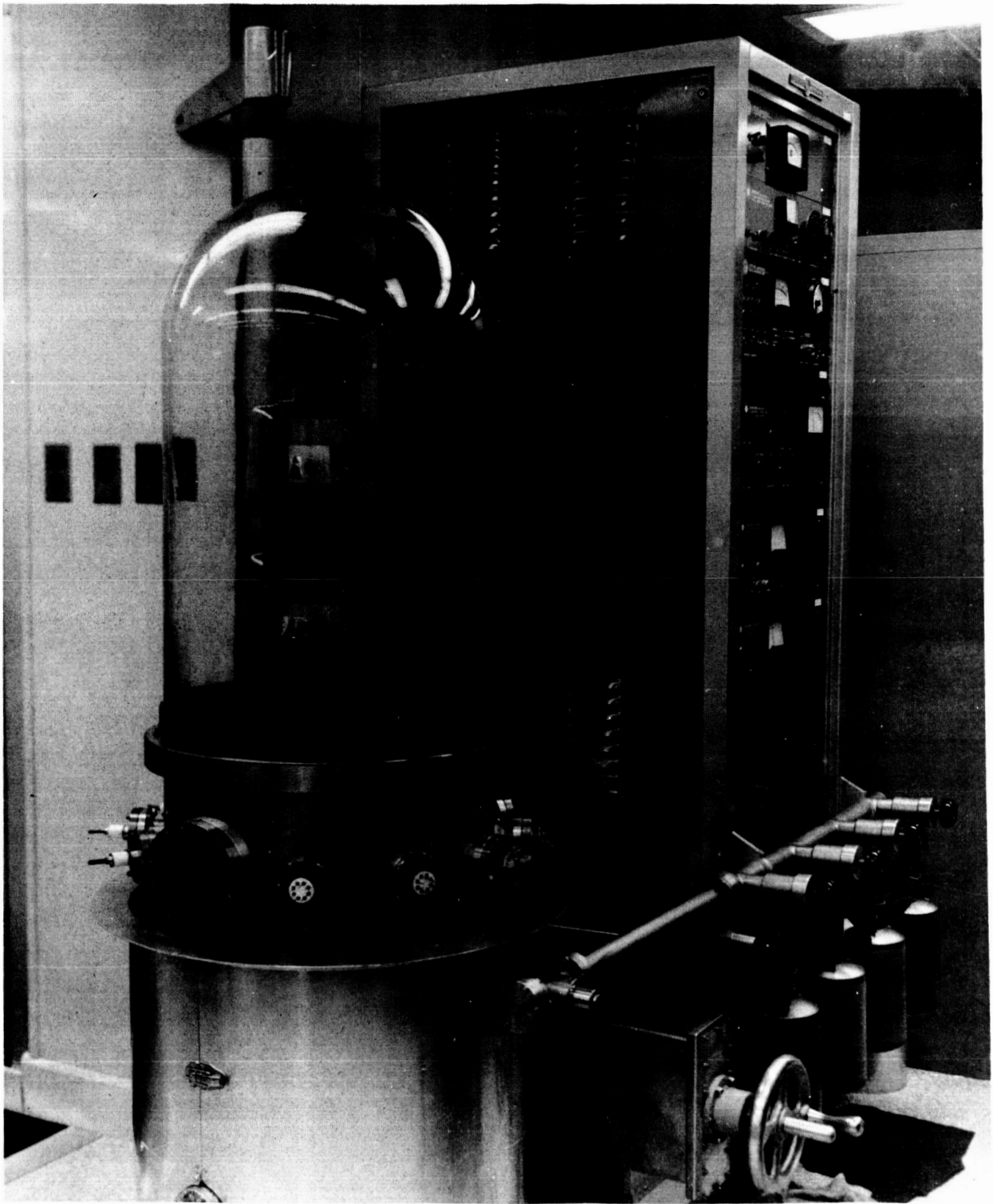


Figure 1-3. SPET Units Undergoing Functional Performance Checks



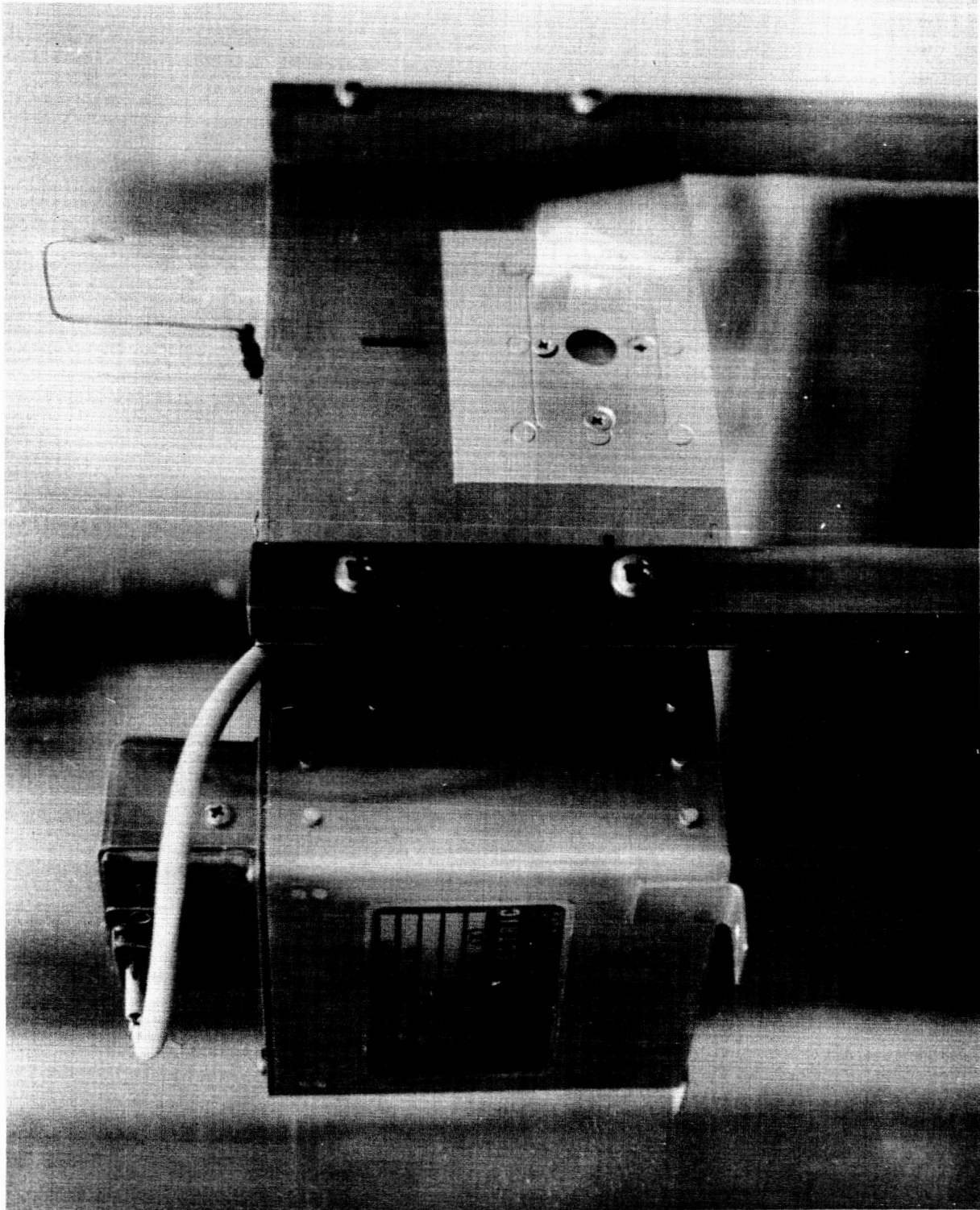


Figure 1-4. SPET System Firing

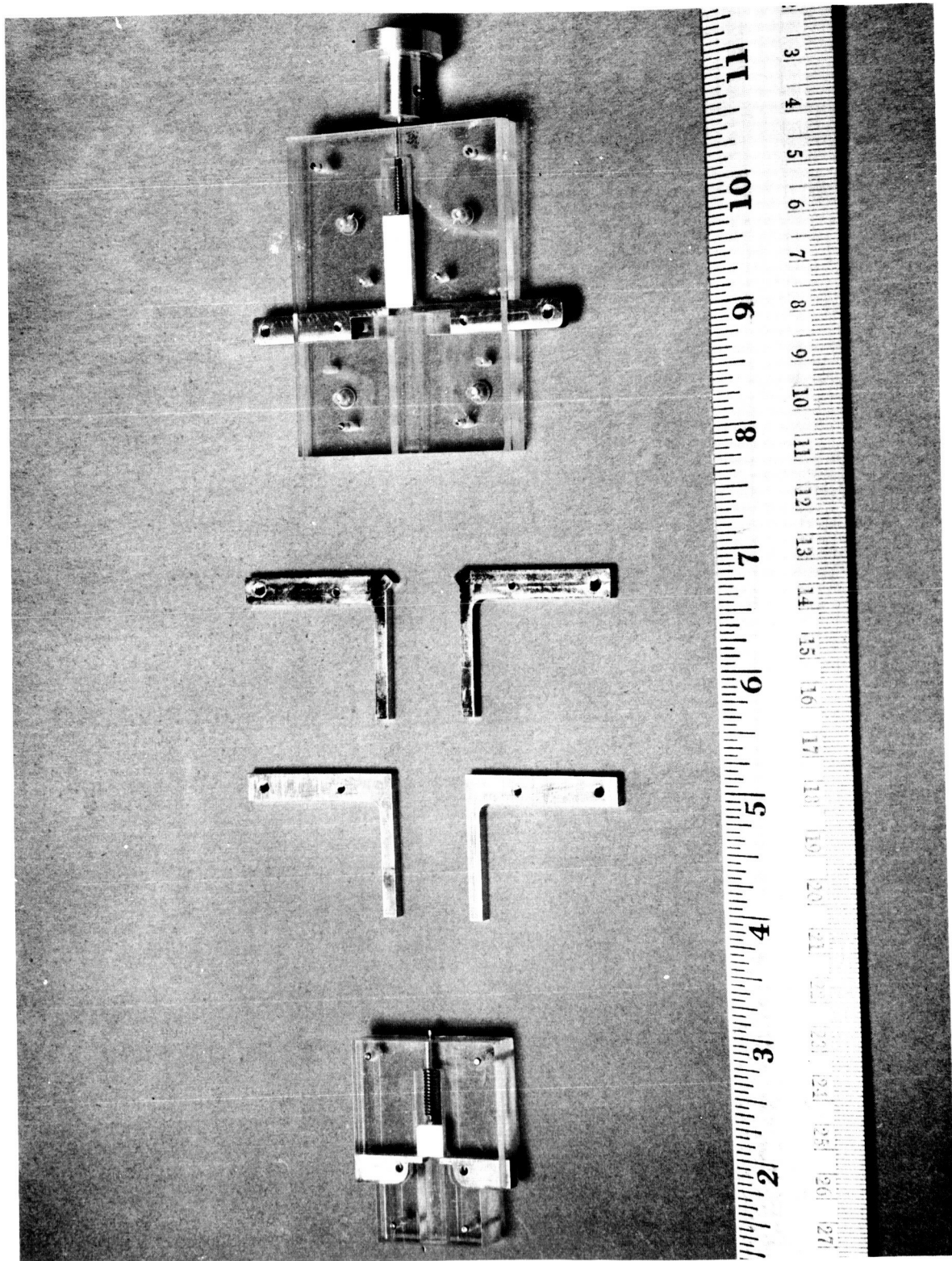


Figure 1-5. Two-Dimensional SPET-D Thrusters

## ARTICLE 1. STATEMENT OF WORK

- (a) The Contractor shall furnish not less than thirteen hundred thirty (1330) man-hours of direct engineering labor (including not more than three hundred thirty (330) man-hours of technicians' labor) directed toward the timely completion of the following Tasks, viz:

- (1) Task I shall be an analytical assessment of the feasibility of producing a "Solid Propellant Electrical Thruster (SPET)" system with a specific impulse characteristic of the order of five hundred (500) to eight hundred (800) seconds and capable of delivering a 0.01 pound thrust. Such analytic studies shall include, but shall not necessarily be limited to:

- (i) Thermofluidynamic analyses of:

Section 3.1

and

Appendix A

- (A) The exothermic chemical reactions involving the ablation of selected materials by electrical discharge and the resultant formation, acceleration, and propagation of impulsive waves.
- (B) The flow evolution process relations between the chamber configuration and the conversion of the electrothermal energies into the kinetic energies of the reaction products.
- (C) The available criteria for the selection of suitable ablative materials for the selection of optimal input combinations of electrical and chemical energies and for the choice of chamber configurations and electrode geometries.

- (ii) Physiochemical and thermochemical analyses of several typical ablative materials considered suitable for use as detonating propellants in the "SPET" system after due consideration of the following preliminary criteria:

Sections 3.6

3.7

3.8

and

Appendix B

- (A) Fluidity in the storage condition.
- (B) Adequate surface tension and wetting properties in the storage condition.
- (C) Low vapor pressure in the storage condition.
- (D) High density in the storage condition.
- (E) Low heat required for the change of phase.
- (F) Low electrical breakdown potential.
- (G) Low molecular weight (high heat capacity) in the gaseous state.

- Sections 3.6 { (H) Absence of stable solid phases (i.e. easily and fully gasifiable).
- 3.7 {
- 3.8 { (I) High exothermic energy content in the decomposition and/or reaction processes.
- and {
- Appendix B { (J) Low flash-back tendency.
- { (K) Low and similar ionization potentials for the gaseous phases.
- Sections 3.2 { (iii) Phase and reaction kinetics analyses of the more suitable ablative
- 3.3 { materials directed toward the determination of reaction rate coefficients
- { and the correlation of these findings with the optimal thermofluidynamic
- { characteristics of the desired "SPET" system.
- (2) { Task II shall be a preliminary investigation of interface problems which might
- { arise between the "SPET" and other spacecraft subsystems, including:
- Section 3.4 { (i) The identification of interface considerations requiring further analysis.
- { (ii) The determination and modification of any radio frequency interferences
- { caused by the electrical discharges within and/or the expulsion of
- { plasmoids from the "SPET".
- (3) Task III shall be the preparation of a Final Report which shall include:
- (i) An exposition of the feasibility assessment problem undertaken pursuant
- to this Contract.
- (ii) The Contractor's recommendations relative to further work toward the
- stated objective.
- (iii) The following specific technical items:
- Section 3.5 { (A) Block diagram of thrusting system.
- { (B) Power profile at input of power supply and at electrode of motor.
- { (C) Typical firing circuitry for motor.
- { (D) Discussion of materials of construction that might be used for
- { flight hardware.
- { (E) Design discussion of propellants and fuel feed system.
- { (F) Problems associated with separating energy storage from thrust device.
- { (G) Problems of all interferences with other circuits.

## SECTION 2

### SUMMARY OF STUDY RESULTS

An analysis of the feasibility of SPET-D operation has indicated that a low density detonation can be initiated and sustained in a constrained range of temperatures and pressures. This confirms the validity of the concept. (Refer to Work Statement Section 1.) (1)

#### NOTE

While not required by the Work Statement, it is important to note that a laboratory demonstration of SPET-D has been successfully accomplished. Magnification of the delivered impulse up to two orders of magnitude were repetitively measured on single pulse firings of metallic films coated with detonating mixtures. (Refer to Appendix F for details.)

The identification and characterization of the interfaces arising between SPET and a typical spacecraft has been completed. It can be concluded that SPET presents no unique problems in the interface area; moreover, the generic simplicity of the SPET concept generally simplifies the usual interfaces which must be met between a spacecraft and a typical alternative low thrust system, such as cold gas. (Refer to Work Statement Section 1.) (2) (i)

A SPET-A system which was available, but did not utilize optimum EMI suppression techniques, was EMI tested in accordance with standard practices. It was determined that most of the generated noise is attributable to the electronics themselves, as opposed to plasma formation and propagation. Thus the SPET is capable of being brought within acceptable EMI spec limits by conventional suppression techniques. (Refer to Work Statement Section 1.) (2) (ii)

Engineering data pertinent to hardware details of the SPET system have been generated and documented in this report. (Refer to Work Statement Section 1.) (3)

## SECTION 3

### STUDY RESULTS

#### 3.1 THERMOFLUIDYNAMIC CONSIDERATIONS

This material is principally in response to Work Statement Section 1. (1) (i)

##### 3.1.1 SUMMARY

In this first theoretical study of the fluid physics of the SPET engine, the techniques of continuum mechanics and kinetic theory are employed to derive fundamental equations which govern the flow of the gaseous reactants within the combustion chamber, and the expansion of the products of combustion into vacuum.

The methods developed by Scala and Gordon for solving the complete time-dependent Navier-Stokes equations are extended herein to include the specific effects of molecular diffusion and non-equilibrium combustion. In this investigation, an exhaustive study of all the possible physical and chemical parameters has not been carried out. Rather, the governing relationships have been derived and a digital computer program has been developed. Furthermore, sample calculations have been obtained for both finite reaction rate kinetics and negligible reaction rates.

The subsequent expansion of this plasma into vacuum is analyzed utilizing the methods of kinetic theory, based on the theoretical techniques developed by Hamel and Willis.

##### 3.1.2 GENERAL DISCUSSION

From the point of view of satellite attitude control and station keeping requirements, it appears to be desirable to develop a long-lived microthruster which combines the use of a chemically active solid propellant with a pulsed electric discharge.

It is envisaged that the electric discharge will cause the propellant to be vaporized into a combustion chamber. If the propellant gas is injected into the chamber sufficiently rapidly, it will form a shock wave and will be ignited by compression heating, if the activation energy is sufficiently low. Once ignition occurs, the gas will proceed to undergo complete combustion if the chemical kinetics are sufficiently rapid. This concept will be investigated herein.

In analyzing theoretically the basic fluid dynamic and physiochemical phenomena associated with the SPET, one should perform an overall analysis which is comprised of certain key aspects. These include the study of the gas generation and combustion processes and the expansion of the resulting plasma into the ambient vacuum. Specifically, it is necessary to perform an:

- a. Analysis of the Vaporization Process.
- b. Estimate of the species formed and their thermodynamic properties.
- c. Analysis of the time history of the development and structure of the very low density shock wave and its propagation down the chamber duct.
- d. Analysis of the chemical kinetics of the chemical reaction and the development of the detonation wave and its propagation down the chamber duct.
- e. Analysis of the employment of a centerbody in order to increase the gas residence time, if this appears necessary.
- f. Analysis of the expansion of the combustion products into vacuum.

Of all these interrelated studies the one requiring the greatest effort is item d. since it requires the solution of a system of non-linear partial differential equations for the dependent variables, in which both time and space are the independent variables.

Fortunately, the general equations for continuum fluid mechanics, the Navier-Stokes equations, have recently been solved for the time-dependent one-dimensional flow of a compressible, viscous, thermally conducting gas (Reference 1). In considering the extension of the above approach to the analysis of the formation and propagation of a detonation wave within the SPET engine, it is clear that one must introduce additional terms and/or equations to account for the presence of more than one chemical species, to include the presence of molecular diffusion and to incorporate the effects of the chemical kinetics of the combustion process in converting chemical energy into internal and kinetic energy.

### 3.1.3 DISCUSSION OF SAMPLE CALCULATIONS

The equations and coefficients<sup>(1)</sup> derived have been programmed in Fortran IV for computation on a digital computer, and two sample calculations were carried out, with and without combustion. The numerical results are shown in Figures 3-1 to 3-7.

Figure 3-1 shows the injection rate parameters  $\rho_w$  and  $v_w$  as a function of time. Note that at time zero, the gas velocity in the chamber is everywhere zero and the chamber density has been taken equal to a constant of  $6.91 \times 10^{-6}$  pound/ft.<sup>3</sup>.

Figure 3-2 depicts the variation of the mass fraction of combustible gas with distance and time. It is seen that due to diffusion and convection the injected gas, which is in largest concentration near the wall, decreases in concentration with distance from the wall. Furthermore, when combustion occurs, the mass fraction of combustible, drops very rapidly as chemical energy is converted into kinetic energy (compare Figures 3-3 and 3-4) and internal energy (compare Figures 3-5 and 3-6). The associated density wave appears in Figure 3-7.

It is clear then, that the rapid injection of a higher density gas into a very low density gas does indeed produce a shock wave. If the reaction kinetics are very slow, the shock wave simply propagates toward the exhaust end. If, on the other hand, the global chemical reaction is rapid, the shock wave becomes a detonation wave and the gas temperature rises

---

(1) See Appendix A



considerably, since the chemical energy is unlocked.

The results presented here should be considered as preliminary, and are representative of the phenomena which occur in the SPET engine in a qualitative way. As the next phase of the investigation it will be necessary to use the new computer program to perform a series of parametric studies to determine the effect of systematically varying the physiochemical parameters and the initial conditions in the SPET chamber. This will help the designer to relate performance to propellant properties and chamber geometry and will help in the interpretation of experimental data.

#### 3.1.4 CONCLUSIONS

During the past five months in which this theoretical investigation was carried out, significant headway has been made in the development of a comprehensive model for the physiochemical processes which occur in the SPET. Analytical models, and numerical techniques have been extended successfully and a new digital computer program for the solution of the complete time-dependent Navier-Stokes equations, including the simultaneous effects of compressibility, viscosity, thermal conduction, molecular diffusion, and combustion has been developed.

In the future, this computer program should be utilized to carry out a comprehensive parametric study to determine the relationship between the physiochemical properties of the propellant and the SPET engine geometry. Once this has been done, the information generated can be factored into the design of advanced SPET devices. It is noted that the theoretical model can be improved by employing more realistic plasma properties and by introducing additional diffusion equations to permit the inclusion of other important chemical species, such as intermediate chain-carrying products of combustion.

Other extensions and refinements in the theory, such as the inclusion of radiation fields and magnetic fields can be accomplished at a still later date when it is planned to consider the presence of these effects in more advanced SPET configurations.

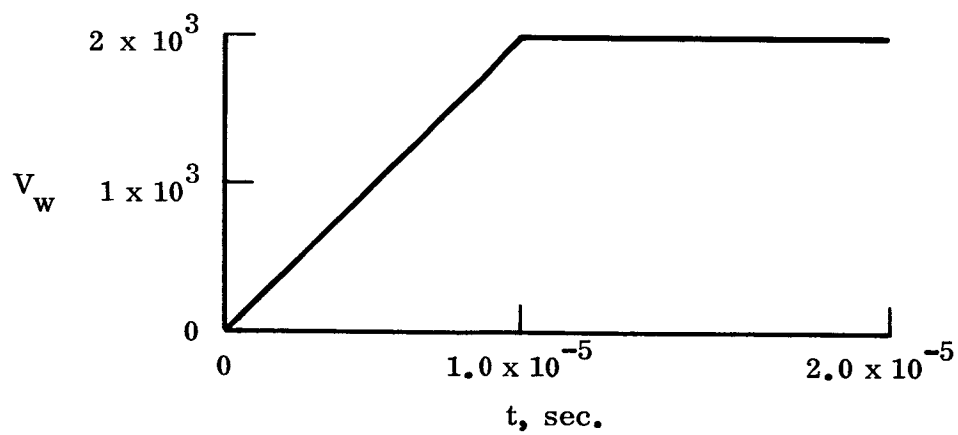
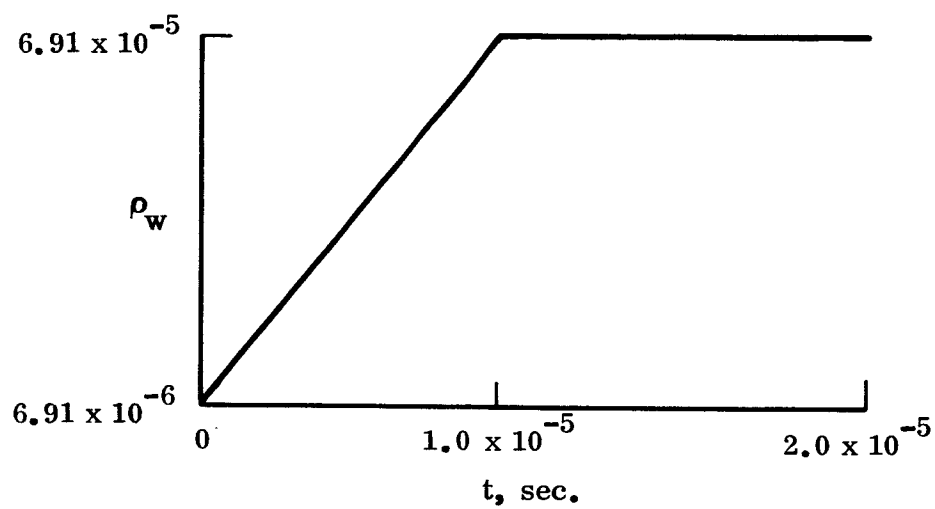


Figure 3-1. Injection of Combustible Gas

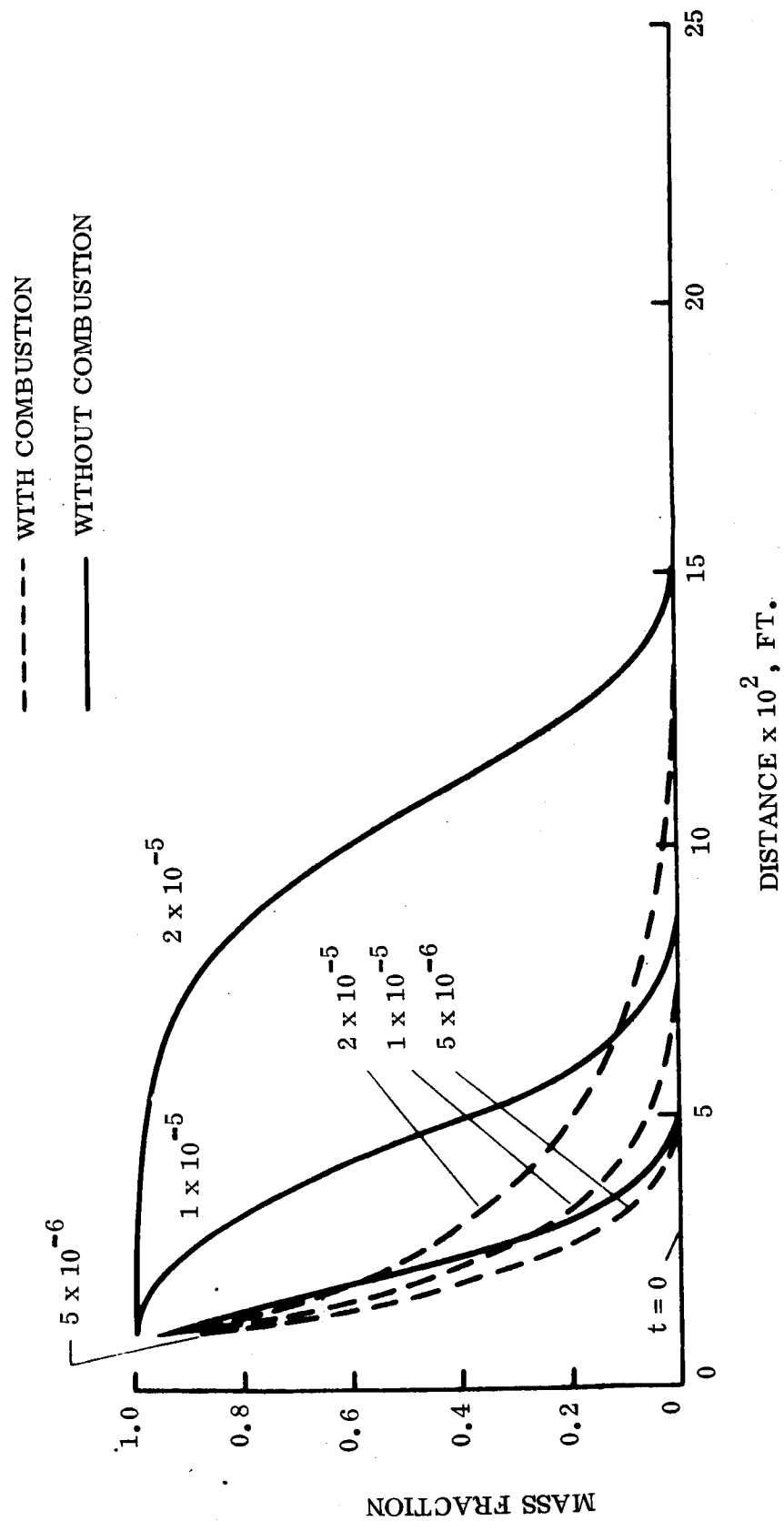


Figure 3-2. Mass Fraction of Combustible Gas

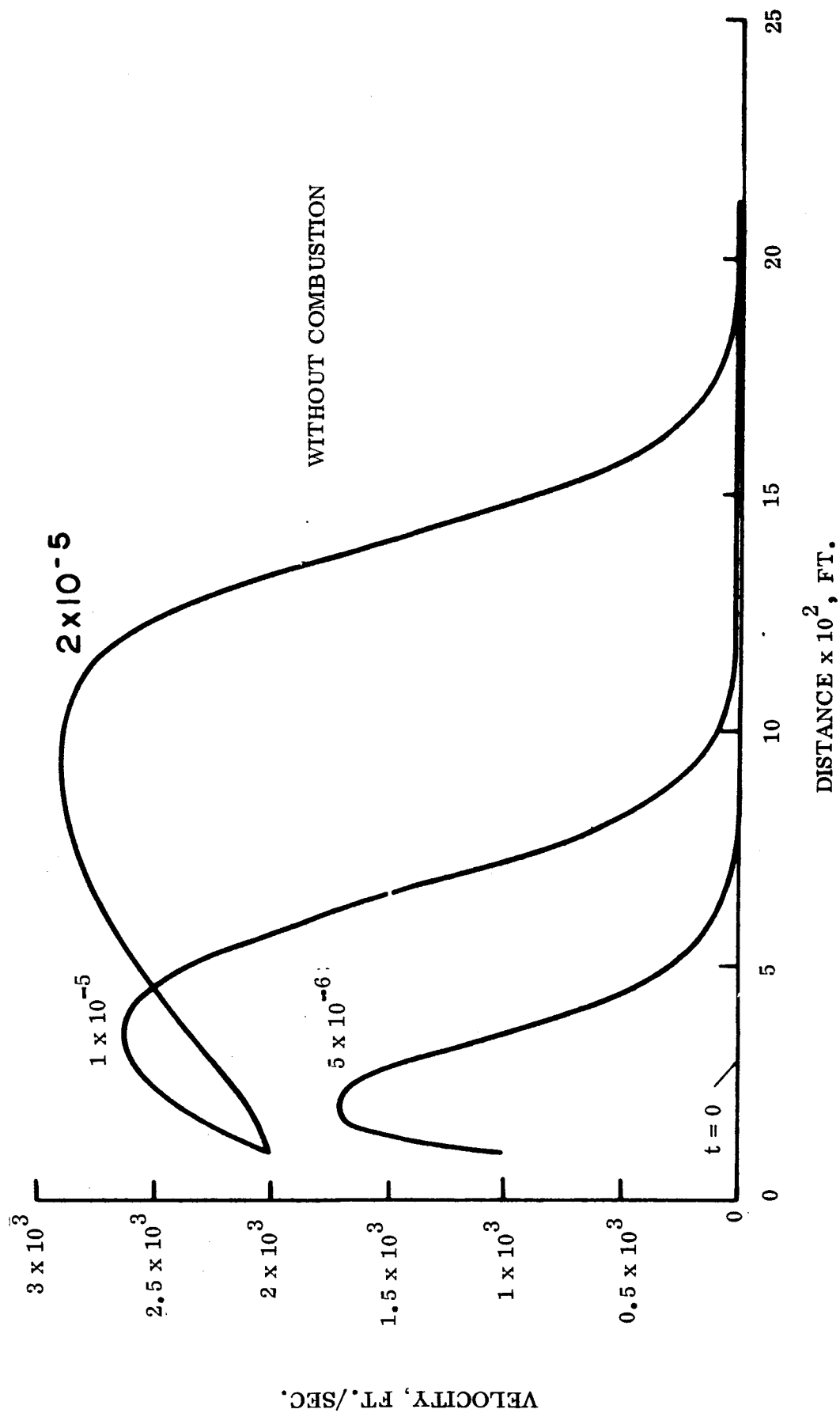


Figure 3-3. Propagation of Shock Wave in SPET Chamber (Without Combustion)

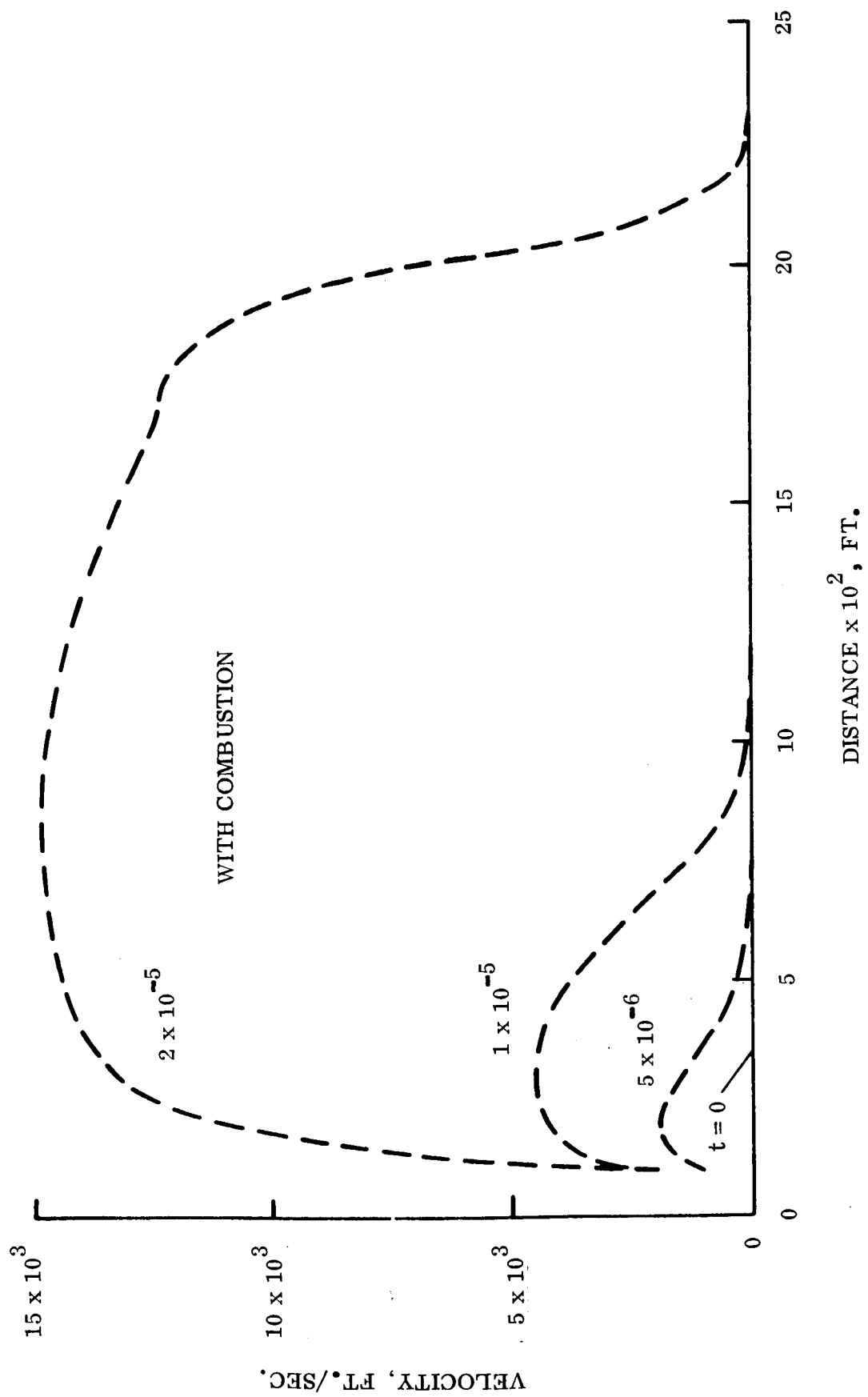


Figure 3-4. Propagation of Detonation Wave in SPET Chamber (With Combustion)

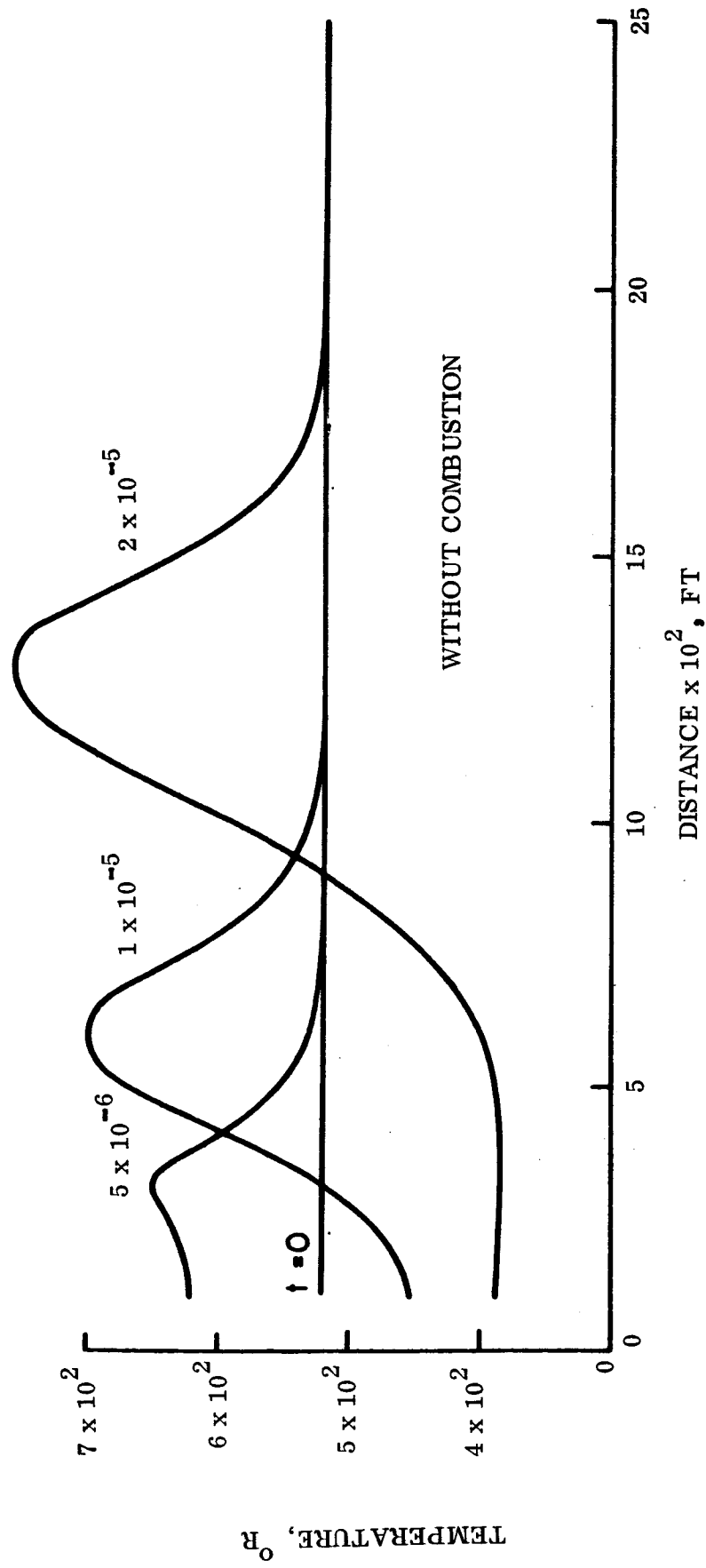


Figure 3-5. Temperature Distribution in SPET Chamber (Without Combustion)

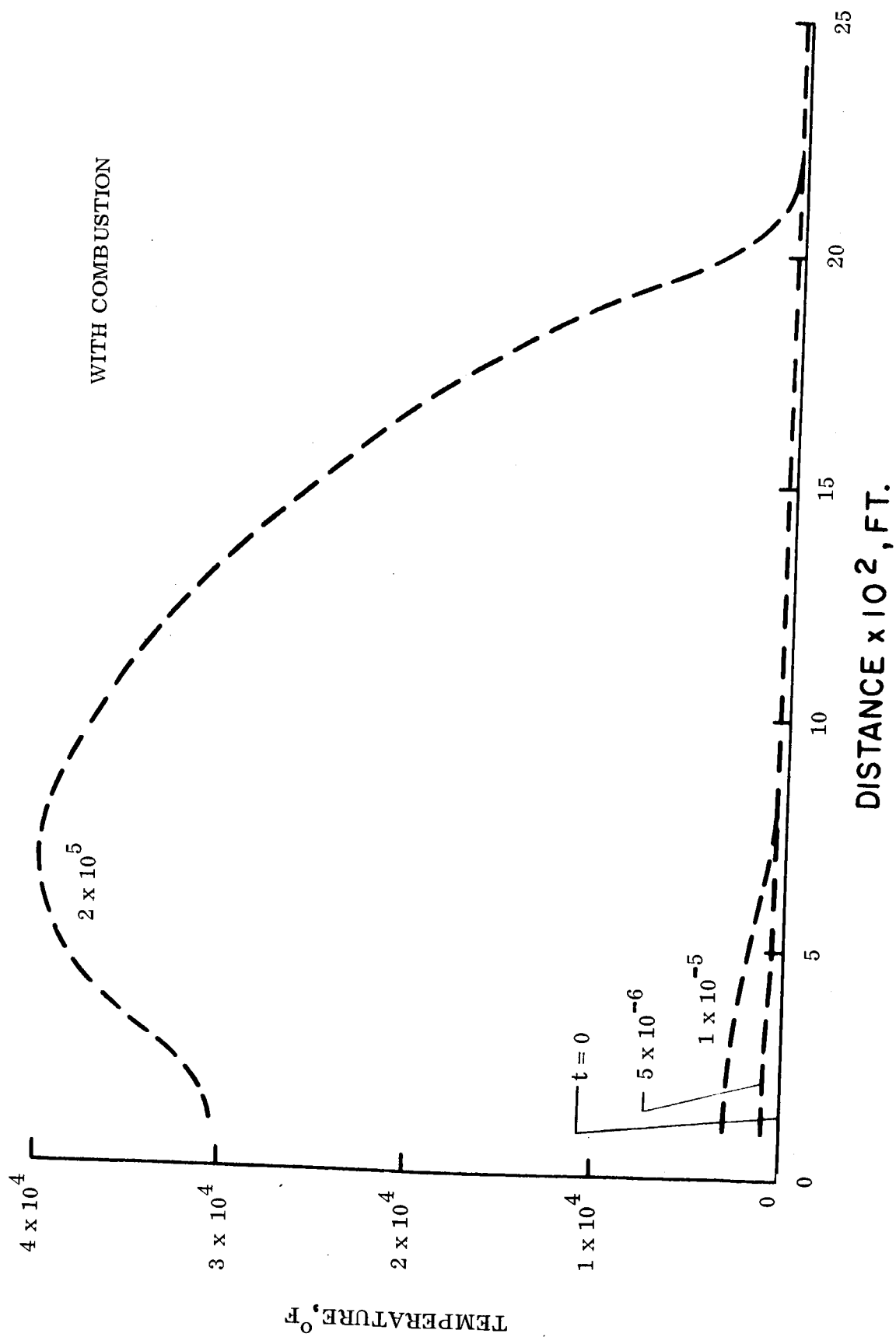


Figure 3-6. Temperature Distribution in SPET Chamber (With Combustion)

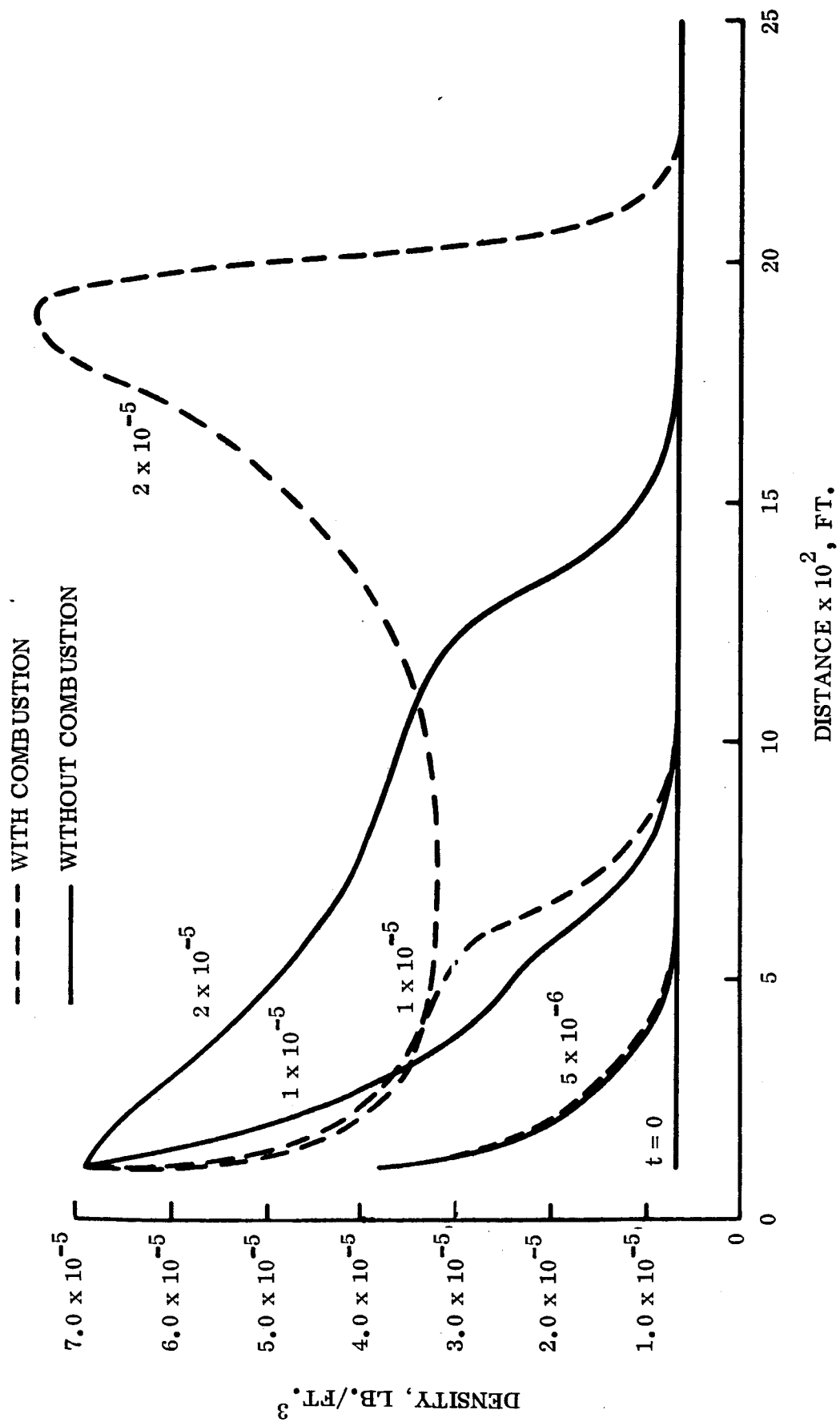


Figure 3-7. Density Distribution in SPET Chamber (With and Without Combustion)



### 3.1.5 RECOMMENDATIONS

The specific recommendations or proposed future theoretical work on the SPET engine are as follows:

- a. Utilizing the newly developed digital computer program, perform a parametric study in which the initial conditions and the physiochemical properties are varied systematically, so that the relationship between propellant properties and plasma at the chamber exit are determined as a function of SPET operating conditions.
- b. Develop a digital computer program for the time-dependent vaporization of the solid propellant so that the initial conditions at the injection end of the chamber can be determined systematically for a number of propellants of interest which are subjected to a range of electrical discharges of the order of 5 to 25 joules. This will provide realistic initial conditions for Paragraph a. above.
- c. Extend the theoretical model for the detonation wave analysis to include the diffusion and chemical reaction of additional chemical species, so that more realistic chemical kinetics can be utilized rather than the simple global reaction utilized herein.
- d. Perform an analysis of the heat losses due to conduction and radiation from the flowing plasma to the SPET chamber side walls, and if significant, incorporate these back into the model for the propagation of the detonation wave. Note that since a one-dimensional treatment was employed here, heat conduction is included at present, but only for the axial direction, and not for the radial direction.
- e. Replace the present one-dimensional representation by an axially-symmetric (two-dimensional) representation, to allow for longitudinal variations in cross sectional area.

- f. Incorporate the Maxwell field equations into the overall system of equations, so that the presence of magnetic fields can be included in further accelerating the flow if desired.
- g. Apply the theoretical model presented here for the analysis of the expansion into vacuum to the specific combustion products which form in the SPET engine.

### 3.2 GAS PHASE KINETICS

This material is principally in response to Work Statement Section 1. (1) (ii)

In evaluating the performance characteristics of the SPET engine in the detonative mode, it is advantageous to separate the overall detonation phenomenon into several component processes. The overall phenomenon comprises the electrical pulse heating of a low vapor pressure liquid or solid whose vaporization products subsequently detonate thereby yielding impulse for propulsion purposes. The individual processes of interest include phase transition, wave formation, and reactions of the vaporization products. It is this last topic which is treated here in detail.

Theories of the structure of a detonation wave represent the supersonic wave as a shock front followed by a reaction zone where the exothermic heat release drives the shock front. The steady-state plane detonation velocity can be satisfactorily predicted by solving the conservation equations for mass, momentum, and energy along with the equation of state-of-the-mixture (Table 3-1). The gases behind the wave front attain equilibrium at the Chapman-Jouguet point where the particle velocity is equal to the local sound speed. It is of prime interest to know whether the gas phase reactions are sufficiently rapid so that detonation is sustained at the low pressures of interest (in order to limit heat transfer) for the SPET engine.

Our current knowledge of combustion chemistry is somewhat incomplete at the present time except for the simplest of fuels, namely, hydrogen. It appears advisable therefore

to restrict our kinetic investigation to the gaseous hydrogen-oxygen system. This choice is appropriate for the additional reasons that hydrogen is a natural degradation product of any candidate propellants which contain hydro-carbons or hydrazine. Also, the kinetics of the  $H_2/O_2$  system are known to be very rapid as is evidenced by its wide detonability limits (Table 3-2) and the fact that it detonates readily with a characteristically high detonation velocity (Table 3-3).

It is of utility in a kinetic analysis of this type to know the equilibrium state which the kinetics attain at infinite time. A series of Chapman-Jouguet gaseous detonation wave calculations have been carried out for a  $2H_2 + O_2$  mixture. The equations for conservation of mass, momentum, and energy in conjunction with the equation of state and the C-J constraint (Table 3-4) have been solved simultaneously. The computation of the equilibrium composition and thermodynamic properties of the detonation products has been performed by a computer analysis which is described in detail in Appendix B. The insensitivity of the detonation velocity to wide variance in the initial temperature and pressure is demonstrated in Table 3-5 which lists the pressure and density ratios across the detonation wave as a function of initial pressure. At atmospheric pressure  $p_2/p_1 = 18$ ; at reduced pressure  $p_2/p_1 \cong 3$ . It is inferred from these results that the structure of a detonation wave may be treated as a shock front followed by a reaction zone only at high pressures. At reduced pressures the two processes are merged.

Figure 3-8 is the Hugoniot curve for a  $2H_2 + O_2$  mixture for various values of  $Q$ , the electrical energy supplied to the initial gas. The Hugoniot curve, computed from a combination of the conservation equations, shows the characteristic detonation and deflagration branches corresponding to supersonic and subsonic wave formation respectively. A line drawn from the initial conditions to the detonation branch of the curve is tangent to the Hugoniot at the C-J point. In Table 3-6 are listed the temperatures and pressures associated with these C-J detonations for various  $Q$  values.

A series of non-equilibrium computations have been performed which examine the time-dependent behavior of  $H_2/O_2$  mixtures at elevated temperatures and reduced pressures.

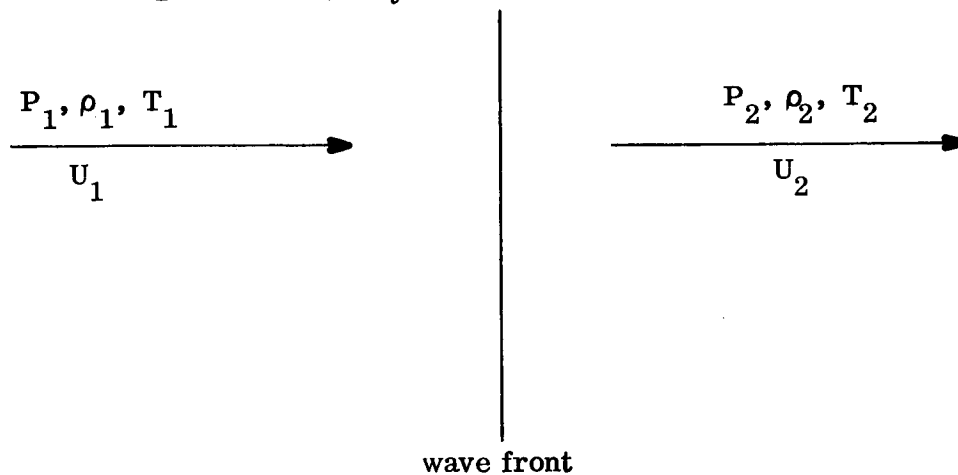
The  $H_2/O_2$  reaction scheme utilized is shown in Table 3-7. This scheme adequately represents the kinetics of the hydrogen-oxygen system over the temperature range  $1,000^\circ$  to  $3,000^\circ$  K. The associated set of kinetic coefficients is shown in Table 3-8. These coefficients are derived from shock tube, flame and discharge flow experiments (Reference 2). The efficiencies of the various collision partners M in the dissociation-recombination reactions cited in Table 3-8 are listed in Table 3-9 where the efficiency of argon is taken to be one.

The species conservation equations have been integrated as a function of flow time for one dimensional inviscid flow behind mach 4 normal shock waves in stoichiometric hydrogen-oxygen mixtures. These equations comprise a set of ordinary first order non-linear differential equations which have been integrated using the Adams-Moulton-Shell integration equations as a function of time. The results of these representative computations are shown in Table 3-10. A range of initial pressures and temperatures have been investigated where the role of electrical pulse heating is restricted solely to preheating the gases from  $300^\circ$  to  $1,300^\circ$  K without reaction. Behind the step function the pressure jump is approximately 19 and the shocked gas temperature at zero time varies from  $1167^\circ$  to  $4321^\circ$  K. For the first shock calculation no significant amount of reaction occurs after 100 microseconds as witnessed by the fact that the composition is unchanged. In the second computation after 220 microseconds, some reaction has occurred at 1.9 mm Hg and a bath temperature of  $\sim 2500^\circ$  K. In the last calculation the reaction temperature falls from  $4321^\circ$  to  $3273^\circ$  K after 70 microseconds as a consequence of extensive dissociation. In no case cited here has the post shock gases attained equilibrium within the specified times. These results introduce doubt as to whether a gas phase detonation can be sustained at these low pressures, even with the aid of considerable heating of the preshocked gases.

On the other hand, the preceding development considers the process of electron heating of the propellants  $H_2$  and  $O_2$  as a simple heating of these gases in the absence of reaction. For the SPET application the electrical pulse heating of a liquid or solid propellant is anticipated. In the process of breaking bonds in the condensed phase vapor may be generated which is partially reacted and ionized. If this occurs, the results of the gas phase kinetic analysis presented previously may have to be modified. One difficulty associated with the electrical

pulse heating of a solid or liquid is that this process is not readily amenable to quantitative analysis at this time. Reliance on experiments is mandatory in order to characterize the performance of the individual propellants.

Table 3-1. Analysis of Plane Detonation Wave



$$\rho_1 U_1 = \rho_2 U_2$$

$$P_1 + \rho_1 U_1^2 = P_2 + \rho_2 U_2^2$$

$$h_1 + \frac{U_1^2}{2} = h_2 + \frac{U_2^2}{2}$$

$$U_2 = C_s$$

where  $U_1$  = DETONATION VELOCITY

$C_s$  = SOUND SPEED

$$P/\rho = R'T/M$$

Table 3-2. Detonability Limits

<u>MIXTURE</u>	<u>LOWER LIMIT</u> % Fuel	<u>UPPER LIMIT</u> % Fuel
$H_2 - O_2$	15	90
$H_2 - \text{Air}$	18.3	59
$CO - O_2$ (moist)	38	90
$NH_3 - O_2$	25.4	75
$C_3H_8 - O_2$	3.2	37
$C_2H_2 - O_2$	3.5	92
$C_2H_2 - \text{Air}$	4.2	50

From "Combustion, Flames and Explosions of Gases," B. Lewis and G. vonElbe, Academic Press, Inc., New York, 1951, page 585.

Table 3-3. Detonation Velocities of Mixtures at Room Temperature and Atmospheric Pressure

<u>MIXTURE</u>	<u>DETONATION VELOCITY</u> meters/sec
$2\text{H}_2 + \text{O}_2$	2821
$\text{C}_2\text{H}_2 + \text{O}_2$	2961
$\text{C}_2\text{H}_2 + 1.5 \text{ O}_2$	2716
$\text{CH}_4 + \text{O}_2$	2528
$\text{C}_2\text{H}_4 + 2\text{O}_2$	2581
$\text{C}_2\text{H}_6 + 3.5\text{O}_2$	2363
$\text{C}_3\text{H}_8 + 3\text{O}_2$	2600
$\text{C}_2\text{N}_2 + \text{O}_2$	2778
$2\text{CO} + \text{O}_2$	1264

From Lewis & VonElbe, "Combustion, Flames and Explosions of Gases,"  
Page 584.

Table 3-4. Detonation Parameters as a Function of Initial Pressure

$P_1$	760 mm Hg	1 mm Hg
$T_2/T_1$	12.3*	8.22
$P_2/P_1$	18.05*	2.07

\*From "Combustion, Flames, and Explosions," B. Lewis, and G. vonElbe, Page 607.

Table 3-5. Effect of Preheat on Chapman-Jouguet Detonation Parameters  
(Stoichiometric  $H_2 - O_2$  Mixture)

Q cal/gr	$T_1$ °K	$P_1$ atmos	$T_2$ °K	$P_2$ atmos
500	1140	$3.18 \times 10^{-4}$	2400	$1 \times 10^{-4}$
950	1800	$1.585 \times 10^{-4}$	2200	$1 \times 10^{-3}$
1800	2955	$1.205 \times 10^{-3}$	2450	$1 \times 10^{-3}$



Table 3-6. Effect of Temperatures and Pressure on Detonation

Velocity for a Stoichiometric  $\text{H}_2 - \text{O}_2$  Systems

INITIAL TEMP =  $300^\circ\text{K}$

INITIAL PRESSURE (atmos)	0.0013	0.263	1	1.98
DETON. VELOCITY (m/sec)	2200	2627 *	2821 *	2872 *

INITIAL TEMP =  $1140^\circ\text{K}$

INITIAL PRESS (atmos.)	0.00032	0.0012
DETON. VELOCITY (m/sec)	2180	2280

\*From "Combustion, Flames, and Explosions," B. Lewis and G. vonElbe, Page 583.

Table 3-7. Reaction Scheme for  $\text{H}_2/\text{O}_2$  System

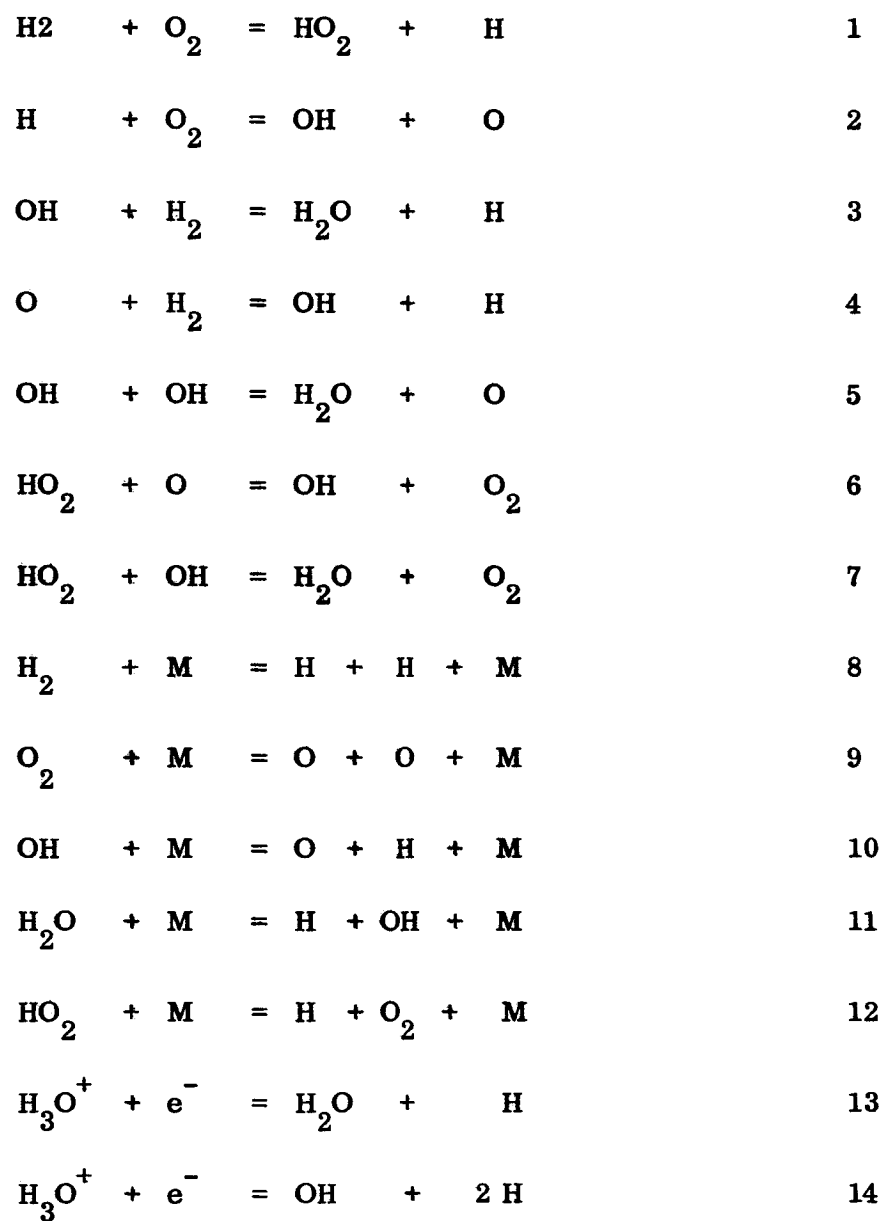


Table 3-8. Kinetic Coefficients for  $H_2/O_2$  System

$$K = AT^n \exp(-E/RT)$$

Units:  $\frac{\text{mol/sec}}{\text{cm}^3}$ ;  $^{\circ}\text{K}$ ; cal/gmol

REACTION	FORWARD COEFFICIENTS			BACKWARD COEFFICIENTS		
	A	n	E	A	n	E
1	1.7/13	0.11	57320	3/13	0	0
2	2.4/14	0	16750	2/12	0.27	98
3	6.3/13	0	5900	2.3/14	0	20687
4	3.3/12	0	7140	1.1/12	0	5192
5	7.6/12	0	1000	8.6/13	0	17734
6	3/13	0	0	5.5/12	0.15	55372
7	3/13	0	0	6.3/13	0.13	72107
8	1.4/18	-0.88	103240	2/18	-1.0	0
9	2.5/16	-0.5	117945	8.9/14	0.44	0
10	7/13	0.21	101292	8/14	0	0
11	6.1/21	-1.31	118027	2.3/21	-1.5	0
12	1.9/16	0.07	45920	1.5/16	0	0
13	1.4/17	0	0	9.9/7	1.54	146487
14	1.2/17	0	0	3.2/7	1.35	28460

1.7/13 represents  $1.7 \times 10^{13}$ .

**Table 3-9. Collisional Efficiencies for Dissociation-Recombination Reactions**

(Argon = 1)

<u>REACTION</u>	H <sub>2</sub>	O <sub>2</sub>	H	H <sub>2</sub> O	OH	O
8	2.5	2	10	7.5	2	5
9	2	5	5	5	2	25
10	2	2	5	5	2	5
11	2	2	2	8	2	2
12	2	2	2	5	2	2

Table 3-10. Kinetic Considerations in  $H_2/O_2$  System

Analysis of reactive flow behind Mach 4 normal shock waves in a 0.67  $H_2$ :0.33  $O_2$  molar mixture.

<u>Pre-Shock</u>			<u>Post-Shock</u>							
$P_\infty$	$T_\infty$	time = 0		Time	$T_2$	$X_{H_2}$	$X_{O_2}$	time = $\infty$		
	$^{\circ}K$	$P_1$	$T_1$		$^{\circ}K$			$T_2$	$X_{H_2}$	$X_{O_2}$
(mm Hg)		(mm Hg)	$^{\circ}K$	(sec)		(mol fraction)		$^{\circ}K$	(mol fraction)	
0.01	300	0.19	1167	$1 \times 10^{-4}$	1167	0.67	0.33	2250	0.155	0.073
0.1	700	1.9	2514	$2.2 \times 10^{-4}$	2518	0.54	0.25	2530	0.168	0.072
1	1300	18.5	4321	$7 \times 10^{-5}$	3273	0.175	0.061	2900	0.15	0.058

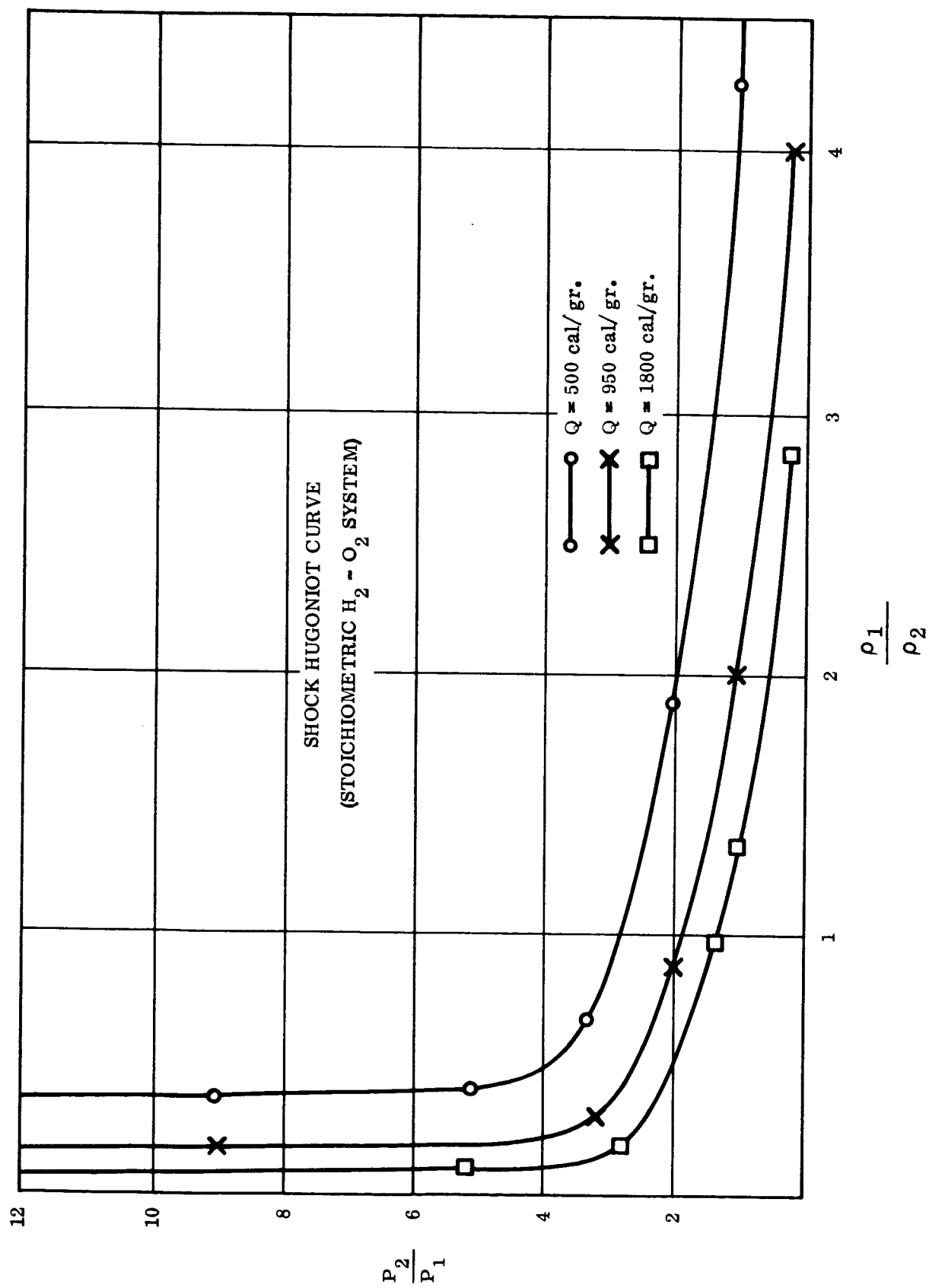


Figure 3-8. Shock Hugoniot Curve (Stoichiometric  $H_2 - O_2$  System)

### 3.3 A PRELIMINARY ANALYSIS OF THE PHASE TRANSITION IN THE SPET

This material is principally in response to Work Statement Section 1. (1) (iii)

#### 3.3.1 STATEMENT OF THE PROBLEM

The SPET is a propulsion device in which a liquid fuel of very low vapor pressure is used. The liquid is intermittently flash evaporated by the energy pulses from discharges of a capacitor. The vapor is generated at high temperatures and pressures, expanding, accelerating, and eventually coalesces into a shock wave which will cause the vapor to ignite. The detonation wave will propagate through an exhaust nozzle.

As an initial hydrodynamic boundary condition it is necessary to calculate quantitatively the amount of liquid vaporized, the pressure and temperature of the vapor pulse in the duration of a discharge. From these initial conditions the wave propagation through a two-phase region and the formation of the shock wave are being studied.

#### 3.3.2 PHASE TRANSITION

When a liquid is evaporated into a space where the pressure is  $p$ , then the expected molecular flux is (Reference 2)

$$J = (p_o - p) / (2 \pi m k t)^{1/2} \quad (3-1)$$

where  $p_o$  is the saturated vapor pressure.

For liquids in general the actual evaporation rate and the expected rate is not equal. The ratio of these two rates is known as evaporation coefficient which must be obtained from experiments. These coefficients have been compiled and published by a number of authors. References 2, 3, 4, and 5.

Based on the theory that the molecular rotation of the liquid is hindered, the ratio of the molecular rotational partition function of the liquid to that of the gas (free-angle ratio) is found to correlate well with the evaporation coefficients (References 2 and 5) for some liquids.

Penner (Reference 6) derived an equation based on the theory of absolute reaction rate which gives a similar form as Equation (3-1), and the evaporation coefficient is identified as the free-angle ratio.

In these formulations, the temperature of the liquid is invariably the same as the gas temperature. It has been shown (Reference 7) that under non-equilibrium conditions these two temperatures are different. If the vapor velocity is not too high the driving force for vaporization is proportional to the difference of the chemical potentials of the liquid and vapor phases (Reference 8). Due to the incomplete description of the liquid, calculation of the chemical potential of the liquid phase from the partition functions imposes considerable difficulty even for a simple liquid.

An approximate rate constant can be obtained, in which the thickness of the liquid surface layer is an unknown at a specific temperature and pressure. As discussed by Hirth and Pend, (Reference 9) and Wylie (Reference 2) this thin layer acts as an intermediate stage in the liquid vapor transition. Frenkel (Reference 10) calculated this thickness as

$$\delta = \left[ \frac{2}{f} kT \right]^{1/2} \quad (3-2)$$

where  $f$  is the second derivative of the potential energy with respect to the intermolecular distance. The statistical theory resulted (Reference 11) in a surface layer thickness as a function of  $T$ ,

$$\delta(T) \sim \frac{a}{|\alpha_1(T)|} \quad (3-3)$$



$|\alpha_1(T)|$  is related to the radial distribution function, the potential energy function, the liquid volume, in addition to the molecular constants  $a$  and  $E$ .

Under the non-equilibrium and transient conditions in this application the energy pulse from the discharge is a function of time but the temperature at which vaporization occurs and the final state of the vapor are not defined. The form of Equation (3-1),

$$J = \Delta p / (2 \pi k m T)^{1/2}$$

which consists of three variables, namely,  $J$ ,  $p$ , and  $T$ , cannot be used. If our problem is considered a constant volume process, the final  $T$  and  $p$  of the vapor depend on the quantity of liquid evaporated. Therefore the molecular flux,  $J$ , must be determined independently. Due to the lack of equilibrium between vapor and liquid, the relationship between  $T$  and  $p$  is not defined. For the same reason neither the free-angle ratio nor the evaporation coefficient is defined. Therefore the equilibrium statistical methods are rendered powerless.

Simultaneous to the search of a rigorous non-equilibrium statistical method, the condition is approximated so that a quasi-steady state may be assumed to exist in a time interval comparable to the length of time during which the liquid molecules become excited and overcome the potential barrier. The liquid is considered to be at a constant temperature,  $T$ , which defines an equilibrium pressure,  $p$ ,  $J$  is then a function of  $T$  alone according to the form of Equation (3-1). For the ignition of the vapor the required shock strength dictates a driving pressure  $p$ , from which  $T$ , and  $J$  are determined.

Under the above assumption the chemical potentials can also be defined. The molecular flux may be expressed as

$$J = k(\mu_{lq} - \mu_{gas}) \quad (3-4)$$

where  $k$  is the rate coefficient and  $\mu$  is the chemical potential which may be calculated

by means of partition functions. Either Equation (3-2) or (3-3) may be used for the thickness of the surface layer in k.

However, Equation (3-4) cannot be solved directly because J is still a function of T. When Equation (3-4) is combined with the hydrodynamic equations, J, P, T, and the vapor velocity, u, can be solved. This is essentially the method described by Vulliet (Reference 8).

The mass flux, the vapor temperature and pressure may be estimated by an ad hoc method. Suppose the thickness of the surface layer is known, and the liquid surface area is known from the actual size of the cell. The volume of liquid evaporated would be  $\delta A$  where  $\delta$  is the evaporation thickness of the surface layer and A, the liquid surface area. This evaporation thickness of the surface layer is not the same as the surface layer under isothermal conditions.

If we consider that thermal equilibrium is obtained by collision then the energy pulse intensity is attenuated by encounters. The attenuation of the energy intensity is exponentially proportional to the mean free path, as given by Slater, (Reference 12)

$$I = I_0 \exp \left( -\frac{N}{V} s x \right) \quad (3-5)$$

where I and  $I_0$  are the final and initial intensities, s, the collision cross section, N/V is the molecular density. The x is defined as the mean free path when  $I/I_0 = e^{-1}$ . We may borrow this idea and consider that  $I_0$  is the kinetic energy of the electrons per unit area of the capacitor under a potential difference v. A suitable value for  $I/I_0$  would give a value of x as the depth of liquid layer penetrated by collision.

The mass of liquid which is vaporized is then,  $\rho xA$ , if the specific heats and the latent heat of vaporization can be defined under the collision conditions, we may write,

$$\rho \times A \left[ (T_b - T_o) C_v (\text{liq}) + \Delta H + C_v (\text{g}) (T - T_b) \right] = E(t) \quad (3-6)$$

The final vapor temperature  $T$  can be calculated from this constant volume consideration. The pressure is determined by a suitable equation of state.

In these methods difficulties will be encountered whenever there are needs to make a quantitative description of the liquid state, such as the formulation of partition functions and the prediction of liquid properties. Therefore, an extensive study of the theories of the liquid state is imperative. Study of other forms of phase transition such as ignition of solid fuel, and detonation of explosives is also necessary because SPET is not limited only in the liquid fuel application.

### 3.3.3 PROPAGATION OF DISTURBANCE AND SHOCK FORMATION

The vapor generated from the energy pulse is going forward as an accelerating piston. Along its path mach waves are generated. The P-compression waves will finally be centered to form a shock wave. The location and the strength of the shock are the two quantities which we are interested to determine. We hope that from the solution of the wave characteristic equations, some conditions may be defined as additional restraints for the energy pulse and the mass flux.

Before we write the hydrodynamic equations we should first consider a region which includes the entire disturbance zone. If we write the continuity equation for the vapor phase,

$$\frac{\partial \rho}{\partial t} + \frac{\partial (\rho u)}{\partial x} = 0 \quad (3-7)$$

then the energy equation does not contain the energy pulse term because the discharge disturbance is initiated entirely in the liquid. If we further neglect the heat conduction term because of short duration, we will have the entropy function  $DS/Dt = 0$  and the

characteristic equations become

$$\begin{aligned}\frac{\delta + P}{\delta t} &= 0 & \text{or } P &= \text{constant} \\ \frac{\delta - Q}{\delta t} &= 0 & \text{or } Q &= \text{constant}\end{aligned}\tag{3-8}$$

This is fine, because the wave propagation can be investigated by the usual method for unsteady continuous motion. However, the initial temperature and pressure remain undetermined, because there is no link between the state in the liquid phase and the state of the vapor phase. We could not hope to achieve what we wanted to accomplish.

If we write the set of hydrodynamic equations describing the motion in the liquid phase, we will be able to study the wave propagation in the liquid phase and the effect it might have to the fuel supply system. We follow the same procedure as we have done for the vapor phase: Substituting continuity equation, with the help of the equation of state, into the momentum equation to obtain the Riemann characteristic equations. Since the equations are written for the bulk of liquid without considerations of the energy input, we are still unable to connect the energy and mass fluxes in the region where the disturbance is generated.

In order to match the wave propagations in the vapor and liquid phases so that additional conditions for the mass flux  $J$ , pressure  $p$ , and temperature  $T$  and velocity can be determined, we should solve another set of equations which will be valid in the phase transition and disturbance generating region.

Instead of continuity equation we write a mass balance equation to describe the removal of vapor,

$$\frac{\partial p}{\partial t} + \frac{\partial (p u)}{\partial x} = -\dot{w}\tag{3-9}$$

where  $-\dot{w}$  represents the net time rate of depletion of material from the region.

Since there is no equilibrium condition in this region we write the momentum equation in terms of momentum flux and replace the energy equation with the equation of change of entropy. Thus, the momentum equation:

$$\frac{\partial u}{\partial t} + u \frac{\partial u}{\partial x} = - \frac{1}{\rho} \frac{\partial p}{\partial x} + \frac{1}{\rho} \sum_i n_i X_i \quad (3-10)$$

where  $P$  is the x-component of the pressure tensor.  $P = \rho U + P$ .

$\sum_i n_i X_i$  is the momentum flux due to a generalized force  $X_i$ , and  $n_i$  is the number density of the particles of the  $i^{\text{th}}$  species.

The entropy equation:

$$\rho \frac{\partial S}{\partial t} + \rho u \frac{\partial S}{\partial x} = - \frac{\partial \sigma}{\partial x} + g \quad (3-11)$$

where  $\sigma$  is the flux representing reversible flow of entropy and  $g$  is the irreversible entropy production.

These equations are quite general, but the solution of them must be specific for individual cases. Further work will be concentrated in establishing methods for solutions to these equations. It may be necessary to start with simple liquids under simplified conditions so that the methods could be established step by step until the complex case could be solved. Once the solutions are obtained we will have the means to predict the energy and mass fluxes and the shock performance as directly related events.


### 3.4 SPET/SPACECRAFT INTERFACE STUDIES

This material is in response to Work Statement Section 2.

TABLE 3-10A. MILLI/MICRO POUND THRUST REQUIREMENTS FOR FUTURE SPACECRAFT MISSIONS

Required Operation	Continuous Thrusting (lb)				
	Vehicle Wt. 10 lb	Vehicle Wt. 100 lb	Vehicle Wt. 1000 lb	Vehicle Wt. 10,000 lb	Vehicle Wt. 100,000 lb
Decoys		GGTS Galactic Probe Adv. Pioneer	ATS-4 ATS 5,6 AM-FM Microwave Nimbus D	Voyager AM-FM P4 AAP	
E-W Stationkeeping	$5.2 \times 10^{-8}$	$5.2 \times 10^{-7}$	$5.2 \times 10^{-6}$	$5.2 \times 10^{-5}$	$5.2 \times 10^{-4}$
N-S Stationkeeping*	$9 \times 10^{-6}$	$9 \times 10^{-5}$	$9 \times 10^{-4}$	$9 \times 10^{-3}$	$9 \times 10^{-2}$
Orbit Adjust*	$1.4 \times 10^{-8}$	$1.4 \times 10^{-7}$	$1.4 \times 10^{-6}$	$1.4 \times 10^{-5}$	$1.4 \times 10^{-4}$
Drag Make-up	$10^{-5}$	$10^{-4}$	$10^{-3}$	$10^{-2}$	$10^{-1}$
110 NM/200 NM					
Attitude Maintenance	$2.3 \times 10^{-11}$	$2.7 \times 10^{-9}$	$1.4 \times 10^{-6}$	$5.9 \times 10^{-4}$	$2.7 \times 10^{-2}$
Attitude Changes	$1.3 \times 10^{-6}$	$2 \times 10^{-5}$	$2.8 \times 10^{-4}$	$4.4 \times 10^{-3}$	$6.5 \times 10^{-2}$
Spin Axis Precession*	$1.7 \times 10^{-8}$	$2.6 \times 10^{-5}$	$3.6 \times 10^{-6}$	$5.7 \times 10^{-5}$	$8.4 \times 10^{-4}$
Inversion Maneuver	$9.3 \times 10^{-7}$	$1.4 \times 10^{-5}$	$1.9 \times 10^{-4}$	$3.1 \times 10^{-3}$	$4.5 \times 10^{-2}$
Station Changes	$7 \times 10^{-7}$	$7 \times 10^{-6}$	$7 \times 10^{-5}$	$7 \times 10^{-4}$	$7 \times 10^{-3}$
Midcourse Correction	$0.3$	$3.0$	$30$	$300$	$3000$

# NOTES

- \*Not Continuous, 16.7% "ON" Duty Cycle
- SPET-A Applicable to items enclosed by .....
- SPET-D Applicable to items shaded by 

### 3.4.1 APPLICABILITY OF SPET-CLASS THRUSTERS TO TYPICAL SPACECRAFT MISSIONS

To define applicability of the system, the following questions were examined:

What thrust level is required to perform typical maneuvers requiring propulsion, as a function of vehicle weight?

What will the propulsion system sized to produce the desired thrust level weigh? (This weight to include the thruster itself, propellants and associated tankage, and the required power conditioning subsystem).

Table 3-10A shows the required thrust level to perform the missions shown as a function of vehicle weight. It shows the striking suitability of SPET class thrusters to perform over the spectrum of interest.

The cross-hatched areas show those missions and spacecraft weight classes for which SPET operating in the detonation mode would be most suitable. The areas indicated by shading show the missions and weight classes best met by SPET operating in the Ablation mode.

Table 1-1 was constructed assuming the physical constants for the space vehicle shown in Table 3-11.

Table 3-11. Assumed Constants of Vehicles

Weight, (Pounds)	10	100	1000	10K	100K
Moment Arm, (Feet)	0.75	1.5	5	15	47.5
Moment of Inertia (Slug Ft. <sup>2</sup> )	0.1	3	140	6,600	307K

The following explanatory notes also pertain to the missions defined in Table 1-1.

#### E-W Stationkeeping - Synchronous Altitude

- a. At worst station
- b. Thrust =  $5.22 \times 10^{-9}$  #/# vehicle continuous

#### N-S Stationkeeping - Synchronous Altitude

- a. Perturbation =  $0.8525^{\circ}$ /year constant
- b.  $\Delta V = 150.4$  ft./sec./year
- c. Thrust =  $9 \times 10^{-7}$  #/# vehicle  $\sim 16.7\%$  "on" time

#### Orbit Adjust - Synchronous Altitude

- a. Correction of  $0.18^{\circ}$  orbit inclination
- b. Correction accomplished in 5 orbits
- c. Thrust =  $1.39 \times 10^{-9}$  #/# vehicle  $\sim 16.7\%$  "on" time

#### Drag Make-Up

- a.  $W/C_{da} = 75\text{#/# ft.}^2$
- b. 110-200 n mi orbit
- c.  $\Delta V = 3$  ft./sec./day
- d. Thrust =  $1.08 \times 10^{-6}$  #/# vehicle continuous

#### Attitude Maintenance

- a. Interplanetary Type Disturbances
- b. Thrust for 1/2 couple =  $4 \times 10^{-10}$  (moment arm)<sup>2</sup> (moment of inertia)



## Attitude Changes

- a. Typical Interplanetary -  $9^{\circ}$  slew in 12.2 min. time
- b. Thrust =  $10^{-5} \frac{(\text{Moment of Inertia})}{(\text{Moment Arm})}$  continuous

## Spin Axis Precession

- a. 1 RPM spin rate
- b.  $1^{\circ}$ /day precession rate (e.g. Sun pointing)
- c. Thrust =  $1.275 \times 10^{-7} \frac{(\text{Moment of Inertia})}{(\text{Moment Arm})}$

## Inversion Maneuver - Synchronous Altitude

- a. Torque mas. =  $\frac{3}{2} \omega_o^2 (\Delta I)$
- b. Time = 1/2 orbital period maximum

## Station Changes

- a. Allow 10 days time to change longitude  $1^{\circ}$
- b. Acceleration  $1/2^{\circ}$  then deceleration  $1/2^{\circ}$
- c. Thrust =  $7 \times 10^{-8}$  #/# vehicle (at zero triaxiality acceleration)

## Mid-Course Correction

- a. Typical  $\Delta V = 200$  ft./sec.
- b. Typical allowable time = 200 seconds
- c. Thrust =  $3.1 \times 10^{-2}$  #/# vehicle

The values of  $I_{sp}$  required to optimize system design for the previously described missions are summarized in the following charts.

Two values of specific power weights typical of present and future power sources are considered as well as tank to propellant weight ratios depicting cryogenic gas, i.e.,  $H_2$  (7.0), cold gas (1.3), liquid (0.15), and high density low vapor pressure (0.05) liquid propellants. The ratio of propellant tank weight to propellant weight is not an all inclusive scaling factor and does not always apply at the low thrust end ( $10^{-6}$  to  $10^{-8}$  pounds) where many devices have "irreducible weight."

The use of the optimum  $I_{sp}$  for weight trade off that is given in the following charts has been generalized. Optimum  $I_{sp}$  (Table 3-12) has been used for weight of system comparisons even though most of the devices (such as, hot gas, resistojet, and cold gas systems) will not meet any of the optimum  $I_{sp}$  requirements given. The overall effect of failing to meet optimum  $I_{sp}$  is, of course, a system weight increase. Data on individual cases can be supplied on request. SPET A and D are the only engine system (Ion engines coming the closest as a second because of their boiler and fixed  $I_{sp}$  and thrust characteristics) that will meet all  $I_{sp}$  optimum under both today's power systems (pounds/kw) and future power systems (pounds/kw).

The methods developed in the References 13 and 14 permit to derive the information illustrated in the previous charts and furnish a more complete framework for comparison and preliminary design.

The particular region of microthruster application has been covered by an analysis which permits to account for the departure from a linear scaling of certain components by factoring them initially as fixed weight contributions.

By taking the ratio of the total impulse to these fixed weights, one obtains a parameter akin to a specific impulse.

$$I_{sp} ) F.W. = \frac{I}{W_{F.W.}} = \text{specific impulse of fixed weight components}$$

Table 3-12. Optimum  $I_{sp}$  for Micro/ Milli Pound Thrusters

Using Present Power Supplies (500 Pounds/kw)

MISSION TIME	$E_c = \frac{\text{PROPELLANT TANK WEIGHT}}{\text{PROPELLANT WEIGHT}}$			
	7.0	1.3	0.15	0.05
1 MONTH	436	233.7	165.3	157.9
6 MONTHS	1067.9	572.7	404.9	386.9
1 YEAR	1510.3	809.8	572.6	547.1
3 YEARS	2616	1402.6	991.8	947.1
5 YEARS	3377.2	1810.8	1280.4	1223.5

OPTIMUM  $I_{SP}$  FOR POWER SUPPLIES (300#/KW)

MISSION TIME	PROPELLANT TANK WT/ PROPELLANT WT			
	7.0	1.3	0.15	0.05
1 MONTH	550	300	213	204
6 MONTHS	1380	740	520	500
1 YEAR	1950	1045	740	705
3 YEARS	3380	1810	1280	1223
5 YEARS	4350	2340	1650	1580

SPET A & D - WILL BE REPRESENTED BY THE 0.05 AND WILL MEET ALL  $I_{SP}$  REQUIREMENTS.

Table 3-12. (Cont'd)  
USING FUTURE POWER SUPPLIES (20 LBS./KW)

MISSION TIME	$E_c$ = PROPELLANT TANK WEIGHT PROPELLANT WEIGHT			
	7.0	1.3	0.15	0.05
1 MONTH	2180	1168.5	966	789.5
6 MONTHS	5339.5	2863	2024.5	1934.5
1 YEAR	7551.5	4049	2863	2735.5
3 YEARS	13080	7013	4959	4735.5
5 YEARS	16886	9054	6402	6117.5

SPET A & D - WILL BE REPRESENTED BY THE 0.05 AND WILL MEET ALL OPTIMUM  
 $I_{SP}$  REQUIREMENTS.

Table 3-12. (Cont'd)

## MICRO/ MILLI POUND THRUSTOR SYSTEM WEIGHT

FOR  $\alpha = 500$ 

$$E_c = 1.3$$

THRUST LEVEL	MISSION TIME				
	1 MONTH	6 MONTHS	1 YEAR	3 YEARS	6 YEARS
10 <sup>-2</sup> LB.	514.829	1253.821	1771.1	3063.97	3954.119
10 <sup>-4</sup> LB.	10.098	17.488	22.661	35.5987	44.491
10 <sup>-6</sup> LB.	5.0502	5.1248	5.17661	5.306	5.394
$E_c = 0.15$					
10 <sup>-2</sup> LB.	361.503	884.05	1249.821	2164.022	2793.449
10 <sup>-4</sup> LB.	4.6051	9.33	13.488	22.6302	28.924
10 <sup>-6</sup> LB.	1.03605	1.088	1.12488	1.2163	1.2793
$E_c = 0.05$					
10 <sup>-2</sup> LB.	345.473	844.783	1194.29	2067.84	2669.277
10 <sup>-4</sup> LB.	4.445	9.438	12.932	21.668	27.683
10 <sup>-6</sup> LB.	1.0345	1.0844	1.1193	1.2066	1.2669

This parameter acquires a very significant role in those cases in which the total impulse is rather limited (few hundreds to few thousands pound sec) and the propulsion time is in the order of months. This happens because certain component weights become nearly independent of both the level of power and of the amount of propellant carried. The results of this analysis show:

- a. Optimizing values of the specific impulse in the range of 1000 → 4000 sec cover most of the applications for a span projected in the future 10 or 20 years as characterized by prospective technology evolution depicted by the energy and mass efficiencies ( $\eta$  &  $\eta_m$  respectively) and specific power weights ( $\alpha = \frac{\text{pound}}{\text{KW}}$ ).
- b. In this region, the specific impulse once brought to the level of one or two thousand seconds furnishes little improvements with any further increase. In other words, one has reached a rather plateau on the performance curve expressed in terms of this parameter. Furthermore, the curve has become monotonic with an asymptotic behavior controlled by the value of the specific impulse of the fixed weight components. In addition, both mass and energy efficiency now play a secondary role. Thus, the design of a device to attain a specific impulse has to be selected exclusively for two purposes.
  1. The elimination of those components which cannot be scaled in weight.
  2. The improvement in life and reliability of the propulsion system.
- c. Further gains can be reaped by increases in specific impulses over the 4,000 sec mark only if drastic reductions in the fixed weight components can be achieved. Thus the ultimate in design can be reached only by those systems which can combine the two characteristics of low fixed weight components and high specific impulses.

The Figures 3-9 and 3-10 illustrate quite clearly this situation. Figure 3-10 is a nomogram which can be used to find the optimizing specific impulse for any application described by the duration in months, the energy, efficiency  $\eta$  and the specific power weight  $\alpha = \frac{\text{lb}}{\text{KW}}$ .

The optimizing specific impulse is in turn given in terms of the mass efficiency  $\eta_m$ . Values of  $I_{sp}$  from 1,000 to 4,000 sec cover the range of most applications of present and future interest.

The effects of  $I_{sp}^{opt}$  and  $I_{sp}^{F.W.}$  on the weights of the propulsion system can be observed in Figure 3-9 where the weights for optimized systems are given for a 1,000 lb sec mission. Other missions can be read by appropriate linear multiplication of the scales.

It is clear that those systems which are limited by low values of specific impulse remain comparatively poor performers even if the fixed weight components can be reduced to values unobtainable at present, say one single pound for the 1,000 pound sec requirement ( $I_{sp}^{F.W.} = 1000$ ). Conversely, a system capable of high specific impulse and having a similar  $I_{sp}^{F.W.}$  will be more than one order of magnitude lighter.

The SPET system is presently the only capable of achieving the necessary combination of low fixed weight components and high specific impulse and thus stands clearly as one of the strongest contenders in the microthruster field. The only other foreseeable contender is the ion engine. The SPET still has a strong edge because of its variable thrust, variable specific impulse and fast response characteristics.

The data presented above shows the eminent suitability of a SPET for a wide variety of mission applications. It would be highly desirable if normal spacecraft slewing and acquisition functions could also be accomplished using the same thruster system.

Figure 3-11 is a plot of time to turn  $30^\circ$  about one control axis versus vehicle moment of inertia about that axis. (Control axes are taken to be the principal vehicle axes). Curves for two thrust levels,  $10^{-4}$  and  $10^{-5}$  pounds, used in pairs to form a couple, are shown.

The control moment arm used varies with vehicle weight, as shown in Table 1-1. The maneuver is accomplished by accelerating constantly for the first half of the total turn angle

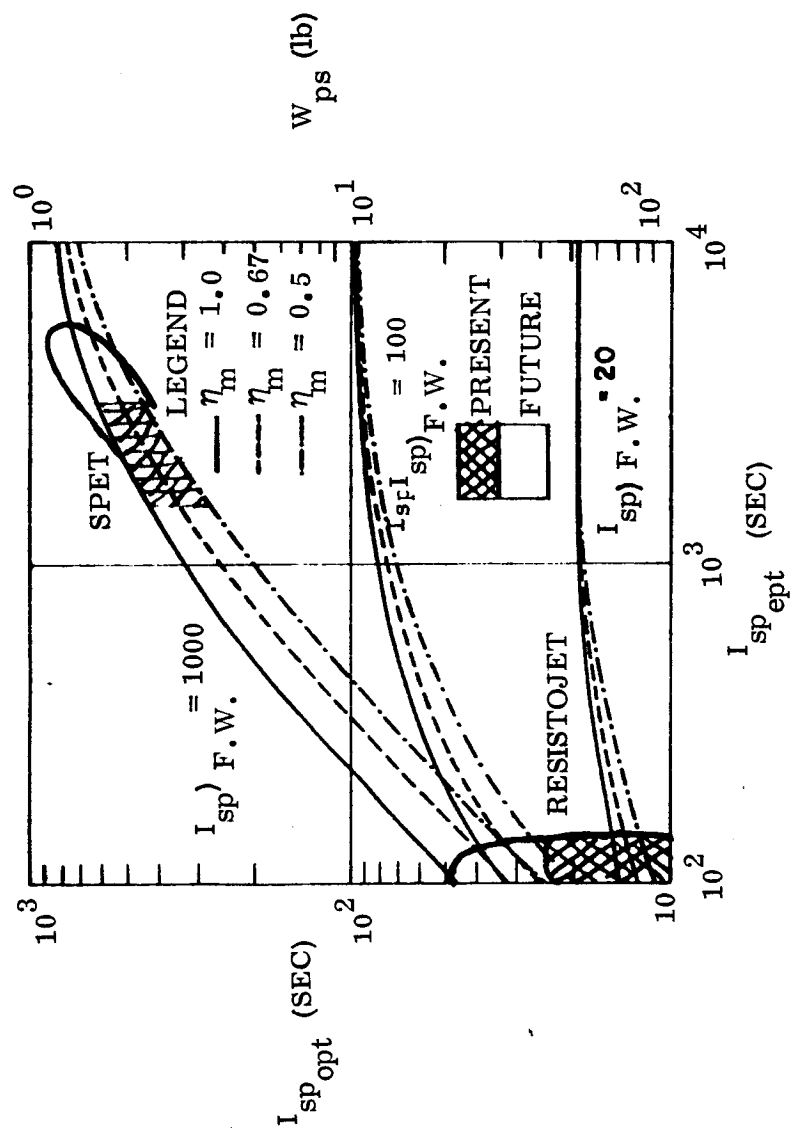


Figure 3-9. Optimized Propulsion System Weights  $\omega_{ps}$  Per 1,000 Pound-Sec Optimum



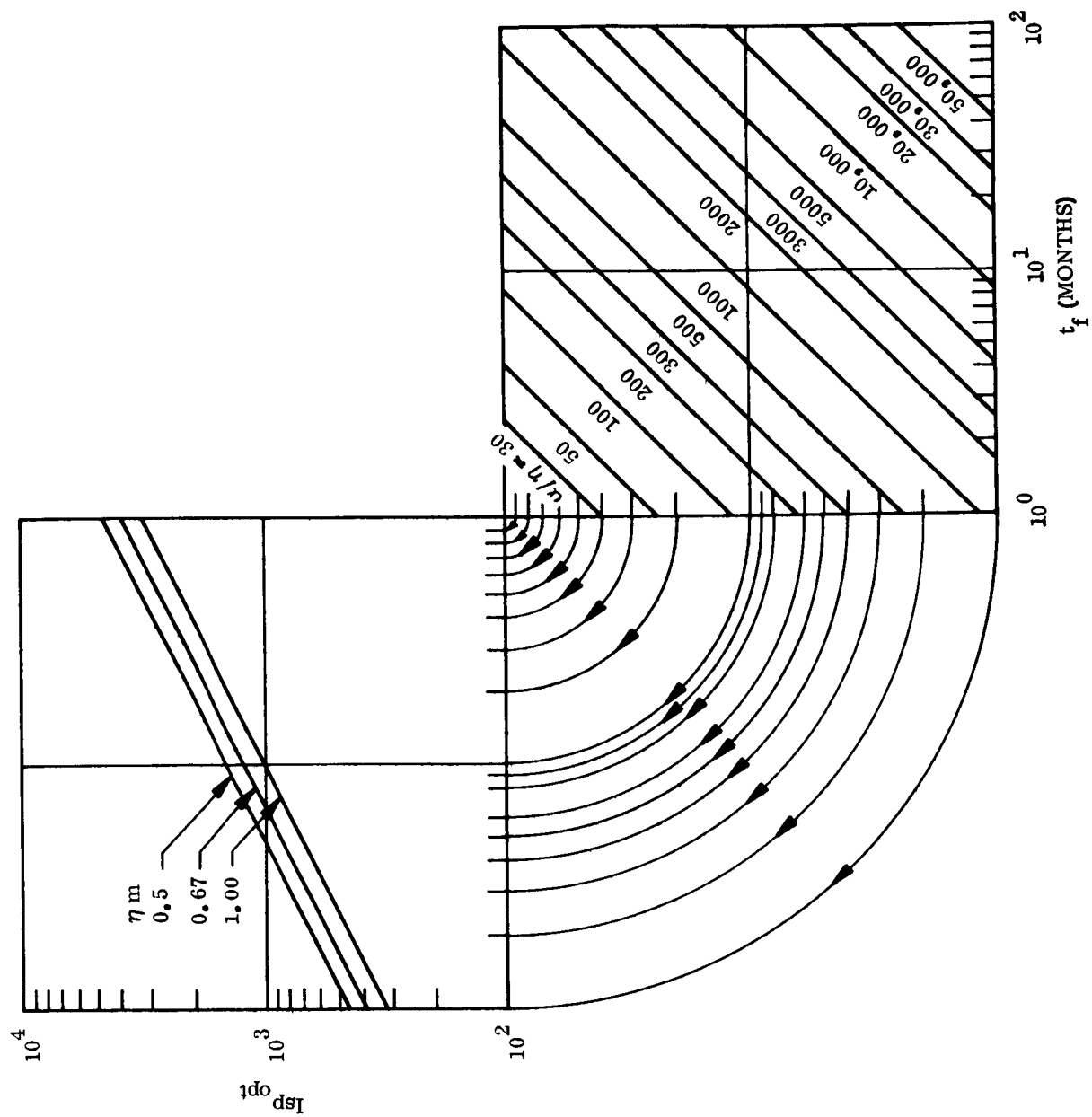


Figure 3-10. Optimizing Specific Impulses

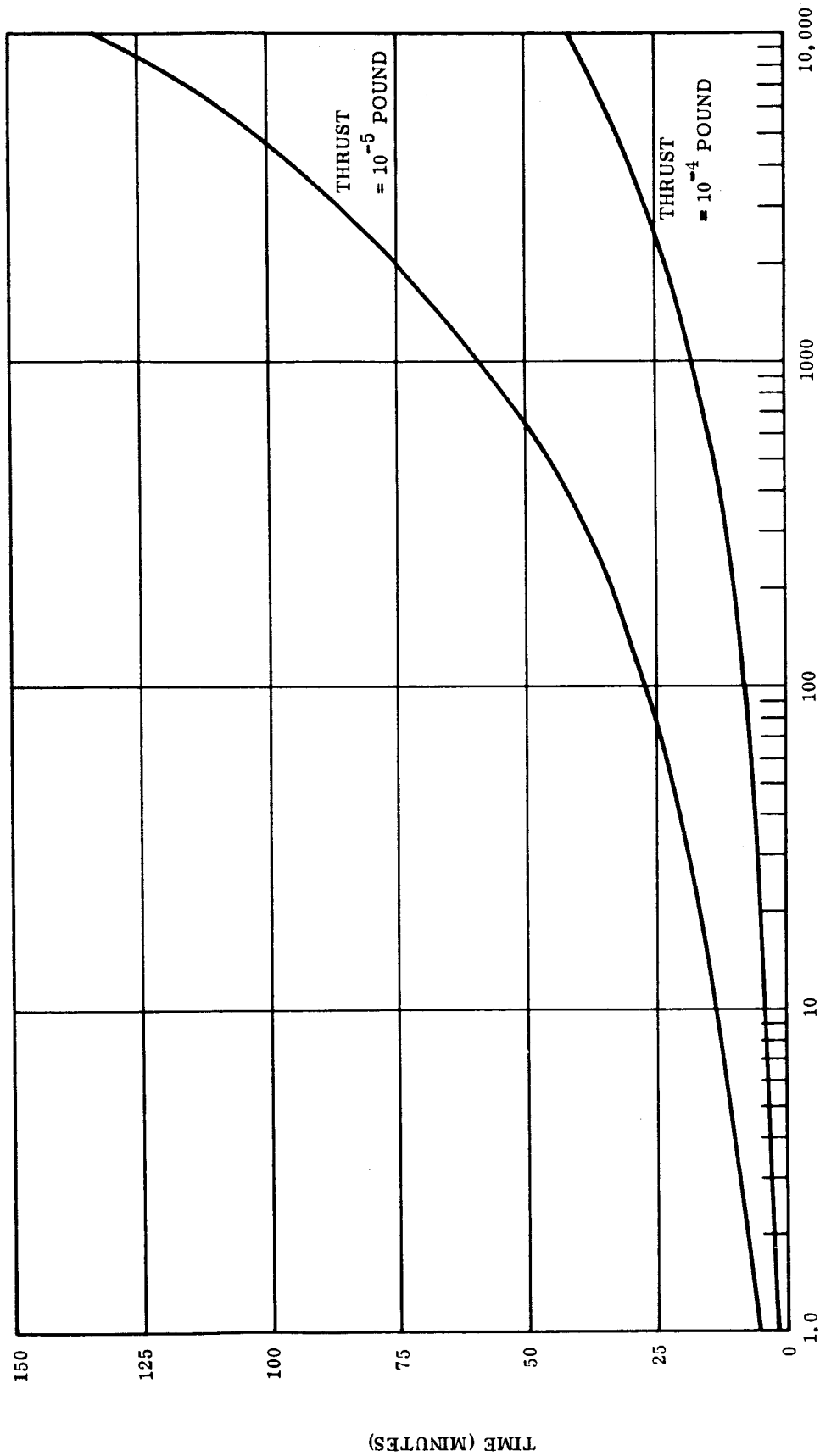


Figure 3-11. 30° Slewing Time vs Moment of Inertia

and decelerating during the second half. Typically a 1,000 pound vehicle, with a moment of inertia of  $140 \text{ slug ft}^2$  can be slewed through a 30 degrees angle in 9 minutes with a  $10^{-4}$  pound thruster. One distinct advantage of slewing with constant acceleration and its attendant minimum body rates is that gyroscopic coupling is minimized, yielding maximum attitude accuracy during the transients.

Figure 3-12 is a similar curve for a slew angle of 90 degrees.

Figure 3-13 is a plot of time required for initial acquisition, defined herein as removal of the initial tumbling rate, as a function of vehicle inertia and thrust level. The initial tumbling rate is assumed to be 0.05 radians per second. For a 1,000 pound vehicle, the initial rate about one axis will be removed in 11.7 minutes, using two  $10^{-4}$  pound thrusters in a couple.

The following is an example of the application of SPET-A to a specific spacecraft-Mariner in this case.

The Mariner attitude control subsystem is required to perform two separate functions; these functions are: (a) stabilize on and hold a fixed angular orientation with respect to inertial references, (b) perform a midcourse maneuver to point the spacecraft's thrust vector to an arbitrary new orientation.

Two Spet engines, one with an impulse of  $10^{-5}$  pound sec per pulse and the other with an impulse of  $10^{-4}$  pound sec per pulse, both having a repetition rate of five pulses per second, are considered. These engines would be physically placed in the same position as the cold gas jets presently in the Mariner design. The vehicle parameters assumed for the calculations are those of the Mariner "C" spacecraft and are given in Table 3-13.

The spacecraft, after having been separated from the final stage of the booster, was assumed to be left with residual rates of three degrees per second about each axis. The attitude control system is required to decrease these body rates and point the roll axis to the sun. This rate reduction is accomplished simultaneously in all three axes with the aid of body

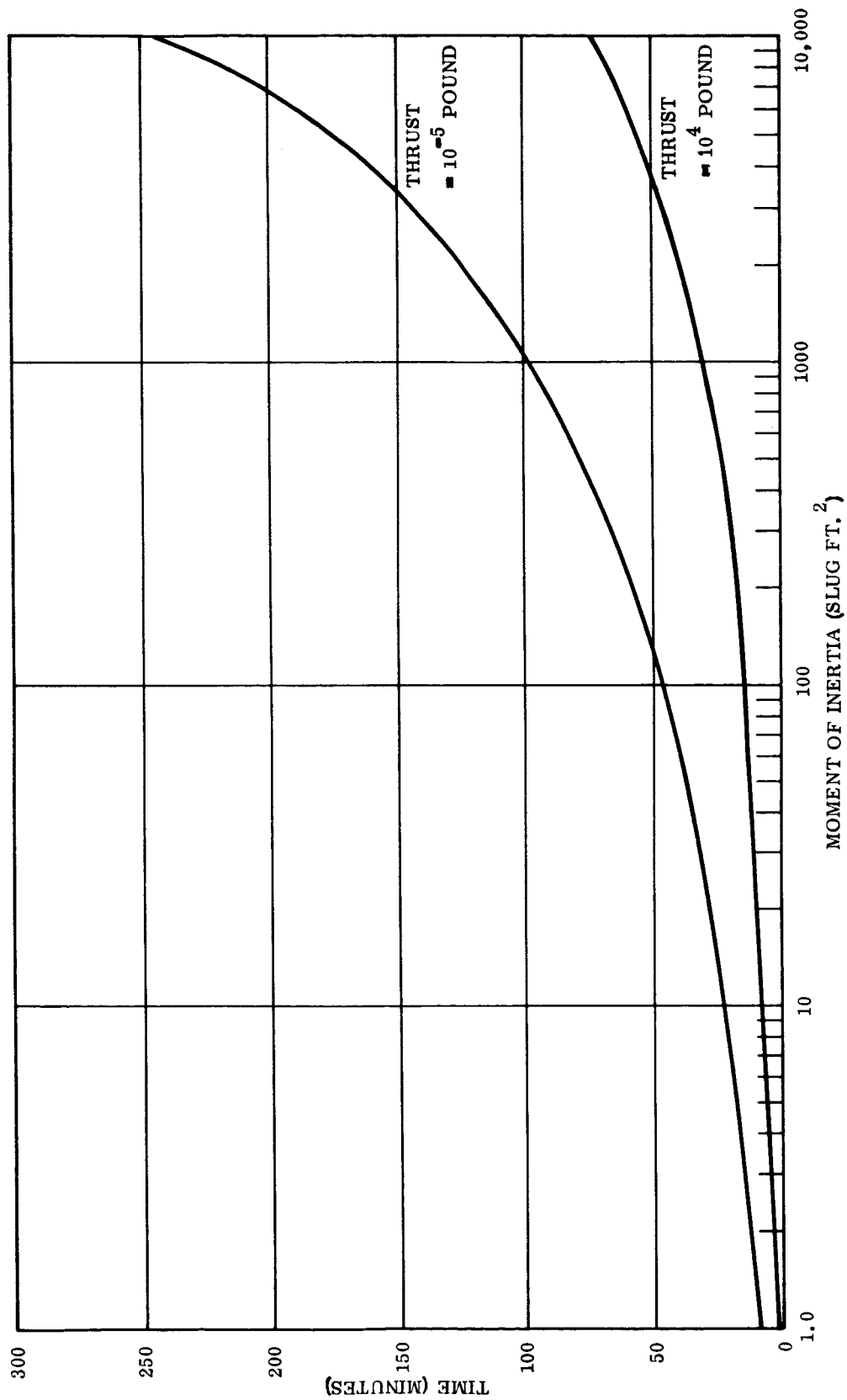


Figure 3-12. 90° Slewing Time vs Moment of Inertia

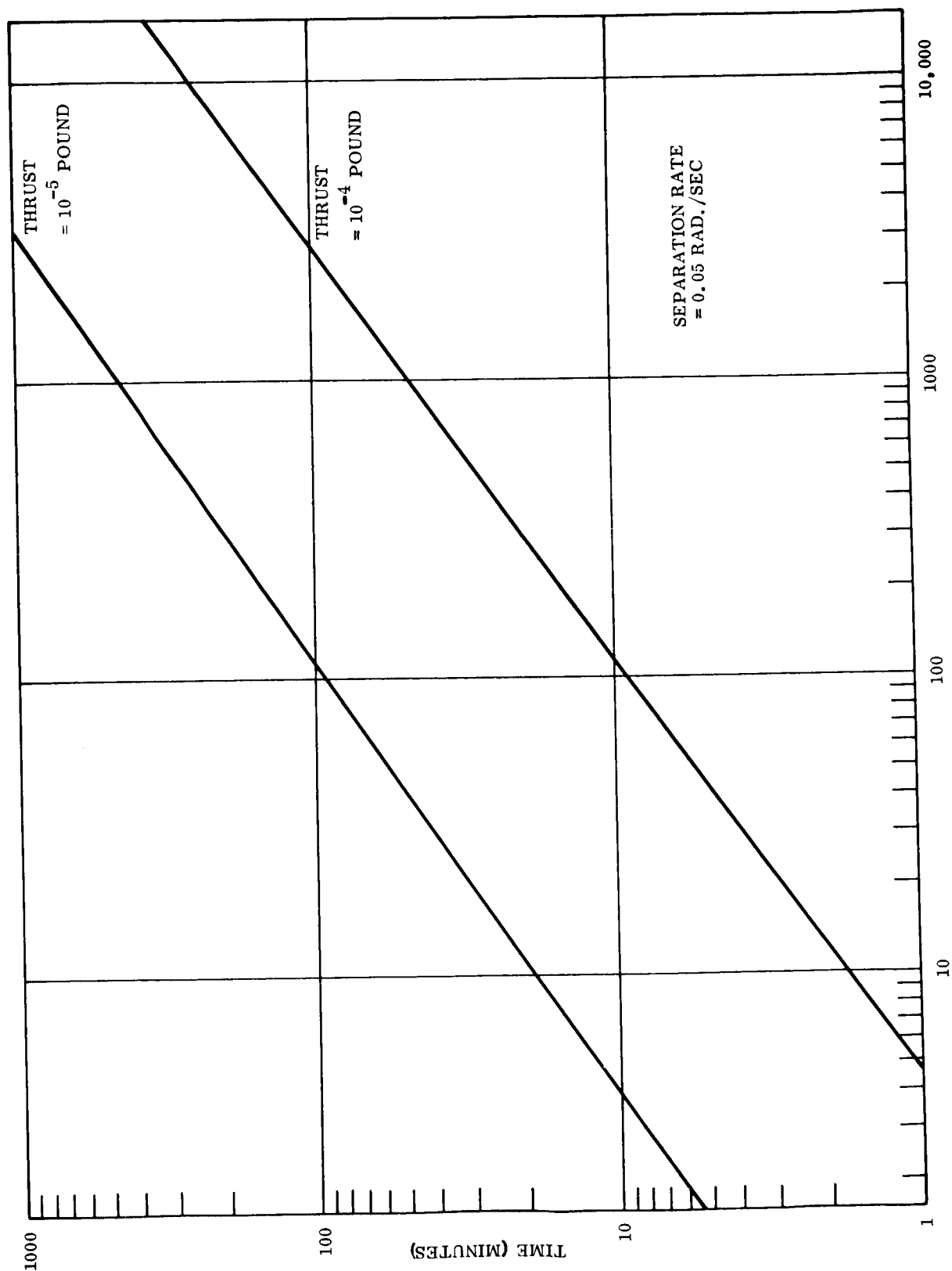


Figure 3-13. Initial Acquisition Time vs Moment of Inertia

mounted rate gyros. The control torques must be applied for the longest period of time about the roll axis, since the moment of inertia about this axis is larger than that of pitch and yaw. The times required to remove this initial momentum are tabulated in Table 3-14. It should be noted here that the calculations for initial stabilization and midcourse maneuver were performed with the assumption made that one of the torquers in each control couple is inoperative.

The Canopus search rates indicated in Table 3-14 are the maximum rates that can be tolerated within the restriction that the star reference must remain inside the four degree field-of-view of the sensor once it is sighted. Since the Canopus search is always performed in the same direction about the roll axis (i.e., it will not necessarily rotate the smallest angle to the reference), a maximum rotation of slightly less than 360 degrees was assumed for the calculation. A SPET engine with an average thrust of  $5 \times 10^{-4}$  pounds ( $1 \times 10^{-4}$  pounds sec per pulse at 5 pps) would be required to operate for a maximum time of 23.4 minutes, and deliver an impulse of 0.7 pounds sec about the roll axis, in order to stabilize the spacecraft to its inertial references.

During the midcourse maneuver, the attitude control subsystem may be commanded to slew the spacecraft by as much as 90 degrees about the pitch axis, and then 180 degrees about the roll axis. The maximum slew rates were calculated on the basis that the gyro, in the position mode, never be allowed to reach its gimbal stops (i.e.,  $\pm 4$  degrees of gimbal rotation was allowed). The maximum reacquisition time was assumed to be the same as the time required to perform a 180-degree roll slew. The larger thrust SPET engine would be required to remain on for a maximum total time of 13 minutes, and supply 0.39 pound sec impulse, in order to perform four midcourse maneuvers.

A solar pressure disturbance torque of  $5 \times 10^{-6}$  ft. pound (68 dyne-cm.) was assumed to act about the pitch and yaw axes, causing a one-sided limit cycle during cruise mode operation. The minimum impulse of the SPET engines is one pulse, and that of the cold gas system is the thrust multiplied by the minimum-on-time of the solenoid (20 milliseconds). As indicated in Table 3-14, the minimum impulse for the larger SPET engine

is approximately six times the minimum impulse of the cold gas system, thereby resulting in longer duration limit cycles about the pitch and yaw axes (where the solar pressure disturbing momentum must constantly be eliminated), and shorter duration limit cycles about the undisturbed roll axis.

A SPET engine that provides an average thrust of  $5 \times 10^{-4}$  pounds would be required to operate for a maximum of 37 minutes (approximately one pound sec of impulse) in order to perform all the attitude control subsystem tasks required during initial stabilization, Canopus search, and four midcourse maneuvers. This time represents the maximum on-time requirements placed upon any one SPET engine. This lifetime is readily attainable, based on laboratory test results.

A SPET engine used for six months of cruise mode operation would be required to deliver an impulse of 4.9 pounds sec; assuming a one-sided limit cycle (i.e., SPET firing only on one side of the position deadband), this impulse requirement corresponds to  $4.9 \times 10^5$  pulses of the  $5 \times 10^{-5}$  pounds thrust SPET engine. This lifetime has been demonstrated on numerous occasions in the laboratory.

The longer time required by the SPET engine (vs cold gas jets) to initially stabilize the spacecraft to the sun necessitates extra power storage capacity. Assuming that each SPET engine consumes 30 watts, that the spacecraft consumes 230 watts, and that battery capacity must not deteriorate below 40% of full power, 5 pounds of additional battery weight must be carried.

The longer time required by the SPET engine to perform the midcourse maneuver will result in an additional thrust vector pointing error of 0.02 degree due to gyro drift (based upon a drift rate 0.25 degree per hour).

It should be noted that it is entirely feasible to operate a given SPET at  $5 \times 10^{-4}$  pounds thrust for initial stabilization and midcourse maneuvers (to minimize elapsed time), and then to operate the same unit at  $5 \times 10^{-5}$  pounds thrust for cruise mode (to minimize

required impulse). The thrust level switching could be easily accomplished by commanding a lower firing voltage when the low thrust mode is desired.

Table 3-13, Mariner "C" Parameters

Roll Moment of Inertia	104 slug-ft <sup>2</sup>
Pitch and Yaw Moment of Inertia	60 slug-ft <sup>2</sup>
Roll Moment Arm	7.5 ft
Pitch and Yaw Moment Arms	8 ft
Roll Position Deadband	<u>±</u> 4 mradians
Pitch and Yaw Deadbands	<u>±</u> 8 mradians
Acceleration Provided by Jets	0.23 mradians/sec <sup>2</sup>
Minimum Jet On-time	20 msec



Table 3- 14. Comparison of SPET vs. Cold Gas

	COLD GAS ( $1.58 \times 10^{-3} \#$ )	SPET ( $5 \times 10^{-4} \#$ )	SPET ( $5 \times 10^{-5} \#$ )
<b>I. INITIAL STABILIZATION</b>			
(a) Initial $3^\circ/\text{sec.}$ Mom. Removal	7.2 min.	22.7 min.	227 min.
(b) Canopus Search			
1. Max. Rate	1.7 mrad/sec.	1.7 mrad/sec.	0.54 mrad/sec.
2. Time to Reach Max. Rate (Jet-On)	16 sec.	46 sec.	146 sec.
3. Time to Search $350^\circ$	4000 sec.	4000 sec.	11500 sec.
4. Total Time Canopus Search	67.5 min.	68.2 min	196 min.
(c) Max. On-Time for One Jet (Roll) Force Impulse	7.5 min. 0.7 # sec.	23.4 min. 0.7 # sec.	229.3 min. 0.7 # sec.
<b>II. MIDCOURSE MANEUVER</b>			
(a) 1. Time to Reach Pitch Slew Rate	26 sec. (3 mr/sec.)	45 sec. (3 mr/sec.)	144 sec. (0.97 mr/sec.)
2. Time to Slew $90^\circ$ (Total Time)	9.2 min.	9.4 min.	29.4 min.
3. Time to Reach Roll Roll Slew Rate	26 sec. (3 mr/sec.)	65 sec. (2.4 mr/sec.)	192 sec. (.71 mr/sec.)
4. Time to Roll $180^\circ$ (Total Time)	17.8 min.	23 min.	76.6 min.
5. Interrogation and Rocket Firing	21 min.	21 min.	21 min.
6. Re-acquisition	17.8 min.	23 min.	76.6 min.
7. Total Maneuver			
Total	65.8 min.	76.4 min.	194.2 min.
(b) Max. On-Time for One Jet Based on 4 Maneuvers (Roll)	314 sec.	780 sec.	2320 sec.
Force Impulse	0.5 # sec.	0.39 # sec.	0.12 # sec.
<b>III. CRUISE MODE</b>			
( $5 \times 10^{-6}$ # ft. Disturbance) (In Pitch and Yaw)			
(a) Min. Limit Cycle Time (Roll)	2 hours	0.64 hours	6.4 hours
(b) Min. Limit Cycle Time (Pitch and Yaw)	55 sec.	320 sec.	32 sec.
(c) 6 Mos. Roll Impulse and No. of Cycles	$7.5 \times 10^{-2} \# \text{ sec}$ (2160 Cycles)	1.36 # sec. (6800 Cycles)	$1.36 \times 10^{-2} \# \text{ sec.}$ (680 Cycles)
(d) 6 Mos. Pitch and Yaw Impulse and No. of Cycles	4.9 # sec. ( $2.84 \times 10^{-5}$ Cycles)	4.9 # sec. ( $4.9 \times 10^{-4}$ Cycles)	4.9 # sec. $4.9 \times 10^{-5}$ Cycles)
(e) Minimum Impulse (Pitch and Yaw)	$1.7 \times 10^{-5} \# \text{ sec.}$	$10 \times 10^{-5} \# \text{ sec.}$	$10^{-5} \# \text{ sec.}$
(f) Minimum Impulse Roll	$3.2 \times 10^{-5} \# \text{ sec.}$	$10 \times 10^{-5} \# \text{ sec.}$	$10^{-5} \# \text{ sec.}$

### 3.4.2 RELIABILITY AND REDUNDANCY CONSIDERATIONS

The passive characteristics of the SPET concept allow us to think in terms of extremely long life potential for this class of thruster devices. To even further enhance reliability of a spacecraft using SPET, it is possible, and in most foreseeable situations, thoroughly practical, to introduce one or two sets of completely redundant thrusters, which would be commanded into operation upon failure or degradation of the primary unit.

The reason for the practicality of this approach is the very low weight of the basic thruster assembly, and its ability to operate off a common propellant supply with any number of other thrusters, as long as they are situated in close proximity to this common propellant supply.

Thus, the weight penalty paid for carrying for example, one set of totally redundant thrusters (assuming one on each of three orthogonal axes) is merely the weight of three very small plastic thruster units, since the propellant supply and most of the power conditioning circuitry would be drawn from the thruster which has failed.

The mechanization of switch over by command to the redundant unit could be accomplished easily by using two AND or NAND gates as shown in Figure 3-14.

### 3.4.3 COMMAND INTERFACES

Excluding switching to redundant thrusters, as discussed above, there are three thruster-associated command functions which might be required, depending on the spacecraft mission application.

#### 3.4.3.1 Selection of Engines for Firing

Assuming complete three axis control is required, a minimum of six rigidly mounted thrusters would be required. A maximum of three of these would operate at one time,

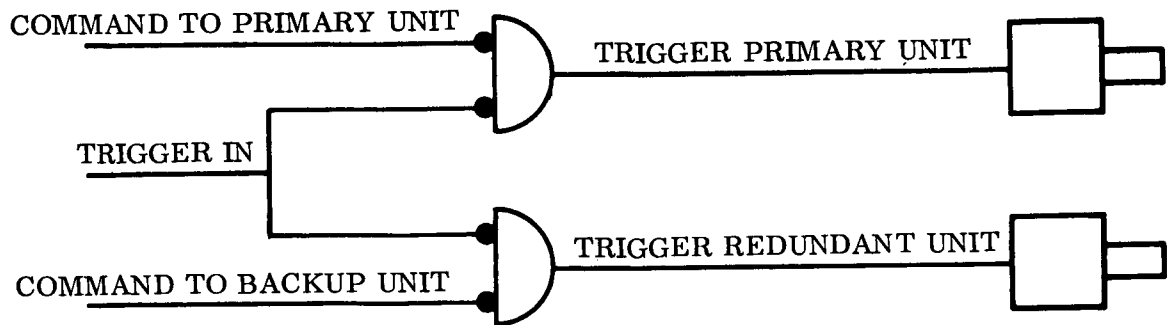


Figure 3-14. Redundant Thruster Switching

since the remaining three, point in the opposite direction. There are eight combinations of three orthogonal thrusters, which requires three command bits for complete specification.

#### 3.4.3.2 Variation of Engine Pulse Rate

The ease of pulse rate variation of a SPET might be utilized in the operational context to provide variable slew rates. If three orthogonally mounted thrusters are used, the capability of varying pulse rates on an individual basis would thus allow any desired vector to be established. Assuming four pulse rates are available for each thruster, it is possible to pre-specify 64 potential thrust vectors per octant. This would require 6 command bits.

#### 3.4.3.3 Variation of Impulse Bit Size

As an alternate means of varying thruster performance, a method of increasing the energy

stored in the capacitor and ultimately discharged through the thruster could be implemented. The mechanization of this function appears to be comparable to that of the pulse rate variation, even though it has yet to be included in an operational system. At any rate, if we again assume four levels of energy storage, 64 thrust vectors per octant are possible, and would require six command bits.

#### 3.4.4 TELEMETRY AND INSTRUMENTATION CONSIDERATION

The pulsed model of SPET operation precludes the necessity of providing high frequency response telemetry capability. Rudimentary PAM/FM, or PDM/FM telemetry would be entirely adequate for SPET performance monitoring and diagnostic instrumentation purposes. It is estimated that three commutator segments per SPET would be entirely satisfactory.

#### 3.4.5 CENTER OF MASS MIGRATION

Two uses for mass expulsion devices on spacecraft are:

- a. Modification of orbit by addition of linear momentum.
- b. Modification of spacecraft orientation by addition of angular momentum.

Mass expulsion devices are required for modification of orbits; they may be selected (from a number of available devices) for control of orientation. Each intended use can result in undesired side effects of the other type on the total spacecraft system; i. e., orbit corrections may introduce disturbances in orientation, and orientation corrections may perturb the orbit. The coupling factor is the actual location of the spacecraft center of mass at the instant of mass expulsion. Therefore, the presence of a mass expulsion device such as SPET requires consideration of the allowable center of mass migration for the total system. One possible conclusion is that the side effects are negligibly small in comparison with other expected disturbances, in which cases no further system constraints are imposed. If the effects are significant the specifications for other subsystems with movable or expendable mass elements (such as solar arrays, booms, propellant

tanks, and deployable antennas) must include constraints to limit excursions of the center of mass to acceptable values, and the location of the line of action of the SPET thruster with respect to nominal center of mass location must be defined.

The SPET is designed to operate with a self-contained propellant supply. If the thrusters are located at the periphery of this vehicle, as would be the use for attitude control, it would seem logical that the migration of vehicle center of mass due to propellant expenditure, would be exacerbated in comparison to, for instance, a cold gas system wherein the gas supply is normally located much closer to vehicle center of mass. However, since the SPET uses such a small quantity of propellant (within order of grams for even a multi-year mission), the resultant migration of vehicle mass center is virtually a negligible systems consideration.

#### 3.4.6 CONTAMINATION OF SPACECRAFT SURFACES

Spacecraft system considerations include assessment of the effects of impingement of the reaction products of mass expulsion devices on other parts of the spacecraft. The most common concern is deposition of material on optical transmission surfaces, such as the cover glass on solar cells or the exterior surfaces of lenses and windows. Another possible concern is the deposition of material on spacecraft exterior surfaces whose emissivity and absorptivity properties are controlled for thermal reasons.

The amelioration of this aspect of SPET thruster interface with other spacecraft systems requires placement of the thrusters so that the discharged products do not impinge on sensitive surfaces. Extensive laboratory experience in high vacuum firings have shown that basically all of the discharged products are contained in a cone of half-angle  $45^\circ$  centered on the thruster axis. Keeping this volume free of sensitive surfaces should prevent degradation of spacecraft function from this cause.

It should also be noted that the extremely high exhaust velocity of SPET (possibly as high as  $2 \times 10^6$  cm/sec) results in a large ordered momentum of the exhaust products. This would tend to further mitigate potential problems of spacecraft surface contamination.

Furthermore it is appropriate to emphasize that the amount of propellant is very small, in other words, only a very limited fraction of it can be involved in this deposition. In other words, the deposition concentration for this area, by appropriate design and installation can be made vanishingly small.

#### 3.4.7 VEHICLE ACCELERATION AND VIBRATION EFFECTS

Prototype SPET flight systems have been vibration tested in accordance with the specified conditions of a booster lift-off environment. Structural dynamic amplification by the enclosing and supporting structures of the SPET system produced g-force in excess of those specified during the tests (up to 75 g.). The systems were functionally tested and visually inspected before and after vibration tests. If the mission requirement includes prolonged acceleration, such as might occur in a spin-stabilized mode, attention must be given in the system design to orientation of the SPET thrusters to minimize propellant flow through the feed systems due to this acceleration. It will generally be possible to orient attitude control thrusters perpendicular to the acceleration vector to minimize this effect; orbit control thrusters, however, may be required to be oriented parallel to this vector for system design reasons. In the latter case, a thin seal of aluminized mylar can be incorporated in the thruster design to contain the propellant for the duration of the spinning mode. When the spinning has ceased the aluminized mylar seal can be broken by the first commanded discharge of the SPET thruster, whereupon normal operation will ensue.

#### 3.4.8 SEPARATION OF POWER CONDITIONING CIRCUITRY FROM THE THRUSTER

The SPET including propellant, instrumentation, and all power conditioning circuitry can be packaged in approximately 20 in<sup>3</sup>, and thus it would appear that many applications would not require consideration of physical separation of power supply circuitry.

If such separation were required, it would be highly desirable that the high voltage capacitor, and trigger tube be kept integral with the thruster at all costs. It is necessary to keep this circuitry in close proximity to minimize circuit inefficiency due to ohmic

losses and distributed inductance. Also, physical separation of the capacitor would require transmission of the large switching transients through appropriate cabling, which would be deleterious to a clean vehicle from the EMI standpoint.

#### 3.4.9 SPET HANDLING

The SPET characteristics of ruggedness, absence of pressurization systems and attendant valving, and shelf life capabilities are pertinent to a discussion of handling problems.

SPETS would ordinarily be installed during factory assembly of the spacecraft. If a seal is incorporated in the thruster design, the propellant can be loaded in the individual thrusters, or thruster clusters, prior to final assembly. In the case of the ablation mode SPET, the propellant presents no hazard of explosion during transportation of the launch site.

In the event that thruster removal is required at any time during the field cycle, including on-stand, the design allows quick, safe, remove/replace cycles, without the necessity of breaking high pressure lines (which normally require re-verification of integrity) or of a great number of electrical disconnections and re-connections. All of this contributes to flexible, safe field and factory operations.

#### 3.4.10 SPET TESTING

In keeping with the highly desirable philosophy of end-to-end testing wherever possible, it is a relatively simple matter, at any time in the factory to launch cycle, to perform a SPET system test with the sole exception of actually discharging a plasma pulse. This can be achieved by electrically starting out the thruster. This type of test can be performed whenever there is vehicle primary power available, or a ground power supply can be tapped into the buss, and when a required command sequence is available via the command programmer or hard wired AGE.

It is even possible to actually fire the thruster, if a small bell jar is placed over the thruster orifice and a reasonably hard vacuum pulled. The bell jar approach would be especially appropriate to factory and field assembly building test sequences, if the situation required it.



### 3.4.11 ATTITUDE CONTROL CONSIDERATIONS

Thrusters are mounted on space vehicles to perform either control torquing functions or to provide a change in linear velocity. (In some instances these two functions are combined.) A common control torque function is the control of the vehicle's attitude. When thrusters are used, the basic vehicle manipulation is given by Newton's second law: The applied external torque is equal to the time rate of change of vehicle angular momentum. It follows at once that a range of control torques, from relatively high to relatively low values will produce the same angular momentum change, if the lower values of control torque are applied for longer time periods than the higher torque values.

$$T = \frac{dH}{dt}$$

$$\int T dt = \int dH$$

Where:

T = Applied external torque

H = Vehicle angular momentum

t = Time

d = Differentiation

With a pair of fixed level thrusters, the vehicle's attitude is controlled by limit cycling through a position deadband, which brackets a nominal position value. In the presence of a disturbance torque, typically in the micropound range, an ideal thrust level would be one where the time integrated control torque will just remove the angular impulse from the vehicle imparted by the disturbance torque. The vehicle's position will be within the deadband limits, reaching one edge of the deadband only, causing only one direction of control torque to be applied. This is illustrated in Figure 3-15, labeled "100% eff.", since all of the propellant is used to overcome unwanted external influences. This will require a thruster in the micropound range. For larger values of thrust, the torque application

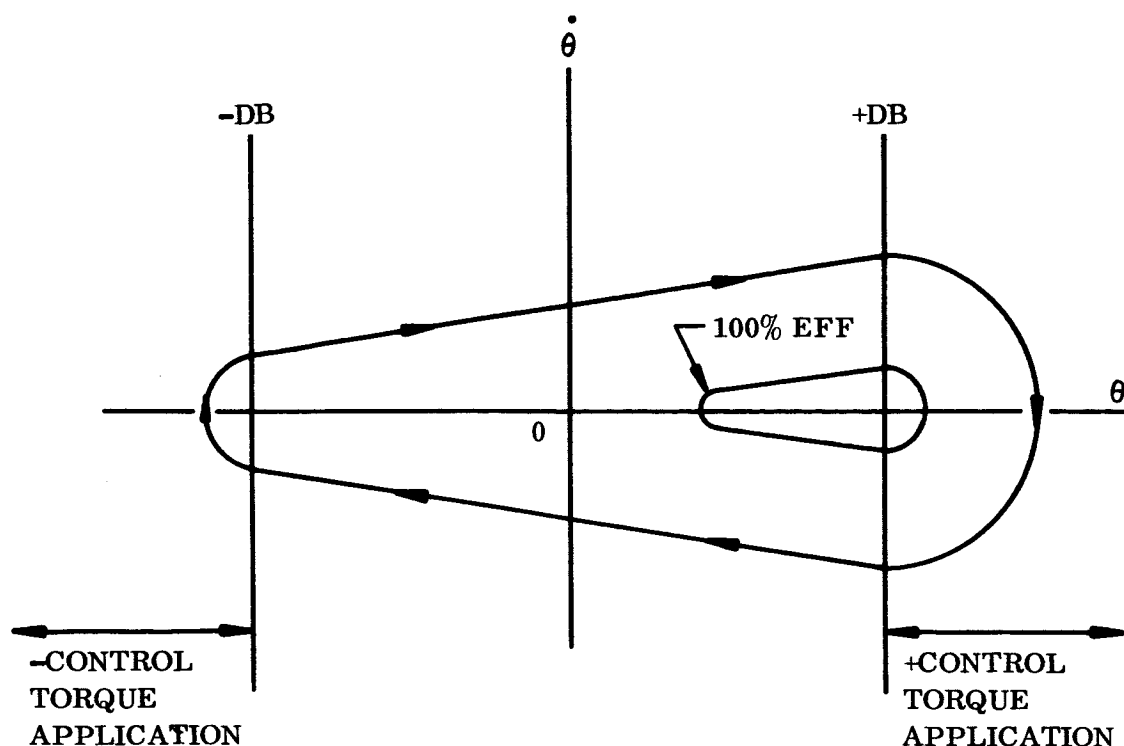


Figure 3-15. Deadband Limits

time must be proportionately reduced, and this is in fact done until a minimum "on" time is reached. With the usual minimum thrust levels available for hot and cold gases, and the usual minimum "on" times of electro-mechanical valves, the resultant control torque impulse will cause both edges of the deadband to be reached in the limit cycle operation with attendant high limit cycle rates. The application of control torque at the negative deadband in Figure 3-15 represents a propellant use inefficiency, since it removes excess energy imparted to the vehicle at the positive deadband.

Higher limit cycle rates also are disadvantageous since they increase the coupling of the control torque about one axis into the other two axes. From Euler's dynamical equations:

$$T_x = L_x + (I_z - I_y) \omega_y \omega_z$$

$$T_y = L_y + (I_x - I_z) \omega_x \omega_z$$

$$T_z = L_z + (I_y - I_x) \omega_x \omega_y$$

Where:

T = Control torque

L = Time Rate of change of angular momentum

I = Moment of inertia about subscript axis

$\omega$  = Vehicle rate about subscript axis

In the same vein, low limit cycle rates make reacquisition of references easier if they are lost by incident or design.

When thrusters are used to change linear velocity, e.g., stationkeeping, orbit inclination adjust, the inevitable misalignments of thrusters and the possible center of mass shifts prevent the thrust vector from passing through the vehicle center of mass, producing a disturbance torque. For a given required velocity change, low level thrusting over a long period is superior to short impulses of a higher level thruster. The latter will cause high amplitude oscillations of a lightly damped system, such as one using gravity gradient restoring torques at high altitudes. High thrust level impulses will require fewer applications per unit time than very low level thrusting. This low pulse rate will approach the vehicle's natural frequencies, giving rise to dynamic amplification of the resultant disturbance torque. Higher pulse rates, possible only with low level thrusters, will permit accurate application of linear impulse, giving greater control resolution.

#### 3.4.12 EMI TESTS OF SPET

##### 3.4.12.1 Introduction

Tests to determine EMI characteristics of the SPET A system have been conducted and the results are presented in the following paragraphs. The objectives were to evaluate the

generic EMI problem presented by a typical SPET system and to assess what levels of EMI are present in a SPET package in a typical flight configuration from a parts placement standpoint, but not in any sense optimized for EMI suppression.

It was thus hoped that the results of the program would indicate whether the measured EMI characteristics were amenable to solution by straight forward, conventional EMI suppression techniques, or whether the physical basis of SPET A operation (plasma formation and propagation) introduced EMI characteristics insoluble by state-of-the-art techniques.

The general conclusion to be drawn from this test program is that the greatest source of EMI in a SPET A system is the electronics, as opposed to plasma phenomena, and therefore it should be possible to attenuate radiated and conducted interference by conventional methods.

#### 3.4.12.2 Description of Test Unit

Two prototype SPET subsystems, electrically identical, and an engineering breadboard model were used in this test program. They are described below.

- a. Prototype Model (Configuration 1). This system is completely enclosed in an aluminum housing (except for the nozzle area) and utilizes rubber impregnated, metal gasketing to reduce EMI leakage and insure continuity across mating surfaces. RF filters are included in the input power and telemetry lines and the filters are isolated in a separate connector box which projects above the main unit. Other EMI suppression measures include isolation of high power interference generators (power converter and trigger circuits) via internal shielding and wave guide assembly described subsequently. The subsystem includes power conditioning (for transforming low voltage DC to high voltage energy), timing (for triggering the electrical discharges), and protection and telemetry circuitry. It has envelope dimensions of 6.7 inch x 4.9 inch 3.5 inch, a volume of 92.5 cu. in.

and a weight of two pounds, five ounces. Input voltage to the unit is 24 volts (+12V, -12V). Average input power varies as a function of selected firing rate; for these tests it was 0.71 watts at 30 ppm.

- b. Breadboard Engineering Model - This unit was an engine firing circuit in breadboard from electrically identical to the firing circuit employed in the prototype. It utilized HV power and trigger sources external to the vacuum chamber. The unit had no enclosure. High voltage was supplied by a standard laboratory variable HV supply, Peschel Instruments Type PP-5c. A breadboard timing circuit electrically identical to that in the prototype supplied the trigger.
- c. Other Configurations. Other test configurations included the basic prototype model with changes in the waveguide attenuation nozzle and/or the position of the engine in its enclosure. These are shown in Figure 3-20 and were as follows:

Configuration No. 2 - waveguide assembly removed

Configuration No. 3 - waveguide assembly reversed and engine removed along its axis approximately 13/16: to edge of enclosure wall.

Configuration No. 4 - waveguide assembly replaced by plate with 7/16 inch hole and engine positioned as in Configuration No. 3.

#### 3.4.12.3 Tests Performed

The following measurements were made in accordance with accepted EMI/RFI standards.

<u>MEASUREMENT</u>	<u>RADIATED INTERFERENCE</u>	<u>CONDUCTED INTERFERENCE</u>
Breadboard #12 (engineering model)	14kc - 1000 mc **ant. pos. 1	14kc - 25mc ±24 VDC power lines

\*See Figure 3-20

\*\*See Figure 3-18

<u>MEASUREMENT</u>	<u>RADIATED INTERFERENCE</u>	<u>CONDUCTED INTERFERENCE</u>
Prototype S/N P3 *Configuration No. 1	14kc - 1000 mc **ant. pos. 1	14kc - 25mc +12VDC return & telemetry lines
Prototype S/N P3 Configuration No. 2	14kc - 1000 mc	
Prototype S/N P2 Configuration No. 2 SPET electrically shorted	14kc - 25mc ant. pos. 1	
Prototype S/N P2 Configuration No. 1	14kc - 25mc ant. pos. 1, 2, 3	
Prototype S/N P2 Configuration No. 2	14kc - 25mc ant. pos. 1, 2, 3	
Prototype S/N P2 Configuration No. 3	14kc - 25mc ant. pos. 1	
Prototype S/N P2 Configuration No. 4	14kc - 25mc ant. pos. 1	
*See Figure 3-20		
**See Figure 3-18		

#### 3.4.12-4 Test Facility and Equipment

The test was conducted in the shielded room in laboratory area at M6422-VFSTC. The following instruments were used in the test:

<u>INSTRUMENT</u>	<u>MANUFACTURER</u>	<u>MODEL NO.</u>	<u>SERIAL NO.</u>	<u>CAL. DATE</u>
Power Supply	Power Design	Model 4005	1cTK0102	NA
Power Supply	NJE Corp.	TR-36-2	OCO191	NA
Power Supply	Harrison	808A	OCO905	NA
RI-FI-Meter	Empire	NF105	NDO578	11/19/65
Tuning Head	Empire	TA105	TA-OKO202	4/22/65
Tuning Head	Empire	TX105	NDO578	5/2/66
Tuning Head	Empire	TI-105	ACO585	4/6/66

<u>INSTRUMENT</u>	<u>MANUFACTURER</u>	<u>MODEL NO.</u>	<u>SERIAL NO.</u>	<u>CAL. DATE</u>
Tuning Head	Empire	T2-105	NDO636	12/1/65
Tuning Head	Empire	T3-105	UEO022	12/1/65
41" Rod Antenna	Empire	VA-105	NDO925	NA
Dipole Antenna	Empire	T1	N/A	N/A
Dipole Antenna	Empire	T2	N/A	N/A
Dipole Antenna	Empire	T3	N/A	N/A
RF Current Probe	Empire	CP-105	1CO630	N/A
Thermovacuum Chamber	Kinney	G12T-3P	TM-0123	NA

#### 3.4.12.5 Test Setup and Procedure

- a. General. The test was set-up as shown in Figure 3-16. The SPET system was mounted on a base plate inside an evacuated bell jar. A cylindrical plexiglass shell replaced the metal grating that normally covers the bell jar for explosion protection.

The prototype SPET (packaged in shielded case) was powered from two separate 12 VDC supplies external to the bell jar. The breadboard SPET received high voltage power and had its power conditioning and triggering functions performed by units external to the bell jar. Provisions were made to minimize affects of the external equipment, and the leads entering the bell jar were shielded.

All broadband interference measurements were made using aural substitution methods with the RI-FI meter set to its Peak detector function. No C-W interference was detected.

Broadband interference readings were obtained at a minimum of three frequencies per octave at which the interference appeared to be maximum. The ambient interference level present with the SPET de-energized was recorded at each measurement frequency.

- b. Conducted Interference Measurements. Current probes were used as pick-up devices, as shown in Figure 3-16, to make measurements of interference currents on lines to the systems.

Measurements were made over the frequency range 14kc to 25mc.

Ambient measurements were made with the dc power supplies removed from the set-up but loaded (500 ohms from each power line to return) in a manner similar to that provided by the SPET.

- c. Radiated Interference Measurements. Radiated measurements were made with the appropriate antenna set at a distance of 1 foot from the energized SPET. A rod antenna was used over the frequency range 14kc to 30mc and a tuned dipole antenna was used from 30 to 1,000 mc. Ambient measurements were made with the BCR de-energized, the power supply turned off, and the thermovacuum equipment operating typically. Each of the configurations listed was tested as shown above.

One prototype was tested with the engine electrically shorted i.e., the pulsed energy was being generated by the electronics but the engine was not allowed to fire.

#### 3.4.12.6 Results and Conclusions

The results of the SPET interference tests are shown in Figures 3-17 and 3-21.

- a. Results. Figure 3-16 shows levels of broadband radiated interference for various SPET systems at a single antenna position. Readings were obtained throughout the frequency of 14kc to 1000mc, ranging from 170db v/mc to 77db v/mc. Interference from the breadboard model was highest. The envelopes of interference from the standard prototype (Configuration No. 1), the prototype with the wave-



guide assembly removed, and the prototype model with the engine shorted, were highest respectively. Interference from these three configurations was detected throughout the frequency range 14kc to 200mc. The interference from the shorted engine configuration represents the noise contributed by the system electronics, and indicates that most of the noise from the normally operated system is not produced by the engine exhaust plasma. The interference from the prototype without the waveguide assembly (Configuration No. 2) is generally 10-20db lower than from the unit with the assembly indicating that a portion of the plasma is absorbed internally. For comparison purposes, a typical composite mil spec limit based on specification MIL I 26-600 modified to include lower frequencies is also shown in Figure 3-16.

Figure 3-17 is a comparison of interference measured at one-foot antenna positions on three sides of the prototype SPET with the waveguide assembly installed. There is no significant difference in the levels measured at the three positions.

Figure 3-18 is the same as Figure 3-17 except for the prototype with the waveguide assembly removed. Again, there is little difference in interference at the three positions.

Figure 3-19 shows levels of interference at antenna position 1 for four set-ups with different enclosure configurations and/or engine positions. Configuration No. 4 produces the most external "noise" and Configuration No. 2 (prototype with the waveguide assembly removed) produces the least. Configurations 1 and 3 have similar interference characteristics between those extremes.

Figure 3-20 is a graph of interference currents, in the frequency range 14kc to 25mc, measured on the +12VDC, return and telemetry lines to the SPET system. The noise characteristics of the power lines and return are quite similar with

noise on the return slightly higher than the other two. Noise on the telemetry line was some 40-80db lower than the other lines and was close to ambient levels.

Figure 3-21 is a plot of interference on the 24VDC power lines to the breadboard system. Noise on the +24 line is generally 20-40db higher than noise on the return line. No significant comparison can be made between noise on the breadboard power lines and lines to the prototype because of major physical differences of the systems. A typical composite mil spec limit for conducted interference based on MIL I 26-600 modified to include lower frequencies is included for comparison purposes on both Figures 3-20 and 3-21.

- b. Conclusions (Previous Results). Prior to initiation of this study, measurements were made of the interference from a prototype SPET, with and without the waveguide assembly, using a non-standard antenna. The measurements were made with a 23-1/2 inch rod antenna mounted inside the thermovacuum chamber. The results of these measurements indicated that interference from the system was some 10 to 80 db lower with the waveguide assembly installed, over the frequency range 14kc to 30mc. The results above 30mc show no consistent pattern and are generally of the same magnitude. These results would seem to indicate that the waveguide is effective in attenuating the interference below 20mc only (a result that indicates a cutoff frequency that is many decades lower than the theoretical cutoff), and that the attenuation at certain frequencies is comparable to that theoretically predictable. These measurements cannot be compared directly to those of the subject tests because of differences in the measurement set-up; however, the results are generally much lower than for the present tests, and this is as expected.

A significant finding concerning compatibility of SPET with EMI-susceptible components is that a successful EMI test of the prototype SPET described herein, and a highly sensitive command receiver supplied by NRL, was conducted on another SPET program. This test was witnessed by NRL personnel, and no degradation of command receiver performance was noted when SPET was operating and a typical SPET/receiver interface was simulated.

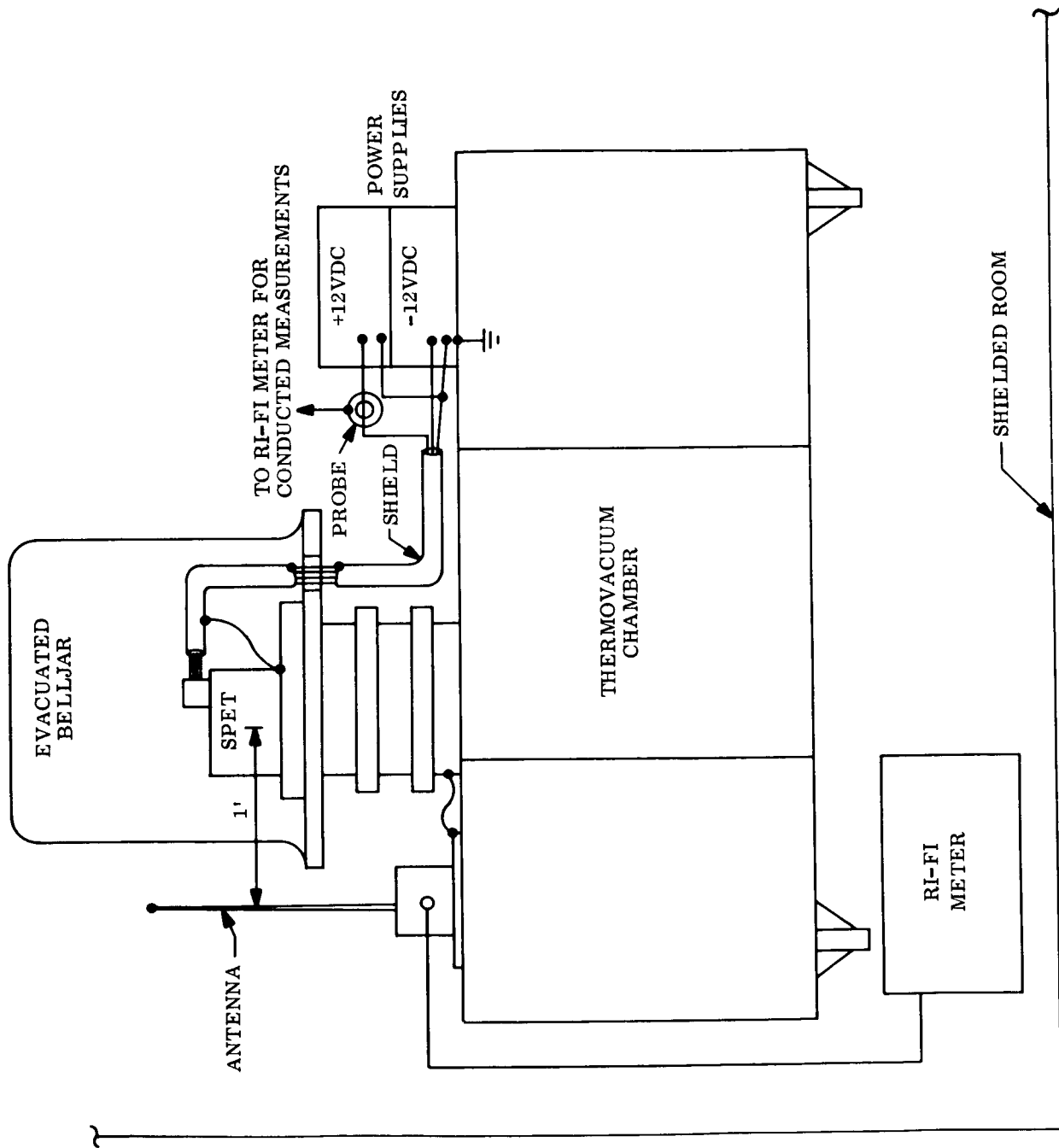


Figure 3-16. Representative Test Setup - SPET EMI Measurements

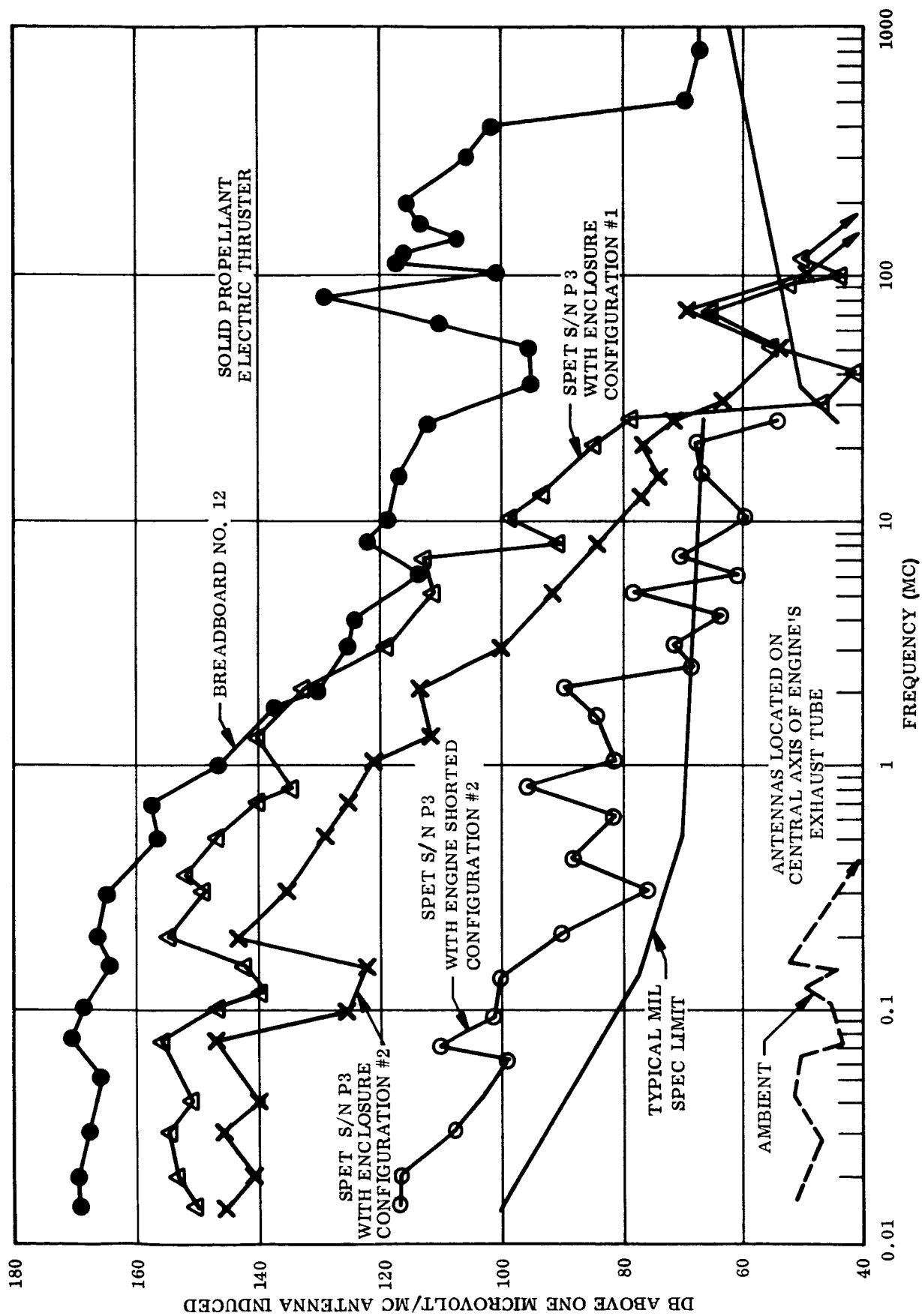


Figure 3-17. Broadband and Pulsed CW Radiated Interference (Measured at One-Foot)

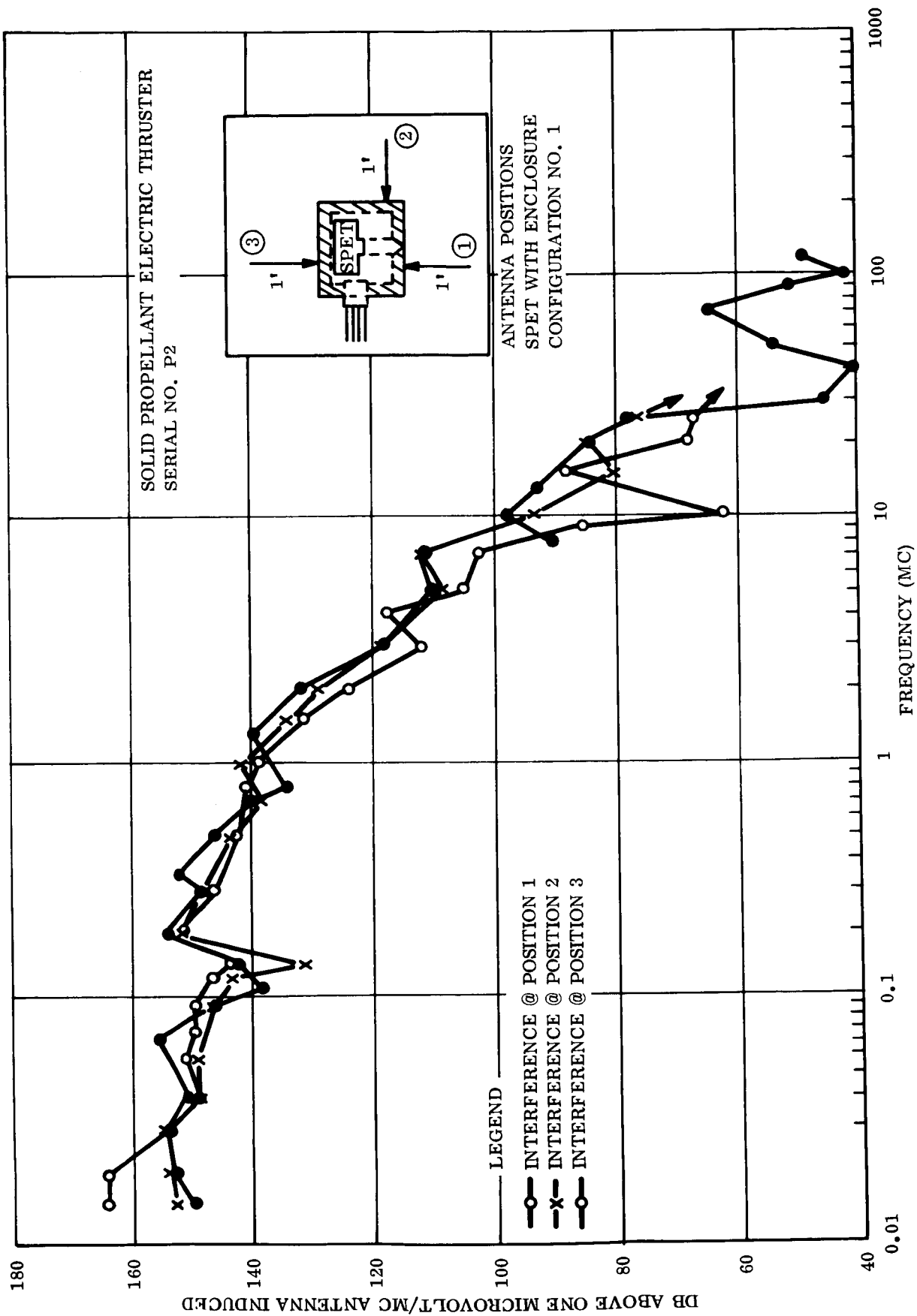


Figure 3-18. Broadband and Pulsed CW Radiated Interference Measured at Various One-Foot Antenna Positions (Configuration No. 1)

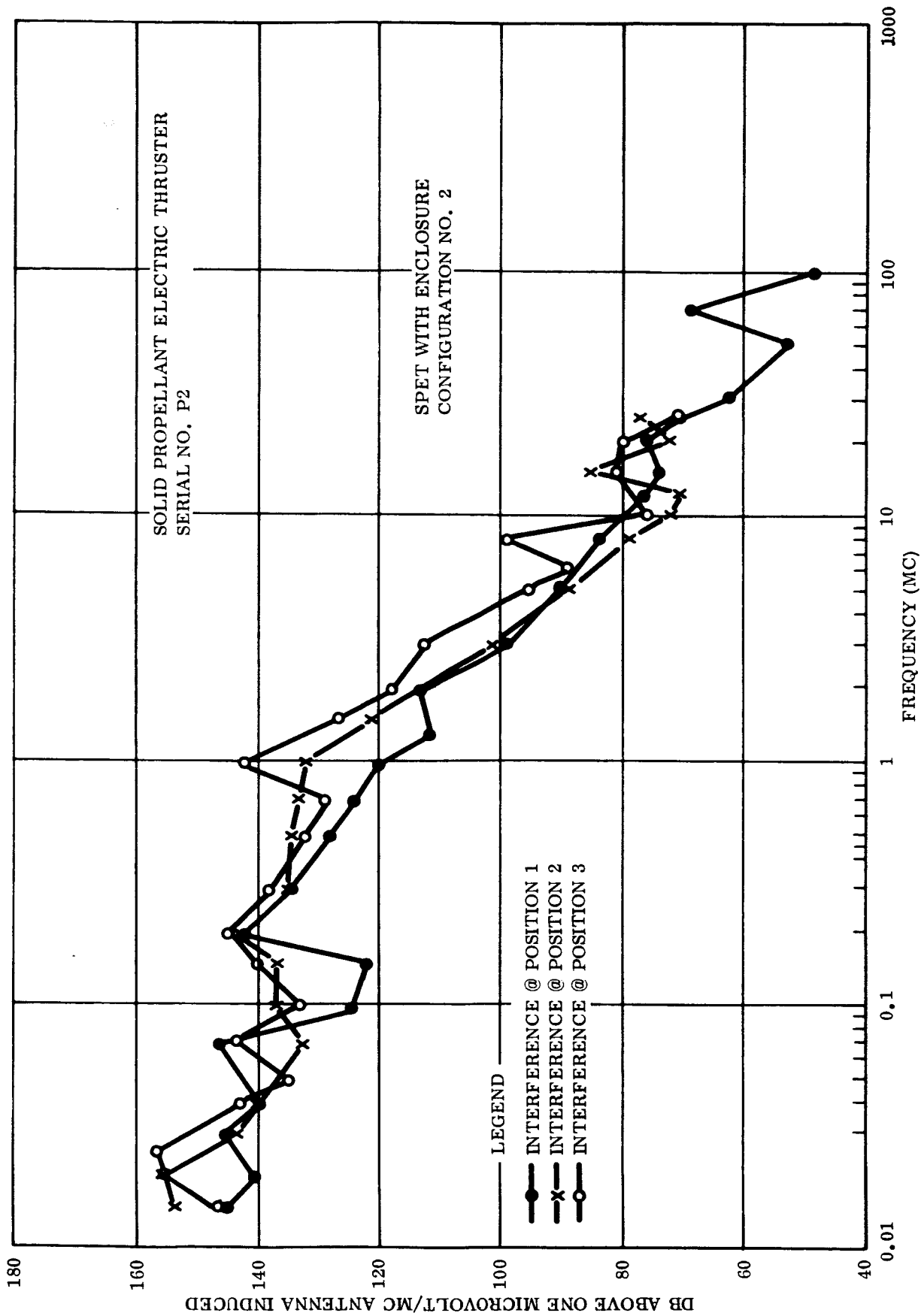


Figure 3-19. Broadband and Pulsed CW Radiated Interference Measured at Various One-Foot Antenna Positions (Configuration No. 2)

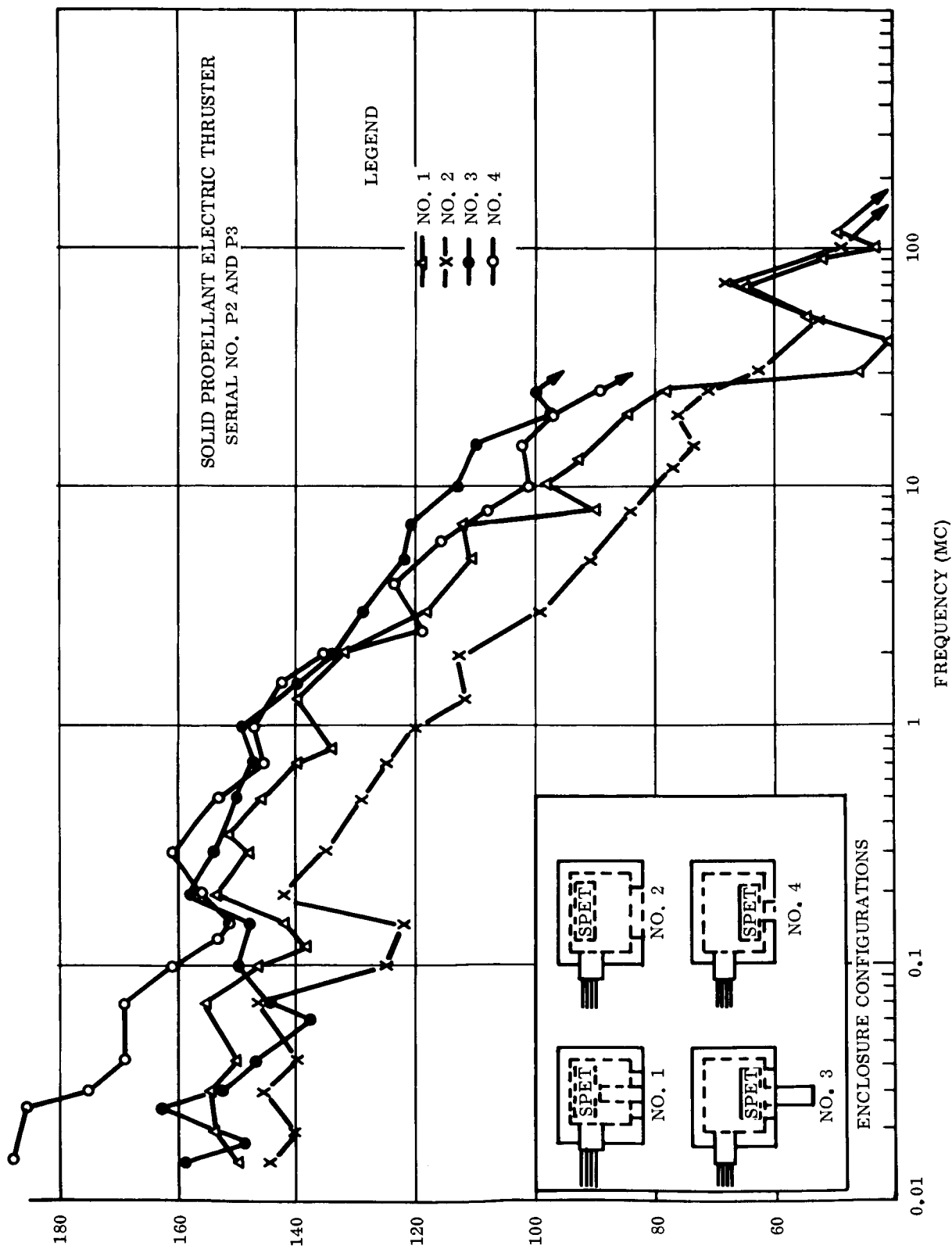


Figure 3-20. Broadband and Pulsed CW Radiated Interference  
Measured at Antenna Position 1

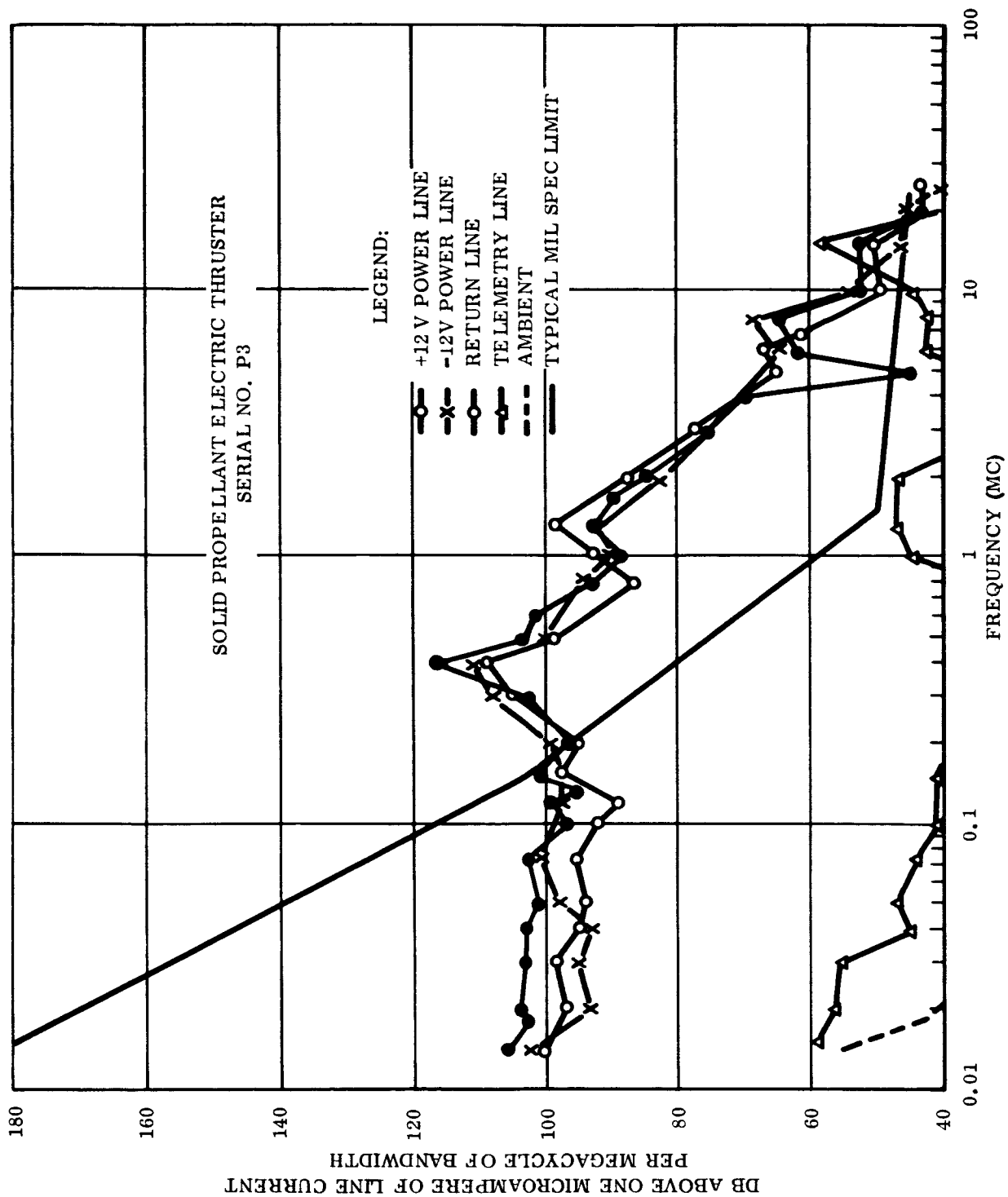


Figure 3-21. Broadband and Pulsed CW Conducted Interference (Current Probes)  
(Sheet 1 of 2)



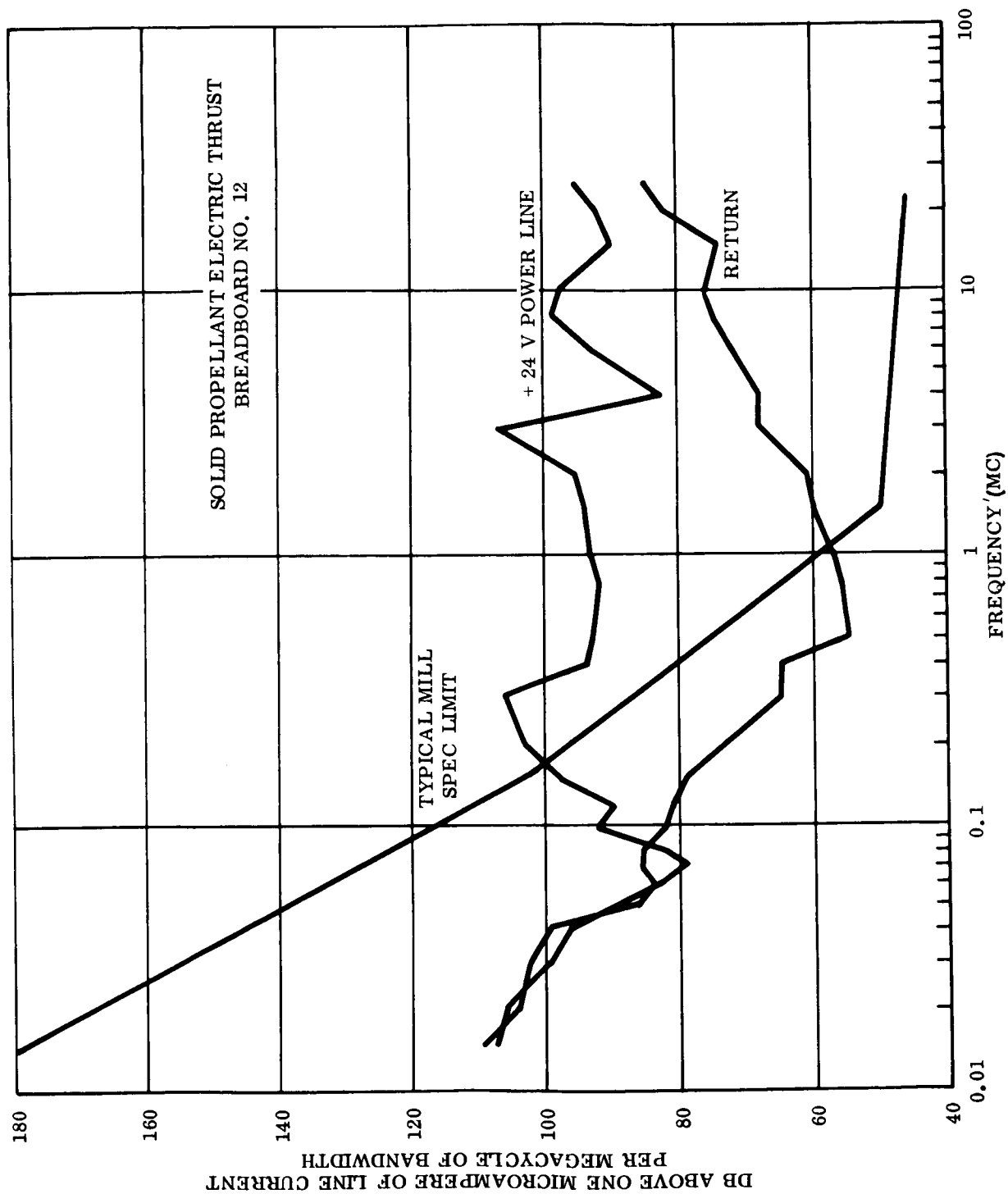


Figure 3-21. Broadband and Pulsed CW Conducted Interference (Current Probes)  
(Sheet 2 of 2)

#### 3.4.12.7 SPET Interference Characteristics

The results of the SPET tests are characteristic of typical electric discharge noise spectrums with broadband noise levels peaking at 15kc and diminishing with frequency to be virtually undetectable between 100mc and 1,000mc. Interference was detected up to 200mc from the enclosed system and the open breadboard interference was detectable up to 1,000 mc. The conducted interference has the same characteristic spectrum but the levels diminish faster with frequency because of the inherent attenuation of the conducting medium. The contribution of the engine exhaust plasma to interference was below typical mil spec limits throughout the spectrum.

#### 3.4.12.8 Shielding

The SPET system enclosure without the waveguide assembly affords some 20 to 60db shielding based on a comparison of interference levels from the open breadboard and the packaged prototype. The same prototype with the waveguide offers less attenuation as indicated above. These values of shielding effectiveness are considerably less than calculated values. This is attributed to the anomalous behavior of the waveguide assembly and the observation that the chassis has high noise currents and is probably a source of radiation itself.

The waveguide exhaust tube is approximately 1 13/16 inch length x 7/16 inch diameter. With those dimensions, the guide should have a cutoff frequency of 12 kmc and an attenuation to all signals passing through it that are below 12 kmc. Comparison of the tests results for the prototype with and without the guide indicates that the guide actually increases the signal by 10 to 20 db. This comparison of the configurations 1 and 2 is adjudged not to be the best demonstration of the effectiveness of the waveguide, because the engine exhaust plasma in configuration No. 1 is concentrated and directed in the guide but in configuration No. 2 is allowed to be partially dispersed inside the enclosure. A comparison of data from configurations 4 and 1 or 4 and 3 are more valid since the only difference between these is

is the presence of the waveguide. Such comparison shows that the waveguide provides 10 to 40 db. attenuation in the frequency range 15 to 150 kc. The departure of the experimental results from the theoretical expectations cannot be definitely traced to any single cause, however, several explanations appear plausible: 1) case radiation appears to have been a substantial contributor to the detected interference; 2) waveguide theory is not entirely applicable in this instance because of the nondescript nature of the source; 3) the guide tends to concentrate and reflect the energy of the engine exhaust in a typical fashion; 4) a combination of such factors. Hence, it appears that the waveguide is of some benefit but its contribution to suppression is small in view of the total radiated energy.

#### 3.4.12.9 Conducted Interference

The conducted interference results indicate that the filters installed at the input to the system are inadequate, and it appears that an additional 60 db. of filtering in the range of 14kc to 25mc is desirable. In particular, the power return should be cleaned up, because it offers a direct path to other systems with no attenuation. This might require changes in the grounding of the system and isolation of the power return from the chassis.

#### 3.4.12.10 Recommendations

It is gratifying to note that the tests indicate only a small contribution to system noise is made by the engine plasma itself, and that the EMI generated by a SPET subsystem did not degrade the performance of a sensitive satellite command receiver. Thus, EMI characteristics of the SPET subsystem can be brought to acceptable levels via normal well understood engineering techniques. It is recommended that an interference reduction study be conducted to determine means of improving the noise characteristics of the device. The study should include as a minimum, an investigation of grounding, filtering, and shielding in the device, to determine the minimum interference configuration.

### 3.5 ENGINEERING DESIGN CONSIDERATIONS

This material is in response to Work Statement Section 1, 3(iii).

#### 3.5.1 TYPICAL FIRING CIRCUITRY

A typical firing circuit for SPET engines, either plasma accelerator or detonation types, is shown schematically in Figure 3-22.

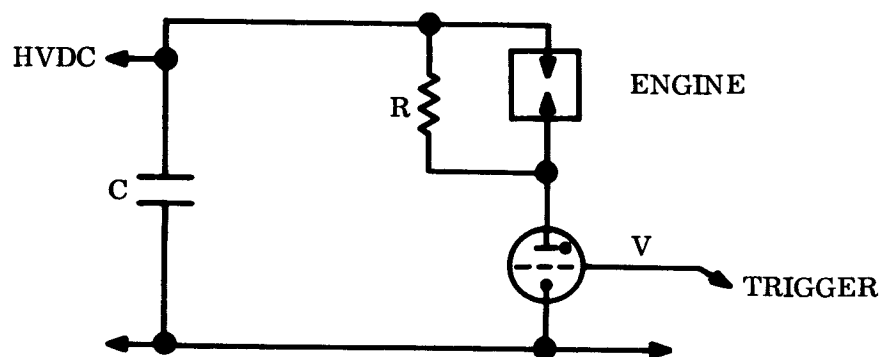


Figure 3-22. Typical Firing Circuit for SPET Engines

The capacitor, C, is an energy discharge type capable of withstanding 30% voltage reversal under repetitive oscillatory discharges. Tube V is a cold cathode thyatron with high peak power and low average power characteristics. Resistance R is a high impedance resistor utilized to insure the voltage drop exists across the tube rather than the engine prior to triggering. This circuit, similar to an electronic photoflash circuit, is nothing more

than a capacitor discharge loop. The physical layout of the circuit and the components employed are of extreme importance to efficiency and life. To minimize circuit losses and provide maximum energy transfer to the engine, the lead lengths between tube, engine and capacitor (those shown in heavy lines in Figure 3-22) must be kept as short as possible and the tube impedance as low as possible when conducting. The inductance of capacitor, tube, and leads must also be minimized to provide maximum peak current and rate of current rise in the loop. While a detailed transmission line analysis has not been performed, a cursory examination of the circuit indicates that remoting the engine from the remaining components of the firing circuit would degrade circuit efficiency. In the case of the detonation engine the electrical efficiency is not of such critical importance so that remoting may be feasible.

From the operating life point of view the cold cathode trigger tube is currently the limiting factor with a life rated at  $10^5$  pulses under non-oscillatory pulse operation. In the SPET application the tube life is degraded to  $10^4$  pulses due to the current reversal of the oscillatory discharge. For the detonation engine, where electrical efficiency is not of such extreme importance and lower pulse energy is required, the existing tubes should be capable of  $10^5$  to  $10^6$  pulses with non-oscillatory firing circuit. Capacitor life is in excess of  $10^6$  pulses. Experimental tubes are currently being developed specifically for the SPET application. Two units have been tested in typical firing circuit operation and provided an average life of  $8 \times 10^5$  pulses. Both units failed as a result of envelope leakage under vacuum, a minor fabrication problem.

Details of a representative SPET power supply for a prototype subsystem are given below.

The SPET power supply is a high voltage, high power pulse generator. The power supply comprises three basic sections:

- a. High voltage generator and storage capacitor
- b. Thyatron and firing circuit
- c. Auxiliary logic

The power supply has the following electrical characteristics:

- a. Supply voltage: + and - 12 volts; tolerance of  $\pm 1$  volt
- b. Average power consumption: 0.5 watts at  $\pm 12$  volts;
- c. Average current drain: 20 ma (maximum) peak current; 50 ma (maximum)
- d. Telemetry channel (2): 0 to 5 volts
- e. Operating temperature range:  $-5^{\circ}\text{C}$  to  $+50^{\circ}\text{C}$
- f. Pulse voltage: 2000 volts
- g. Pulse energy: 0.5 joule
- h. Pulse rate: 15 ppm

The SPET power supply block diagram is shown in Figure 3-23, and the timing diagram is shown in Figure 3-24. The method for delivering the high power, short duration pulse is by capacitor discharge. A high voltage, energy storage capacitor is used for this purpose. A resonant charger is employed to generate high voltage because of its high efficiency; actual efficiencies of 75 to 80% are obtained. Auxiliary logic consists of two timers and a flip flop. This circuit provides protection against a continuous power drain resulting from a type of engine misfire designated as the conductance mode. In the event of such a misfire, leaving the engine and thyatron in conduction, a 5-second timer fires, disabling the high voltage generator, allowing the energy storage capacitor to discharge and the thyatron to be extinguished. Simultaneously with disablement of the high voltage generator, a 20-second timer is initiated. At the end of the 20-second period the high voltage generator is enabled, restarting the unit in its normal mode.

Waveforms 1 through 8 on the block diagram are shown in Figure 3-24 and Figure 3-25 is the electrical schematic; Table 3-15 lists the component parts specified on the schematic.

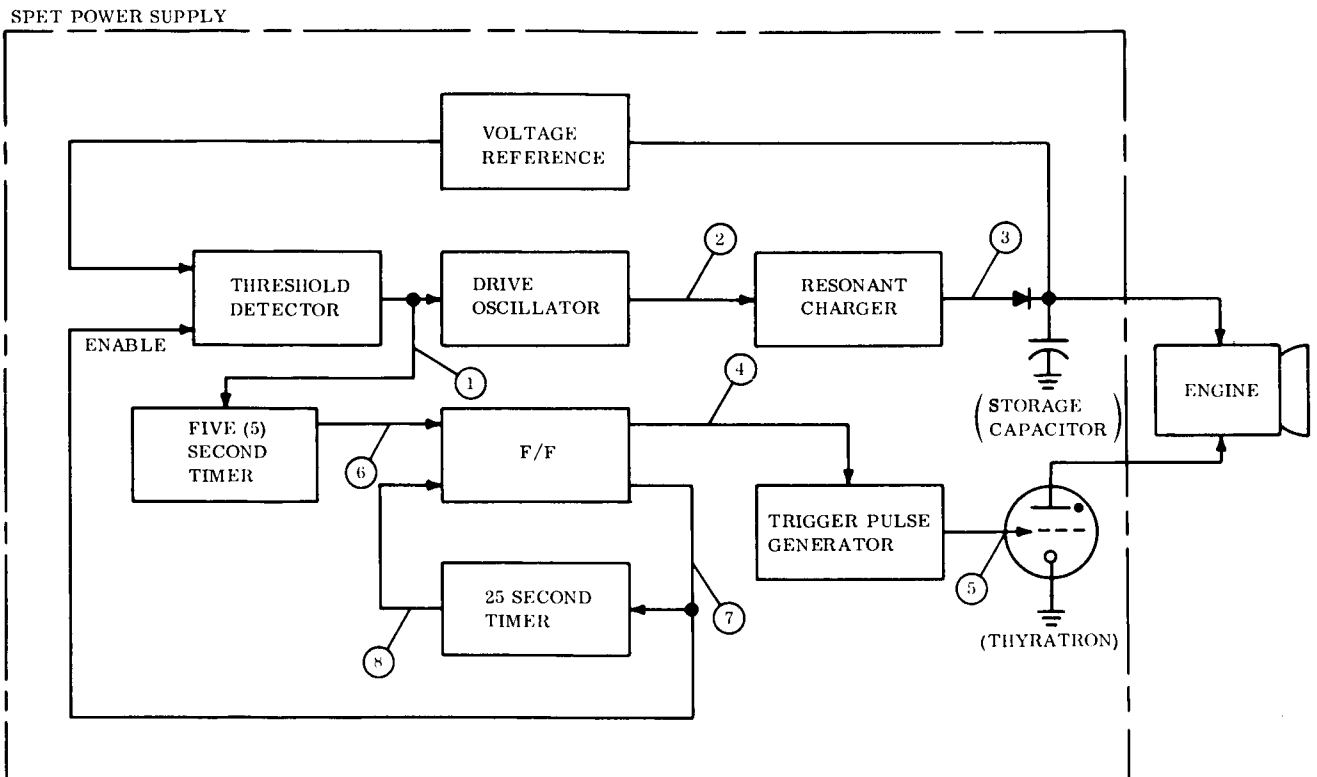


Figure 3-23. SPET Power Supply Block Diagram

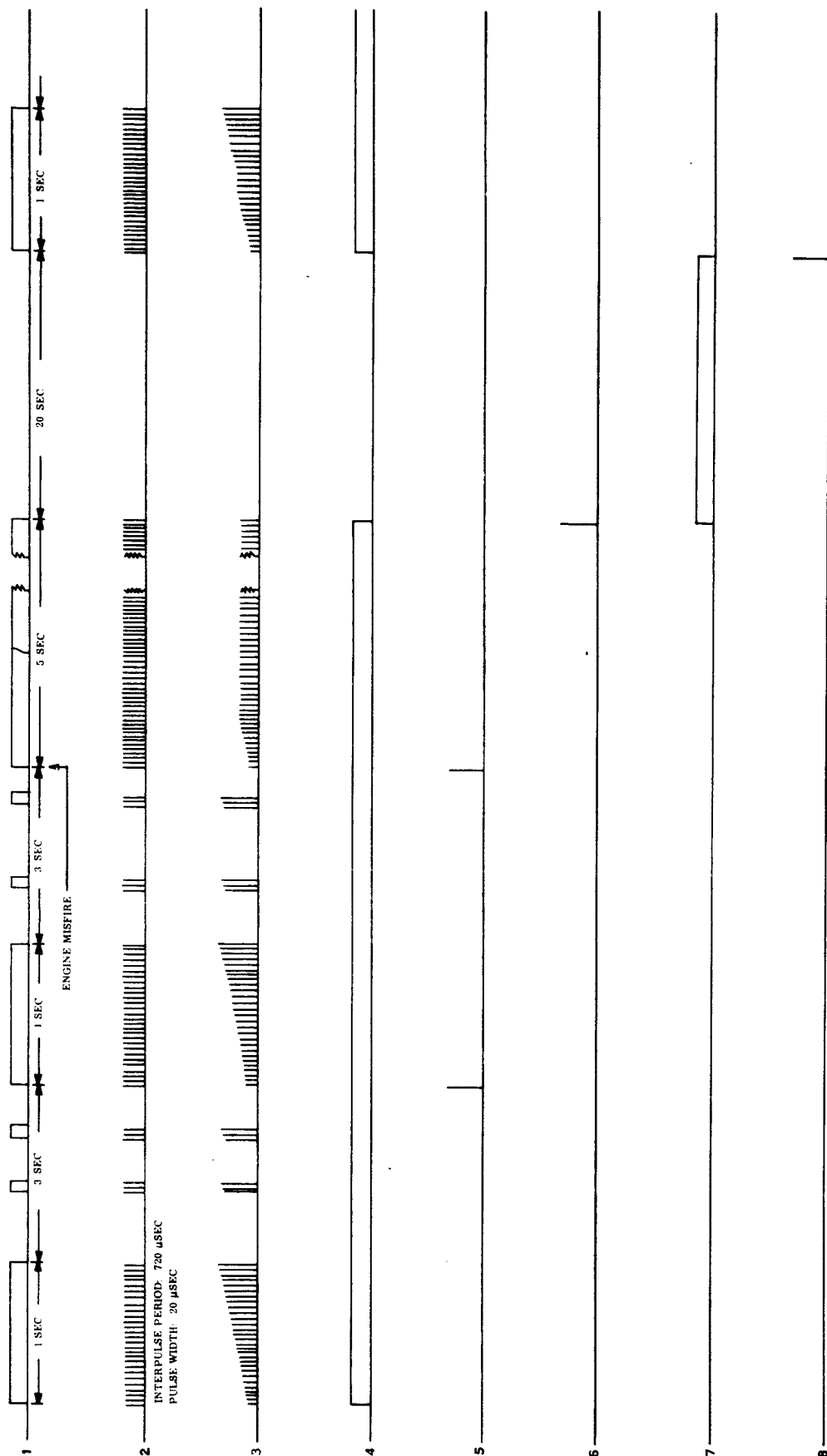
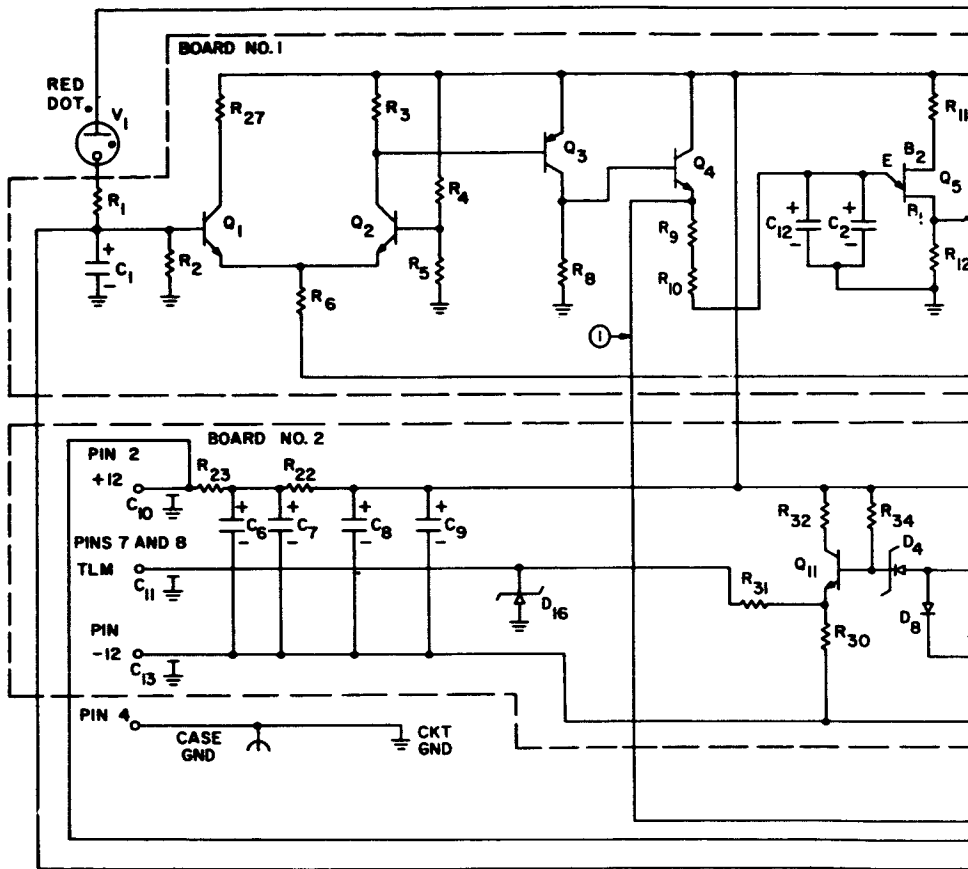
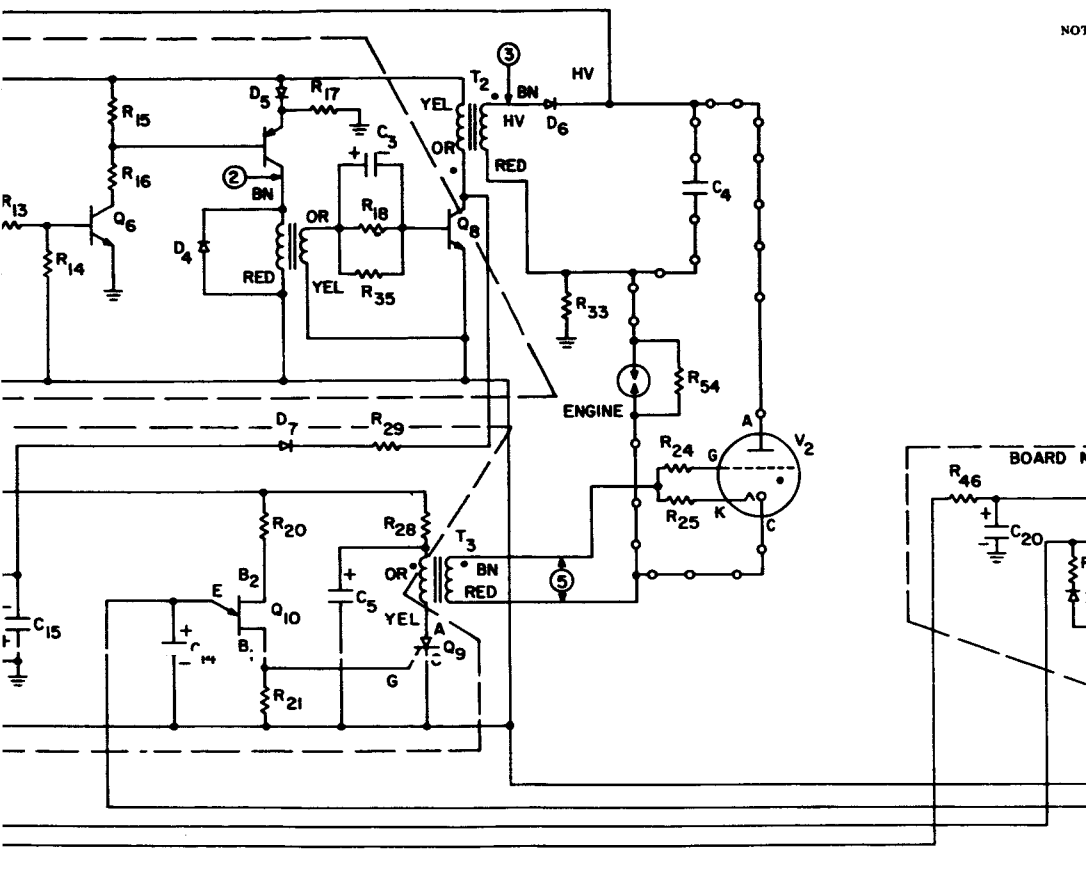


Figure 3-24. SPET Power Supply Timing Diagram






3-85 (1)



~~2~~ 2

- ALL LINES MARKED HV USE HIGH VOLTAGE WIRE.
- KEEP LEADS MARKED  AS SHORT AS POSSIBLE.
- R45 MUST BE MOUNTED NEAR Q15;  
R26 MUST BE NEAR Q13.
- R29 AND R25 MUST BE MOUNTED  
NEAR V2.

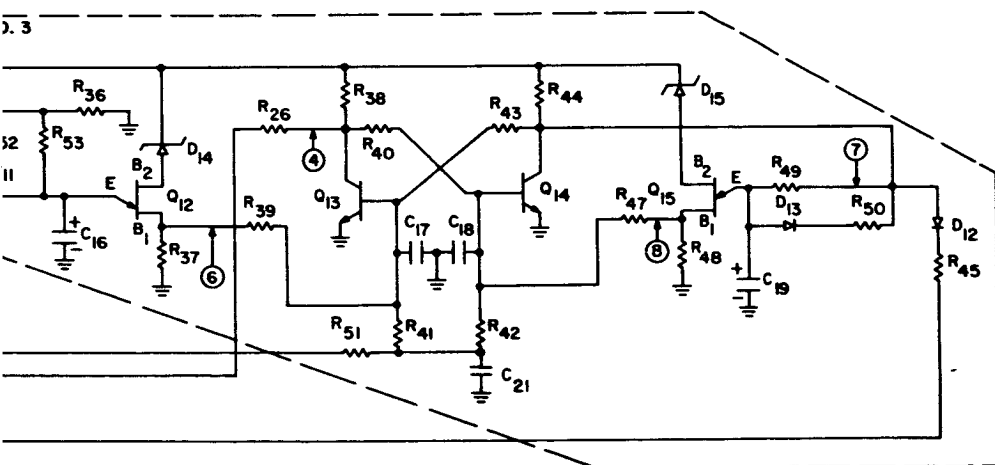
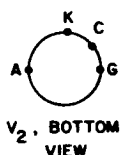


Figure 3-25. SPET Power Supply Schematic

Table 3-15. Spet Power Supply Component Parts List

RESISTORS (All resistors are RC07 unless otherwise specified)				CAPACITORS			TRANSISTORS		DIODES	
Designation*	Value (ohms)	Designation*	Value (ohms)	Designation*	Value (ohms)	Designation*	Value (μ uf)	Voltage Rating	Designation*	Type
R1	10M	R22(RC20)	15	R43	330K	C1	0.0047	35v150D	Q1	2N930
R2	1M	R23(RC20)	15	R44	47K	C2	0.01	35v150D	Q2	2N930
R3	82K	R24(RC20)	1M	R45	3M	C3	1	35v150D	Q3	2N2605
R4	1M	R25(RC20)	1M	R46	100	C4	GE619x22			
R5	200K	R26	Selected 470K-NOM	R47	100K	C5	4.7	35v150D	Q4	2N3354
R6	68K	R27	10K	R48	47	C6	4.7	35v150D	Q5	2N264
R7	Deleted	R28	47K	R49	Selected 330K-NOM	C7	4.7	35v150D	Q6	2N708
R8	24K	R29	Selected 5.6K-NOM	R50	47K	C8	4.7	35v150D	Q7	2N1132
R9	15K	R30	47K	R51	100	C9	4.7	35v150D	Q8	2N3421
R10	Selected SIR NOM	R31	100	R52	47K	C10	Sprague 103P6		Q9	2N2346
R11	100	R32	100	R53	Selected 330K-NOM	C11	Sprague 103P6		Q10	2N2647
R12	270	R33	100	R54	10M(1/2W)	C12	0.0056	35v150D	Q11	2N930
R13	1K	R34	1M			C13	Sprague 103P6			
R14	33K	R35(RC20)	10			C14	6.8	35v150D	Q12	2N2647
R15	620	R36	22K			C15	100	20v150D	Q13	2N930
R16	1.2K	R37	47			C16	15	20v150D	Q14	2N930
R17	100K	R38	47K			C17	1000pfc-15 <sup>c</sup> 102K		Q15	2N2647
R18	10	R39	100K			C18	1000pfc-15 <sup>c</sup> 102K		TRANSFORMERS	
R19	Deleted	R40	330K			C19	47	35v150D	T1 Tresco YT021	TUBES
R20	470	R41	3M			C20	47	35v150D	T2 Tresco YT022	V1 GVIA - 2000 Victoreen
R21	47	R42	3M			C21	47	35v150D	T3 Tresco YT023	V2 KNG - EG&G

\*Component designations refer to Figure 3-25, SPE T Power Supply Elect'ic Schematic

The resonant charging circuit is shown in Figure 3-26. A switched load is shown since resonant charging has the greatest advantage in a system where a capacitor is cycled between full charge and nearly full discharge, and in the SPET unit. Note the polarities of the battery, transformer, and diode; these polarities are such that  $i_1$  and  $i_2$  do not flow simultaneously. Operation is as follows:

- Switch  $S_1$  closes at  $T_1$  and current  $i_1$  flows according to  $i_1 = \frac{V_1}{L_{N1}} t$ , assuming negligible series resistance.
- At time  $T_2$  ( $t = T_1 - T_2$ ),  $S_1$  opens. At this instant there is energy stored in the magnetic field of  $N_1$  which is  $\frac{1}{2} L_{N1} (i_1 \text{ peak})^2$ .
- This energy is delivered to  $C_1$  in a period of time determined by the turns ratio  $\frac{N_2}{N_1}$ , the peak primary current  $i_1 \text{ peak}$ , and the charge on the capacitor. It is important to note the peak secondary current  $i_2$  is  $(i_1 \text{ peak}) \times \frac{N_1}{N_2}$ . Because no resistance is required to limit the peak value of  $i_1$  or  $i_2$ , the theoretical limit efficiency is 100%.

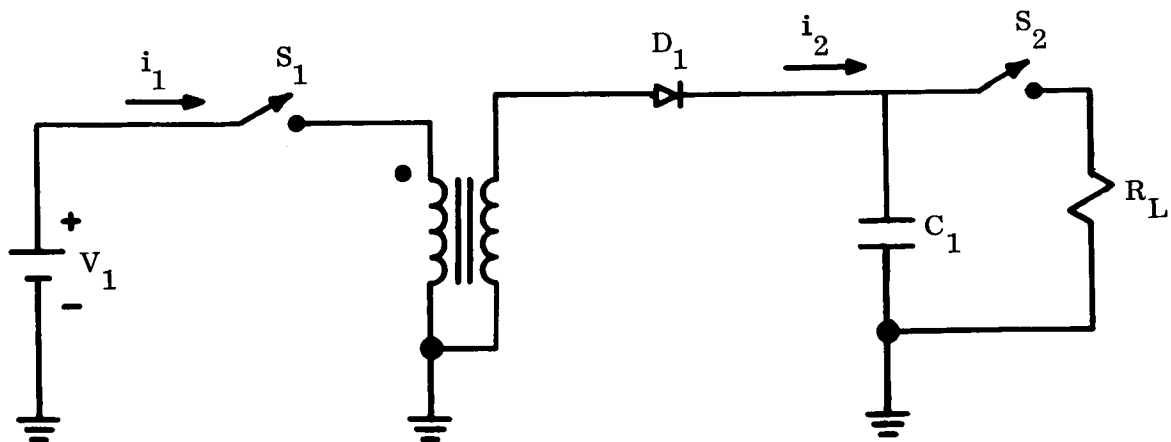


Figure 3-26. Resonant Charging Circuit

For high efficiency in a practical design, attention must be paid to:

- a. Switch losses
- b. Core losses
- c. Wire losses
- d. Distributed capacitance in  $T_1$  windings
- e. Leakage inductance in  $T_1$
- f. Diode voltage drop and reverse leakage.

Resonant charging has one other important characteristic. There is no fixed relationship between the primary power voltage  $V_1$  and the voltage that can be developed across the storage capacitor. A closed loop voltage regulation system is therefore a necessity. For efficiency, its feedback current requirement must be small.

Special components used in the SPET system are listed as follows:

- a. Thyratron. The thyratron in the SPET power supply is a 4-electrode, cold cathode, low pressure gas filled type. It includes a source of ionizing radiation (nickel 63) which reduces trigger requirements and results in low sensitivity to ionizing radiation from without its envelope.

Note: The manufacturer of the thyratron is Edgerton, Germeshausen, and Grier Inc., and its trade name is Krytron. The model KN6, used in SPET, has been used in space vehicles and is flight proven. Under SPET operating conditions, the lifetime of the Krytron is expected to be about 100,000 operations. General Electric, with the aid of a vendor, has initiated development of a long life thyratron for use specifically on the SPET application.

- b. High Voltage Reference. The high voltage reference is a corona voltage regulator manufactured by Victoreen Instruments. The GVIA model, trade named Corotron, is space flight proven. Operating life in SPET service is expected to be in excess of five years.

- c. High Voltage Diode. This is a standard General Electric part and has controlled avalanche characteristics for highest reliability.
- d. Energy Storage Capacitor. General Electric manufactures this as a special item. It is a mylar dielectric type which has been tested beyond 1,000,000 operations in SPET service.
- e. Operating Conditions. In normal operation the SPET units require 20 ma average current; 36 ma peak current. The load is unbalanced with the -12 volt input requiring about 16 ma average. All flight units operate in the range of one shot every 4 to 5 seconds.

Telemetry is derived in such a way that output voltage is approximately inversely proportional to power demand. Only one telemetry signal is produced but it is available at two connector pins. Both outputs can be used to obtain more frequent readout.

Telemetry output is:

+1.8  $\pm$  0.35 volts - Normal operation

+3.3  $\pm$  0.35 volts - Conductance mode

+4.5 to +5.0 volts - Open mode. Power demand is low. Unit may be left on.

+0.2 to 0.0 - Abnormal operation. Power input is probably excessive. Remove power.

The first generation of firing circuits represented by the SPET prototype subsystems described above and by laboratory test units are not optimum with respect to the requirements discussed. Primarily, the availability of components as related to a compressed time schedule for engine development and experimental evaluation of engine performance has prevented firing circuit optimization. Furthermore, firing circuit optimization depends to great extent on engine size and envelope configuration which in turn depend on the engine operating requirements for a particular application. Preliminary efforts in pursuit of this goal have been made including discussions with vendors interested in tailoring components for the SPET application.

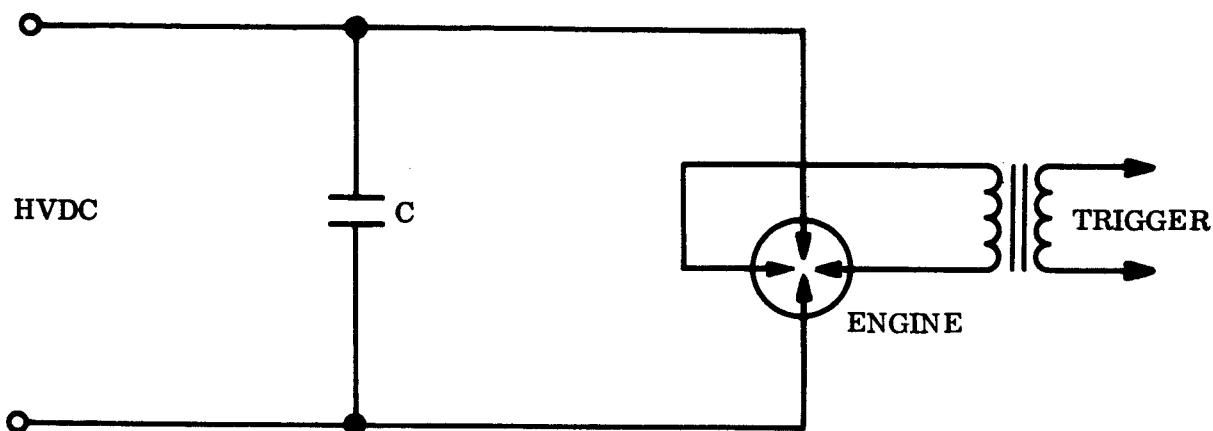


Figure 3-27. Internal Trigger Firing Circuit

SPET POWER SUPPLY

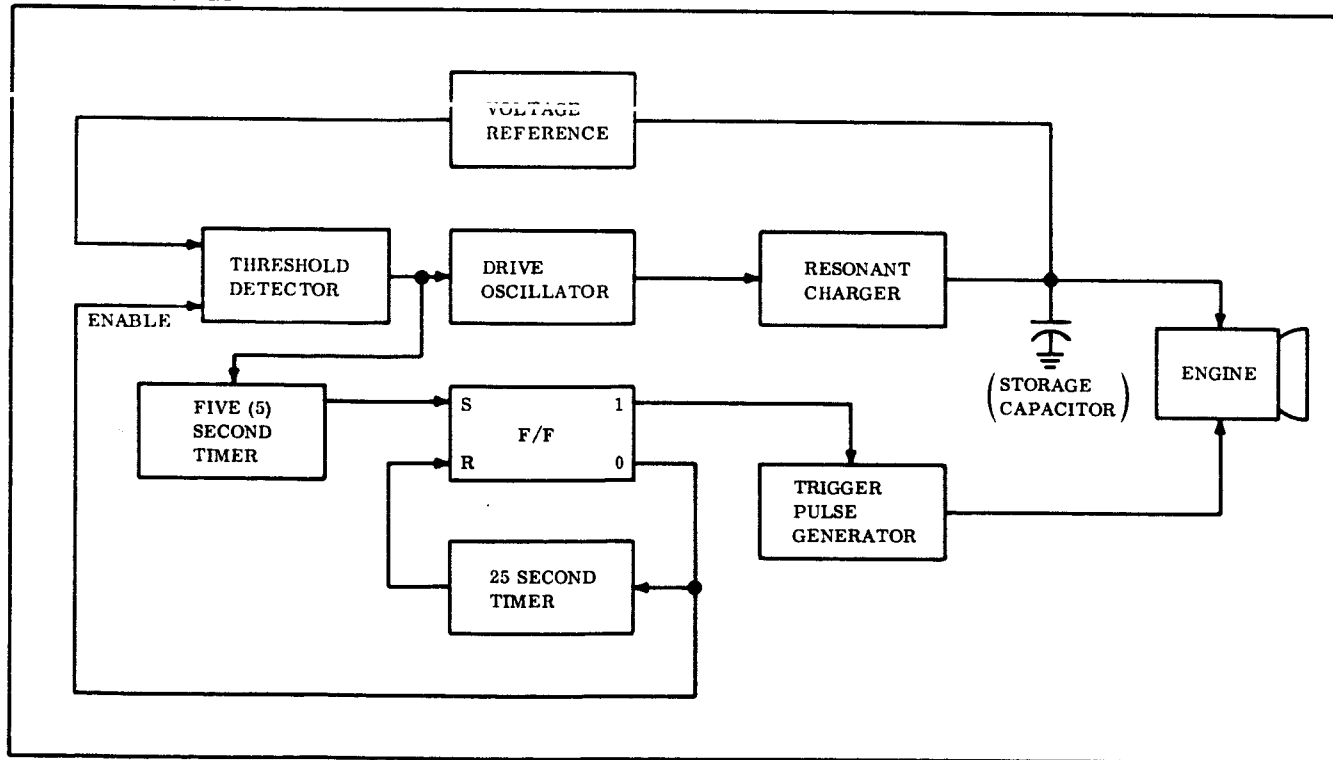


Figure 3-28. SPET Power Supply Block Diagram With Internal Trigger Engine



An alternate approach to the solution to the current tube life problem is to eliminate the tube by performing the switching function within the engine itself. The feasibility of this approach has been demonstrated in the laboratory. An auxiliary pair of electrodes is added to the basic SPET engine and physically arranged to initiate the main discharge by vaporizing a small quantity of propellant at low energy between the main electrodes. The same type trigger circuit is employed as for the cold cathode thyatron. In the SPET circuit in common use, two electrodes are connected in series with a capacitor and a cold cathode trigger tube. The cold cathode tube is ignited by a trigger obtained by stepping up a small 0.03 joule capacitor discharge. This energy is thus 3% of the one joule involved in the main discharge across the electrodes (1 joule).

The presence of the switching tube is justified by the fact that it permits to apply to the film of propellant a voltage well above its breakdown value. In this manner the pyrolyzing and electrolyzing effects ("precooking") which the application of a lower voltage would have on the propellant are minimized. As a matter of fact, SPET engines employing only one set of two electrodes have been run for the duration of one to two days in the self-triggering mode. This mode is obtained by connecting the electrodes directly to the main power capacitor. The firings are then controlled by the charging time of the R. C. circuit and by the propellant feed rate. Both the energy efficiency and the propellant deposit situation suffer in this case by the fact that voltages below those of the breakdown value are applied to the propellant.

A way of eliminating the switching tubes without incurring the "precooking" problem has been successfully demonstrated. The same small energy pulse which was previously applied to the grid of the switching tube is now made to appear across two small triggering electrodes in contact with the propellant film as shown in Figure 3-27. This causes the propellant to vaporize in a small amount which is sufficient to switch the main discharge across the exploding-accelerating electrodes. Furthermore, these electrodes are now no longer in contact with the propellant film but are switched on to the film by the vaporized charge. In this manner, the "precooking" is eliminated. The block diagram of a subsystem utilizing this engine concept would be modified to that shown in Figure 3-28.

The advantages that accrue with this scheme are several:

- a. The efficiency is increased because the cold cathode tube has a dc resistance of approximately 1.5 ohm which is three times as great as the engine's resistance. Furthermore, when a cold cathode trigger tube is used longer leads are required, which further add to the resistance and inductance of the external circuit. These additional sources of losses can also be eliminated. As a result, the efficiency of the engine can be almost doubled.
- b. The problem of short tube life as a source of failure of the engine is eliminated.
- c. Because the accelerator electrodes are now uncoupled from the fuel breakdown process, greater flexibility in design and in operating conditions (larger variation in thrust and specific impulse) is made possible.
- d. The triggering electrodes operate at low power and moderate rate of current change. The problem of designing them for long life is thus of greatly smaller magnitude. The only major problem foreseen which is unique to this design is the maintenance of adequate insulation between the main electrodes which depends primarily on residue formation and conceivably on fuel wetting on surfaces common to the two main electrodes.

### 3.5.2 POWER PROFILES

The electrical input power characteristic of a typical prototype SPET subsystem, as defined by the schematic diagram shown in Figure 3-29, is a periodic function with a frequency corresponding to the engine firing rate. Since the subsystem is designed to operate from a constant DC voltage supply, the input power characteristic follows the input current characteristic. The current (or power) characteristic can be approximated by rectangular pulses as shown in Figure 3-29.

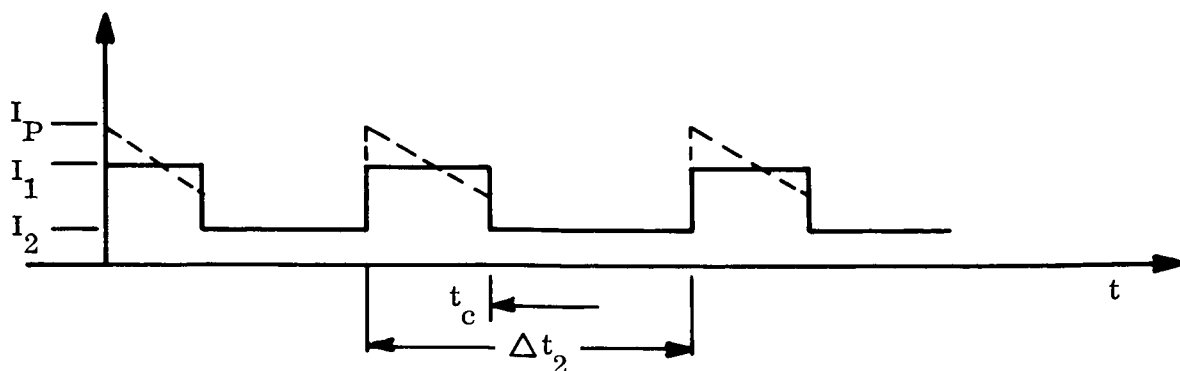


Figure 3-29. Characteristic Current Pulses

The actual current characteristic has trapezoidal portions as indicated by the dashed lines. This characteristic is primarily established by the cycling of the resonant charging circuit of the power conditioning; the decreasing current results from the decrease in load as the capacitor charges.  $I_1$  is the average input current of the subsystem during the charge time,  $t_c$ , of the power conditioning. Note that  $t_c$  can be expressed in terms of the firing cycle period  $\Delta t_2 = t_w + t_p$  as  $K(t_w + t_p)$  where  $0 < K < \frac{t_w}{t_w + t_p}$  consistent with the terminology of Appendix D.

$I_2$  is the average current representing overall circuit operating currents during the firing cycle period  $\Delta t_2$ . Some filtering has been employed in the existing prototype subsystems to limit the peak current,  $I_p$ .

With the input current characteristic thus defined and with a DC supply voltage,  $V$ , the average input power at a constant firing rate can be expressed as

$$\overline{P}_i^* = V \left[ \frac{I_1 t_c + I_2 (\Delta t_2 - t_c)}{\Delta t_2} \right]$$

or

$$\overline{P}_i^* = V \left[ \frac{t_c}{\Delta t_2} (I_1 - I_2) + I_2 \right]$$

The corresponding input energy per cycle is:

$$\overline{E}_i^* = P_i T = V \left[ t_c (I_1 - I_2) + I_2 \Delta t_2 \right]$$

The portion of the input power required for charging the energy discharge capacitor is seen to be

$$\overline{P}_c^* = V \frac{t_c}{\Delta t_2} (I_1 - I_2)$$

and the corresponding input energy per cycle

$$\overline{E}_c^* = \overline{P}_c^* \Delta t_2 = V t_c (I_1 - I_2)$$

The energy stored in the firing circuit discharge capacitor,  $C_s$ , when charged to a voltage,  $V_s$ , during each cycle is

$$\overline{E}_s^* = 1/2 C_s V_s^2$$

corresponding to an average power of

$$\overline{P}_s^* = \frac{\overline{E}_s^*}{\Delta t_2} = 1/2 \frac{C_s V_s^2}{\Delta t_2}$$

The efficiency,  $\eta_{p_c}$  of the power conditioning circuit up to the energy storage capacitor is, neglecting bias and auxiliary circuit power,

$$\eta_{p_c} = \frac{\overline{P}_s^*}{\overline{P}_c^*} = \frac{\overline{E}_s^*}{\overline{E}_c^*} = 1/2 \frac{C_s V_s^2}{V t_c (I_1 - I_2)}$$

With bias and auxiliary power included, the subsystem efficiency at the energy storage capacitor is

$$\eta_{pc} = \frac{P_s^*}{P_i^*} = \frac{E_s^*}{E_i^*} = 1/2 \frac{C_s V_s^2}{V [t_c (I_1 - I_2) + I_2 \Delta I_2]}$$

The efficiency of the engine firing circuit,  $\eta_e$ , is now required to determine the overall efficiency of a SPET subsystem  $\eta$  and the output power  $\bar{P}_{EX}^*$ .  $\eta_e$  can be determined from the ratio of the engine exhaust kinetic energy per pulse to the electrical energy discharged per pulse exhaust kinetic energy per pulse,  $E_{EX}^*$ , being calculated from measurements of engine impulse,  $i$ , and specific impulse  $I_{sp}$  as

$$E_{EX}^* = \alpha i I_{sp} \text{ where } \alpha \text{ is a dimensional constant depending on the system of}$$

units employed. Since the energy discharged is the energy stored in the capacitor the engine firing circuit efficiency is

$$\eta_e = \frac{\bar{E}_{EX}^*}{\bar{E}_s^*} = \frac{\alpha i I_{sp}}{1/2 C_s V_s^2}$$

The overall subsystem efficiency is then

$$\eta = \eta_{pc} \eta_e = \frac{\alpha i I_{sp}}{V [t_c (I_1 - I_2) + I_2 \Delta t_2]}$$

The output power of the engine exhaust  $\bar{P}_{ex}^*$  in terms of input power  $\bar{P}_i^*$  and subsystem efficiency  $\eta$  is

$$\bar{P}_{ex}^* = \eta \bar{P}_i^*$$

and in terms of engine exhaust kinetic energy per pulse is

$$\bar{P}_{ex}^* = \frac{\alpha i I_{sp}}{t_2}$$

It should be noted the SPET subsystem output power as defined by the engine exhaust power  $P_{EX}$  is of little value as a design parameter or as a measurement of performance; impulse or average thrust as functions of electrical input power are more useful parameters.  $\overline{P}_i^*$  and  $\overline{P}_{ex}^*$  represent average powers but as derived above are based on a single firing cycle. A more rigorous derivation of the average powers can be made utilizing a summation over a train of  $n$  pulses as done for the case of average thrust given in Appendix D.

This would lead to average powers expressed as a function of a constant firing cycle period as follows:

For the input power:

$$\overline{P}_i = VI_2 + \frac{V T_c}{T_w + T_p} \cdot (I_1 - I_2)$$

$$\text{where } T_c = \sum_j^n (t_c)_j = K \sum_j^n (t_w)_j + K \sum_j^n (t_p)_j = K (T_w + T_p)$$

for the power delivered to the energy storage capacitor:

$$\overline{P}_s = \frac{\eta C_s V_s^2}{Z (T_w + T_p)}$$

for the output power of the engine exhaust:

$$\overline{P}_{ex} = \alpha \overline{F} I_{sp}$$

where

$$F = \frac{\sum_j^n (i)_j}{T_w + T_p}$$

If average time periods are defined as  $\bar{t}_w = \frac{T_w}{\eta}$ ,  $\bar{t}_p = \frac{T_p}{\eta}$  and  $\bar{t}_c = \frac{T_c}{\eta}$ ,

$$\bar{P}_i = V I_2 + V \frac{\bar{t}_i}{\bar{t}_w + \bar{t}_p} (I_1 - I_2)$$

$$\bar{P}_s = \frac{1}{2} \frac{C_s V_s^2}{\bar{t}_w + \bar{t}_p}$$

$$\bar{P}_{ex} = \frac{\alpha \sum_j^n (i)_j}{n (\bar{t}_w + \bar{t}_p)} I_{sp} = \frac{\alpha \bar{i} I_{sp}}{\bar{t}_w + \bar{t}_p}$$

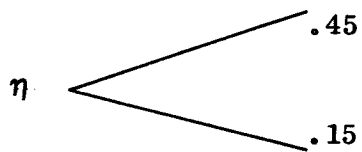
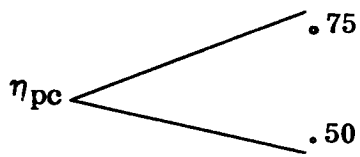
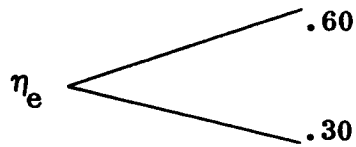
where

$$\bar{i} = \frac{1}{n} \sum_j^n (i)_j$$

is the average impulse per firing cycle. The restriction that  $\bar{t}_w + \bar{t}_p > \bar{t}_c$  must of course be enforced to maintain validity of these expressions.

The terms in the expression for input power  $P_i$  having  $I_2$  coefficients represent the constant bias power for power conditioning and trigger circuitry plus the power required for any auxiliary logic and telemetry circuits which may be included in a SPET subsystem. The  $I_2$  terms will therefore remain essentially constant for a broad range of total subsystem power. Obviously if the total subsystem input power is limited by specification to levels approaching the bias and auxiliary circuit power, the subsystem efficiency will be poor. It can also be seen from the expression for  $P_i$  that the degrading of efficiency by  $I_2$  is more severe when the firing cycle time period  $(\bar{t}_w + \bar{t}_p)$  is long compared to the charge time,  $\bar{t}_c$ , since the power loss represented by the  $I_2$  terms is constant and independent of  $\bar{t}_c$  whereas the useful power is proportioned to the firing cycle time.

A subsystem design including power conditioning, firing circuitry and bigger timing circuitry optimized within practical design limitations is estimated to be capable of providing efficiencies in the ranges shown below:



These efficiencies can be realized providing that input powers above 0.5 watts are permissible. Below 0.5 watts input power, circuit bias power requirements become a significant power loss.



### 3.6 PROPELLANT AND FEED CONSIDERATIONS

Before discussing the several aspects involved in the development of a successful combination of a feed and propellant system for the SPET, it is appropriate to formulate a set of preliminary criteria to be used in the selection of the working fluid:

- a. Fluidity or the capability of migrating under suitable fields of forces, in the storage condition
- b. For the surface action scheme, adequate tension and wetting properties in the storage conditions
- c. Low vapor pressure in the storage condition
- d. High Density in the storage condition
- e. Low energy required for the change of phase
- f. Low Electrical breakdown potential
- g. Low molecular weight (or better high heat capacity) in the gaseous state
- h. Absence of stable solid phases (i.e., easily and fully gasifiable)
- i. High exothermic energy content in the decomposition and/or reaction processes
- j. Low flash-back tendency
- k. Low and similar ionization potentials for the gaseous phases

The relative importance of these criteria changes with the particular form of the SPET system which, in turn is dictated by the characteristics of the application.

A number of "first generation" propellants were developed using those components which would simplify handling and preparation procedures. Dispersions of powdered aluminum metal have been prepared using silicone oils SF-96 of various degrees of viscosity as the carrier.

A 50/50 by weight dispersion of aluminum powdered metal in SF-96 No. 50 viscosity was found satisfactory and its physical properties used empirically to determine the geometry of a feeding plug. This plug was fabricated by means of molding a thermo setting epoxy. The resulting plug contained a row of ten tapered capillary tubes with diameter varying from 20 to 8 mils of an inch. The face of the plug containing the smaller end of the tapered tubes was covered with two glass plates 6 mils thick forming a channel (trough) 3 mils wide and 250 mils long. The monotonically decreasing mean radius of curvature of the passages constituted by the tubes and the trough drives the propellant dispersion by capillary action until a stable configuration of the free liquid surface is reached. This configuration is obtained when the trough is filled with fluid for its entire length. In this manner a ribbon of propellant is brought to establish contact with two appropriately located electrodes. Electrical breakdown is then caused by the application of a potential differential which can be as low as 600 volts.

No sign of ablation or of any other damage was observable on the surface of the plug exposed to the electrical discharge proving the principle of ablative protection which is one of the key features of the scheme. To facilitate manufacturing, plastic plates were used to form the feed throughs in the subsequent manufacturing of plugs. These also showed no trace of any damage after several tens of thousands of firings.

A qualitative demonstration of the stability of the feed formation was achieved by having basically the same number of firings out of the same plug fired with successive fuel loadings.

Further in a second test an engine was fired intermittently during a storage period of over ten days in the vacuum chamber at a pressure held at  $10^{-7}$  mm of hg. During the firing periods of the order of a few hours, however, the pressure reached the  $6 \times 10^{-6}$  mm hg range.

In conclusion the principles and several interconnected phenomena used in the feeding scheme were properly predicted in a preliminary design which succeeded in a convincing demonstration of feasibility.

A development program was then conducted to produce storage and feed system of 20 to 250 cc capacity, adequate for propulsion times from few months to few years duration at the propellant flow rates of 1/3 to 3  $\mu$ gm/sec with propellants of specific gravity close to unity. The development of systems of higher capacity is a straight forward task.

The specific forms of the schemes employed are several comprehending nested cones--capillary tubes, radial blades center wicks combinations, and a single axial symmetric monotonically decreasing channel with a wick or capillary tube arrangement.

The systems developed have an acceptable degree of control and stability. Further work is required, by all means, to establish better defined design criteria with particular emphasis on the interaction of the feed and ablation phenomena.

The only problem item, brought to light in this initial phase of the program has been that of deposit formation. This is due to the presence in the carrier of constituents of high chemical stability, not easily gassifiable and of higher ionization potential than the seeding metal. As a consequence, they tend to be bypassed by most of the energy in the discharge and most of the electromagnetic ponderomotive forces. This results in the return to the solid or liquid state of a residue of those stable components leading to a formation of deposits. For the case of the silicone carrier the deposits have the aspect of gummy and occasionally glassy deposition on the lower part of the acceleration channel and on the plug surface. On the other hand they did not impede the operation of the device. The engine stopped firing

only when the capillary tubes were depleted of metallic dispersion.

To eliminate the very stable  $\text{Si O}_2$  radical present in the silicone oil, a substitution of a hydrocarbon was made for the carrier. A dispersion of the aluminum metal in Apiezon oil was used. This resulted in a carbon like powder deposit with the occasional formation of an elastic brown looking film.

For the purpose of eliminating this latter deposit and improve also the breakdown and specific heat characteristics of the propellant a new dispersion was made in the same carrier using aluminum metal and lithium hydrides and aluminum lithium hydrides.

Some lithium dispersions were made by dissolving the metal in liquid ammonia and pouring this into a precipitating substrate followed by evaporation of the ammonia. The latter procedure gave dispersions in which the metal tended not to settle. Some examples of dispersion made and successfully tried in the thruster in the preliminary experiments are:

- a. Aluminum powder (18 M) in Apiezon oil or silicone oil SF-96-(50).
- b. Lithium Hydride and aluminum metal powder (18 M) in Apiezon or silicone oil SF-96-(50).
- c. Lithium aluminum hydride powder in Apiezon oil.
- d. Colloidal lithium precipitated from liquid ammonia in Apiezon oil.

The above mixtures were made by concentrations of about 50% by weight of powder in oil. They had adequate capillary action and performed satisfactorily in the early experiments.

The main problems encountered with these techniques have been in the selection of a compatible oil with adequately low vapor pressure, the tendency of the dispersions to settle and/or conglomerate, and the deposit of residues in the thruster by the propellant after

many firings. The deposition characteristic was sensibly improved but the deposits (especially those of carbon) were not totally eliminated.

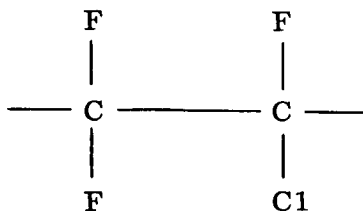
The following phase of the program which was directed to the development of laboratory and engineering prototypes of the system did produce a number of advanced propellants using different carries, ultrafine, and colloidal dispersions and solutions of metallic salts.

Some of the propellants identified, tested, and used in this phase were:

Fluorlube MO-10

- a. Formula  $(CF_2CFC1)_x$
- b. Average molecular weight - 670
- c. Pour point -  $40^{\circ}F$
- d. Density @  $100^{\circ}F$  - 1.895 g/cc  
                   @  $160^{\circ}F$  - 1.840 g/cc
- e. Vapor pressure @  $100^{\circ}F$  - 70 microns Hg  
                                   @  $160^{\circ}F$  - 600 microns Hg
- f. Viscosity @  $100^{\circ}F$  - 18 cs.  
                   @  $160^{\circ}F$  - 5 cs.  
                   @  $100^{\circ}F$  - 35 cps  
                   @  $160^{\circ}F$  - 9 cps
- g. Surface tension @  $77^{\circ}F$  - 23 dynes/cm

Fluorlube is a non-reactive linear polymer built up of a recurring unit which is



It has high electrical resistivity and dielectric strength, properties which do not indicate that it would make a good fuel. Its relatively high vapor pressure also diminishes its usefulness. Other grades of fluorolube are available with lower vapor pressures, but there is a corresponding rise in pour point temperature and viscosity.

Fluorolube	S-30	T-80
Pour point, °F	5	35
Vapor pressure @ 100°F,	15	5
Microns Hg		
Viscosity @ 100°F, cs	100	500

Favorable factors for use of fluorolubes are its chemical stability, no special handling procedures are necessary; its low surface tension and ability to wet surfaces readily; its lack of attack toward metals and other materials; and its safety lack of toxicity and its low cost.

#### Polyglycidalnitrate (PGN)

- a. Formula  $\text{HO} - \text{CH}_2 - \text{CH}(\text{OONO}_2) - \text{O} - n(\text{CH}_2)_3\text{CH}_2\text{OH}$
- b. Average molecular weight -  $n(119.08) + 90.12$
- c. Pour point - mixture of 10% Al powder and PGN 1010 -  $-25^\circ\text{F}$
- d. Density @  $15^\circ\text{C}$  - 1.3-1.4 g/cc
- e. Vapor pressure - unknown but low
- f. Viscosity @  $25^\circ\text{C}$  - 5750 cps
- g. Surface tension - unknown

PGN is a polymer of glycidal nitrate with the formula shown above. Although no data is available on the vapor pressure, it is known to be low. Material with an equivalent molecular weight was distilled in our laboratory using a molecular still. Pressures below one micron of Hg at temperatures above  $200^\circ\text{C}$  were observed.

Polypropyleneglycol 1025 and 2025

a.	Formula	$\text{HO} \leftarrow \text{CH}_2 - \overset{\text{CH}_3}{\underset{ }{\text{CH}}} - \text{O} \rightarrow$	$n$
b.	Average molecular weight	- 1025	-2025
c.	Pour point	- 39°C	-32°C
d.	Density @ 20°C	- 1.007 g/cc	-1.005 g/cc
e.	Vapor pressure @ 20°C	- .01 mm Hg	-.01 mm Hg
f.	Viscosity @ 100°F	- 200 cps	-438 cps
g.	Surface tension	-unknown	

Polypropyleneglycol is a polymer of the basic structure shown above. The material with certain additives has been used as a fuel for the SPET engine with varying degree of successes. The material has been stripped of volatile material in our laboratory on a molecular still with pressures as low as 0.1 micron at 200°F. Additives used with this material have been lithium perchlorate and aluminum powder.

### 3.7 HIGH ENERGY PROPELLANT FOR SPET-D

Investigation of high energy organic and inorganic propellant using additives aimed to complete gassification of the carrier and able to operate in the detonating mode (SPET-D) have been conducted with varying degree of success.

For applications where added thrust is needed at minimum drain on electrical power, engines designed to make use of the chemical combustion energy of special fuels can be used. In one case the SPET engine design of fuel feed and vaporization is used. The fuel is selected to produce vapors in the electrical discharge, which will detonate in the chamber adding much thrust to the engine. During test of SPET engines several occurrences of the detonation mode of operation have been observed. To further develop this concept, fuels need to be obtained and engines designed and fuel-engine systems tested. Many complex chemical, kinetic, and physical factors are involved. To help understand these, fundamental studies of liquid and solid phase have been conducted. Their discussion is given in other sections of this document.

Chemically speaking, there are a wide variety of explosive compounds which might be suitable for test. The main problem is to develop one which will provide the right gas phase ingredients to detonate after vaporization by electrical discharge.

#### 3.7.1 SPET-D FUEL CONCEPTS

##### Wafers

This solid state fuel concept requires alternating layers of detonable material with a layer of "inert" material to prevent propagation of the detonation down the stack. Definite leads to such a system have been developed. The practical advantages permitted by this approach are: The possibility of precisely measuring the amount of propellant used per shot and the reduction of back flash effects especially important in the early stages of a hardware program. In this manner some of the most formidable difficulties in mass metering, impulse measuring and handling of potentially hazardous material are minimized during the initial learning



stages. The need of special equipment and the enforcement of strict safety measures are bypassed.

From a final product standpoint the thin wafer concept may also develop into devices of extreme simplicity capable to deliver large impulses in the number of several thousands. They may be eminently suited for short duration applications such as evasive or emergency maneuvers of spacecraft, final corrections, of re-entry vehicles and anti-discrimination maneuvers of decoys.

The laboratory demonstration of the wafer concept has been successfully accomplished by the electrically triggered detonation of metallic films coated with lacquered KDNBF explosive. Discussion of this phase is covered in Appendix F of this report.

#### Gases or Volatile Liquids

The concept of using gases or volatile liquids like water, ammonia, or hydrazine is attractive from the lack of residue and energy standpoint, but poses problems from the standpoint of evaporation in space and handling and metering.

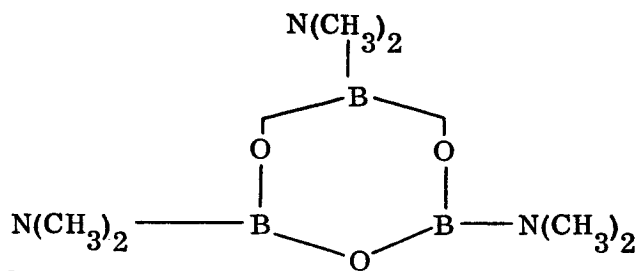
The best approaches to a passive system for dealing with the evaporation problems of volatile materials in a microthruster involve electrolytic gating or decomposition of solids or low vapor pressure liquids to yield the desired gases. Electrolytic gating means that one would deposit by electro-plating a metal in capillaries or pores to plug them up. Then, when firing was to be done, the deposits would be redissolved electrolytically allowing the gases to pass. The process should be reversible under the right conditions and even allow throttling by only partial dissolution or deposition.

The electrolytic decomposition of solids or low vapor pressure liquids to yield detonable gases is certainly feasible chemically, but may require more energy consumption than desirable. Energy balance calculations can be readily made for proposed systems to check their desirability. Hydrogen and oxygen could be produced for instance from a coordination compound which would tie up the water in a solid.

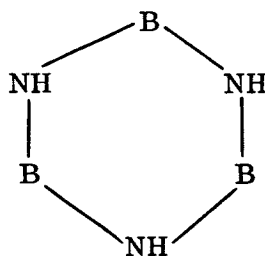
## Inorganic Liquid Fuels

A cursory look at the literature in the fields of boron and phosphorus chemistry indicated that the possibility of liquid inorganic compounds of low vapor pressure may exist. Although specifically suitable materials have not been located in the literature, the existence of compounds such as tris (dimethylamino) boraxole,

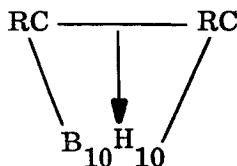
b.p.  $221^{\circ}\text{C}$



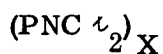
or borazene, b.p.  $53^{\circ}\text{C}$



or carboranes



or phosphoro nitrilic chlorides



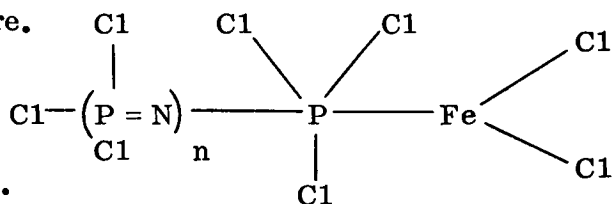
(where x may vary over a wide range)

leads us to believe that suitable compounds may exist or can be synthesized. The lower ionization potential, possibly higher electrical conductivity, and low average atomic weight of such compounds make them attractive SPET detonation engine fuels.

As a result of this literature search fairly extensive leads were established throughout the industry and the research centers. They succeeded in locating an ironchloride stabilized phosphonitrilic chloride and in obtaining samples of this material from the research center of the Dupont Company. The use of this propellant has extended the life of the SPET engine several folds. The characteristics of this propellant are:

- |                                     |                                    |
|-------------------------------------|------------------------------------|
| a. Formula                          | $(\text{PNC1}_2)_x \text{ FeCl}_3$ |
| b. Average molecular weight         | -1178                              |
| c. Pour point                       | $-51^\circ \text{F}$               |
| d. Density @ $25^\circ \text{C}$    | -1.92 g/cc                         |
| e. Vapor pressure                   | ?                                  |
| f. Viscosity @ $100^\circ \text{F}$ | -23.3 cs                           |
| @ $210^\circ \text{F}$              | -5.8 cs                            |
| @ $400^\circ \text{F}$              | -2.1 cs                            |
| g. Surface tension                  | ?                                  |

Iron chloride stabilized phosphonitrilic chloride is a thermally stable material with a wide fluid range. Its probable form is a nearly equimolar mixture of two polymers having the following structure.



While the vapor pressure and surface tension are not known, they are both low. The fluid, during preparation, is heated to  $450^\circ \text{C}/0.32 \text{ mm Hg}$  to remove any volatile components.

The fluid is subject to hydrolysis and precautions should be taken to exclude atmospheric moisture as much as possible. Another drawback to its use is its extremely high cost -

\$2,100 per pound, one pound minimum order.

No information is available on its compatibility with other materials nor on its toxicity, therefore it should be treated with caution shown all chemicals of unknown toxicity. In general, it is expected that since the material hydrolyzes to phosphoric acid and hydrochloric acid its compatibility with materials and toxicity will be similar to these acids. In other words, avoid getting it on the skin. Flush with water if contact is made accidentally.

#### Liquid Oxidizer and Reacting Liquid Fuels

Several explosive manufacturers have been contacted in a search for a liquid oxidizer with very low vapor pressures.

Negotiations were started with Aerojet--General Corp. and the Navy to obtain samples of high energy liquid fuels being made by Aerojet under Navy contract. Unfortunately the classified nature of these materials did not permit to make them available for this unclassified program.

### 3.8 PHYSIO-CHEMICAL CONSIDERATIONS OF SPET PROPELLANTS

A treatment of the SPET fuel and thrust phenomenon can be outlined and broken into three phases, which are summarized below:

- a. Film Breakdown - Disruption of film into high density, partially ionized gas.
- b. Plasma Formation - Increase of temperature and increased ionization.
- c. Expansion - Expansion of plasma due to heating followed by recombination and condensation.

One may identify some parameters associated with these phases: Phase I is governed both by the rate of energy dissipation due to  $I^2 R$  heating which is in turn dependent upon the sheet resistance of the fuel and by the energy required to overcome the film stability and cause a change of state. These include the specific heat of the liquid phase, the surface-free energy (especially important in high surface tension, extremely thin films) and the heat of vaporization. Phase II involved largely constant volume processes where the governing factor is the energy required to promote ionization and the degree of ionization achieved before the gas begins to expand (Phase III). Phase III is largely governed by ion-field interactions in a situation where ion density and temperature may drop radically due to re-combination, expansion or condensation effects.

One should have data of the following types to permit accurate calculations of thermal behavior.

Specific Heat - One may approximate the specific heat by assuming adherence to the Dulong-Petite law: Then

$$C_v = \frac{1/2 N(1.987)}{NW} \text{ cal/g}^\circ\text{C}$$

MW = average molecular wt (grs)

N = number of degrees of freedom:  $N_{\text{solid}} \approx 6$

$N_{\text{DIA. gas}} \approx 5$

$N_{\text{MDN. gas}} \approx 3$

Thus we may estimate  $C_v$  for  $N_{ak}$  as 0.21 and so forth for other materials.

Thus the energy required to heat a fuel from ambient ( $T_A$ ) to the point of vaporization ( $T_v$ ) is:

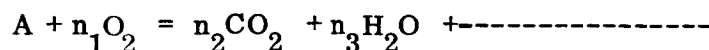
$$E_1 = \frac{(T_v - T_A) \frac{N}{2} (1.987)}{MW} \text{ cal/g}^\circ\text{C}$$

in the same way, the energy required in Phase II to heat the gas to some plasma temperature ( $T_p$ ), before expansion is:

$$E_3 = \frac{(T_p - T_v) \frac{N}{2} (1.987)}{MW^1} \text{ cal/g}^\circ\text{C}$$

where  $MW^1$  is the average molar weight of the gaseous species and N corresponds to the gaseous state (most probably nonatomic).

Heat of Vaporization - This may be gotten fairly easily if the heat of combustion is known. Thus, if



and the  $\Delta H$  for the reaction is known, then the knowledge of the  $\Delta H$  of formation for  $CO_2$ ,  $H_2O$ , etc. (all fairly simple) permits one to determine the heat of vaporization of the unknown, complex substance, A. Unfortunately, a search failed to uncover data of this sort for the fuels specified.

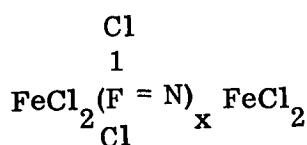
One may calculate  $E_2$ , the heat of vaporization directly by examining the individual bond energies. However, this treatment is handicapped by lack of knowledge of the exact structure of the fuels and the difficulty of making such calculations as the carbon chains lengthen. The reader is referred to "The Strength of Chemical Bonds" by T. L. Cottrell, Butterworths, 1954, for a more complete discussion of this point.

The determination of condensation products is nearly impossible due to the indication that electrical gradients present in Phase I are sufficient to break all chemical bonds and even, in some cases to preferentially strip electrons from inner shells. Thus condensation products depend more on the gas phase dynamics than on the original structures. Determination of structures of condensates must await further lucidation of gas conditions by detailed experiments.

In conclusion, due to the complexity of these fuels and the lack of research on the thermochemical properties of the chemicals, evaluation of fuels is perhaps better conducted by actual experiment than by detailed calculations of dubious merit. Table 3-16 gives a list of selective candidate fuels.

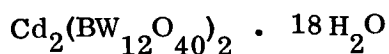
Table 3-16. Candidate Fuels

1. Phosphonitric Chloride



For MW  $\cong$  2,000,  $x \cong$  15

2. Cadmium Borotungstate



MW  $\cong$  6,600

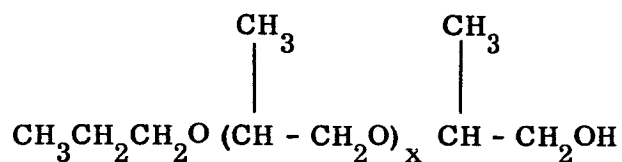
### 3. Fluorolube



For  $\text{mw} \cong 560$ ,  $x \cong 3$

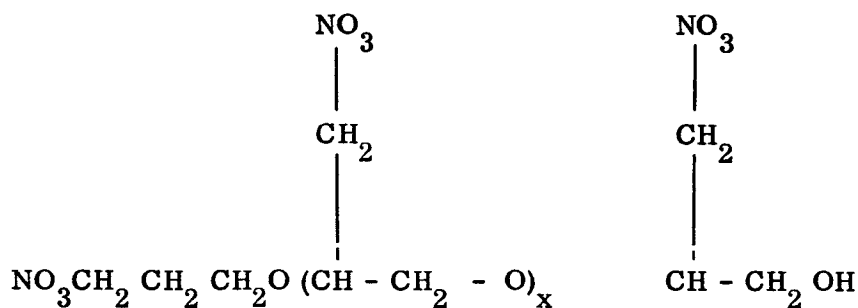
$C_v = 0.32$  (cal)

### 4. Polyoxypropyleneglycol (PPG) (with 10% by wt. $\text{LiClO}_4$ )



For  $\text{mw} \cong 2000$ ,  $x \cong 33$

### 5. Polyglycidynitrate (PPN) (with 10% by wt. $\text{LiClO}_4$ )



For  $\text{mw} \cong 2000$ ,  $x \cong 15$

### 6. Liquid Metals

Typically: NaK eutectic      - 78.28 wt % K  
    21.74 wt % Na  
 $C_v \cong .21$                       M.P. -  $12^\circ\text{C}$



7.  $\text{SbKC}_s$  eutectic

Wt %

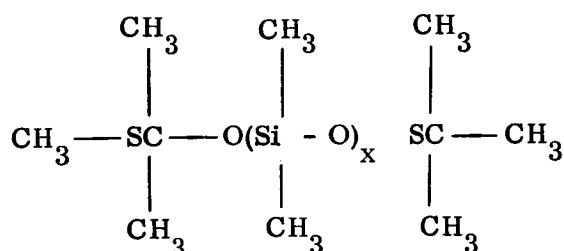
73%  $\text{SbCl}_3$

10%  $\text{KBr}$

17%  $\text{C}_s \text{Cl}_2$

$$\Delta H_{l-g} \cong 17.6$$

8. Silicone oil suspension



For mw  $\cong$  2000, x  $\cong$  25

with 30 wt % Al and 30 wt % Li

### 3.9 REFERENCES

1. Langan, W. T., Cresswell, J. D., and Browne, W. G., "Effects of Alabation Products on Ionization in Hypersonic Wakes", GE-MSD Tech. Inf. Ser. Rpt. No. 65SD208, January 25, 1965.
2. Wyllie, G., Proc. Roy. Soc. (London) 197A, 383 (1949).
3. Hirth, J., & Pound, G. M., J. Phys. Chem. 64, 619 (1960)
4. Paul, B., ARS J., 32, 1321 (Sept. 1962)
5. Erying, Henderson, Stover, & Erying, "Statistical Mechanics and Dynamics," p. 479, John Wiley & Sons, N. Y. 1964.
6. Penner, S. S., J. Phys. Chem., 56, 475 (1952).

7. Kucherov, R. Ya, and Pikenglaz, L. E., Soviet Phys. JETP, 37 (10), 88, (1960) (English Translation).
8. Vulliet, W. G., J. Chem. Phys., 41, 521 (1964).
9. Hirth, J. P., and Pound, G. M., "Condensation and Evaporation," Macmillan, 1963.
10. Frenkel, J., "Kinetic Theory of Liquids," Dover, 1955
11. Fisher, I. Z., "Statistical Theory of Liquids," University of Chicago Press, 1964, p. 169.
12. Slater, J. C., "Introduction to Chemical Physics," p. 328, McGraw-Hill, 1939.
13. LaRocca, A. V., "Parametric Performance Studies of Electrical Thrust Generators for Space Applications," Proceedings of Fifth Symposium of Ballistic Missile and Space Technology, Vol. II, Los Angeles, August 1960.
14. LaRocca, A. V., "Solid Propellant Electric Thrusters," AIAA Propulsion Joint Specialist Conference, Colorado Springs, Colorado, June 14-18, 1965.

**APPENDIX A**

**FLUID PHYSICS OF SPET IN THE DETONATION MODE**

**S. SCALA, B. HAMEL, AND P. GORDON  
SPACE SCIENCES LABORATORY  
MISSILE AND SPACE DIVISION  
GENERAL ELECTRIC COMPANY**

## 1.0 INTRODUCTION

From the point of view of satellite attitude control and station keeping requirements, it appears to be desirable to develop a long-lived microthruster which combines the use of a chemically active solid propellant with a pulsed electric discharge.

It is envisaged that the electric discharge will cause the propellant to be vaporized into a combustion chamber. If the propellant gas is injected into the chamber sufficiently rapidly, it will form a shock wave and will be ignited by compression heating, if the activation energy is sufficiently low. Once ignition occurs, the gas will proceed to undergo complete combustion if the chemical kinetics are sufficiently rapid. This concept which has been proposed by Dr. A. La Rocca and named the SPET<sup>\*</sup> will be investigated herein.

In analyzing theoretically the basic fluid dynamic and physicochemical phenomena associated with the SPET, one should perform an overall analysis which is comprised of certain key aspects. These include the study of the gas generation and combustion processes and the expansion of the resulting plasma into the ambient vacuum. Specifically, it is necessary to perform the following:

- a. Analysis of the Vaporization Process.
- b. Estimate of the species formed and their thermodynamic properties.
- c. Analysis of the time history of the development and structure of the very low density shock wave and its propagation down the chamber duct.

---

\* Acronym for Solid Propellant Electrical Thruster

- d. Analysis of the chemical kinetics of the chemical reaction and the development of the detonation wave and its propagation down the chamber duct.
- e. Analysis of the employment of a centerbody in order to increase the gas residence time, if this appears necessary.
- f. Analysis of the expansion of the combustion products into vacuum.

Of all these interrelated studies, the one requiring the greatest effort is item (d) since it requires the solution of a system of non-linear partial differential equations for the dependent variables, in which both time and space are the independent variables.

Fortunately, the general equations for continuum fluid mechanics, the Navier-Stokes equations, have recently been solved for the time-dependent one-dimensional flow of a compressible, viscous, thermally conducting gas (Reference 1). In considering the extension of the above approach to the analysis of the formation and propagation of a detonation wave within the SPET engine, it is clear that one must introduce additional terms and/or equations to account for the presence of more than one chemical species, to include the presence of molecular diffusion and to incorporate the effects of the chemical kinetics of the combustion process in converting chemical energy into internal and kinetic energy. This analysis is carried out in paragraph 3.0. In addition, the method of solving these equations is discussed and sample calculations are given.

An analysis of the solid propellant gasification process is given in paragraph 2.0, and the theoretical approach to the analysis of the expansion of the combustion products into vacuum is given in paragraph 4.0.

Where appropriate, consideration is given, of course, to the question of species which are present and their thermochemical properties. No analysis is presented herein of the effects of a centerbody, since it is only when one performs a parametric study of chamber

dimensions necessary for particular propellants that this consideration arises and is a relatively straightforward computation.

Finally, specific recommendations are given for future theoretical work.

## 2.0 THERMOPHYSICAL MODEL FOR SOLID PROPELLANT GASIFICATION PROCESS

As already mentioned, a vapor is generated by the release of electrical energy from the power supply and represents the initial conditions for the analysis of the detonation process. Hence, we are concerned herein with a consideration of the vaporization of the SPET fuel which is assumed to be a solid propellant, somewhat like polyoxi-propylene glycol.

In first approximation one could write:

$$\dot{m}_w(t) = \frac{\Delta E(t)}{\Delta H_{\text{vap}}} \quad (2-1)$$

which states that the mass rate of formation of combustible gas is simply the available electrical energy deposited in the solid divided by the heat of vaporization of the solid.

However, this represents a tremendous oversimplification since in fact, much theoretical and experimental work has been done on the phenomenon known as an "exploding wire", (Reference 2 and 3) which is very much related to the present problem. Moreover, a detailed study of non-equilibrium vaporization is given in Reference 4 and an analysis of the combined effects of transient heat conduction within a solid and surface mass transfer is given in Reference 5.

Therefore, it is recognized that the speed of the vaporization process is critically dependent upon the rate of energy delivery to the propellant and the resulting rise in propellant temperature. Experimental observations show that the behavior of the solid propellant can range from "slow burining" to explosive ablation. This leads to the definition of an electrothermal time constant, which is the time for a temperature equal to the "boiling point" to penetrate to a depth  $x/e$ , (Reference 2 and 3).

Analysis (Reference 4) shows that we may write the equation for the vaporization kinetics in the form:

$$\dot{m}_w(t) = \frac{\alpha M_p}{\sqrt{2 \pi M_p R T_p}} \left( P_p - P_{p \text{ eq.}} \right) \quad (2-2)$$

where  $\dot{m}_w$  is the mass rate of propellant vaporized per unit area, per unit time,  $\alpha$  is the vaporization coefficient,  $M_p$  is the molecular weight of the vaporizing propellant,  $P_p$  is the actual vapor pressure of the propellant, where the subscript eq. denotes equilibrium.

It is important to observe that since we are dealing with non-equilibrium vaporization, a knowledge of a  $\alpha$  becomes critical. However, the essential theoretical difficulty has now been converted into a problem in which one must specify the relationship between the time rate of flow of electrical energy through the propellant and the corresponding rise in temperature of the propellant.

The heating of the solid propellant, is given by  $I^2 R(t)$  where the instantaneous resistance is

$$R_w = \frac{V_w - L_w \frac{dI}{dt}}{I} \quad (2-3)$$

where  $R_w$  is the resistance of the propellant,  $V_w$  is the voltage across it,  $L_w$  is the wire inductance,  $I$  is the current and  $dI/dt$  is the rate of change of current. This equation must be solved simultaneously with the electrothermal equation for the propellant. In general terms this may be written.

$$\rho C \frac{\partial T}{\partial t} = \Delta \cdot (K \Delta T) + \sum_i \dot{w}_i h_i + \psi \quad (2-4)$$

where  $\psi$  is the electrical dissipation term.

If we assume that the propellant is a cylindrical disk, then the governing electrothermal equation becomes: (Reference 3 and 5)



$$\rho C \frac{\partial T}{\partial t} = \frac{1}{r} \frac{\partial}{\partial r} \left( Kr \frac{\partial T}{\partial r} \right)$$

$$\frac{\partial}{\partial z} \left( K \frac{\partial T}{\partial z} \right) + \sum \dot{w}_i h_i - \frac{K}{LT} \left( \frac{\partial V}{\partial z} \right)^2 \quad (2-5)$$

where V is the potential associated with the electric field and L is the Lorenz number.

It is noted that if the vapor which is generated is non-conducting, then the current has a single path through the solid, otherwise, the second path through the plasma must be considered. At the present time, a digital computer program exists to which the electrical dissipation term must be added if we wish to make a significant improvement over Equation (2-1).

Thus, to summarize, Equation (2-2) can be utilized to predict the injection rate and represents an improvement over Equation (2-1) only if one solves Equation (2-5) numerically.

### 3.0 APPLICATION OF THE TIME DEPENDENT NAVIER-STOKES EQUATIONS TO THE ANALYSIS OF DETONATION WAVE PROPAGATION IN THE SPET

Analysis of equation applications is included in the following:

- a. Definition of the Physical Problem - In this section of the study, we will describe our application of the complete time-dependent Navier-Stokes equations to the analysis of the formation and propagation of a detonation wave within the combustion chamber of the SPET engine. In this theoretical investigation, we will for the first time include the simultaneous time-dependent effects of gas compressibility, viscosity, thermal conductivity, diffusion and chemical reactions for a one-dimensional flow.

In the physical situation of interest, the initial conditions are that the SPET combustion chamber contains a very low density motionless gas, (e.g., the gaseous remains from the previous cycle). Upon the discharge of an electrical current through the solid propellant at the injection end, the propellant is vaporized and unburned gas enters the combustion chamber at the end  $x = 0$ , at the initial time,  $t = 0$ . The freshly injected unreacted gas flows into the chamber by the process of convection and diffusion and undergoes laminar mixing with the initially motionless gas. The injected gas acts to compress the gas already in the chamber, much like a moving gas piston. A pressure wave is set up which also acts to heat the flowing gas mixture. If the chemical kinetics of the essentially irreversible chemical reactions are sufficiently rapid and sufficient energy is available to raise the temperature of the injected gas to the ignition point, then the injected gas which is propagating away from the inlet end begins to burn rapidly and the pressure wave becomes a detonation wave. That is, one observes the formation of a propagating shock wave which is followed by a moving zone of rapid chemical reactions.

When the combined wave process occurs, the injected species are burned rapidly, heat is released, and the velocity, temperature, and density of the propagating gas

mixture all rise simultaneously. This resulting high speed gas propagates toward the nozzle end where it then expands into free space.

If on the other hand, the chemical reaction process is very sluggish, then the injected unburned gas simply expands toward the exhaust nozzle and into free space but at a much lower velocity and temperature. In this case, the enhancement of the velocity and temperature due to the conversion of chemical energy into kinetic energy and internal energy does not occur within a combustion chamber of reasonable length and the chemical energy of the gas is wasted. It is therefore clear that the chemical kinetics can be quite critical in determining the optimum operating chamber temperature and its length.

In general, one notes that the physical problem dictates that transient effects are critical, and hence a steady state, or quasi-steady, model is not applicable for the prediction of phenomena within the SPET chamber. Rather, one must retain all time dependent terms in the governing equations. Moreover, since we are dealing with the propagation of a detonation wave into a low density gas, we are concerned with low Reynolds number flows in which viscous effects are important, and hence one cannot use an inviscid gas model. Furthermore, we are interested in how the heat release affects the temperature distribution in the combustion chamber so that heat conduction must be included. Finally, since we are treating a chemically reacting gas mixture, it becomes necessary to include the effects of diffusion and non-equilibrium chemical reactions. In order to analyze this complex physicochemical problem, it becomes necessary to extend our previous work (Reference 1) on the complete time-dependent Navier-Stokes equations for a compressible, viscous, thermally conducting gas to include the effects of diffusion and chemical reactions. Since one requires a separate diffusion equation for each species but one, the order of the mathematical system rises by two for each chemical species included in the model.

Since this investigation represents the first attempt to include both diffusion and chemical reactions in the numerical solution of the complete Navier-Stokes equations, we have decided to assume that the unburned gas (the vaporized propellant) can be treated as a single averaged chemical species, and that the products of reaction can be represented by another suitably averaged species. By "averaged", we mean a fictitious species which is used to represent a collection of species and has the average thermal, chemical and molecular properties of the group of species which are actually present in the chamber. For the case of the thermal and molecular properties, this type of averaging can be an excellent approximation, however, we note that for the chemical properties, particularly, the chemical kinetic rate properties, this type of averaging is difficult to achieve, since a chain reaction, for example, cannot be readily approximated by a single step reaction of the form  $A \rightarrow B$ . The complete set of macroscopic conservation laws may therefore be written as follows:

The conservation of mass is:

$$\frac{\partial \rho}{\partial t} + \frac{\partial}{\partial x} (\rho v) = 0 \quad (3-1)$$

The conservation of momentum (Navier-Stokes) is:

$$\rho \left( \frac{\partial v}{\partial t} + v \frac{\partial v}{\partial x} \right) = - \frac{\partial P}{\partial x} + \frac{4}{3} \frac{\partial}{\partial x} \left( \mu \frac{\partial v}{\partial x} \right) \quad (3-2)$$

Here we take note of the fact that the presence of diffusion and chemical reactions does not affect either the global conservation of mass or the conservation of momentum. However, it is now necessary to consider the conservation of the individual chemical species, which is given by the partial differential equation which appears to be a first order equation as (3-1):

$$\frac{\partial \rho_i}{\partial t} + \frac{\partial}{\partial x} \left( \rho_i v_i \right) = \dot{w}_i \quad (3-3)$$

In this equation,  $v_i$  is the absolute velocity of the  $i^{\text{th}}$  species given by

$$\vec{v}_i = \vec{v} + \vec{V}_i \quad (3-4)$$

where  $\vec{v}$  is the macroscopically observed streaming velocity, and  $\vec{V}_i$  is the diffusion velocity.

For a binary gas mixture, the diffusion velocity of a species is related to the concentration gradient of the species by means of the relationship known as Fick's Law. This is written:

$$j_i = \rho_i V_i = - \rho \mathcal{D}_{ij} \frac{\partial C_i}{\partial x} \quad (3-5)$$

where  $\mathcal{D}_{ij}$  is the binary diffusion coefficient,  $C_i$  is the mass fraction of species  $i$ , and thermal diffusion is neglected.

Consequently, upon introducing Equations (3-4) and 3-5) into Equation (3-3) and also making use of Equation (3-1) to simplify the result, one obtains the second order equation:

$$\rho \frac{\partial C_i}{\partial t} + \rho v \frac{\partial C_i}{\partial x} - \frac{\partial}{\partial x} \left( \rho \mathcal{D}_{ij} \frac{\partial C_i}{\partial x} \right) = \dot{w}_i \quad (3-6)$$

In the foregoing,  $\dot{w}_i$  is the chemical source term which represents the net rate of formation of species  $i$  by chemical reaction, and will be discussed further when the specific chemical kinetic model is introduced.

The conservation of energy becomes:

$$\begin{aligned} \rho \bar{C}_v \left( \frac{\partial T}{\partial t} + v \frac{\partial T}{\partial x} \right) &= \frac{\partial}{\partial x} \left( k \frac{\partial T}{\partial x} \right) - p \frac{\partial v}{\partial x} \\ &+ \frac{4}{3} \mu \left( \frac{\partial v}{\partial x} \right)^2 - \frac{\partial}{\partial x} \left( \sum_i \rho_i v_i h_i \right) \\ &- \sum_i e_i \dot{w}_i - \sum_i e_i \frac{\partial}{\partial x} \left( \rho v_{ij} \frac{\partial C_i}{\partial x} \right) \end{aligned} \quad (3-7)$$

In the latter equation the internal energy and enthalpy of species  $i$  are given by:

$$e_i = \int C_{v_i} dT + \Delta e_{f_i}^o \quad (3-8)$$

and

$$h_i = \int C_{p_i} dT + \Delta h_{f_i}^o \quad (3-9)$$

respectively, and also

$$\bar{C}_v = \sum_i C_i C_{v_i} \quad (3-10)$$

Finally, one has the equation of state:

$$P = \rho \bar{R} T \quad (3-11)$$

where the gas constant is composition dependent and is given by:

$$\bar{R} = \sum_i C_i R_i \quad (3-12)$$

It is also noted that the sum of the mass fractions is unity:

$$\sum_i C_i = 1.0 \quad (3-13)$$

and the sum of the chemical source terms is zero.

$$\sum_i \dot{w}_i = 0 \quad (3-14)$$

For convenience, we will use the subscript 1 to represent the averaged injected combustible gas mixture and the subscript 2 to represent the averaged products of combustion. Hence, we note that:

$$C_2 = 1 - C_1 \quad (3-15)$$

$$\dot{w}_2 = -\dot{w}_1 \quad (3-16)$$

Let us now consider the initial conditions and the boundary conditions. As already mentioned, at time zero, before the injection process has begun, the gas in the chamber is motionless and has a constant density and temperature.

Furthermore, the gas consists entirely of species 2. Hence, we may prescribe the following initial conditions:

$$v(0, x) = 0 \quad (3-17)$$

$$T(0, x) = T_o(x) = \text{constant} \quad (3-18)$$

$$\rho(0, x) = \rho_o(x) = \text{constant} \quad (3-19)$$

$$C(0, x) = 0 \quad (3-20)$$

As the vaporization process begins, gas starts streaming into the combustion chamber, and hence the boundary conditions at the injection end wall are:

$$v(t, x_w) = v_w(t) \quad (3-21)$$

$$\rho(t, x_w) = \rho_w(t) \quad (3-22)$$

Moreover, since species 2 cannot flow through the injection end wall, we have the added constraint:

$$\rho_2 v_2(t, x_w) = 0 \quad (3-23)$$

Hence introducing Equations (3-4), (3-5), and (3-15) into Equation (3-23) we obtain the differential relationship for the mass fraction of combustible gas at the wall.

$$\begin{pmatrix} 1 & - & C_{1_w} \\ - & & \end{pmatrix} v_w = - \left( \vartheta_{ij} \frac{\partial C_1}{\partial x} \right)_w \quad (3-24)$$



In addition, we may specify the temperature at the wall or its derivative. We have found it convenient to assume that no heat is conducted back into the wall from the hot gas:

$$\frac{\partial T}{\partial x} (t, x_w) = 0 \quad (3-25)$$

Since we will be determining the propagation of the detonation wave toward the exhaust nozzle end, it will not be necessary to prescribe any boundary conditions at that end, but will assume that the calculated detonation wave structure will provide the initial conditions for the expansion of the products of combustion into the ambient atmosphere, (vacuum).

At this point, we are faced with solving the simultaneous set of coupled non-linear partial differential equations with variable coefficients (3-1), (3-2), (3-6), and (3-7) employing the auxilliary Equations (3-8) to (3-14) subjected to the initial conditions (3-17) to (3-20) and the boundary conditions (3-21), (3-22), (3-24) and (3-25).

In order to solve this set of equations on a digital computer, we introduce a space transformation as suggested by Landau and utilized previously in Reference 1. In this case, Equations (3-1), (3-2), (3-7), and (3-6) become:

$$\frac{\partial \rho}{\partial t} = -a_1 \frac{\partial \rho}{\partial \eta} - a_2 \frac{\partial v}{\partial \eta} \quad (3-26)$$

$$\begin{aligned} \frac{\partial v}{\partial t} = & \bar{b}_1 \frac{\partial^2 v}{\partial \eta^2} + \bar{b}_2 \frac{\partial v}{\partial \eta} - b_2 \frac{\partial \rho}{\partial \eta} \\ & - b_3 \frac{\partial T}{\partial \eta} - b_4 \frac{\partial C_1}{\partial \eta} \end{aligned} \quad (3-27)$$

$$\begin{aligned}
\frac{\partial T}{\partial t} = & \bar{c}_1 \left( \frac{\partial^2 T}{\partial \eta^2} \right)^2 + \bar{c}_2 \frac{\partial T}{\partial \eta} + \bar{c}_3 \left( \frac{\partial T}{\partial \eta} \right)^2 \\
& + \bar{c}_4 + \bar{c}_5 \left( \frac{\partial C_1}{\partial \eta} \right) \left( \frac{\partial T}{\partial \eta} \right) - \bar{c}_6 \left( \frac{\partial C_1}{\partial \eta} \right)^2 \\
& + \bar{c}_7 \frac{\partial^2 C_1}{\partial \eta^2} + \bar{c}_8 \frac{\partial C_1}{\partial \eta} - \bar{c}_1 \frac{\partial T}{\partial \eta} \\
& - \bar{c}_2 \frac{\partial v}{\partial \eta}
\end{aligned} \tag{3-28}$$

$$\begin{aligned}
\frac{\partial C_1}{\partial t} = & \bar{d}_1 \frac{\partial^2 C_1}{\partial \eta^2} - \bar{d}_2 \left( \frac{\partial C_1}{\partial \eta} \right)^2 + \bar{d}_3 \frac{\partial C_1}{\partial \eta} \\
& + \bar{d}_4 \frac{\partial C_1}{\partial \eta} \frac{\partial T}{\partial \eta} + \bar{d}_5 - d_1 \frac{\partial C_1}{\partial \eta}
\end{aligned} \tag{3-29}$$

Note that the barred quantities signify the viscous terms and the coefficients are given in the appendix.

As discussed earlier in Reference 1, uniqueness theorems for systems of this kind are not well established. However, at this point an examination of the characteristics of the mathematical system indicates that we are dealing with a well posed initial value problem.

- b. Gas Property Data. In the model treated here, as noted earlier, it was necessary to utilize averaged properties for the two chemical species. It was therefore assumed that the injected gas (species 1) was a mixture of light-weight hydrocarbons with an average molecular weight of 8 pounds/pound - mole. The products of combustion were taken to be a mixture of gases with an average molecular weight of 20 pounds/pound - mole. There follow immediately:

$$R_1 = 193 \frac{\text{ft. - pound}}{\text{pound}^{\circ} \text{R}} \quad (3-30)$$

$$R_2 = 77.3 \frac{\text{ft. - pound}}{\text{pound}^{\circ} \text{R}} \quad (3-31)$$

$$C_{v1} = 0.621 \frac{\text{BTU}}{\text{pound}^{\circ} \text{R}} \quad (3-32)$$

$$C_{v2} = 0.248 \frac{\text{BTU}}{\text{pound}^{\circ} \text{R}} \quad (3-33)$$

It was also assumed that the energies and heats of formation of the reactants and products were:

$$\Delta e_{f1}^0 = 100 \frac{\text{BTU}}{\text{pound}}$$

$$\Delta e_{f2}^0 = -8000 \frac{\text{BTU}}{\text{pound}}$$

(3-34)

$$\Delta h_{f_1}^0 = 200 \frac{\text{BTU}}{\text{pound}}$$

$$\Delta h_{f_2}^0 = -7800 \frac{\text{BTU}}{\text{pound}}$$

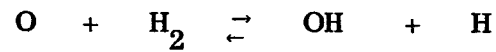
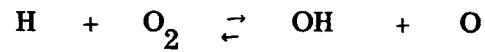
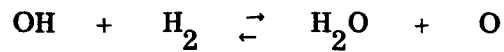
Although more complicated transport properties (e.g. Reference 6) can readily be introduced into the computer program, it was felt that this type of refinement was not warranted at this stage and consequently, simple kinetic theory representations were utilized in which the viscosity, thermal conductivity and diffusion coefficient were taken to be:

$$\mu = 1.28 \times 10^{-6} \sqrt{T (^{\circ}\text{R})}, \frac{\text{pound}}{\text{ft. sec.}} \quad (3-35)$$

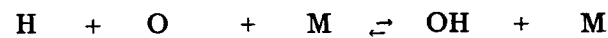
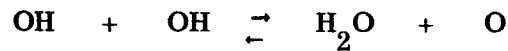
$$K = 4.49 \times 10^{-7} \sqrt{T (^{\circ}\text{R})}, \frac{\text{BTU} - \text{ft.}}{\text{ft.}^2 \text{ sec. } ^{\circ}\text{R}} \quad (3-36)$$

$$\vartheta_{ij} = \frac{1.2 \times 10^{-4} T (^{\circ}\text{R})^{3/2}}{P \frac{\text{pound}}{\text{ft.}^2}}, \left( \frac{\text{ft}^2}{\text{sec}} \right) \quad (3-37)$$

Finally, we discuss the chemical kinetic model selected. W. G. Browne (Reference 7) has considered in detail the chemical kinetic rate processes associated with the combustion of hydrogen and hydrocarbons with oxygen. In general, he finds that a total of seven simultaneous chemical reactions are necessary in order to adequately treat the  $\text{H}_2 - \text{O}_2$  system. The number of reactions rises rapidly for energy new chemical element introduced into the system. As noted earlier, in the present investigation, we have allowed for the presence of two averaged species. Consequently, rather than using a system such as (Reference 7):



(3-38)



where M denotes any third molecule, we will simplify the chemical kinetic model to the form:



where A denotes the averaged mixture of combustible gases which are injected and B represents the averaged products of combustion. Thus, we obtain for the chemical source term:

$$\dot{w}_1 = k \rho_1^n \quad (3-40)$$

where the specific reactivity  $k$  is given by:

$$k = a T^b e^{-E/RT} \quad (3-41)$$

and  $n$  is the order of the reaction. Note that  $E$  is the activation energy for the chemical reaction.

- c. Discussion of Sample Calculations - The equations and coefficients derived in Paragraphs 3a and 3b have been programmed in Fortran IV for computation on a digital computer, and two sample calculations were carried out, with and without combustion. The numerical results are shown in Figures A-1 to A-7.

Figure A-1 shows the injection rate parameters  $\rho_w$  and  $v_w$  as a function of time. Note that at time zero, the gas velocity in the chamber is everywhere zero and the chamber density has been taken equal to a constant of  $6.91 \times 10^{-6}$  pounds/ft<sup>3</sup>. This is in accordance with the initial conditions discussed in Paragraph 3a.

Figure A-2 depicts the variation of the mass fraction of combustible gas with distance and time. It is seen that due to diffusion and convection the injected gas, which is in largest concentration near the wall, decreases in concentration with distance from the wall. Furthermore, when combustion occurs, the mass fraction of combustible drops very rapidly as chemical energy is converted into kinetic energy (compare Figures A-3 and A-4) and internal energy (compare Figure A-5 and A-6). The associated density wave appears in Figure A-7.

It is clear then, that the rapid injection of a higher density gas into a very low density gas does indeed produce a shock wave. If the reaction kinetics are very low, the shock wave simply propagates forward to the exhaust end. If, on the other hand, the global chemical reaction is rapid, the shock wave becomes a detonation wave and the gas temperature rises considerably, since the chemical energy is unlocked.

The results presented here should be considered as preliminary, and are representative of the phenomena which occur in the SPET engine in a qualitative way. As the next phase of the investigation, it will be necessary to use the new computer program to perform a series of parametric studies to determine the effect of systematically varying the physicochemical parameters and the initial conditions in the SPET chamber. This will help the designer to relate performance to propellant properties and chamber geometry and will help in the interpretation of experimental data.

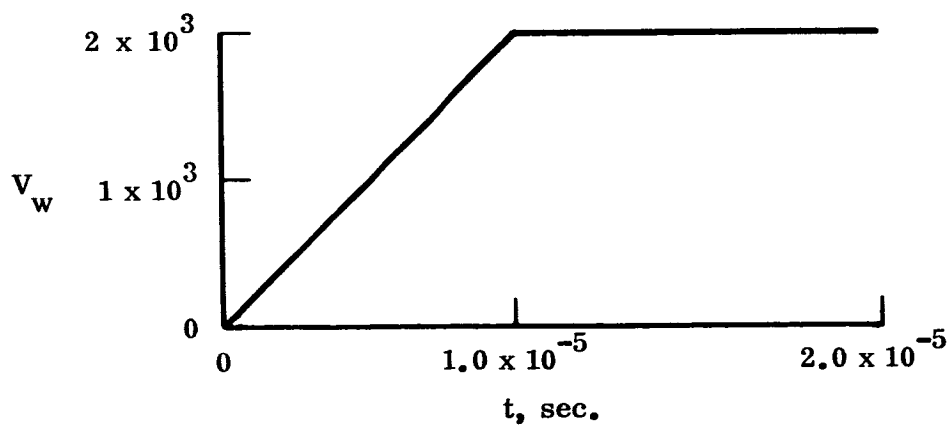
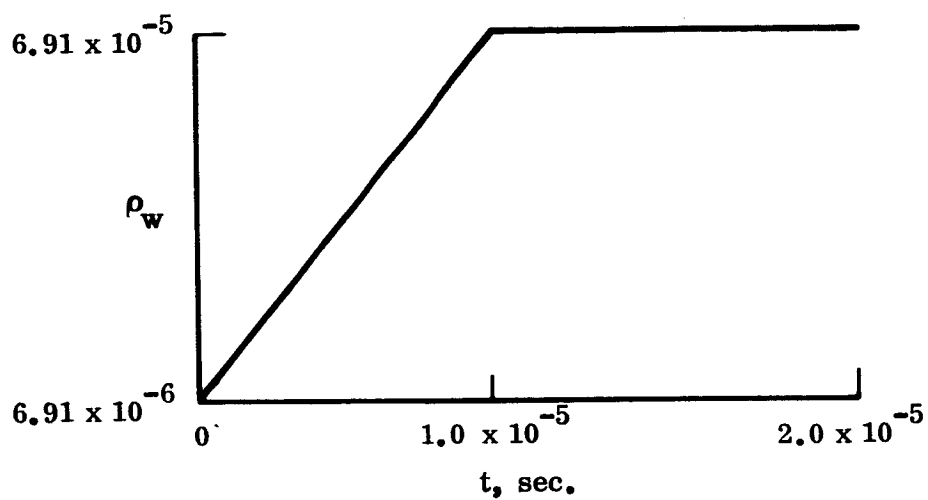


Figure A-1. Injection of Combustible Gas

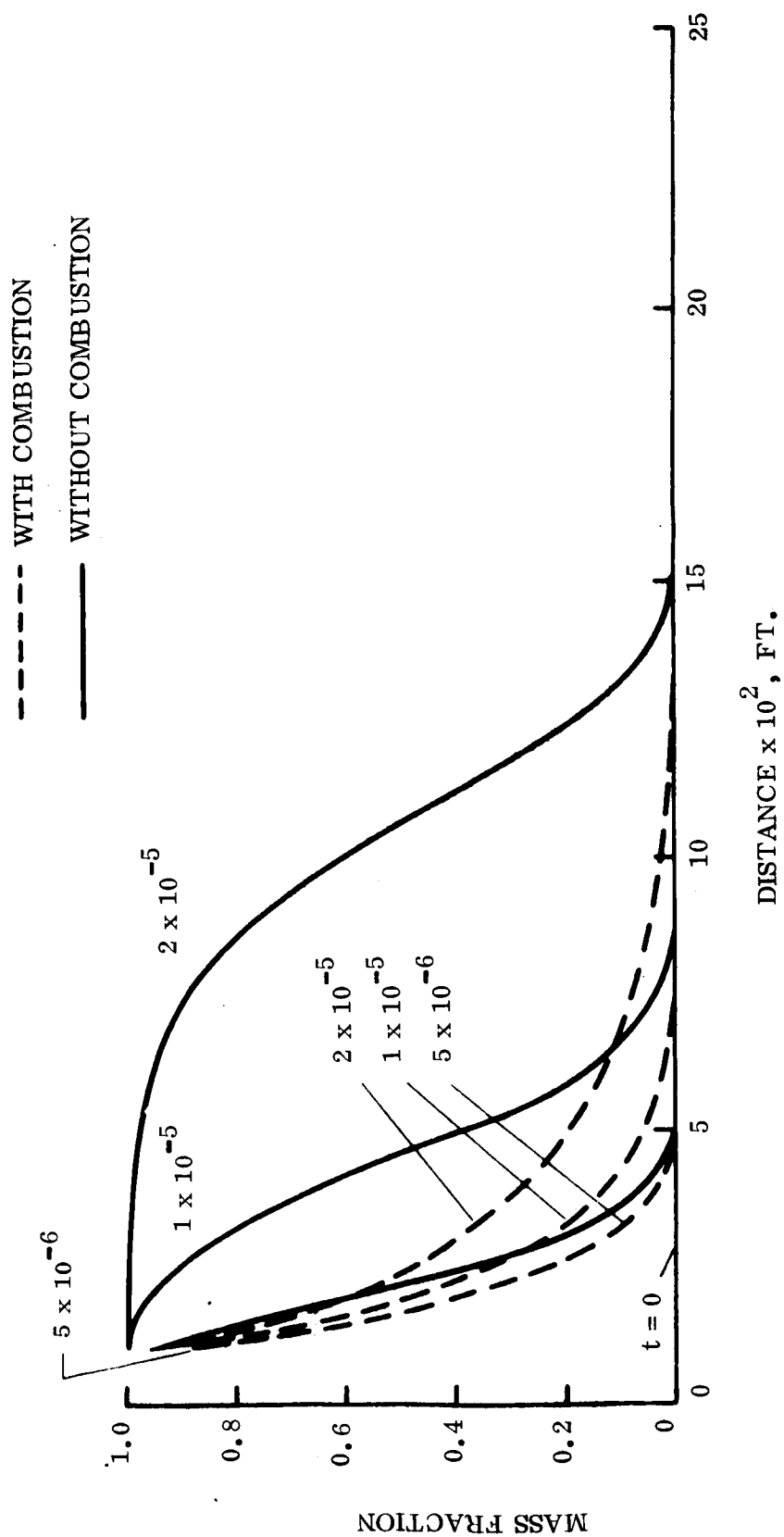


Figure A-2. Mass Fraction of Combustion Gas



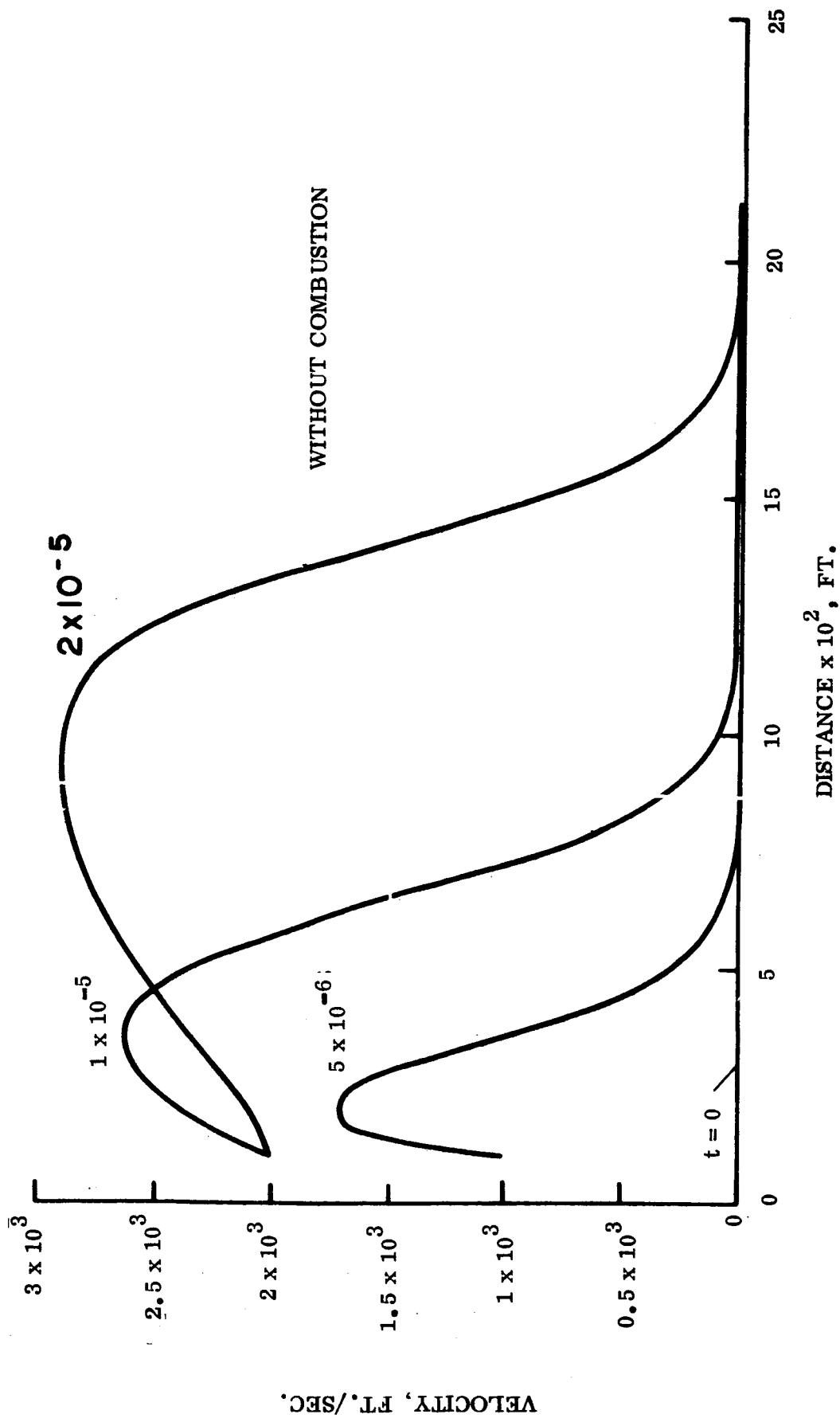


Figure A-3. Propagation of Shock Wave in SPET Chamber (Without Combustion)

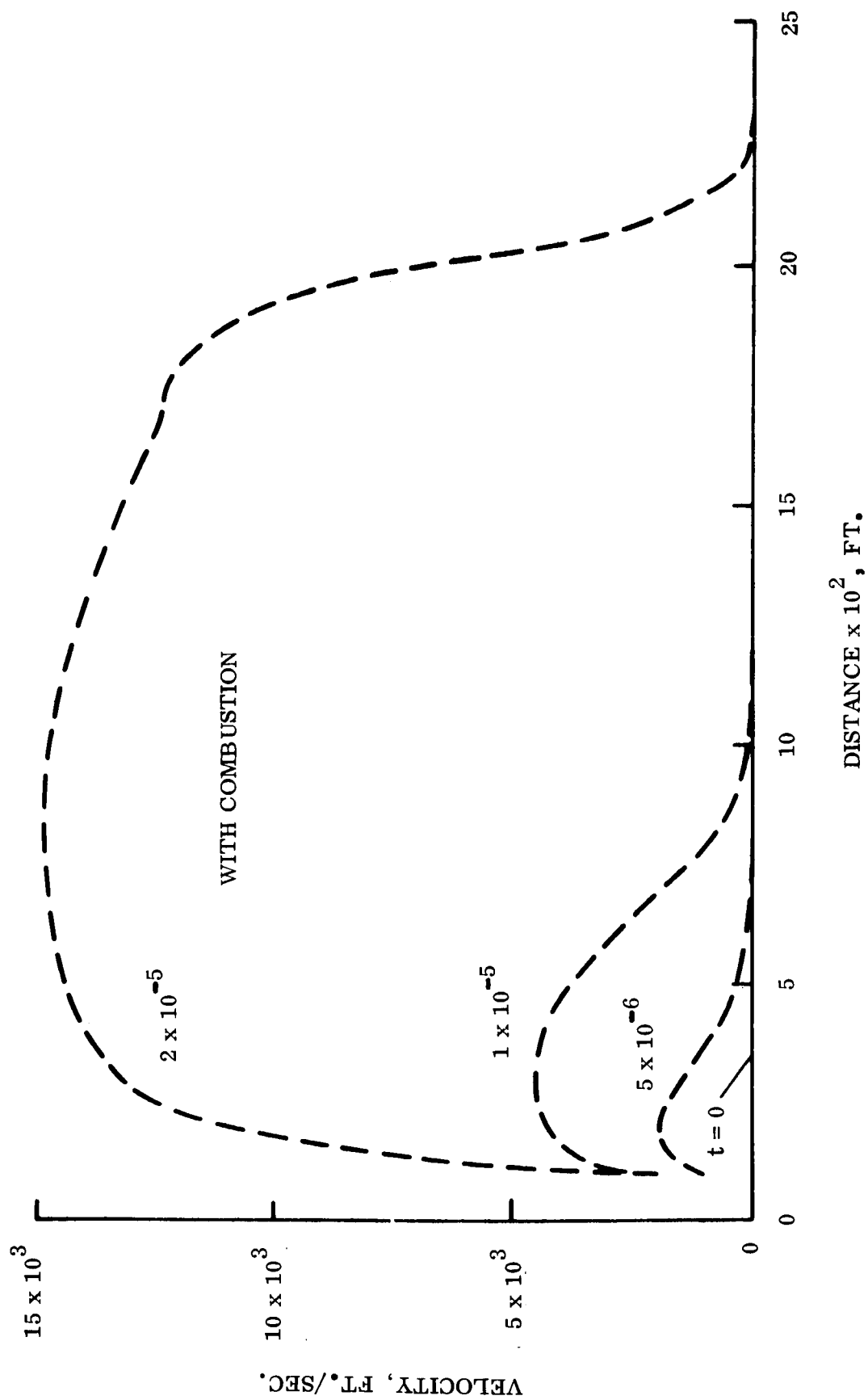


Figure A-4. Propagation of Detonation Wave in SPET Chamber (With Combustion)

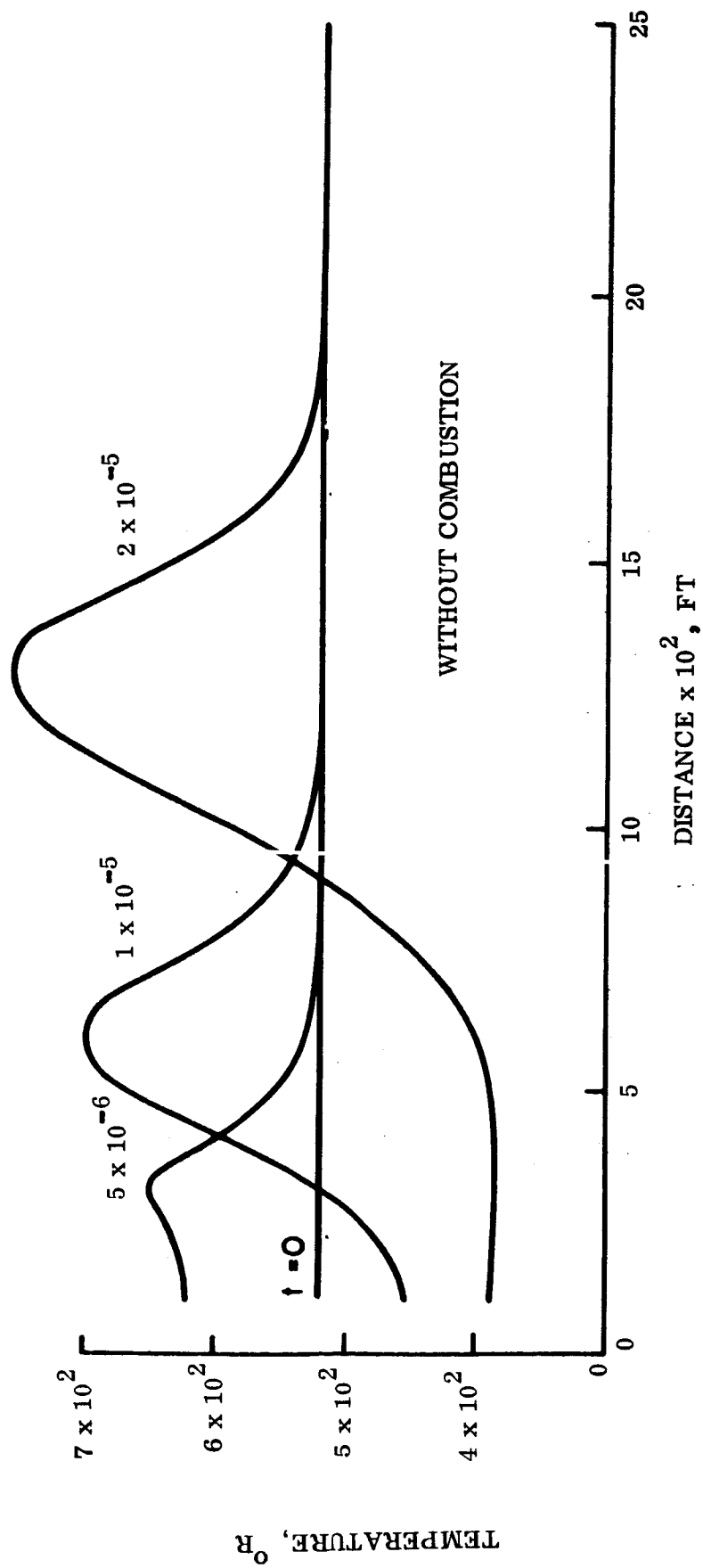


Figure A-5. Temperature Distribution in SPET Chamber (Without Combustion)

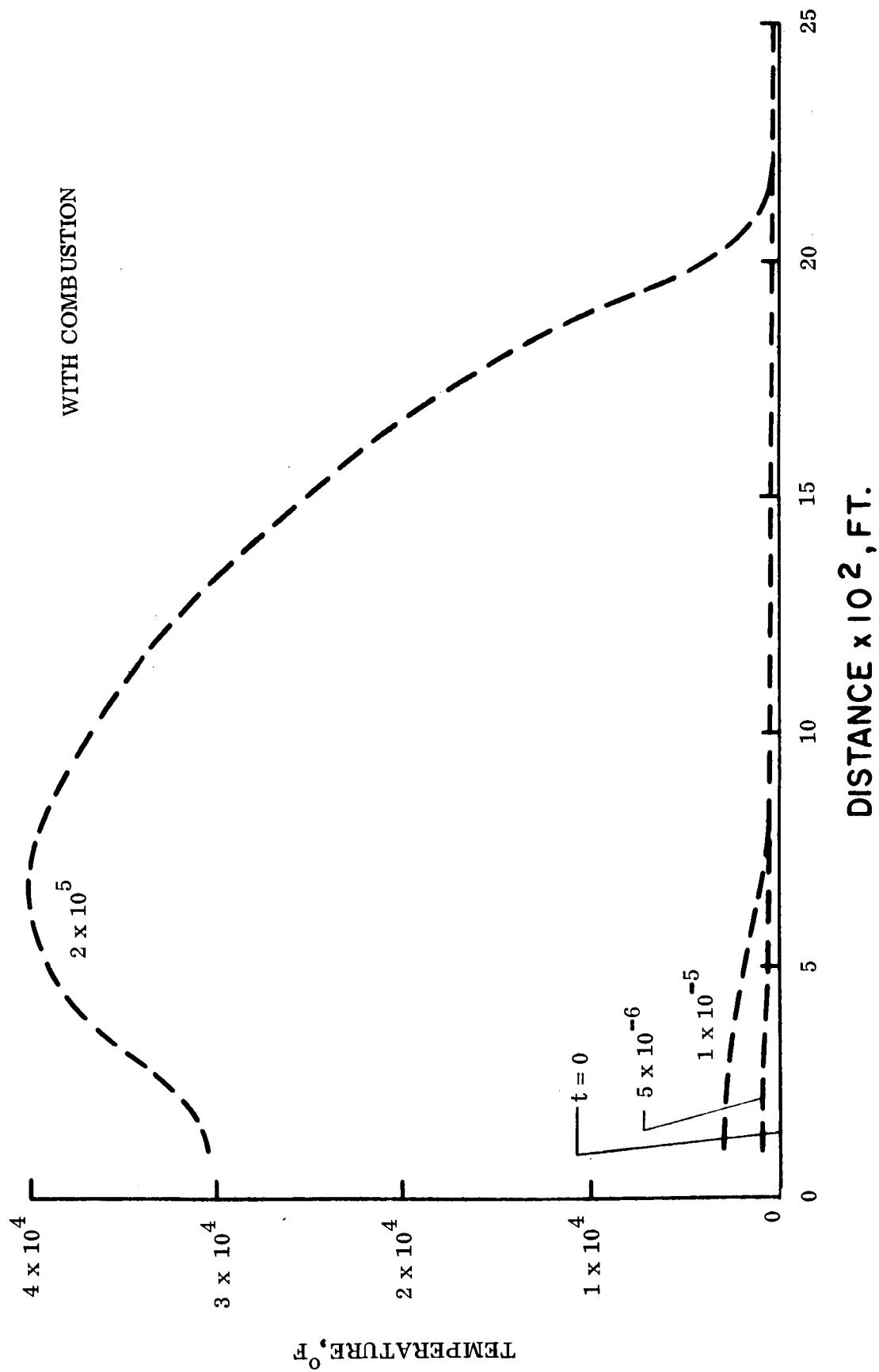


Figure A-6. Temperature Distribution in SPET Chamber (Without Combustion)

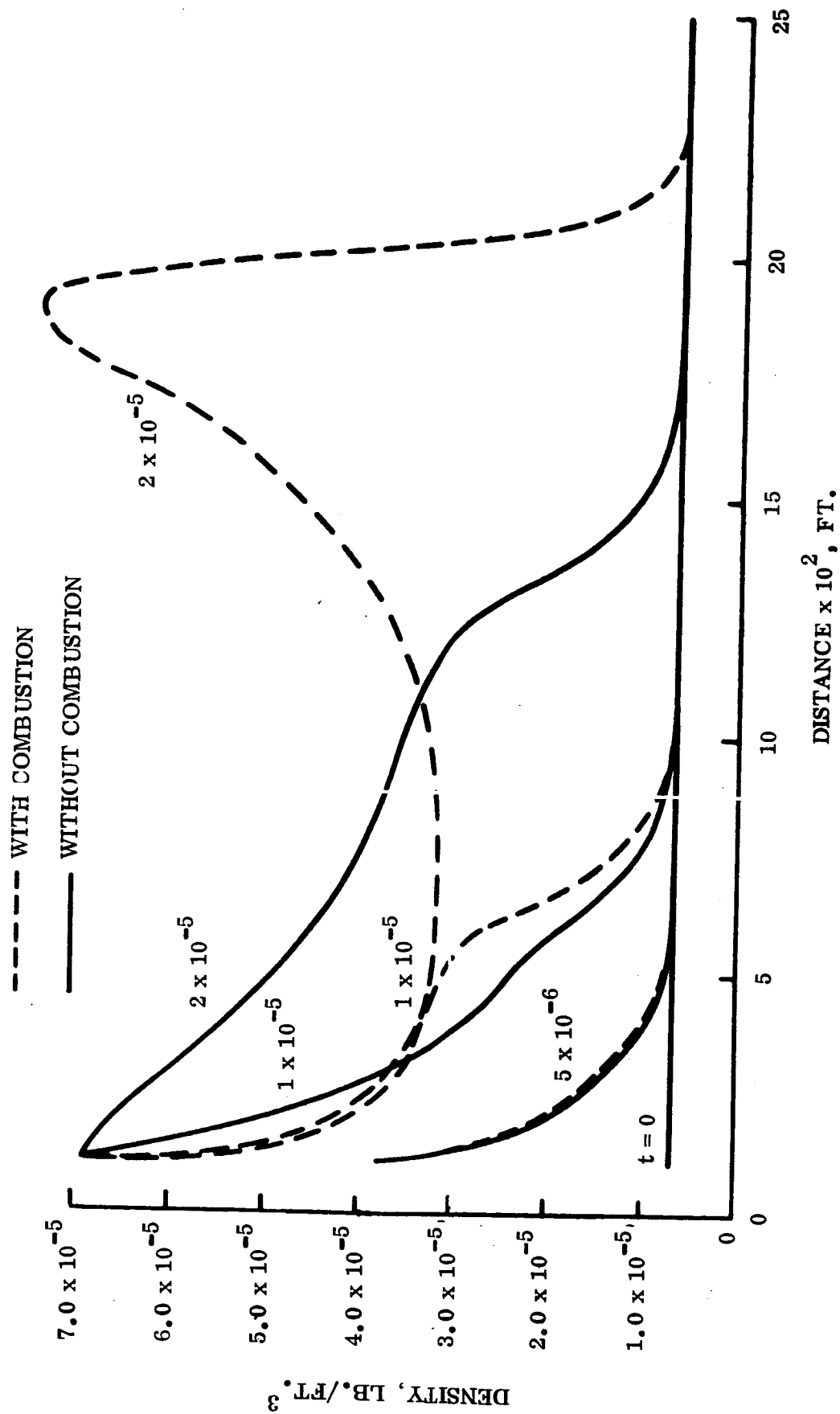


Figure A-7. Density Distribution in SPET Chamber (With and Without Combustion)

#### 4.0 ANALYSIS OF EXPANSION OF COMBUSTION PRODUCTS INTO VACUUM

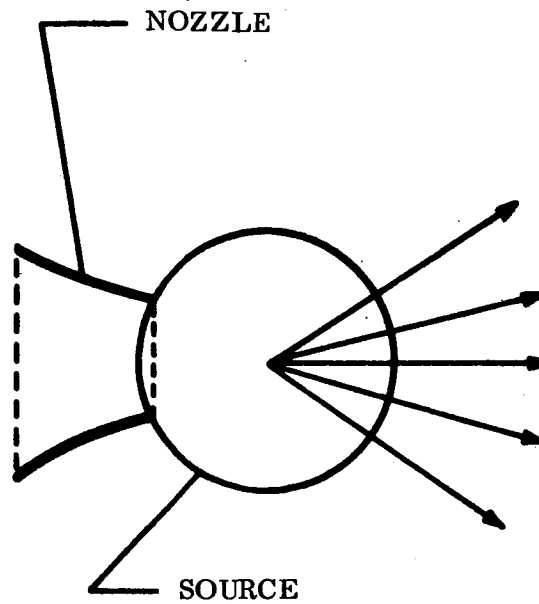
- a. Introduction - In its "exploding wire" phase of operation, the SPET engine produces a column of gas at high temperature and pressure. This gas then expands into the vacuum region in the vicinity of the engine, generating thrust. To analyze the expansion of these gases requires an analysis of the non-linear Navier-Stokes and Boltzmann Equations. In the vicinity of the original gas column, we have a dense collision-dominated expansion and continuum considerations apply. While far from the source, collisions are less frequent and the Boltzmann Equation is required.

To analyze this expansion, we have made a number of simplifications, which can readily be improved so that quantitative predictions can be made.

We first assume that the cylindrical source the gas issues from is quasi-steady, that is to say gas is continuously issuing from a cylinder of radius  $a$ . This source flow model of the expansion is valuable in many areas of engineering. For example in Figure A-8, we show the analog of the spherical-source flow to nozzle expansion and additionally the cylindrical source flow model that we employ for the SPET engine expanding flow. For simplicity, we further assume that the gas is made of monatomic particles of the same species.

Our point of view, then is to develop a self-consistent approximation to the Boltzmann Equation which will be appropriate to the hypersonic, rarefied flow in the expanding stream and so avoid the controversies about the relative merits of the various ad-hoc moment approaches. The fundamental idea will be that instead of establishing the approximation on the magnitude of the collision frequency (and Knudsen number), either near-continuum or near free molecular, we only demand that the mach number or speed ratio of the flow (ratio of the ordered velocity to the thermal velocity) be large compared to one. In what follows we sketch the analysis of this flow and then finally summarize our conclusions and recommendations.

A. SPHERICAL SOURCE FLOW



B. SPET EXPANSION

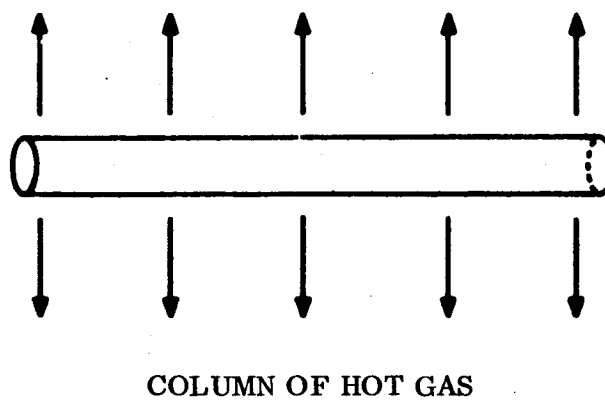


Figure A-8. Schematic Diagram of Expansion Process

- b. The Cylindrically Symmetric Expansion - We first write the complete set of moment equations up to the stress tensor equation.

$$\rho' V' r' = \text{constant} \quad (4-1)$$

$$\frac{dp'_{rr}}{dr'} + \left( \frac{p'_{rr} - p'_{\theta\theta}}{r'} \right) + p' V' \left( \frac{dV'}{dr'} \right) = 0 \quad (4-2)$$

$$\frac{1}{r'} \frac{d}{dr'} (r' V' p'_{rr}) + 2p'_{rr} \left( \frac{dV'}{dr'} \right) = -\nu' (p'_{rr} - p') - \frac{1}{r} \frac{d}{dr'} (Q'_{rr} r') \quad (4-3)$$

$$\frac{1}{r'} \frac{d}{dr'} (r' v' p'_{\theta\theta}) + \frac{2V'}{r'} p'_{\theta\theta} = -\nu' (p'_{\theta\theta} - p') \quad (4-4)$$

$$\frac{1}{r'} \frac{d}{dr'} (r' v' p'_{zz}) = -\nu' (p'_{zz} - p') \quad (4-5)$$

where  $(r', \theta, z')$  represent the obvious choice of cylindrical coordinates.

Again taking

$$r = r'/r'_*, \quad T = T'/T'_s, \quad V = V'/(RT'_s)^{1/2} \quad (4-6)$$

and restricting ourselves to the case where

$$\nu' = p'/\mu' \quad (4-7)$$

and  $\mu' \sim (T')^\omega$  the equations reduce to

$$v^2 r \frac{dT_{rr}}{dr} + T_{rr} r \frac{dV^2}{dr} = -\alpha (T_{rr} - T) T^\beta$$



$$v_r^2 \frac{dT_{\theta\theta}}{dr} + 2V^2 T_{\theta\theta} = -\alpha (T_{\theta\theta} - T) T^\beta \quad (4-8)$$

$$v_r^2 \frac{dT_{rr}}{dz} = -\alpha (T_{zz} - T) T^\beta - \frac{1}{r} \frac{d}{dr} r Q_{rrr}$$

where  $\beta = 1 - \omega$ , and  $\alpha$  has the same meaning as before.

Taking an inner expansion of the form

$$T_{tt} = T_{rr0} + (1/\alpha) T_{rr1}, \text{ etc.} \quad (4-9)$$

we find that the leading form is the inviscid solution, given by

$$T_{rr0} = T_{\theta\theta0} = T_{zz0} = T_0 \quad (4-10)$$

where

$$T_0^3 (1 - T_0) = (1/4) (3/4)^3 r^{-2} \quad (4-11)$$

and for  $r \gg 1$

$$T_0 \sim (1/4)^{1/3} (3/4) r^{-2/3} \quad (4-12)$$

We can estimate  $T_{rr1} - T_1$  from Equations (A2-A7) and find for  $r \gg 1$

$$T_{rr1} - T_1 \sim a_0 r^{-2/3} r^{2\beta/3} \quad (4-13)$$

where  $a_0$  is of order unity. In other words for  $\beta = 0$ , we find that the inner solution is uniformly valid i.e., that the continuum solution continues to be a good approximation for all  $r$ . (Strictly for  $r < \exp(\alpha)$ ) For  $\beta \neq 0$ , we choose outer variables

$$x = \ln(r \epsilon^\delta) \quad (4-14)$$

$$T_{rr} = \epsilon (t_{rr0}(x) + \dots$$

$$T_{\theta\theta} = \epsilon (t_{\theta\theta 0}(x) + \dots \quad (4-15)$$

$$\epsilon = (5/\alpha)^{1/\beta}$$

The equations for  $t_{rr0}$  again utilizing the hypersonic approximation are to lowest thermal order:

$$\frac{dt_{rr0}}{dx} = - (t_{rr0} - t_0) t_0^\beta$$

$$\frac{dt_{\theta\theta}}{dx} + 2t_{\theta\theta} = - (t_{\theta\theta 0} - t_0) t_0^\beta \quad (4-16)$$

$$\frac{dt_{zz0}}{dx} = - (t_{zz0} - t_0)^\beta$$

Which can be rearranged into

$$t_{\theta\theta 0} = - (3/2) (dt_0/dx) \quad (4-17)$$

$$t_{rro} = t_{zz0} = (3t_0 - t_{\theta\theta 0}) / 2 \quad (4-18)$$

$$\frac{d^2 t_0}{dx^2} + (2 + t_0^\beta) \frac{dt_0}{dx} + \frac{2}{3} t_0^{\beta+1} = 0 \quad (4-19)$$

For  $t_0 \gg 1$  the solution to Equation (4-19) is

$$t_0 \sim B e^{-2x/3} = B \epsilon^{-2\delta/3} r^{-2/3} \quad (4-20)$$

which formally matches with the inner solution providing

$$B = (1/4)^{1/3} (3/4) \epsilon^{(2\delta/3 - 1)} \quad (4-21)$$

This is consistent with  $t_0 \gg 1$  providing  $2\delta/3 < 1$  and  $x \leq 1$ , i.e. providing  $r \leq \epsilon^{-\delta}$ . On the other hand the inner solution is from Equation A8, still valid providing  $r^{2\beta/3} < \alpha$  or  $r < \epsilon^{-3/2}$  while at the same time  $r \gg 1$ . Clearly for any  $r$  of order  $\epsilon^{-\delta}$  where  $0 < \delta < 3/2$  there is an overlap region.

For  $x \gg 1$  the solution to Equation (4-19) is of the form

$$\frac{dt_0}{dx} + \frac{1}{3} t_0^{\beta+1} = 0$$

i.e.  $t_0 \rightarrow (\beta x/3)^{-1/\beta} + \dots$

$$(\beta (\ln(r) + \delta \ln \epsilon) / 3)^{-1/\beta} \quad (4-22)$$

$$(\beta/3)^{-1/\beta} (\ln r)^{-1/\beta}$$

A much more detailed matching of the inner and outer expansions could presumably be effected. However, the main result is contained in Equations (4-17, (4-18) and (4-22) which say that  $T_0$  and hence  $T_{rr}$  and  $T_{zz}$  goes to zero, with  $r \rightarrow \infty$ , like  $\ln(r)$  and  $T_{\rho\theta}$  goes to zero more rapidly namely as  $\ln(r)^{-(1/\beta+1)}$ . Therefore while for  $\beta \neq 0$  (or molecules harder than inverse fifth power) there is no longer an isotropic pressure, there is no freeze, so the cylindrical expansion differs fundamentally from the spherical expansion. This result would be difficult to envision using a sudden freeze criterion.

- c. Discussion of Results - Our main conclusion is that the expansion of the original cylinder of gas will be quite efficient (in fact a great deal more efficient than if we considered a spherical source) in converting thermal energy into directed kinetic energy, so that the losses due to incomplete translation expansion should be small. We can make this point quite graphically by noting in Figure A-9, a plot of temperature as a function of distance from the source, for spherical source flow. We note that the temperature approaches an asymptote at some distance from the source.

From the equation for flow velocity:

$$kT_{\text{stag}} = \frac{1}{2} m V^2 + kT \quad (4-23)$$

we observe that if  $T$  reaches an asymptotic value this will represent incomplete expansion and the flow velocity will be reduced so that a loss of thrust results.

For cylindrical expansion, of inverse fifth power molecules  $T = \left(\frac{1}{4}\right)^{1/3} \frac{3}{4} r^{-2/3}$ ; so that  $T \rightarrow 0$  as  $r \rightarrow \infty$  and the losses in flow velocity and thrust due to uncomplete expansion are minimized.

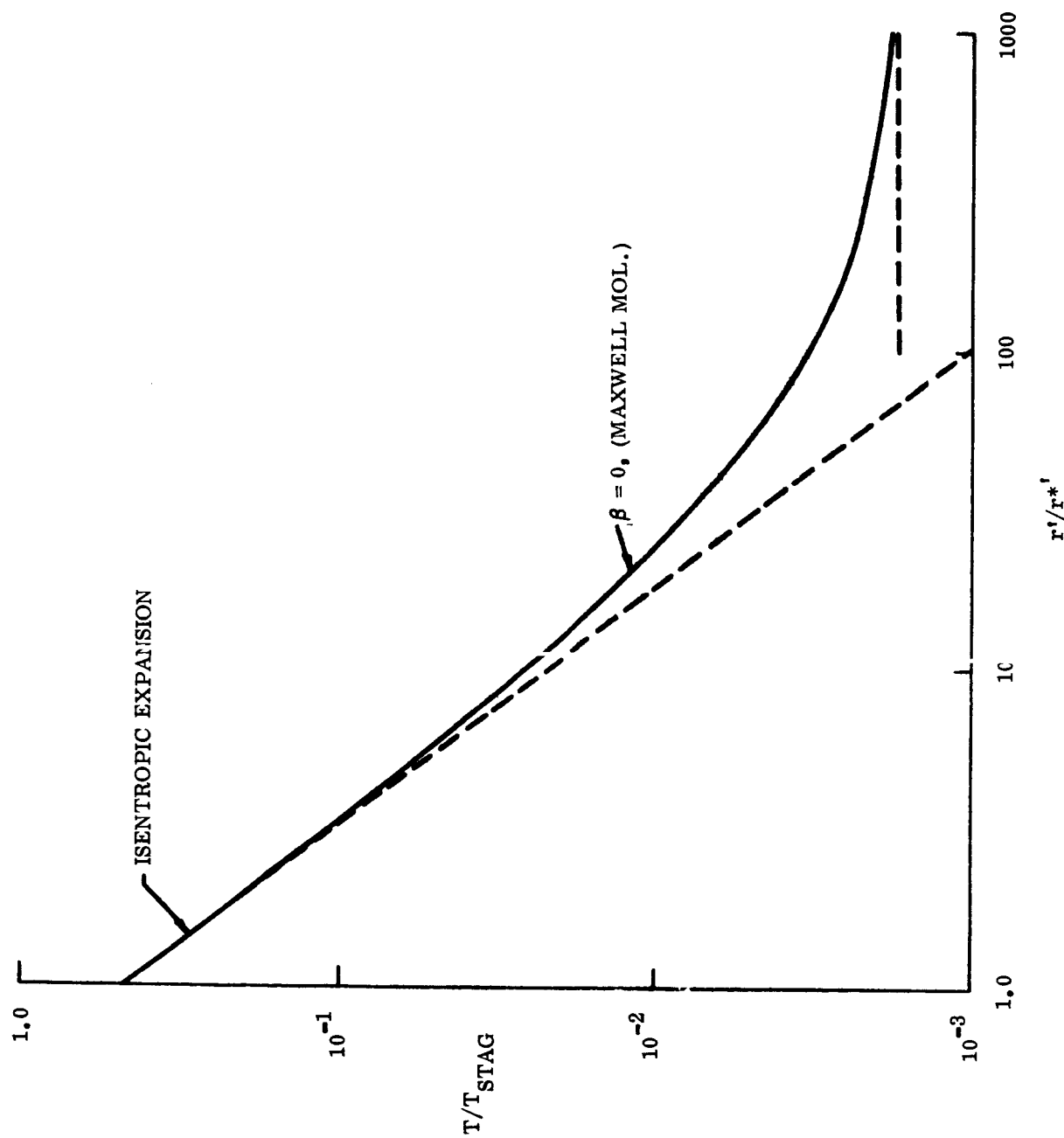


Figure A-9. Freezing of the Temperature  $T_{11}$  (Knudsen Number  $\approx 1,000$ )

## 5.0 RECOMMENDATIONS

The specific recommendations for proposed future theoretical work on the SPET engine are as follows:

- a. Utilizing the newly developed digital computer program, perform a parametric study in which the initial conditions and the physicochemical properties are varied systematically, so that the relationship between propellant properties and plasma at the chamber exit are determined as a function of SPET operation conditions.
- b. Develop a digital computer program for the time-dependent vaporization of the solid propellant so that the initial conditions at the injection end of the chamber can be determined systematically for a number of propellants of interest which are subjected to a range of electrical discharges of the order of 5 to 25 joules. This will provide realistic initial conditions for paragraph 1 above.
- c. Extend the theoretical model for the detonation wave analysis to include the diffusion and chemical reaction of additional chemical species, so that more realistic chemical kinetics can be utilized rather than the simple global reaction utilized herein.
- d. Perform an analysis of the heat losses due to conduction and radiation from the flowing plasma to the SPET chamber side walls, and if significant, incorporate these back into the model for the propagation of the detonation wave. Note that since a one-dimensional treatment was employed here, heat conduction is included at present, but only for the axial direction, and not for the radial direction.
- e. Replace the present one-dimensional representation by an axially-symmetric (two-dimensional) representation, to allow for longitudinal variations in cross sectional area.

- f. Incorporate the Maxwell field equations into the overall system of equations, so that the presence of magnetic fields can be included in further accelerating the flow if desired.
- g. Apply the theoretical model presented here for the analysis of the expansion into vacuum to the specific combustion products which form in the SPET engine.

## 6.0 SUMMARY

In this first theoretical study of the fluid physics of the SPET engine, the techniques of continuum mechanics and kinetic theory are employed to derive fundamental equations which govern the flow of the gaseous reactants within the combustion chamber, and the expansion of the products of combustion into vacuum.

The methods developed by Scala and Gordon for solving the complete time-dependent Navier-Stokes equations are extended herein to include the specific effects of molecular diffusion and non-equilibrium combustion. In this investigation an exhaustive study of all the possible physical and chemical parameters has not been carried out. Rather, the governing relationships have been derived and a digital computer program has been developed. Furthermore, sample calculations have been obtained for both finite reaction rate kinetics and negligible reaction rates.

The subsequent expansion of this plasma into vacuum is analyzed utilizing the methods of kinetic theory, based on the theoretical techniques developed by Hamel and Willis.



## 7.0 CONCLUSIONS

During the past five months in which this theoretical investigation was carried out, significant headway has been made in the development of a comprehensive model for the physicochemical processes which occur in the SPET. Analytical models, and numerical techniques have been extended successfully and a new digital computer program for the solution of the complete time-dependent Navier-Stokes equations, including the simultaneous effects of compressibility, viscosity, thermal conduction, molecular diffusion and combustion has been developed.

In the future, this computer program should be utilized to carry out a comprehensive parametric study to determine the relationship between the physicochemical properties of the propellant and the SPET engine geometry. Once this has been done, the information generated can be factored into the design of advanced SPET devices. It is noted that the theoretical model can be improved by employing more realistic plasma properties and by introducing additional diffusion equations to permit the inclusion of other important chemical species, such as intermediate chain-carrying products of combustion.

Other extensions and refinements in the theory, such as the inclusion of radiation fields and magnetic fields can be accomplished at a still later date when it is planned to consider the presence of these effects in more advanced SPET configurations.

## 8.0 REFERENCES

1. Scala, S. M. and Gordon, P., "Reflection of a Shock Wave at a Surface", General Electric Co., M.S.D., TIS Report No. 65 SD 24, June 1965, (accepted for publication in the **Physics of Fluids**).
2. Exploding Wires, Vol. I, Edited by William G. Chase and Howard K. Moore, Plenum Press, New York 1959.
3. Exploding Wires, Vol. II, Edited by William G. Chase and Howard K. Moore, Plenum Press, New York, 1962.
4. Scala, S. M. and Vidale, G. L., "Vaporization Processes in the Hypersonic Laminar Boundary Layer", Int. Journal of Heat and Mass Transfer, Vol. I, No. 1, pp. 4-22, 1960.
5. Nolan, E. J. and Scala, S. M., "Aerothermodynamic Behavior of Phrolytic Graphite During Sustained Hypersonic Flight", ARS Journal, Vol 32, No. 1, pp. 26-35, January 1962.
6. Sherman, M., "The Transport Properties of Partially Ionized Nitrogen Methods and Results", General Electric Co., M.S.D., TIS Report No. R 65 SD44, October 1965.
7. Browne, W. G., "Kinetics of the  $H_2/O_2$  System for use in the Spet Engine Development Program", letter dated September 9, 1965.

## 9.0 NOMENCLATURE

$a_i$	- see Index (Paragraph 10.0)
$b_i$	- see Index (Paragraph 10.0)
$c_i$	- see Index (Paragraph 10.0)
$C_i$	- mass fraction of species i
$C_{p_i}$	- specific heat at constant pressure
$C_{v_i}$	- specific heat at constant volume
$d_i$	- see Index (Paragraph 10.0)
$\vartheta_{ij}$	- binary diffusion coefficient
$\Delta e_{f_i}$	- energy of formation
$E$	- activation energy
$\Delta E$	- energy absorbed
$h$	- enthalpy, including chemical
$\Delta h_{f_i}^o$	- heat of formation
$j_i$	- diffusion flux vector
$k$	- specific reactivity, Boltzmann constant
$K$	- thermal conductivity coefficient
$M$	- molecular weight
$n$	- order of chemical reaction
$p$	- pressure
$Pr$	- Prandtl number
$r$	- radial coordinate
$\overline{R}$	- gas constant

$R$	-	electrical resistance
$t$	-	time coordinate
$T$	-	temperature
$v$	-	gas velocity
$V$	-	diffusion velocity, voltage
$\dot{w}_i$	-	chemical source term
$x$	-	spatial coordinate
$z$	-	axial coordinate
$\alpha$	-	vaporization coefficient
$\beta$	-	see Index (Paragraph 10.0)
$\eta$	-	transformed spatial coordinate
$\mu$	-	viscosity coefficient
$\rho$	-	density
$\theta$	-	tangential coordinate

#### Subscripts

$i$	-	species $i$ , index
$s$	-	stagnation
$vap$	-	vaporized
$w$	-	wall
$0$	-	initial undisturbed state
$1$	-	unreacted gas mixture
$2$	-	burned gas mixture

## 10.0 INDEX

$$a_1 = \frac{\partial \eta}{\partial t} = v \frac{\partial \eta}{\partial x}$$

$$a_2 = \rho \frac{\partial \eta}{\partial x}$$

$$\bar{b}_1 = \frac{4}{3} \mu \left( \frac{\partial \eta}{\partial x} \right)^2 \left( \frac{1}{\rho} \right)$$

$$\bar{b}_2 = \frac{4}{3} \left( \frac{d\mu}{dT} \right) \left( \frac{\partial T}{\partial \eta} \right) \left( \frac{\partial \eta}{\partial x} \right)^2 \left( \frac{1}{\rho} \right)$$

$$b_1 = a_1$$

$$b_2 = \left( \frac{\bar{R} T}{\rho} \right) \left( \frac{\partial \eta}{\partial x} \right)$$

$$b_3 = \bar{R} \left( \frac{\partial \eta}{\partial x} \right)$$

$$b_4 = T \left( \frac{\partial \eta}{\partial x} \right) \left( \frac{d\bar{R}}{dC_1} \right)$$

$$\bar{c}_1 = \frac{K}{\rho \bar{C}_V} \left( \frac{\partial \eta}{\partial x} \right)^2$$

$$\bar{c}_2 = \bar{c}_1 \frac{\left( \frac{\partial^2 \eta}{\partial x^2} \right)}{\left( \frac{\partial \eta}{\partial x} \right)^2}$$

$$\bar{c}_3 = \left( \frac{dK}{dT} \right) \frac{\bar{C}_1}{K}$$

$$\bar{c}_4 = \frac{4}{3} \frac{\mu}{\rho \bar{C}_v} \left[ \left( \frac{\partial \eta}{\partial x} \right) \left( \frac{\partial v}{\partial x} \right) \right]^2 - \frac{w f_2}{\rho \bar{C}_v}$$

$$\bar{c}_5 = \frac{f_3 f_5 \left( \frac{\partial \eta}{\partial x} \right)^2}{\bar{C}_v}$$

$$\bar{c}_6 = \frac{f_1 f_3 f_4 \left( \frac{\partial \eta}{\partial x} \right)^2}{\bar{C}_v}$$

$$\bar{c}_7 = \frac{f_1 f_3 \left( \frac{\partial \eta}{\partial x} \right)^2}{\bar{C}_v}$$

$$\bar{c}_8 = \frac{f_1 f_3 \frac{\partial^2 \eta}{\partial x^2}}{\bar{C}_v}$$

$$d_1 = a_1$$

$$\bar{d}_1 = f_3 \left( \frac{\partial \eta}{\partial x} \right)^2$$

$$\bar{d}_2 = f_3 f_4 \left( \frac{\partial \eta}{\partial x} \right)^2$$

$$\overline{d}_3 = f_3 \frac{\partial^2 \eta}{\partial x^2}$$

$$\overline{d}_4 = \frac{f_3 \left( \frac{\partial \eta}{\partial x} \right)^2}{2T}$$

$$\overline{d}_5 = \frac{\dot{w}}{\rho}$$

$$f_1 = (h_1 - h_2) - (e_1 - e_2)$$

$$f_2 = e_1 - e_2$$

$$f_3 = \frac{\kappa_1 T^{1/2}}{R \rho}$$

$$f_4 = \frac{d \overline{R}}{d C_1} / \overline{R}$$

$$f_5 = \frac{f_1}{2T} + \beta_4$$

$$\beta_1 = \frac{P \vartheta_{ij}}{T^{3/2}}$$

$$\beta_4 = C_{p1} - C_{p2}$$

**APPENDIX B**  
**EQUILIBRIUM COMPOSITION**  
**OF THE**  
**COMBUSTION PRODUCTS**

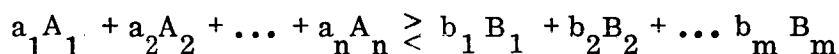


The method for determining the equilibrium composition of the combustion gas will be shown by considering a fuel and oxidizer which produce compounds containing only C, H, O, and N.

It will be assumed that the following products are formed: CO, CO<sub>2</sub>, H, H<sub>2</sub>, H<sub>2</sub>O, OH, O, O<sub>2</sub>, N, N<sub>2</sub>, and NO. At the combustion temperatures T<sub>C</sub>, it is assumed that the products are perfect gases in equilibrium.

For the assumed equilibrium there are seven equations for the required equilibrium constants K<sub>1</sub>, K<sub>2</sub>, ..., K<sub>7</sub>.

Consider the general chemical reaction equation



where a<sub>i</sub> is the number of moles of the i<sup>th</sup> species of the reactants A<sub>i</sub> and b<sub>j</sub> the number of moles of the j<sup>th</sup> species of the products B<sub>j</sub>.

For a chemical reaction conducted so that ΔT = Δp = 0, which is the case of measuring the enthalpy of reaction, the free energy is given by

$$\Delta F_{T,p} = \sum_{j=1}^m b_j F_{B_j} - \sum_{i=1}^n a_i F_{A_i}$$

where F<sub>B<sub>j</sub></sub> and F<sub>A<sub>i</sub></sub> are the free energies of the species B<sub>j</sub> and A<sub>i</sub> respectively. If ΔF° is the standard free energy change for the products and reactants,

$$\Delta F^\circ = \sum_{j=1}^m b_j F^\circ_{B_j} - \sum_{i=1}^n a_i F^\circ_{A_i}$$

and the free energy change for the reaction is given by:

$$F_{T_{1,p}} - \Delta F^\circ = RT \ln \left[ \frac{\prod_{j=1}^m (B_j)^{b_j}}{\prod_{i=1}^n (A_i)^{a_i}} \right]$$

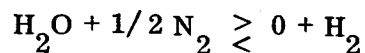
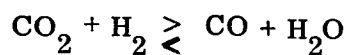
where  $\pi$  is the product sign.

When the chemical reaction is in equilibrium  $\Delta F_{T_{1,p}} = 0$ . Now, since the standard free energy change is a constant, the expression in the brackets is also a constant called the equilibrium constant represented by  $K_p$

$$K_p = \left[ \frac{\prod_{j=1}^m (B_j)^{b_j}}{\prod_{i=1}^n (A_i)^{a_i}} \right]$$

The seven reaction equations available for determining the equilibrium constants and the constants themselves are:

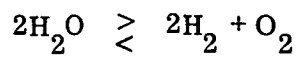
#### Reaction Equations



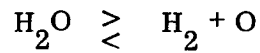
#### Equilibrium Constants

$$K_1 = \frac{(P_{\text{CO}})(P_{\text{H}_2\text{O}})}{(P_{\text{CO}_2})(P_{\text{H}_2})}$$

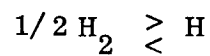
$$K_2 = \frac{(P_{\text{NO}})(P_{\text{H}_2})}{(P_{\text{H}_2\text{O}})(P_{\text{N}_2})^{1/2}}$$



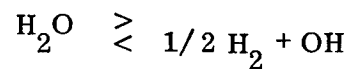
$$K_3 = \frac{(P_{\text{H}_2})^2 (P_{\text{O}_2})}{(P_{\text{H}_2\text{O}})^2}$$



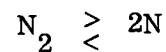
$$K_4 = \frac{(P_{\text{H}_2})(P_{\text{O}})}{(P_{\text{H}_2\text{O}})}$$



$$K_5 = \frac{(P_{\text{H}})}{(P_{\text{H}_2})^{1/2}}$$



$$K_6 = \frac{(P_{\text{H}_2})^{1/2} (P_{\text{OH}})}{(P_{\text{H}_2\text{O}})}$$



$$K_7 = \frac{(P_{\text{N}})^2}{(P_{\text{N}_2})}$$

For the determination of the number of moles for the assumed gas products four additional relationships are needed. These are provided by the requirement that each of the elements C, H, O, and N be conserved.

Therefore:

$$\Sigma \text{C} = n_{\text{CO}_2} + n_{\text{CO}}$$

$$\Sigma \text{H} = 2n_{\text{H}_2\text{O}} + n_{\text{OH}} + 2n_{\text{H}_2} + n_{\text{H}}$$

$$\Sigma O = 2n_{O_2} + n_O + n_{H_2O} + n_{NO} + n_{CO} + 2n_{CO_2}$$

$$\Sigma N = 2n_{N_2} + 2n_N + n_{NO}$$

where  $\Sigma C$ ,  $\Sigma H$ , etc., represent the total number of gram atoms of carbon, hydrogen, etc., and  $n_H$ ,  $n_O$ , etc., represent the number of gram atoms in the products of the gas indicated by the subscripts on the n's.

The conservation equations can be rewritten in terms of partial pressures by:

$$CO_2 + CO = \frac{RT}{V} \Sigma C$$

$$2H_2O + OH + 2H_2 + H = \frac{RT}{V \Sigma H}$$

$$2O_2 + O + H_2O + OH + NO + 2CO_2 + CO = \frac{RT}{V \Sigma O}$$

$$2N_2 + N + NO = \frac{RT}{V \Sigma N}$$

The seven equations for the equilibrium constants together with the four equations of conservation comprise a set of eleven equations with eleven unknowns which are solved simultaneously using the Newton-Raphson method to give the equilibrium composition of the combustion products.

#### Thermodynamics Properties of an Equilibrium Mixture

The following equations are used to calculate the thermodynamic properties for the combustion products in equilibrium:

Molecular Weight gr/ mole

$$M = \sum_{i=1}^q M_i X_i$$

Enthalpy cal/ gr

$$h = \frac{RT}{M} \sum_{i=1}^q X_i \left( \frac{H_i}{RT} \right)$$

Entropy cal/ gr oK

$$S = - \frac{R}{M} \left[ \sum_{i=1}^q H_i \left\{ \ln X_i + \left( \frac{\phi S_i^0}{R} \right) \right\} + \ln p \right]$$

where

$$\frac{S_i^0}{R} = \left[ \frac{H_i^0}{RT} - \frac{F_i^0}{RT} \right]$$

Frozen Specific Heat cal/ gr oK

$$C_p = \frac{R}{m} \sum_{i=1}^q X_i C_{Pi}$$

Specific Volume cm<sup>3</sup>/ gr

$$U = \frac{1}{q} = 82.0592 \frac{T}{Mp}$$

where

- $p$  = pressure in atmosphere
- $T$  = temperature in degrees Kelvin
- $X$  = mole fractions of the species
- $q$  = total number of constituents in the system
- $R$  = gas constant in cal/mole oK
- $F_i$  = free energy of the  $i^{\text{th}}$  species in cal/gr.
- $H_i$  = absolute enthalpy per mole of  $i$

### Specific Impulse

The calculation of the theoretical specific impulse  $I_{sp}$  is the same as the determination of the isentropic enthalpy change ( $h_c - h_{ext}$ ). To compute the specific enthalpy  $h_c$ , the equilibrium composition of the gases produced by a combustion reaction and the combustion temperature must be determined.

Calculation of the combustion temperature  $T_c$  involves calculating the equilibrium composition of the combustion products and the heats of reaction.

From the foregoing statements it is shown that calculation of the theoretical specific impulse involves determining:

- a. The combustion temperature  $T_c$ .
- b. The composition, gamma, and molecular weight of the gas.
- c. The specific enthalpy of the gas.
- d. The exit temperature  $T_{exit}$  of the gas in the exit plane of the nozzle.
- e. The composition, gamma, and molecular weight of the gas at  $T_{exit}$ .
- f. The specific enthalpy of the gas at the exit plane  $h_{exit}$ .

When  $P_{exit} = P_o$ , the combustion gases are expanded completely to the predominating back pressure and the specific impulse is a maximum value.

**APPENDIX C**  
**VACUUM BALANCE**  
**IMPULSE MEASUREMENT**

## 1.0 INTRODUCTION

A thrust measurement problem encountered during the development of a micropound electric thruster lead to this unusual application of an analytical vacuum balance. The thruster engine operates in a pulsating mode at pulse rates ( $f$ ) up to a current maximum of about ten pps. The electrical input pulse produced by a charged capacitor is extremely short, on the order of microseconds. The pulse duration ( $\tau_P$ ) and the pulse shape  $F(t)$  of the engine thrust are not exactly known. The impulse ( $I$ ) prior to measurement was estimated to be in the range of 0.1 to 1 dyne-seconds per joule input. The engine impulse is defined as:

$$I = \int_0^{\tau_P} F(t) dt = \int_{v_1}^{v_2} m dv = \Delta m v \quad \begin{array}{l} \text{(change in} \\ \text{momentum)} \end{array}$$

and the average thrust ( $\bar{F}$ ) as

$$\bar{F} = I f$$

For a firing rate ( $f$ ) of a few times per second, the average thrust was expected to be on the order of 1 dyne per joule input. (4 dynes  $\approx$  4 milligrams force  $\approx 10^{-5}$  pound force). The average thrust over the firing interval  $\tau_P$  is  $I/\tau_P$  and is estimated to be on the order of tenths of pounds; the peak thrust is even higher.

A spacecraft employing the electric thruster will respond to the average thrust of the engine. The immediate measurement problem, therefore, was to measure the impulse per firing or, alternately, the average thrust of a number of pulses at some fixed firing rate for a given electrical input energy.

From an engine design standpoint, it would also be desirable to have knowledge of the actual engine thrust pulse as a function of time. Because of the large inertia of the engine, measurements of this type may have to be made indirectly, on the thrust particles, by measuring their number and momentum as a function of time.



Several devices are inherently capable of making the impulse or average thrust measurement; a torsion wire pendulum, a ballistic pendulum, an analytical balance, or a long flexible shaft anchored at one end are among the possibilities. All these devices have time periods very long compared to the engine pulse and on the order of the engine firing rate. If the firing interval can be made small compared to the period of the measurement device, we have an integrator and can measure the average thrust of a large number of firings. If the period of the measuring device is insufficiently long to permit integration, we can still measure the peak deflection produced by a single firing and relate this to the engine impulse.

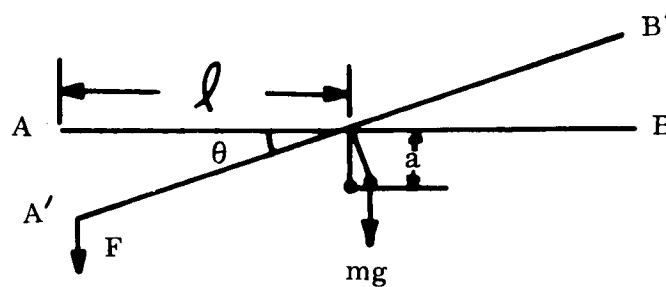
Of the various devices mentioned, an analytical balance is most convenient to use in the sense that a direct calibration in terms of static weight is possible. For example, with a damped balance, it would be possible to mount the engine and power source on one pan, balance out the static weight, then fire the engine at a high pulse rate compared to the balance period, and measure the average resulting thrust directly in terms of weight. An Ainsworth Type AV balance of 200 grams capacity and having a sensitivity of less than 1 milligram designed for use in a vacuum was available. The balance readout, an integral part of the balance system consisting of a transducer coupled to an electro-mechanical driven chart recorder, indicated weight by sensing balance arm position.

In consideration of these factors, analytical and experimental determination of the balance response to an impulse were initiated.

## 2.0 DYNAMIC CHARACTERISTICS OF AN ANALYTICAL BALANCE

This section analytically describes the motion of the balance under the influence of impulsive forces. An expression is derived which relates deflection of the balance under impulsive forces in terms of static weight. This relationship thus determines the calibration of the balance to impulsive forces.

Let us now examine the dynamics of a balance under the influence of a disturbing torque.



Let AB represent a rigid rod of mass  $m$ , of length  $2\ell$ , balanced at 0, with the CG a distance  $a$  below the balance point. Then, inertial moment = disturbing moment - restoring moment

$$I \ddot{\theta} = F \ell \cos \theta - mga \sin \theta$$

Assume the system loses energy through damping proportional to  $\dot{\theta}$ . The damping coefficient is  $C$ , acting at  $\ell$ . The moment of inertia of the beam is  $m \ell^2/48$  normal to the length at the center. The basic differential equation is thus

$$\ddot{\theta} + \frac{48C}{m \ell} \dot{\theta} + \frac{48ga}{\ell^2} \theta = \frac{48F}{m \ell}$$

where the equation has been linearized for small  $\theta$ , i.e.,  $\cos \theta \approx 1$ ,  $\sin \theta = \theta$ . It is interesting to note the equation also holds for the ballistic pendulum except that the coefficients must be modified.

Let

$$\frac{48C}{m \ell} = k$$

$$\frac{48ga}{\ell^2} = \rho^2$$

$$\rho^2 - \frac{k^2}{4} = \omega^2$$

Now let the disturbing force be constant and acting for a duration  $\tau$ . The equations of motion become:

$$\ddot{\theta} + k \dot{\theta} + \rho^2 \theta = \frac{48F}{m\ell} \quad 0 \leq t \leq \tau \quad (1)$$

$$\ddot{\theta} + k \dot{\theta} + \rho^2 \theta = 0 \quad t > \tau \quad \text{with the quantities} \quad (2)$$

$\theta_\tau$  and  $\dot{\theta}_\tau$  being the initial conditions for the second equation.

The solution of Equation (1) is

$$\theta = \frac{F\ell}{mga} \left[ 1 - \frac{k}{2\omega} e^{-\frac{kt}{2}} \sin \omega t - e^{-\frac{kt}{2}} \cos \omega t \right] \quad 0 \leq t \leq \tau$$

for  $\theta = 0, \dot{\theta} = 0$  at  $t = 0$

Now

$$\theta_\tau = \frac{I \ell \omega^2 \tau}{2 mga}, \quad \dot{\theta}_\tau = \frac{I \ell \omega^2}{mga} \quad \text{where } I = F \tau$$

The solution to Equation (2) above is

$$\theta = e^{-\frac{kt}{2}} \left[ \left( \frac{I \ell \omega}{mga} + \frac{k}{4} \frac{I \ell \omega \tau}{mga} \right) \sin \omega t + \frac{I \ell \omega^2 \tau}{2 mga} \cos \omega t \right] \quad t > \tau$$

without damping, we have

$$\theta = \frac{I \ell \omega}{mga} \left[ \sin \omega t + \frac{\tau \omega}{2} \cos \omega t \right]$$

allowing that

$$\frac{k \tau}{4} \approx 0, \quad \frac{\tau \omega}{2} \approx 0$$

we have

$$\theta_d = \frac{I \ell \omega}{mga} e^{-\frac{kt}{2}} \sin \omega t$$

with damping

$$\theta = \frac{I \ell \omega}{mga} \sin \omega t$$

without damping.

Actually  $\omega$  in the second equation differs from that in the first, as a function of damping factor ( $k$ ).

The first maximum deflection for the undamped case occurs at  $t_{\theta_{\max}} = T/4$  where  $T = 2\pi/\omega$  is the balance time period. For the damped case, the maximum deflection occurs at

$$t_{\theta_d \max} = \frac{T}{2\pi} \tan^{-1} \frac{4\pi}{kT}$$

$$\approx \frac{T}{4} \text{ with low damping.}$$

The maximum deflection in response to an impulse is therefore,

$$\theta_{\max} = \frac{\ell}{mga} \cdot \frac{2\pi}{T} I \quad \text{without damping}$$

and

$$\theta_{d \max} = \frac{l}{mga} \cdot \frac{2\pi}{T} I e^{-\frac{k}{2} \left( \frac{T}{2\pi} \tan^{-1} \frac{4\pi}{kT} \right)} \quad \text{with damping}$$

$$\dot{=} \frac{l}{mga} \cdot \frac{2\pi}{T} I e^{-\frac{kT}{\theta}} \quad \text{with low damping}$$

The static deflection independent of damping is  $\theta_s = l/mga \cdot F$  where  $F$  is a constant force or deadweight. The constant  $l/mga = \theta_s/F$  is a normal balance sensitivity factor and can be easily verified with known weights. The damping factor ( $k$ ) and time period ( $T$ ) can be experimentally determined from the balance motion after release from an initial deflection. The balance motion as monitored on the recorder appears as a damped oscillation. The time period ( $T$ ) can be determined by timing one or more oscillatory cycles. The damping factor can be computed from recorded values of two successive peak deflections ( $\theta_1, \theta_2$ ) occurring at an interval of one time period apart as follows:

$$\theta_2/\theta_1 = e^{-\frac{k}{2} T}$$

$$\ln \theta_2/\theta_1 = -\frac{k}{2} T$$

$$k = -\frac{2}{T} \ln \theta_2/\theta_1 = \frac{2}{T} \ln \theta_1/\theta_2$$

In terms of the known or experimentally determined constants, the balance impulse response can be expressed as:

$$\frac{I}{\theta_{d \max}} = \frac{F}{\theta_s} \cdot \frac{T}{2\pi} e^{\frac{kT}{8}}$$

With low damping, the exponential term can be neglected with little error giving.

$$\frac{I}{\theta_{\max}} = \frac{F}{\theta_s} \cdot \frac{T}{2\pi}$$

### 3.0 CALIBRATION METHODS AND TEST RESULTS

The balance has a period of about three seconds undamped when loaded with about 50 grams on each pan, i.e., the weight of the thruster engine. This is too fast to permit operation as an integrator, but would permit the impulse measurement of a single firing. An experimental arrangement was set up by mounting the engine on one pan, and balancing out the static weight of the engine. Thin flexible silver ribbon leads were connected to the engine so as to apply minimum restoring torque on the balance. Heavy leads obviously cannot be used. When the engine was fired, a thermal deformation of the leads was noted. This deformation was permanent, and ruled out the possibility of connecting high current leads directly to the engine on the pan.

A mercury pool contact mechanism was devised to overcome the lead deformation problem. The mercury was covered with oil because of its relatively high vapor pressure at room temperature. The mercury-oil combination acted as a heavy viscous damper and introduced errors due to the change in buoyant force with displacement of the leads and the capillary forces at the conductor oil interface. These errors were minimized by using a detergent in the oil to prevent wetting of the lead wires and by keeping the lead wire area submerged as small as possible relative to the contact surface area.

With the mercury contact configuration, the balance was loaded to about 75 grams on both the engine and counter-balance sides. Under these conditions, the balance sensitivity factor ( $\theta_s/F$ ) was determined to be  $\theta_s/F = 0.6$  recorder scale divisions per dyne, the time period (T) measured as  $T = 1.8$  seconds, and the damping factor (k) computed from successive peak deflections to be  $k = 0.78 \text{ sec}^{-1}$ . The resultant impulse response was then computed from

$$\theta_{d \text{ max}} = \theta_s/F \cdot \frac{2\pi}{T} e^{-kT/8}$$

as

$$I/\theta_{d \max} = 0.6 \text{ dyne-sec/division}$$

Under actual operation, the high current pulses produced a boiling action in the mercury indicating a significant energy loss.

As an alternate to mounting the ion engine on the balance pan, one can rigidly support the engine near the balance and impinge the engine exhaust against a plate connected to the balance arm. This method was also set up and the engine fired; however, consideration of the possible errors in this method discounted the resultant deflections measured.

The impingement method assumes several characteristics that may be invalid and hence produce significant error. First, it has yet to be shown whether the presence of the plate in the exhaust proximity influences the engine impulse. Secondly, unless the plate absorbs the total momentum of all exhaust particles, the method is in error. If elastic scattering is taking place, for example, the measured impulse could be high by a factor of two maximum. Finally, it is assumed that no secondary particles are emitted from the plate and that no static field is built up between the plate and engine. All of these factors are difficult to assess, and lead one to the conclusion that the impingement method should be relied on only as a last resort and then, only after attempting to evaluate the unknowns. The measured impulse of the engine by this method may be in error by 100% or more.

While the floating mercury contact approach satisfactorily overcame the mechanical restriction problem associated with the flexible ribbon leads, the inherent energy loss in excessive lead length was further increased by the mercury contact drop. Since any firing circuit loss is detrimental to engine performance, it was decided to mount the thruster together with a compact firing circuit on the balance. This minimized the firing circuit losses and eliminated high current inputs to the mounted assembly. An additional connection was required for triggering purposes, however. A third mercury pool contact was added to meet this requirement. With this setup, an electrostatic force of sufficient magnitude to produce impulse errors on the order of 40% existed between the energized firing circuit

and the surrounding grounded balance components. Several attempts were made to compensate for this effect by installing grounded and biased planes above and below the firing circuit. Some success with this approach was obtained but in general, repeatability and stability were poor. In order to facilitate installation of compensating bias planes during these attempts, the mercury pool contact system was replaced by a flexible wire hookup with the leads entering the balance system in a coiled fashion along the axis of the main knife edge pivot. This input hookup proved to be superior to the mercury pool system with respect to damping and sensitivity. The final steps taken to reduce electrostatic deflection to an acceptable level were to enclose the engine and compact firing circuit in a grounded shield and to dress the input leads straight in along the main pivot axis. This arrangement is depicted schematically in Figure C-1. The leads were secured to the top of the pivot blade and along the balance arm, then were coiled down clear of the end pivot to mate with small spring clip connectors on the shielded thruster assembly. The static and dynamic noise level at the recorder output of the balance has been repeatably controlled to less than one division corresponding approximately to a force of one dyne or an impulse of  $1/2$  dyne-sec.

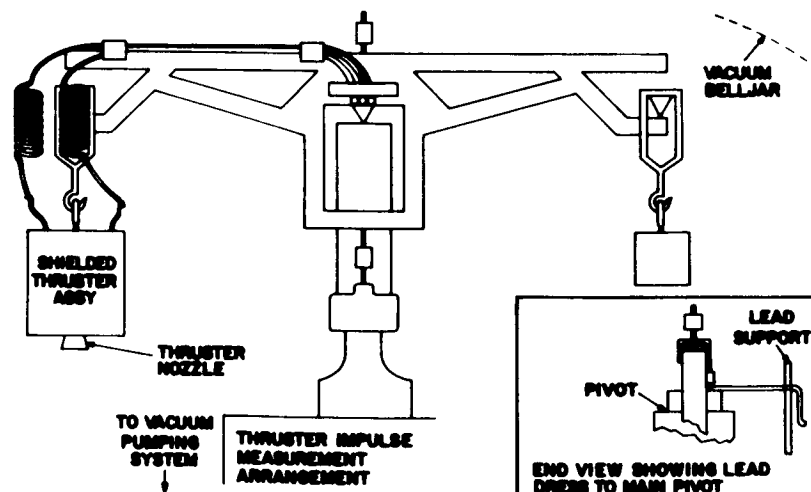


Figure C-1. Engine Impulse - Balance Fixture



Calibration of the balance was performed for dynamic impulse through the simple expedient method of dropping known weights through a known distance onto the balance. Knowing the dynamic response characteristics of the balance and the impulse imported to the balance by the weight, then a correction factor can be used for correlation with the actual engine thrust measurements.

From the dynamic response, we found that

$$\theta = e^{-k T/2} \left[ \left( \frac{I \ell \omega}{mga} + \frac{k \tau}{4} \frac{I \ell \omega}{mga} \right) \sin \omega t + \frac{I \ell \tau \omega^2}{2 mga} \cos \omega t \right]$$

setting  $d\theta/dt = 0$  and solving for  $t_0$  where  $t_0$  is the time required to reach  $T/2$  from  $t = 0$  gives:

$$\theta_{\max} = \frac{\ell}{mga} \left[ I \omega \sin \omega t_0 + \omega (1 - \cos \omega t_0) \right]$$

substituting in the test values (example = 10 milligram mass) produces

$$\begin{aligned} \theta_{\max} &= \frac{\ell}{mga} \quad 3.2 (0.3) + 10 (1 + 0.95) \\ &= \frac{\ell}{mga} \quad (20.46) \end{aligned}$$

Since the sensitivity of the balance is 1 mg = 1 division then for a mass of 10 mg an impulse displacement of 20 divisions would be expected at 0 cm height. Therefore, the additional impulse due to momentum would be 0.46 divisions at 10 centimeters height drop.

Figure C-2 represents the expected displacement due to a 10 mg mass dropping through known distance (Table C-1). It becomes apparent that due to the small mass tolerance and the heights needed to provide adequate momentum that this technique for calibration leaves much to be desired. Errors include air damping, air currents, etc. so that the practical momentum imparted at say 16 cm can be obliterated by these factors.

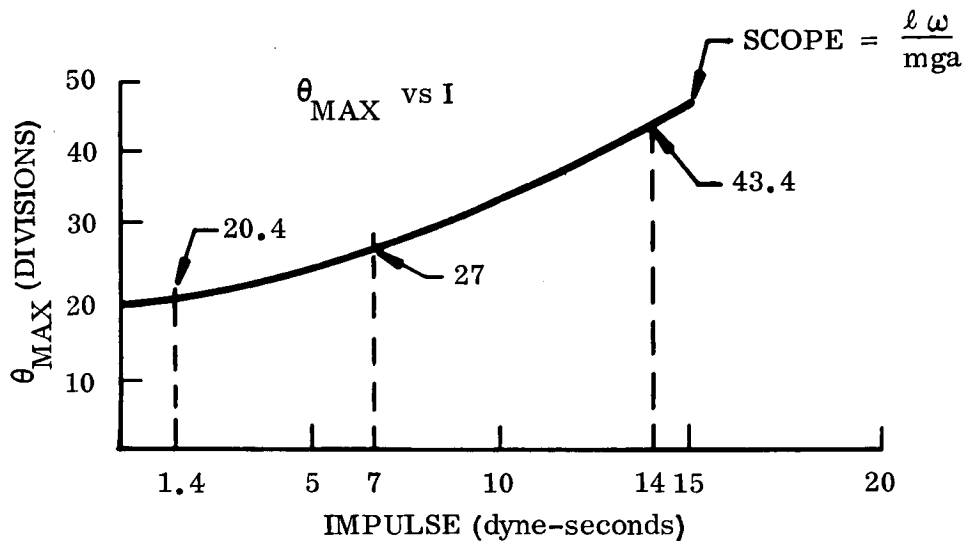


Figure C-2. Displacement Due to a 10 mg Mass Dropping Through Known Distance

An electric field forcing device was selected to overcome the problem of dropping small weights within the confines of the balance bell jar when under vacuum. The forcing device consisted of two parallel disks, one supported by the balance arm, the other mounted on the base plate as shown in Figure C-3. Electrically, the disk on the balance was grounded through one of the input leads, the other connected to a voltage source. The gap between disks was set at approximately 50 mils under balanced conditions. For static calibration, known weights were added to the counter balance side. The voltage levels required to return the balance to its initial position were then determined to establish the force vs. voltage characteristic at the original disk gap. Impulse type inputs in the form of high peak, exponentially decaying voltage pulses were then applied to the disks. Both peak voltage level and pulse width (time constant) were varied to determine the balance impulse response. The balance static sensitivity, oscillatory time period, and peak deflection ratio were measured for calculation of the theoretical response.

TABLE C-1. IMPULSE CALIBRATION DROPPING MASS METHOD

STATIC MASS (MILLI- GRAMS)	HEIGHT (cm)	MEASURED TOTAL STEP IMPULSE (DIVISIONS)	IMPULSE (DIVISIONS)	CALCULATED IMPULSE DYNE-SEC OR $\frac{\text{GR-CM}}{\text{SEC}}$	MEASURED SCALE FACTOR DYNE- SEC DIV.	BALANCE DAMPING 1 2 3 (SWINGS)
1) 10	10	22.5	12.5	1.4	0.56	12.5 10 9.6
2) 3	10	5	2	0.42	-	2.1 2.3 -
3) 3	16	6.4	3.4	0.53	1.2	3.2 3.5 2.7
4) 7.5	16	17	9.5	1.33	0.67	9.5 8.0 7.5
5) 4	16	8.2	4.2	0.71	0.4	5 4 4
6) 10	16	29.5	19.5	1.78	-	10 10.5 9.5

Sensitivity 1 mg = 1 scale divisions

Constants:

$$1 \text{ dyne} = 1.02 \times 10^{-3} \text{ grams} = 1.02 \text{ mg}; 1 \text{ dyne} - \text{sec} = 1 \frac{\text{gram-cm}}{\text{sec}}$$

$$v = v_o + at$$

$$y = v_o t + \frac{1}{2} at^2$$

$$@ 10 \text{ cm} = t_1 = 0.143 \text{ sec}; v_1 = 140 \text{ cm/sec}$$

$$@ 16 \text{ cm} = t_2 = 0.181 \text{ sec}; v_2 = 178 \text{ cm/sec}$$

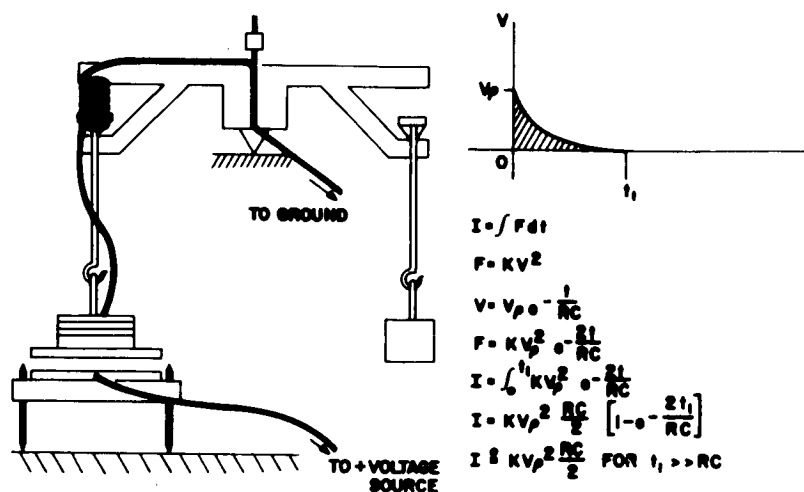


Figure C-3. Electrical Impulse - Balance Calibration

The electric field force between thin parallel disks is given by:

$$F = \frac{1}{2} E_o A \frac{V^2}{d}$$

where  $E_o$  = is the dielectric permeability of the medium between the disks

$A$  = is the area of each disk

$V$  = is the potential difference between disks

$d$  = is the gap distance between disks

The calibration approach used eliminated the need for computing disk area, accurately measuring the gap, and compensating for firings effects. The force-voltage relationship was directly determined to obtain the ratio constant  $K = F/V^2$  (dynes/sq. volt) as described above. The impulse acting on the balance by applying a voltage pulse to the disks is then

$$I = \int_0^{t_1} F(t) dt$$

$$I = K \int_0^t V(t)^2 dt$$

Figure C-4 shows the static force-voltage relationship for two disk gaps plotted on log-log scale to verify that  $F \propto V^2$ . For the impulse response calibration run the ratio constant K for a gap of about 40 mils was determined to be:

$$K = \frac{F}{V^2} = \frac{20.4 \times 0.980}{(187.6)^2} \quad \frac{\text{milligrams} \times \text{dynes/milligrams}}{(\text{volts})^2}$$

$$K = 5.68 \times 10^{-4} \text{ dynes}/(\text{volt})^2$$

The balance impulse response, taken as peak deflection ( $\theta_{d \max}$ ) from the recorder chart shown in Figure C-5, measured for several voltage pulses and the resultant impulse sensitivity factor computed are tabulated in Table C-2. For comparison, the theoretical impulse sensitivity factor and response to the same impulses were calculated and are also included in Table C-2. The balance time period and peak deflection ratios measured for use in the calculation of theoretical response were:

$$T = 2.9 \text{ seconds}$$

$$\frac{\theta_2}{\theta_1} = e^{-kT/2} = 0.93$$

$$k = -\frac{2}{T} \ln \frac{\theta_2}{\theta_1} = 0.050$$

$$e^{-kT/8} = 0.982$$

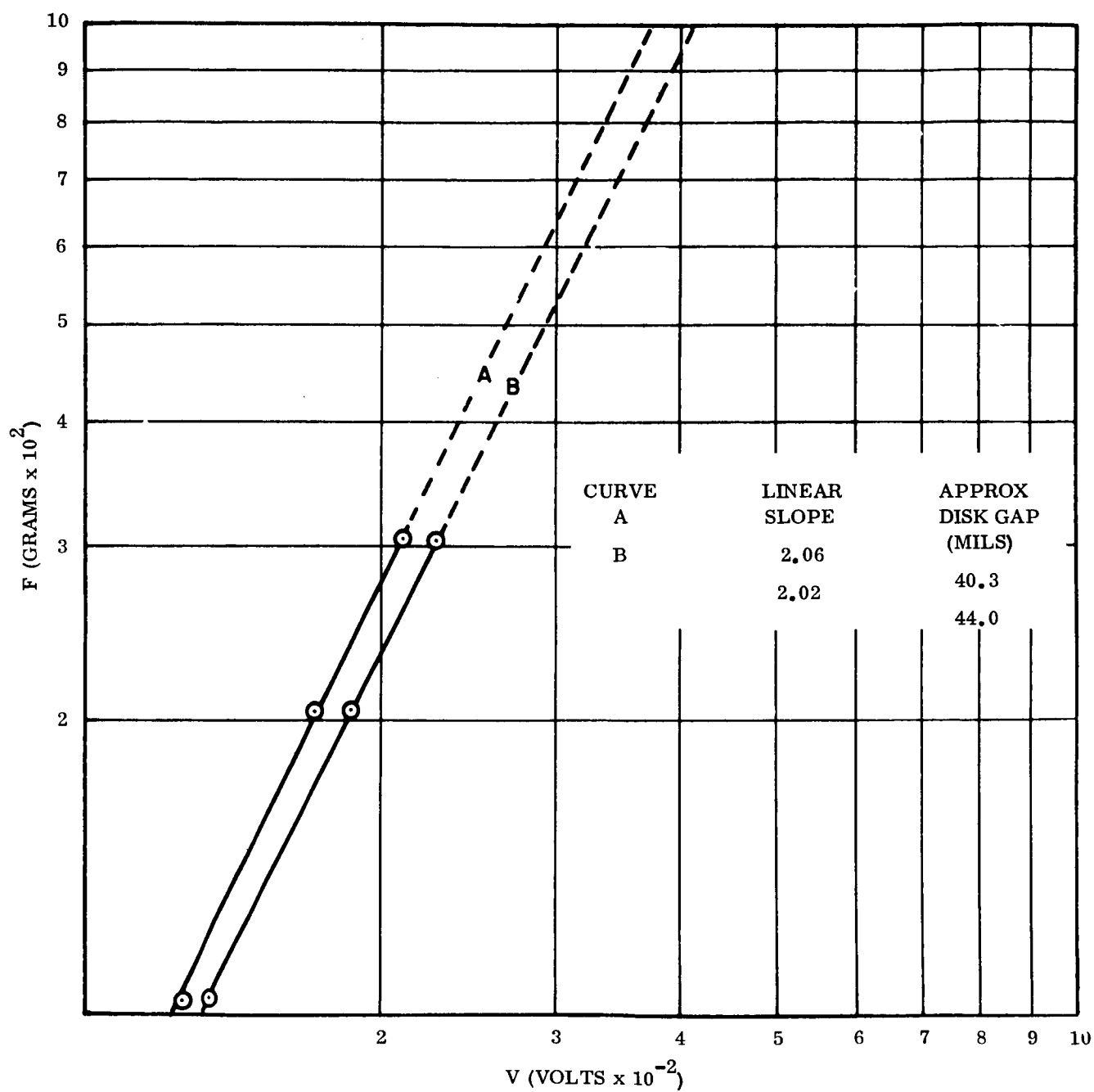


Figure C-4. Disk Force vs. Voltage

with the balance sensitivity  $\frac{F}{\theta_s} = 1 \text{ milligram/division} = 0.98 \text{ dynes/division}$ . The theoretical impulse response calculated was:

$$\begin{aligned} I/\theta_{d \max} &= \frac{F}{\theta_s} \frac{T}{2\pi} e^{kT/8} \\ &= 0.462 \frac{\text{dyne-sec}}{\text{division}} \end{aligned}$$

with  $V(t) = V_p e^{-t/\tau_c}$  for the exponential pulse used, where  $V_p$  is the peak voltage applied to the disks and  $\tau_c$  is the exponential time constant of the voltage pulse,

$$\begin{aligned} I &= K \int_0^{t_1} V_p^2 e^{-2t/\tau_c} dt \\ &= K V_p^2 \frac{\tau_c}{2} \left( 1 - e^{-2t_1/\tau_c} \right) \end{aligned}$$

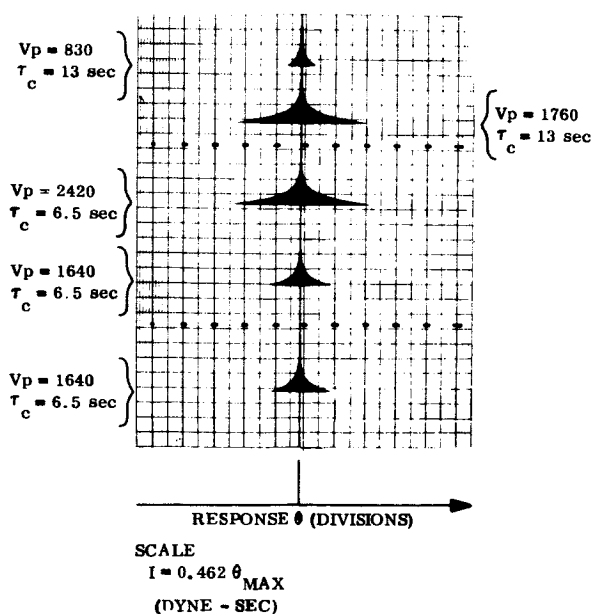


Figure C-5. Dynamic Calibration Electrical Impulse

For  $t_1 \gg \tau_c$

$$I \doteq K V_p^2 \cdot \frac{\tau_c}{2}$$

The circuit employed to generate the voltage pulse is a triggered capacitor discharge circuit as shown schematically in Figure C-6.

The resistor R was selected to control decay time constant (pulse duration). An oscilloscope with HV probe was used to monitor the voltage amplitude and waveshape at the disks.

The major source of error in this calibration procedure lies in the measurement of the transient voltage pulse. With the oscilloscope, the amplitude and time constant of the exponential waveshape could be measured to within only  $\pm 5$  percent. The static voltage was measured with a digital voltmeter to within less than 1% accuracy. Since the full scale balance deflection (100 divisions at the recorder) produces 35 mils displacement of the disks, the error in disk gap was controlled to less than one percent for a gap of 50 mils by returning the balance to within one division of the reference position for each weight-voltage combination. The maximum error in the generated impulse was then less than  $\pm 17$  percent with an rms error of less than  $\pm 12\%$  on these bases.

The impulse measurement data for a typical thruster are tabulated in Table C-3. The balance dynamic characteristic parameters for these measurements were the same as those determined for the electric field force impulse calibration configuration; i.e., the balance impulse response was 0.462 dyne-sec/division. The tabulated values of Impulse (I)/Input Energy (E) indicate a variation of almost 3:1 in this measure of thruster performance. The variation in I/E is characteristic of the engine tested and should not be interpreted as variations in balance impulse response. The balance impulse response ( $I/\theta_{d_{max}}$ ) calibration with the electric field force impulses varied less than  $\pm 7\%$  from the



average value as tabulated in Table C-2. Figure C-7 shows the recording of the balance response to the thruster impulse from which the tabulated impulse measurement data were derived.

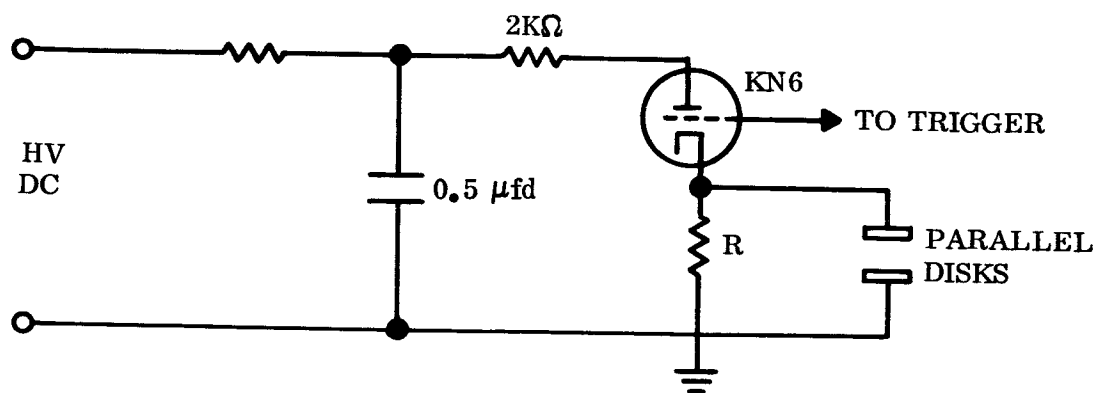


Figure C-6. Pulse Generator Circuit

## CONCLUSIONS

The analytical and experimental data can be summarized as follows:

- a. A vacuum analytical beam balance proved remarkably rugged and adaptable to making dynamic impulse measurements.
- b. Extreme care had to be used to prevent electrostatic deflection of the balance by thruster power leads. Electrostatic errors were minimized by lead dress geometry and shielding.
- c. Impulse calibration was accomplished satisfactorily with an electric field forcing device to within  $\pm 15\%$  of the calculated theoretical impulse response of the balance.
- d. With the proper selection of balance characteristics, this technique can be used to provide impulse and thrust measurements on pulsed or continuous microthrust engines.

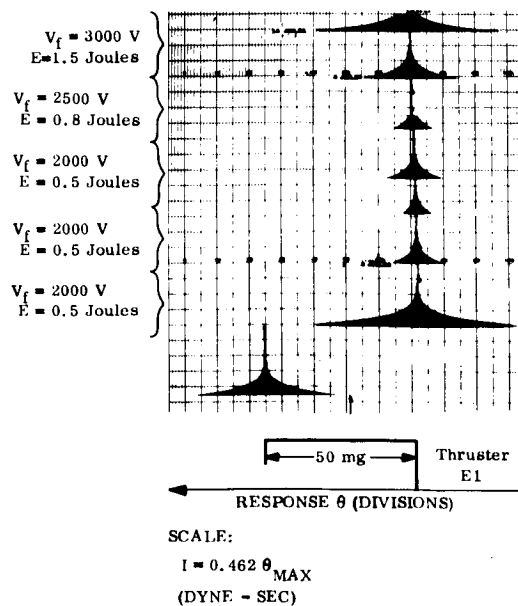


Figure C-7. Thruster Impulse Measurement

Table C-2. Impulse Response Calibration Data

INPUT IMPULSE				RESPONSE		
				MEASURED		THEORETICAL
V Volts	e (M sec)	K dynes/volt <sup>2</sup>	I (dyne-sec)	$\theta$ <sup>max</sup> (Div)	I/ $\theta$ <sup>max</sup> (dyne-sec/div)	$\theta$ <sup>max</sup> (Div)
1638	6.5	5.68x10 <sup>-4</sup> ↓	4.92	10.2	0.462 ↓	10.6
2420	6.5		10.8	22.5		23.4
1760	13.0		11.44	21.7		24.8
830	13.0		2.54	5.1		5.5
1795	13.0		11.9	25.3		25.7
AVG. 0.491						

Table C-3. Thruster Impulse Data

Firing Voltage V (Volts)	Pulse Energy E (Joules)	Maximum Deflection $\theta_{\max}$ (Divisions)	Impulse I = 0.462 $\theta_{\max}$ (Dyne-sec)	Impulse/Input Energy I/E (dynes/Joule)
2000	0.5	8.6	3.96	7.9
2000	0.5	4.0	1.85	3.7
2000	0.5	9.1	4.20	8.4
2000		6.4	2.95	5.9
2500	0.8	14.7	6.77	8.4
3000	1.5	32.0	14.77	9.8

**APPENDIX D**  
**DEFINITION OF AVERAGE PARAMETERS**  
**OF PULSED PROPULSION DEVICES**

## 1.0 DEFINITION OF AVERAGE PARAMETERS OF PULSED PROPULSION DEVICES

The average thrust  $\bar{F}$  of a pulsed device can always be defined over any duration of time as

$$\bar{F} = \frac{1}{t_2 - t_1} \int_{t_1}^{t_2} F dt \quad (1-1)$$

where  $F$  is the instantaneous value of the thrust.

Of the time intervals  $(t_2 - t_1)$  few are physically significant; starting from the smallest

$$\Delta t_1 = t_p = \text{duration of a single pulse}$$

$$\Delta t_2 = t_p + t_w = \text{period between two successive pulses}$$

$$\Delta t_3 = t_t = T_p + T_w = \sum_{j=1}^n (t_p)_j + \sum_{j=1}^{n-1} (t_w)_j = \text{period in which a train of } n \text{ pulses}$$

is delivered by maintaining the thruster continuously "on"

$$\Delta t_4 = \sum_K^m (t_t)_K + \sum_K^{m-1} (t_{\text{off}})_K = \text{period in which } m \text{ trains of duration } (t_t)_K \text{ are}$$

sent with  $(m-1)$  off periods of duration  $(t_{\text{off}})_K$  in between

$$\Delta t_5 = T_M = \sum_i^c (t_t)_i + \sum_i^{C-1} (t_{\text{off}})_i = \text{total mission duration during which } t \text{ trains}$$

of duration  $(t_t)_i$  are sent with a number of  $(C-1)$  "off" periods in between (and possibly one

more before first or after last train)

NOTE. A duty cycle can be properly defined only for the periods  $\Delta t_4$  and  $\Delta t_5$  respectively as:

$$(DC) = \frac{\sum_K^m (t_t)_K}{\Delta t_4} = 1 - \frac{\sum_K^{m-1} (t_{\text{off}})_K}{\Delta t_4}$$

$$(DC) = \frac{\sum_i^c (t_t)_i}{T_M} = 1 - \frac{\sum_i^{C-1} (t_{\text{off}})_i}{T_M}$$

Of these intervals the most significant is  $\Delta t_3$ . The corresponding average value of the thrust

$$(\bar{F})_{t_t} = \frac{1}{t_t} \int_0^{t_t} F dt = f_t (\bar{i})_{t_t} \quad (1-2)$$

where

$$f_t = \frac{n}{t_t} = \text{pulse frequency}$$

$$(\bar{i})_t = \frac{\sum_{j=1}^n (i)_j}{n} = \text{average pulse amplitude}$$

fully characterizes the pulsed device performance and makes it equivalent from a dynamical point of view to that of a "continuous while on" device provided that the pulse frequency is a decade or more larger or smaller than all of the characteristic frequencies of the vehicle. These frequencies are:

$f_s$  = structural frequency

$f_r$  = rigid body oscillation about center of mass

$f_{or}$  = orbit frequency

Of great physical significance is the time integral of the force  $F$  over the interval

$$\Delta t_1 = t_p \int_0^{t_p} F dt \quad (1-3)$$

which defines the magnitude of a single pulse. This characterizes the size of the bit and has bearings on sensing and command logic. On the other hand the average value of the thrust over the same time interval is devoid of any physical interest. The mechanical or dynamical effects are completely and exclusively defined by the impulse. As it is been pointed out in the discussion the quantity

$$\bar{F}^* = \frac{1}{t_p} \int_0^{t_p} F dt \quad (1-4)$$

acquires the significance of a mere physical oddity because of the conditions imposed on  $F$  and necessary to maintain finite the value of the integral however small the interval  $t_p$ .

A relation between  $\bar{F}$  the average thrust of a train, and  $\bar{F}^*$ , that of a single pulse can be written as

$$F = F^* \frac{1}{1 + \frac{T_w}{T_p}} \simeq \bar{F}^* \frac{T_p}{T_w} \quad (1-5)$$

where the last form of the right side is valid with increasingly good approximation for the fraction at numerator acquiring values increasingly larger than unity

$$\frac{T_w}{T_p} \rightarrow \gg 1$$

## 2.0 ENERGETIC OF THE PULSED THRUSTER

The thrust  $F$  delivered by a reaction device such as a rocket in absence of pressures acting on its boundary because of fluid dynamic or other fields effects can be related to the change in momentum of the following propellant. Thus, it can be immediately written as

$$F = \dot{m} (V_{ex} - V_o) \cong \dot{M} V_{ex} \quad (2-1)$$

where

$\dot{m}$  = propellant massflow

$V_{ex}$  = propellant exhaust velocity

$V_o$  = propellant incoming velocity

negligibly small in comparison with  $V_{ex}$

A proper definition of the specific impulse (of the propellant) can be given as

$$I_{sp} = \frac{F}{\dot{W}} = \frac{\text{Thrust}}{\text{Propellant weight flow}} \quad (2-2)$$

which only with the assumptions of zero pressure terms and zero incoming propellant velocity reduces to

$$I_{sp} = \frac{V_{ex}}{g} \quad (2-3)$$

where  $g$  is the standard acceleration of gravity in appropriate units.

In the case of pulsed devices the above equation can be immediately transformed to give the magnitude of the pulse in term of the specific impulse

$$i = \int_g^t F dt = m V_{ex} = w I_{sp} \quad (2-4)$$

with  $m$  and  $w$  representing respectively the mass and the weight of the propellant which has been accelerated, during the pulse, to the exit velocity  $V_{ex}$ .

The kinetic energy of the leaving mass is equal to the useful work  $W$  done on it by the forces acting in the devices, thus, it is equal to the  $\eta E$  fraction of the energy input,  $\eta$  being an overall efficiency.

$$\frac{1}{2} m V_{ex}^2 = \eta E$$

This energy input may come from sources internal to the propellant, that is from its total enthalpy  $H$  and from sources external to the propellant, such as for example from addition of an amount  $E_E$  of electrical energy

$$\frac{1}{2} m V_{ex}^2 \cong \eta_H H + \eta_E E_E \quad (2-6)$$

$$\text{or} \quad \frac{1}{2} m (V_{ex}^2 + V_{ex_o}^2) = \eta_H H + \eta_E E_E \quad (2-7)$$



Having assumed linearity in the process and thus used the principle of superposition.

The term

$$\frac{1}{2} m V_{ex_0}^2 = \eta_H H = \frac{1}{2} \eta_H m V_{ex}^2 \quad (2-8)$$

represents the transformation of the propellant total enthalpy in exit kinetic energy by acceleration to a directed velocity  $V_{ex_0}$ . This velocity is by definition the  $\sqrt{\eta_H}$  fraction of the ideal velocity  $V_{ex_0}$  obtainable by complete isentropic expansion to vacuum.

The term

$$\frac{1}{2} m (V_{ex}^2 - V_{ex_0}^2) = \eta_E E_E \quad (2-9)$$

represents the additional conversion of the energy applied from an external electrical source for further acceleration to the final exit velocity  $V_{ex}$ .

By using the definition of specific impulse and the numerical factors required for appropriate conversion of units the input of electrical energy necessary for each pulse to obtain the desired specific impulse  $I_{sp}$  is given as

$$E = \frac{22}{\eta} w I_{sp}^2 \left[ 1 - \frac{I_{sp_0}}{I_{sp}} \right] \quad (2-10)$$

$E = (\text{Joules})$   
 $w = (\text{pound})$   
 $I_{sp} = (\text{sec})$

where

$$I_{sp_0} = \sqrt{\eta_H} I_{sp_\infty} \quad (2-11)$$

is the specific impulse obtainable by direct expansion to vacuum, thus the  $\sqrt{\eta_H}$  fraction of the ideal specific impulse  $I_{sp}$

The pulsed thruster while operating requires an average power

$$\bar{P} = \frac{\sum_{j=1}^n (E)_j}{t_t} = \frac{n}{t_t} (\bar{E}) = f_t (\bar{E})_{t_t} \quad (2-12)$$

where

$$(\bar{E})_{t_t} = \frac{\sum_{j=1}^n (E)_j}{n} \quad (2-13)$$

is the average energy per pulse.

Assuming  $I_{sp}$  and  $\eta$  to be constant and using Equations (2-4) and (4-23) this other expression for the average power can be obtained

$$\bar{P} = \frac{22}{\eta} \bar{F} I_{sp} \left[ 1 - \left( \frac{I_{spo}^2}{I_{sp}^2} \right) \right] \quad (2-14)$$

Finally, if it is also assumed that the pulses are identical and equally spaced then the average power over the entire operating period given by Equation (2-14) becomes numerically identical to the average power over the time interval between two successive pulses.

Notice that the  $I_{sp}$ ,  $H$  and other associated parameters as the stagnation temperature etc., are identical to those used in the treatment of steady state devices.

### 3.0 CHARACTERISTICS OF SPET THRUSTERS

The firing frequency of the SPET engines has been selected in the range 0.2 - 2 CPS which is safely away from the resonance frequencies of typical space vehicles. In this manner the SPET's behave from a mechanical and dynamical point of view as "continuous while on" thrusters of ratings numerically equal to those described by the SPET average parameters  $\bar{F}$ ,  $\bar{P}$  and  $(\bar{i})t_t$ .

Typical SPET thrusters have demonstrated an impulse bit or "pulse" of 10  $\mu$  pound/sec with an energy input of 0.5 Joules. The duration of the "pulse" is of order of few microseconds (1 - 8).

For sake of simplicity consider a duration of the "pulse" equal to five microseconds. It will be apparent from what follows that its exact value is for the purpose of this analysis irrelevant. The dynamics are fully characterized by the size of the impulse.

As it is characteristic for impulsive motions the average thrust of the SPET during the length of the "pulse" acquires large values necessary to maintain finite the impulse bit or in our terminology the "pulse." For example for said typical SPET thruster (Equation 4-5).

$$\bar{F}^* = \frac{10 \times 10^{-6} \text{ pound sec.}}{5 \times 10^{-6} \text{ sec.}} = 2 \text{ (pound)} \quad (3-1)$$

If the interval between firings is one second, then the approximation  $t_p/t_w \ll 1$  is well justified. Thus by Equation 4-11 the average thrust is

$$\bar{F} = \frac{2 \text{ (pound)}}{1 + 2 \times 10^5 \text{ (sec)}} = 10^{-5} \text{ (pound)} \quad (3-2)$$

The same result can be obtained more directly by using Equation 4-8

$$\bar{F} = \frac{\sum_{j=1}^n (i)_j}{t_t} = \frac{10 \times 10^{-6} \text{ (pound sec.)}}{1 \text{ (sec)}} = 10^{-5} \text{ (pound)} \quad (3-3)$$

If a train of ten "pulses" identical to the one described is fired in a second substitution of the pertinent values

$$\overline{F}^* = 2 \text{ (pound)}$$

$$t_t = 1 \text{ (sec)}$$

$$n = 10$$

$$t_p = 5 \times 10^{-6} \text{ (sec)}$$

$$t_w = \left[ \frac{1}{9} - \frac{5}{9} \times 10^{-5} \right] \text{ (sec)}$$

Equation 4-17 would give

$$\overline{F} = \frac{\overline{F}^*}{1 + \frac{n-1}{n} \frac{t_w}{t_p}} = \frac{2 \text{ (pound)}}{1 + \frac{9}{10} \frac{1}{9} \frac{1}{5 \times 10^{-6}}} 10^{-4} \text{ (pound)} \quad (3-4)$$

which of course checks as it should up to the fourth significant digit, with the value obtained from Equation 4-8

$$\overline{F} = \frac{\sum_{j=1}^n (i)_j}{j} = \frac{10 \times 10^{-5} \text{ (pound sec.)}}{1 \text{ (sec.)}} = 10^{-4} \text{ (pound)} \quad (3-5)$$

In a similar manner considerations of the energetics may seem to lead to paradoxical values if the same degree of caution is not applied in dealing with the impulsive relations. For example one may be astounded by the large value of  $\overline{F}^*$  and deduct as a consequence that because of the small mass employed (in the order of few micrograms) tremendously large specific impulse and stagnation temperature must be involved. From this it is easy to conclude that since such temperatures are not easily obtainable in the laboratory, the measured SPET performance should be categorically questioned. As a matter of fact, carried off by the ways of thinking developed by working with continuous devices, one might take

$$F = 2 \text{ pound} \quad \dot{W} = 10^{-8} \text{ (pound)}$$

$$I_{sp} = 2 \times 10^{-8} \rightarrow \text{to } ? \gg 100,000 K^0$$

and thus become quite an unbeliever of the quoted measurements. A look at the energetic equations may clear this misconception.

If one insists in using the of time-energy equations over the duration of the pulse one has also to realize that both the power and the mass flow acquire tremendously large values. Thus what was mistakenly taken for  $F$  was instead

$$\int_0^{t_p} \dot{W} dt = W$$

while  $\dot{W}$  averaged over the five microsecond duration of the pulse is

$$\dot{W} = \frac{10^{-8}}{5 \times 10^{-6}} = 2 \times 10^{-3} \left( \frac{\text{pound}}{\text{sec.}} \right)$$

Similarly the average power over the same five microsecond is

$$P = \frac{1}{5 \times 10^{-6}} = 2 \times 10^5 \text{ (watts)} = 200 \text{ (KW)}$$

The specific impulse thus needs to be

$$I_{sp} = \frac{2}{2 \times 10^{-3}} = 1000 \text{ (sec.)}$$

which obviously checks that obtained from

$$P = \frac{0.022}{\eta} F I_{sp} = \frac{0.022}{\eta} 2 \times 1000 \text{ (KW)}$$

$$I_{sp} = 1000 \text{ (sec.)}$$

having assumed conservatively

$$\eta = 22\%$$

The stagnation temperatures depending on the nature of the gas and on the processes involved surely does not need to be extravagantly high.

#### 4.0 DISCUSSION

A first integral of the equation of dynamic motion gives the expression

$$i = \int_{t_0}^{t_1} F dt = \int_{t_0}^{t_1} m \frac{dv}{dt} dt = m (v_1 - v_0) \quad (4-1)$$

which relates over the time interval  $(t_1 - t_0)$  the impulse of the force  $F$  to the change in momentum of the mass  $m$  on which said force is acting.

This equation becomes the governing relation of impulsive motion, provided that the force  $F$  acquires sufficient magnitude to maintain finite the value of the integral

$$\int_{t_0}^{t_1} F dt \text{ however small the time interval } (t_1 - t_0).$$

A mean value for  $F$  can always be defined in the small interval  $(t_0 - t_1)$  in which the impulsive event occurs

$$\overline{F^*} = \frac{1}{t_1 - t_0} \int_{t_0}^{t_1} F dt = \frac{i}{t_1 - t_0} \quad (4-2)$$

Both the average force as defined and the peak value of  $F$  are amenable to analytical determination depending on the knowledge and character of the prescribed function  $F(t)$ .

It is always possible by appropriate translation of the  $t$  coordinate axis to write the small interval of time or pulse duration as

$$t_1 - t_0 = t_p \quad (4-3)$$

and the equation of impulsive motion

$$i = \int_0^{t_p} F dt = m (v_1 - v_0) \quad (4-4)$$

and the mean value of the force as

$$\overline{F^*} = \frac{i}{t_p} \quad (4-5)$$

where  $i$  is the elemental impulse, or impulse bit in our terminology "pulse".

Consider the case in which a train of  $n$  pulses each of magnitude ( $i$ ) is given over a time period  $t_t$  by definition greater than the sum total of the pulse duration

$$t_t > \sum_j^n (t_p)_j$$

In other words a truly pulsed behavior of operation is enforced by having the device on for a time always greater than that of a single "pulse"  $t_p$ . Notice that this definition includes that of a single pulse preceded or followed by a wait time period, during which the device is operational in the sense that it absorbs power. For example such is the case of a slow start or heat sink resisto-jet. This definition is therefore necessary to assure a proper account of the energy and power requirements of the device. Then one can write

$$t_t = \sum_j^n (t_p)_j + \sum_j^{n-1} (t_w)_j = T_p + T_w \quad (4-6)$$

where  $(t_w)_j$  has been defined as the wait period between "pulse"  $j$  and  $j + 1$ .

An average force over this period can always be defined (whatever the shape and form of the  $(t_p)_j$  and  $(t_w)_j$  intervals) as:

$$\overline{F} = \frac{1}{t_t} \int_0^{t_t} F dt = \frac{I}{t_t} \quad (4-7)$$



I being the total impulse delivered over the time  $t_t$  defined in Equation 4-6. By breaking the integral of Equation 4-7 in a summation of as many integrals as the propulsive and wait periods, the average thrust  $\bar{F}$  reacquires the most general form in term of the single "pulses"  $(i)_j$  whatever their shape and relation might be:

$$\bar{F} = \frac{1}{t_t} \left( \int_0^{t_{pj1}} F dt + \dots \int_{t_f - t_{pjn}}^{t_f} F dt \right) = \frac{1}{t_t} \sum_j^n (i)_j \quad (4-8)$$

Equation 4-6 and the definition of mean value of the force  $\bar{F}^*$  over the "pulse" time intervals permit to write this other expression of the average force  $F$  over the pulsed propulsion on period  $t_f$

$$\bar{F} = \frac{\sum_j^n (i)_j}{T_p + T_w} = \bar{F}^* \frac{1}{1 + \frac{T_w}{T_p}} \quad (4-9)$$

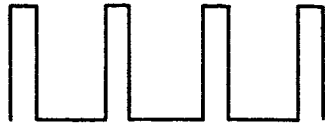
which for

$$\frac{T_w}{T_p} \gg 1 \quad (4-10)$$

reduces to

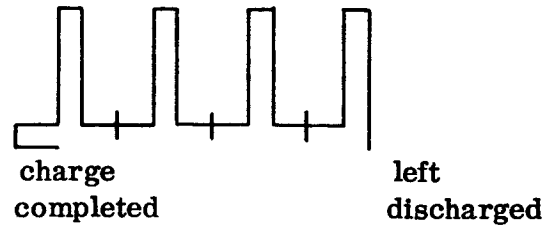
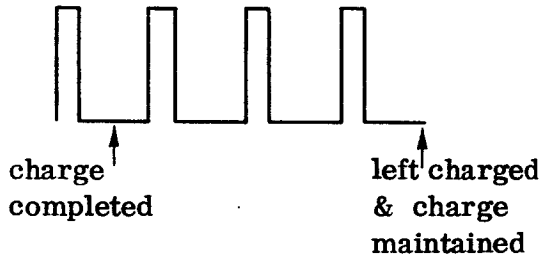
$$\bar{F} = \bar{F}^* \frac{T_p}{T_w} \quad (4-11)$$

Consider a more special case in which these additional constraints are added: The  $n$  "pulses" in the train are equal and equally spaced. Thus, here it has been assumed that the response to the on command is immediate. The wait period is not limiting this response .



$n$  pulses  $n - 1$  wait periods

From the energetic point of view instead a wait period may be required to average uniformly the power. Only for the cases in which the charge time or peak power are largely different from the average then the above condition  $n t_p, (n - 1) t_w$  is applicable



Otherwise the coefficient of  $\frac{t_w}{t_p}$  instead of  $\frac{n-1}{n}$  becomes unity.

Consider the first case, then

$$t_t = n (t_p + t_w) - t_w \quad (4-12)$$

and

$$\overline{F} = \frac{ni}{nt_p} \cdot \frac{1}{1 + \frac{n-1}{n} \frac{t_w}{t_p}} = F^* \cdot \frac{1}{1 + \frac{n-1}{n} \frac{t_w}{t_p}} \quad (4-13)$$

which for

$$\frac{t_w}{t_p} \gg 1 \quad (4-14)$$

gives

$$\bar{F} = \bar{F}^* \left( \frac{n}{n-1} \frac{t_p}{t_w} \right) \quad (4-15)$$

and with the addition condition

$$n \gg 1.$$

Reduces to

$$\bar{F} = \bar{F}^* \frac{t_p}{t_w} \quad (4-17)$$

of a form very similar to that of Equation (4-11).

Typical SPET thrusters, (This part with the numerical examples has been repeated in the section of the text called Characteristics of SPET Thrusters.) have demonstrated an impulse bit or pulse of 10 micro pound/second with an energy input of 0.5 Joules. The duration of the "pulse" is on the order of few microseconds (1-8).

For sake of simplicity consider a duration of the pulse equal to five microseconds. It will be apparent from what follows that its exact value is for the purpose of this analysis irrelevant. The dynamics are fully characterized by the size of the impulse.

As it is characteristic for impulse motions, the average thrust of the SPET during the length of the pulse acquires quite large values necessary to maintain finite the impulse bit or in our terminology the pulse. For example for the said typical SPET thruster Equation (4-5).

$$\bar{F}^* = \frac{10 \times 10^{-6} \text{ pound/second}}{5 \times 10^{-6} \text{ seconds}} = 2 \text{ (pounds)} \quad (4-18)$$

If the interval between firings is one second, then the approximation  $t_p \ll 1$  is well justified. Thus by Equation (4-11) the average thrust is:

$$\bar{F} = \frac{2 \text{ (pound)}}{(1 + 2 \times 10^{-5} \text{ (sec.)})} = 10^{-5} \text{ (pound)} \quad (4-19)$$

The same result can be obtained more directly by using Equation (4-8)

$$\bar{F} = \frac{\sum_{j=1}^n (i)_j}{t_f} = \frac{10 \times 10^{-6} \text{ (pound/second)}}{1 \text{ (second)}} = 10^{-5} \text{ (pound)} \quad (4-20)$$

If a train of the "pulses" identical to the one described is fired in a second substitution of the pertinent values

$$\bar{F}^* = 2 \text{ (pound)}$$

$$t_f = 1 \text{ (second)}$$

$$n = 10$$

$$t_p = 5 \times 10^{-6} \text{ (second)}$$

$$t_w = \frac{1}{9} - \frac{5}{9} \times 10^{-5} \text{ (second)}$$

In Equation (4-17) would give

$$\bar{F} = \frac{\bar{F}^*}{1 + \frac{n-1}{n} \frac{t_w}{t_p}} = \frac{2 \text{ (pounds)}}{1 + \frac{9}{10} \frac{1}{9} \frac{1}{5 \times 10^{-6}}} \approx 10^{-4} \text{ (pounds)} \quad (4-21)$$

which of course checks as it should up to the fourth significant digit, with the value obtained from Equation (4-8).

$$\bar{F} = \frac{\sum_{j=1}^n (i)_j}{t_f} = \frac{10 \times 10^{-5} \text{ (pound/second)}}{1 \text{ (second)}} = 10^{-4} \text{ (pounds)} \quad (4-22)$$

We might have clouded with an excessive formalism the basic significance which should have been extracted immediately from Equation (4-1). Namely, that the magnitude  $i$  of the "pulse" is the only parameter of relevance from the dynamical and mechanical point of view.  $\bar{F}$  acquires the significance of a mere physical oddity.

It may have been perhaps of value to have emphasized this fact with an example pointing to an extravagant size completely devoid of any mechanical meaning. It is in the nature of the physical processes involved to perform "a physical integration" which gives all of its significance and importance to Equation (4-1), one of the basic governing equation of physics. This also explains the intrinsic simplicity of an equation such as (4-8) which is expressed in terms of  $(i)_j$  the magnitudes of the single pulses, that is of the parameters proper to the physical description.

The significance and the role played by the other governing parameter  $\bar{F}$  the average thrust can now be appreciated by similar considerations.

The solutions of the dynamical equations of mechanical systems for most general case including potential, resistive and external forcing forces, indicate that regions of response which is linear to very good approximation are obtained for the cases in which the frequency of the forcing function is a decade smaller or larger than those characteristic of the mechanical system. In these regions it is then possible to substitute for the time depending force its average value.

In other words the mechanical systems are mobile to such an extent that they can freely follow the action of the force, or are so slow in response to sense only the integrated effect.

For this latter case one may be tempted to extract an analogy with the case previously treated when defining the impulsive motion. The analogy is somewhat curtailed by the independence of periodicity which is particular of that case.

A space vehicle response from the point of view of structural, rigid-body, and orbit mechanics to a train of pulses, is equivalent to that which it shows to a force which acts continuously over the same time interval and which has a magnitude equal to the average value  $\overline{F}$  of the train provided that the frequency of this latter is more than ten times smaller or larger than those characteristics of the vehicle response.

The frequency  $f_t$  of the train can be defined from:

$$\overline{F} = \frac{\sum_j^n (i)_j}{t_t} = \frac{n \overline{(i)}}{t_t} = f_t \overline{(i)} \quad (4-23)$$

as

$$f_t = \frac{n}{t_t} = \frac{\overline{(i)}}{\overline{F}}$$

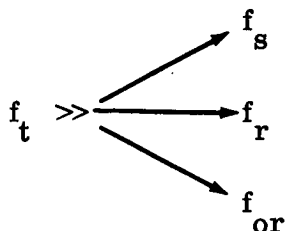
where

$n$  = number of pulses in the train

$t_t$  = duration of the train

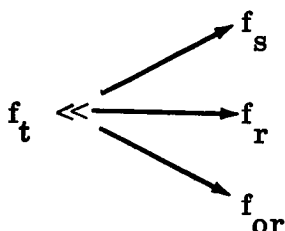
$\overline{(i)} = \frac{\sum_j^n (i)_j}{n}$  = average size of pulses in the train.

Thus



or

(4-24)



where

$f_s$  = vehicle structural frequency

$f_r$  = vehicle frequency to rigid body oscillation about its center of mass

$f_{or}$  = vehicle orbit frequency

define one of the two conditions which permit to substitute from a dynamical point of view a "pulsed while on" with a "continuous while on" thruster rated at the average thrust of the pulsed device.

Of course it is still possible with both of these systems to excite resonances by commanding them on and off in synchronism with any vehicle resonant frequencies. This would be tantamount to applying a step forcing function of impulse  $I = \bar{F} t_p$  and frequency  $f_{on} = \frac{1}{T}$ , there  $T$  is the time in between "on" commands.

For the case of pulsed system the possibility still exists of another periodicity of the forcing function to creep in by having the distribution of the  $(i)_j$  pulses around their average value

$$\overline{(i)} = \frac{\sum_{j=1}^n (i)_j}{n}$$

acquire a periodic rather than a random character. The frequency of this periodicity might have values much smaller than  $f_t$ , being lower limited, in principle, only by the duration  $t_t$  of the train. Thus it may no longer satisfy one of the conditions, Equation (4-24). On the other hand any periodic variation in the pulse train needs to possess sufficient amplitude to become a significant source of resonance such cases are excluded by proper design and operating techniques of these devices.

The characteristic frequencies of typical space vehicles are very low of order

$\frac{1}{100} \sim \frac{1}{1000}$  CPS. A pulsed thruster which would operate at a frequency of the order of one CPS would thus satisfy the conditions for being dynamically equivalent to a "continuous while one" thruster of a rating equal to the average thrust  $\overline{F}$  of the pulsed device.

The above considerations have led to the selection of firing frequencies of that order for the SPET engines and to the definition of their performance in terms of the average thrust  $\overline{F}_i$  and of the pulse magnitude. The first parameter thus permits direct comparison and substitution with "continuous while on" devices. The second characterizes the size of the thrusting bit and has bearings on the sensing and command logic.



**APPENDIX E**  
**A CHARACTERIZATION OF**  
**THE SPET-A**

The characterization of SPET involves many parameters, some of which are measured directly and others which are derived from measured quantities. The specific impulse ( $I_{sp}$ ) is one parameter of great importance which is defined<sup>(1)</sup> as the impulse produced from a unit weight of propellant or;  $I_{sp} = \frac{I \text{ (gm - sec.)}}{W \text{ (gm)}}$

The pulse can be measured with the vacuum balance impulse test fixture and the mass of the propellant used can be measured on an analytical balance. From these measurements  $I_{sp}$  is calculated. Table E-1 lists three typical engine's characteristics. The averages given will be used in the succeeding calculation but it should be pointed out that the averages do not represent any one particular engine and are used only for very general computations.

TABLE E-1. TYPICAL ENGINE CHARACTERISTICS

ENGINE NUMBER	CAPACITOR VOLTAGE (VOLTS)	ENERGY PER PULSE (JOULES)	FIRING RATE (PPS)	AVERAGE IMPULSE ( $\mu$ LB-SEC)	MASS USED (MG)	NO. OF PULSES	MASS USED PER PULSE ( $\mu$ g)	$I_{sp}$ (sec)	EFFICIENCY
M-1-A	2500	0.78	0.5	5.6	21.8	9,150	2.38	1033	0.157
103-2A	3000	1.13	0.5	13.7	17.4	7,976	2.18	2777	0.713
104-1	2500	0.78	0.5	6.9	31.2	10,450	2.99	1020	0.192
104-1	3000	1.13	0.5	9.2	33.2	8,885	3.74	1100	0.192
Average	2750	0.955	0.5	8.9	25.9	9,115	2.82	1482	0.31

These three engines have the same general form but differ in the fuel feeding mechanism and the area of the fuel film to be ablated. All of these engines have a fuel reservoir of 10 cc, in which a carborundum wick is inserted, which feeds the fuel up into the firing chamber by capillary action, where it is vaporized and heated by an electrical arc and expelled out through a stack.

<sup>(1)</sup>See Appendix D

Engine M-1-A is a slow feeder with an electrode gap of 20 mills and an electrode width of 1/16-inch.

Engine 103-2A is a slow feeder with an electrode gap of 10 mills and an electrode width of 1/8-inch.

Engine 104-1 is a fast feeder with an electrode gap of 30 mills and an electrode width of 1/16-inch.

NOTE: The A following the engine number indicates accelerating rails in the stack.

The fuel used in the engines was polyoxipropylene glycol (PPG) with 10% lithium perchlorate by weight. PPG, density of 1.007 gm/cc, is a long polymer with basic groups  $(C_3 H_6 O)_X$  where X has a mean value of 2,000. In preparing the fuel all chains of less than 500 basic groups were separated out. PPG's formula molecular weight is 58 gm/mole and the molecular weight of lithium perchlorate is 105 gm/mole. Lithium perchlorate is added because pure PPG is a very good electrical insulator but when it is mixed with lithium perchlorate the breakdown potential is lowered sufficiently so it will breakdown in our engine. From Table E-1 the average mass of propellant used per pulse is  $2.82 \times 10^{-6}$  gm and the number of atoms per gram of the fuel is  $0.96 \times 10^{23}$  atoms/gm. Thus the number of atoms expelled per pulse is  $2.7 \times 10^{17}$  atoms.

The average pressure in the nozzle can be determined from the measured impulse which when divided by the half period of the capacitor discharge will give the thrust. The half period is 0.8 microseconds giving a thrust of  $5 \times 10^6$  dynes. Thus the pressure is just this thrust divided by an effective area. From past experiments we have shown that the  $I_{sp}$  is not dependent on the shape of the nozzle to any measurable degree. This would tend to indicate the effective area on which the thrust acts is just the area of the base of the nozzle which is  $0.2 \text{ cm}^2$ . This assumption yields a pressure on the base of the nozzle of  $2.5 \times 10^7$  dyne/sq cm.

By observing the voltage at any point in the circuit and measuring the period of discharge and the logarithmic decrement, one is able to calculate the current as a function of time,  $I(t)$ , the total circuit's inductance and the total circuit's resistance. The measured logarithmic decrement is three and the period of discharge is measured to be 1.6 microseconds which yields the circuit's inductance and resistance to be  $0.67\mu\text{h}$  and 2.5 ohm respectively for a circuit having a capacitor of  $1/4\text{-}\mu\text{f}$ . This gives

$$I(t) = 2.8 \times 10^3 e^{-1.9 \times 10^6 t} \sin(3.94 \times 10^6 t) \quad (1-1)$$

where  $I$  is in amperes

$t$  is in seconds

The time of maximum current is 0.4 microseconds after the start of the discharge which corresponds to the first quarter cycle. Thus the maximum current is 1,300 amperes.

From Equation (1-1) the voltage drop over any circuit element can be obtained if one knows the element's impedance. From this the power consumed by any circuit element can be determined.

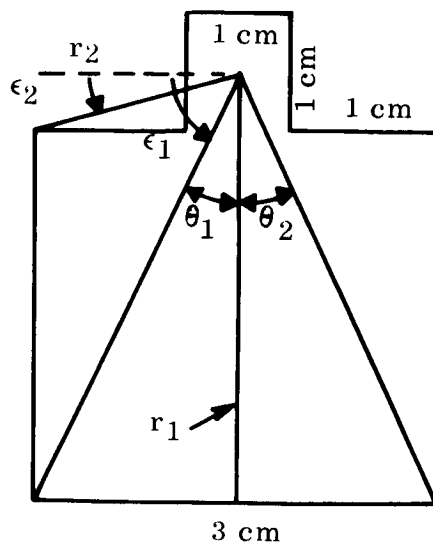


Figure E-1. Dimensions of Current Carrying Leads

Figure E-1 gives the dimensions of the current carrying leads of a typical circuit. The 3cm base is the length of the capacitor with 4 cm leads going around the fuel tank and connecting to the 1cm accelerating rail electrodes. Calculating the magnetic field "B" in the center of the accelerating electrodes one sums up the contribution from each segment of the circuit which is:

$$B = \frac{\mu_o I}{4\pi} \left[ \frac{1}{r_1} (\sin\theta_1 - \sin\theta_2) + \frac{1}{r_2} (\sin\epsilon_1 - \sin\epsilon_2) + \dots \right] \quad (1-2)$$

This gives a magnetic field of  $B = 83 \mu\text{oI}$ . The maximum field occurs at the first quarter cycle when the current is at its maximum value of 1.3K amperes. This corresponds to  $0.136 \text{ webers/m}^2$ .

The maximum magnetic force for this case is  $f = BIL = 1.76 \text{ newtons}$  which is quite small when compared to the force produced by the plasma pressure in the nozzle.

This result has been verified experimentally by taking individual engine and measuring the impulse generated with and without accelerating rail electrodes. This result points out the fact that engines with specific impulses of 2,000, or less can be obtained by electrical joule heating alone and magnetic acceleration is not needed. However, for engines of specific impulse of greater than 3,000 seconds magnetic acceleration becomes necessary. This could be accomplished by just designing a circuit which has a ringing frequency in the megacycles. For a circuit having a ringing frequency of two megacycles, the peak current would be about 9,000 amperes which would produce a magnetic force of 85 newtons which would increase the thrust by a factor of 2.6.

Thus an engine operating with a capacitor ringing frequency of the order of megacycles switches from predominantly joule heating of the plasma to magnetic acceleration. It should be pointed out here that when magnetic acceleration becomes predominant it is quite questionable whether or not the plasma will be in equilibrium. Also when magnetic acceleration is present, one has to check and be sure the plasma is Taylor stable and that there are no gross instabilities of the form of spoking. Thus an engine using magnetic acceleration has

a completely new set of problems associated with it that must be overcome and is not a mere extension of a previous engine.

This form of plasma acceleration has been demonstrated in the laboratory where the ringing frequency was 10 megacycle. The plasma seems to be formed with no visible instabilities which would disturb the plasma flow. In this particular engine the total circuit inductance was 0.01  $\mu$ h and the total resistance was 0.03 ohms with the engine having 55% of the inductance and resistance. This compares to the normal SPET engine which has 25% of the circuit inductance and resistance.

Another question of importance is whether or not the current that flows in the SPET firing circuit will produce any sizeable impulsive torque to the spacecraft. For this calculation we will assume the worse cases possible; the magnetic field is perpendicular to the current carrying leads and the current in the leads will be assumed to be the maximum current of 1.3K amperes. The impulse of the torque produced is:

$$I_t = Biat$$

where

- B is in webers/m<sup>2</sup>
- i is in amperes
- a is in square meters
- t is in seconds
- $I_t$  is in newton-meter seconds

The impulse of the torque is  $1.35 \times 10^{-12}$ ,  $1.35 \times 10^{-13}$  and  $1.35 \times 10^{-14}$  newton-meter seconds for a magnetic field of  $10^{-2}$ ,  $10^{-3}$ , and  $10^{-4}$  gauss respectively.

From Table E-1 the average impulse delivered by the SPET engine is 8.9 micropound-seconds, equal to  $2.0 \times 10^{-4}$  newton seconds which gives an impulse of the torque of  $3.04 \times 10^{-4}$  newton-meter seconds for a spacecraft with a moment arm of five feet. Clearly the impulsive torque produced by the thrust of the SPET engine is much greater than that resulting from the interaction of the magnetic field and the current carrying elements.

**APPENDIX F**  
**RESULTS OF SPET-D**  
**LABORATORY DEMONSTRATIONS**

In the detonation mode, the thrust developed by the SPET engine is derived from an exothermic chemical reaction which is triggered by an electrical discharge. Demonstration of the feasibility of the detonation mode has been accomplished by triggering the metallic film coated with appropriate detonating mixtures.

Specifically:

- a. Sheets of one-half mill, aluminized mylar have been coated with a film of exothermic material.
- b. One-fourth by one-eighth inch portions of this coated mylar is positioned between two triggering electrodes.
- c. A high voltage, low energy, electrical pulse is then passed through the aluminum foil which explodes the foil and ignites the exothermic propellant.

The primary considerations in selecting the propellant is its speed of reaction and its sensitivity. Because the detonation will occur in a vacuum, the detonation must be completed in a time shorter than the time needed for the diffusion of the products away from the combustion zone. The sensitivity of the propellant must be such that it will be ignited by the electrical discharge.

Two different detonable propellant were tested: ammonium perchlorate ( $\text{NH}_4\text{ClO}_4$ ) and potassium-dinitrobenzofuroxan (KDNBF).  $\text{NH}_4\text{ClO}_4$  was not sensitive enough for this mode of triggering and thus was discarded. The KDNBF, however, has been shown to be sensitive enough for this engine and produced thrusts orders of magnitude above that assignable to the electrical energy pulse. Several different thicknesses of the propellant layer were then tried ranging from 1 to 8 joule/0.031 in<sup>2</sup>. For KDNBF, the foils with less than 5 joule/0.031 in<sup>2</sup>. would not operate satisfactorily, but the higher energy foils, that is, the 5, 6 and 8 joule/0.031 in<sup>2</sup> worked reasonably well. The main problem in preparing this propellant is to obtain a good bond between the aluminized mylar and the explosive coating.



The electrical triggering system is a small capacitor which is charged to 3KV and then discharged through the aluminum foil. A 0.005  $\mu$ f capacitor having an energy storage of 0.0225 joules is sufficient to ignite the propellant. As one can clearly see the electrical energy is negligible in comparison with the chemical energy so that all the thrust produced is a result of the chemical detonation.

The measured impulse produced varies from 30 to 60 dyne-sec for the 5 joule/0.031 in.<sup>2</sup> and the 8 joule/0.031 in.<sup>2</sup> respectively. The mass of propellant used in each pulse varies from 1 to 2 milligram respectively which gives a rather constant specific impulse of a mean value of 28 seconds. This specific impulse is approximately one-third of the theoretical maximum which indicates that the fuel is not reacting completely. Being that no attempt was made to optimize the engine, fuel, or circuitry and that the question of a detonation wave being established in a vacuum is still debated, this experiment is feasible and is quite encouraging.

The next parameter of interest for this type of an engine is the specific impulse due only to the chemical reaction  $I_{spo}$ . It can be shown that the electrical energy added is related to the measured specific impulse  $I_{sp}$  and the chemical specific impulse  $I_{spo}$  by the following equation:

$$E = \frac{K}{\eta} I_{sp}^2 W \left( 1 - \frac{I_{spo}^2}{I_{sp}^2} \right) \quad (1-1)$$

where

- E = is the electrical energy
- $\eta$  = is the efficiency
- $I_{sp}$  = is the specific impulse produced
- W = is the weight of propellant used
- $I_{spo}$  = is the chemical specific impulse
- K = is a conversion factor depending on the units used

By measuring the specific impulse  $I_{sp}$  for various electrical trigger energy one can show that  $E \rightarrow 0$  and if  $\eta$  and  $W$  are assumed to remain constant, the measured  $I_{sp} \rightarrow I_{spo}$ . This information has been taken for the 8 joule/0.031 in.<sup>2</sup> foil which was detonated in air and gives  $I_{spo} = 20$  seconds.

Figure F-1 is a graph of  $I_{sp}$  (sec) vs the added electrical energy in joules for the 8 joule/0.031 in.<sup>2</sup> KDNBF fuel in air. This yields an  $I_{spo}$  of approximately 20 seconds.

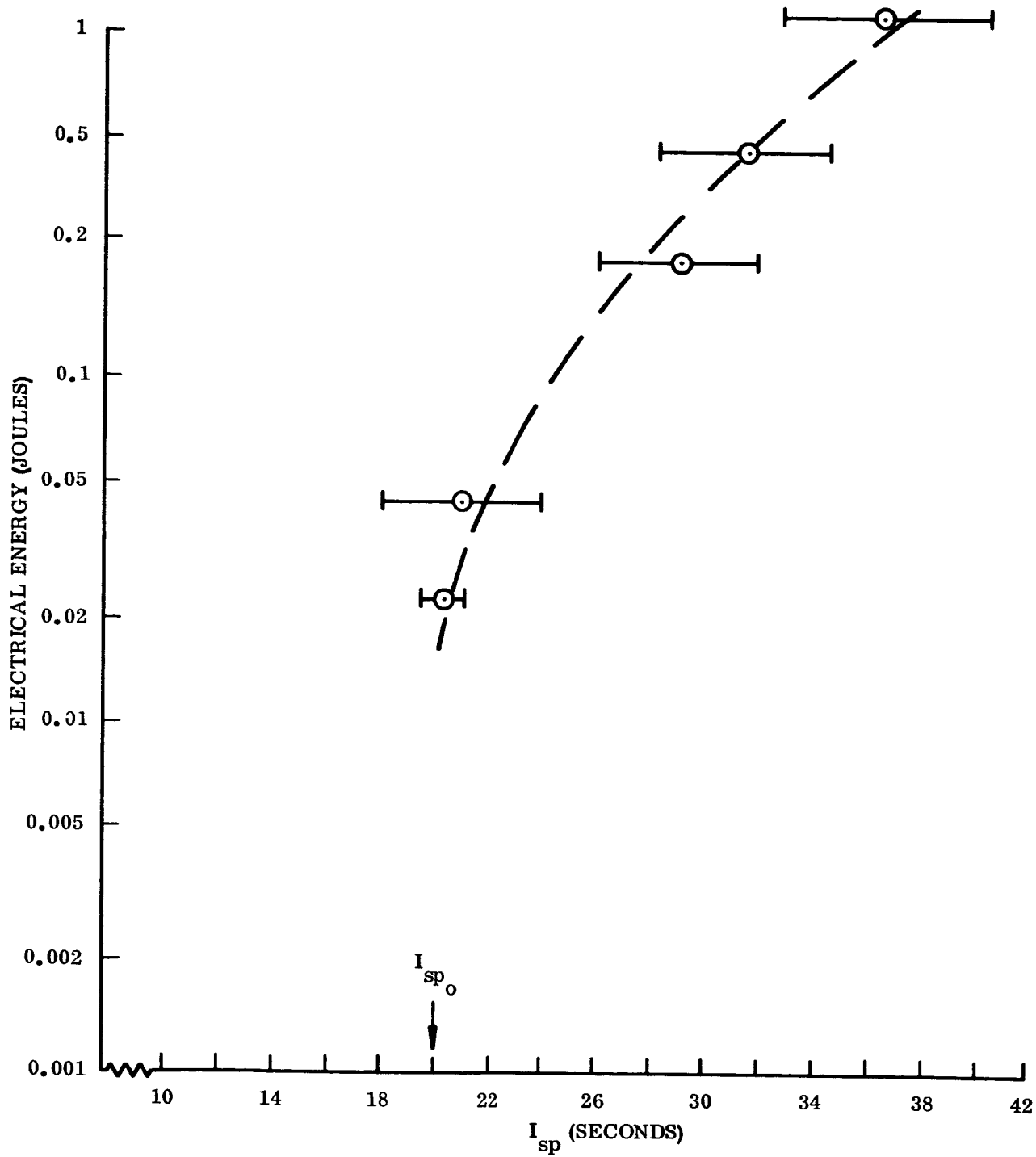


Figure F-1.  $I_{sp}$  vs Electrical Energy

7. Kucherov, R. Ya, and Pikenglaz, L. E., Soviet Phys. JETP, 37 (10), 88, (1960) (English Translation).
8. Vulliet, W. G., J. Chem. Phys., 41, 521 (1964).
9. Hirth, J. P., and Pound, G. M., "Condensation and Evaporation," Macmillan, 1963.
10. Frenkel, J., "Kinetic Theory of Liquids," Dover, 1955
11. Fisher, I. Z., "Statistical Theory of Liquids," University of Chicago Press, 1964, p. 169.
12. Slater, J. C., "Introduction to Chemical Physics," p. 328, McGraw-Hill, 1939.
13. LaRocca, A. V., "Parametric Performance Studies of Electrical Thrust Generators for Space Applications," Proceedings of Fifth Symposium of Ballistic Missile and Space Technology, Vol. II, Los Angeles, August 1960.
14. LaRocca, A. V., "Solid Propellant Electric Thrusters," AIAA Propulsion Joint Specialist Conference, Colorado Springs, Colorado, June 14-18, 1965.

Da

23 MAY 66 46144

2



**GENERAL  
ELECTRIC**

**SPACECRAFT DEPARTMENT  
MISSILE AND SPACE DIVISION  
VALLEY FORGE COMPLEX**

P.O. Box 8555 • Phila. Penna., 19101